

Design, Implementation and Control of Microwave Plasma Gasification System for Syngas Production

Belal Kabalan

A thesis submitted in partial fulfilment of the requirements
of Liverpool John Moores University
for the degree of Doctor of Philosophy

Built Environment and Sustainable Technologies

(BEST)

December 2012

LIVERPOOL JMU LIBRARY



3 1111 01309 1648

Dedicated to Moutasim, Randa, Lubna and Yazan

My supportive and loving family

Abstract

This thesis provides a solution for sustainable energy production. It applies the newest technologies of microwave plasma on a traditional method known as gasification. The simulation of this system has been achieved through a high frequency structure simulator to decide the best design of the structure. Microwave radiation at the frequency of 2.45 GHz has been applied to ionise argon gas and convert it into plasma. It has been proven that plasma can be self-initiated with an appropriate electric field applied. This microwave-induced plasma is the heart and soul of the Liverpool John Moores University's gasification system. It is coupled to a gasification chamber to gasify the feedstock placed inside and extract its energy as synthesis gas (i.e. hydrogen and carbon monoxide). Feedstock used in this study is carbon based material including pieces of wood and palm date seeds. This work is novel as no other work upto the date of this thesis completion has studied the different variables affecting plasma creation, plus the automation and the fully control of the microwave plasma gasification system.

Results reveal that after improvement of the microwave-induced plasma by automated control, it was possible to increase the synthesis gas production to 25.7% hydrogen and more than 57.6% carbon monoxide. This study has included the effects of some parameters on the plasma created, thus on its efficiency. These parameters are; the power of the microwave radiation, the reflected power from the system, the flow rate of argon and the pressure inside the gasification chamber. Other effects were taken into consideration throughout the project such as the study of the sample's moisture levels on the gas production and the use of helium gas instead of argon for plasma creation. The system has

proved the benefits of applying microwave-induced plasma technology on the gasification technology. These benefits can be summarised as the reduction of the input power needed for the procedure from the range of megawatts to 1 kilowatt, and the flexibility achieved through controlling the plasma jet for an improved process.

Acknowledgements

The completion of this project and the writing of this thesis has been the most significant academic and personal challenge I have ever had to face. Without the support, patience and guidance of my supervisors, colleagues, friends and family, this study would have not been completed. I would like to thank my director of studies and mentor Dr. Alex Mason for his continuous and unconditional help and support throughout this study. A big thank you goes to Professor Ahmed Al-Shamma'a. I would not be where I am now without the guidance and the support he has given me in the past two years. Also my thanks go to Professor Rafid Al-Khaddar and Doctors Andy Shaw, Stephen Wiley and Jeffrey Cullen for their help and of course their collaboration and guidance in those difficult or complicated parts of the research.

I would like to mention that my study in Liverpool would not have been the same without my friends who have also become a family; Ghaith, Ehab, Elena, Benjamin amongst many others, thank you for your understanding and your support when I was down.

Finally, my greatest gratitude goes to my family; my father who always has supported me both emotionally and financially, my mother who is always there for me with her loving heart and thoughts. My sister, she is my best friend and my focal point when I feel weak and tired, and my brother who always puts a smile on my face.

Thank you all!

Table of Contents

Chapter One: Introduction.....	1
1.1. Introduction and Project Scope	1
1.2. Aims and Objectives	2
1.3. Background	4
1.3.1. The Need for Renewable Energy	4
1.3.2. Market Drivers for Renewables.....	10
1.4. Current Renewable Solutions.....	11
1.5. Energy from Biomass.....	15
1.6. The Waste Issue	18
1.7. Gasification for Energy Generation	20
1.8. Chapters Overview.....	21
1.9. Summary	23
Chapter Two: Gasification	25
2.1. Introduction	25
2.2. History of Gasification.....	25
2.3. Gasification Theory.....	30
2.4. Stages of Gasification	33
2.5. Types of Gasifiers	34
2.5.1. Moving-bed Gasifiers.....	34
2.5.2. Fluidised-bed Gasifiers.....	36
2.5.3. Entrained-flow Gasifiers	37
2.6. Waste Streams for Gasification.....	39
2.7. Power Generation from Gasification	42
2.7.1. Integrated Gasification Combined Cycle IGCC.....	42
2.7.2. Fischer Tropsch Process.....	43
2.7.3. Conventional Heating Gasification Projects	44
2.8. Environmental Consideration and Advantages of Biomass Gasification	45
2.9. Summary	47
Chapter Three: Microwaves and Plasma.....	49

3.1. Introduction	49
3.2. Electromagnetics	50
3.2.1. Electromagnetic Radiation and Spectrum	52
3.3. Waveguides	55
3.3.1. Waveguide Transmission Modes	59
3.3.2. Cut-off Frequency	62
3.3.3. Impedance of Transmission Lines.....	63
3.3.4. Voltage Standing Wave Ratio (VSWR), Reflection Coefficient and Q factor	64
3.3.5. S-Parameters.....	66
3.4. Microwave components	68
3.4.1. Magnetrons	70
3.4.2. Circulators	72
3.4.3. Tuning system	73
3.5. Horn Antenna	75
3.6. High Frequency Structure Simulator HFSS.....	76
3.7. Plasma	82
3.7.1. Definition of Plasma.....	82
3.7.2. Plasma Excitation Sources	83
3.7.3. Gas Interaction with Microwaves.....	84
3.8. The Potential Benefits of Microwave Plasma Gasification	85
3.9. Key Microwave Plasma Gasification Parameters.....	86
3.10. Current Plasma Gasification Technologies.....	87
3.11. Summary	90
Chapter Four: Microwave Plasma Gasification System.....	92
4.1. Introduction	92
4.2. Initial LJMU's Gasification System.....	92
4.2.1. Microwave Components.....	93
4.2.2. Gasification Chamber.....	97
4.2.3 Microwave Plasma Cavity Modelling.....	99
4.3. Microwave Plasma System Simulation.....	104
4.4. System Improvements.....	108

4.5. Instrumentation and LabVIEW Interface.....	110
4.5.1. The Use of LabVIEW.....	111
4.5.2. cDAQ Chassis	116
4.5.3. Power Control.....	118
4.5.4. Gas Feed Control	121
4.5.5. E-H Tuner Control.....	123
4.5.6. Temperature.....	127
4.5.7. Gas Analyser	128
4.6. Gasification System Control	132
4.7. System Limitations.....	135
4.8. Summary	136
Chapter Five: Experimental Methodology	137
5.1. Introduction	137
5.2. System Calibration	137
5.2.1. Power.....	137
5.2.2. Argon Flow.....	139
5.2.3. E-H Tuner	142
5.2.4. Hydrogen Sensor	142
5.3. Feedstock Preparation	144
5.3.1. Samples Properties Determination	145
5.3.2. Samples Analysis Using Microwave Sensor.....	146
5.4. System Experimentation	148
5.4.1. Plasma Temperature Profile	149
5.4.2. Quintox Limitation	150
5.4.3. Pressure Effects on Gasification Process	151
5.4.4. Argon Flow Rate Effects on Gasification Process	152
5.4.5. Sample Moisture Effects on Gasification Process.....	152
5.4.6. Improvement of the Gasification Process	152
5.4.7. Argon Plasma versus Helium Plasma.....	153
5.4.8. Different Feedstock Study	153
5.5. Summary	154

Chapter Six: Results and Discussion.....	156
6.1. Introduction.....	156
6.2. System Calibration.....	156
6.2.1. Power.....	156
6.2.2. Argon Flow.....	158
6.2.3. E-H Tuner.....	159
6.2.4. Hydrogen Sensor.....	161
6.3. Feedstock Preparation.....	162
6.3.1. Samples Properties Determination.....	162
6.3.2. Sample Analysis Using Microwave Sensor.....	163
6.4. System Experimentation.....	170
6.4.1. Plasma Temperature Profile.....	171
6.4.2. Quintox Limitation.....	173
6.4.3. Pressure Effects on Gasification Process.....	178
6.4.4. Argon Flow Rate Effects on Gasification Process.....	185
6.4.5. Sample Moisture Effects on Gasification Process.....	190
6.4.6. Improvement of the Gasification Process.....	193
6.4.7. Argon Plasma versus Helium Plasma.....	197
6.4.8. Different Feedstock Study.....	200
6.5. Strengths and Limitations.....	202
6.6. Summary.....	205
Chapter Seven: Conclusion and Future Work.....	207
7.1. Conclusion.....	207
7.2. Future Work.....	210
References.....	212
Appendix A – Publications List.....	220
Appendix B – Gasification Plants Worldwide.....	221
Appendix C – LabVIEW Block Diagram.....	223

List of Figures:

Figure 1.1: Renewables share of global final energy consumption, 2009.....	5
Figure 1.2: Temperature variance in the past 100 years.....	7
Figure 1.3: GHG sources, 2006.....	7
Figure 1.4: Greenhouse gas emissions, 2006.	7
Figure 1.5: CO ₂ historical levels.	8
Figure 1.6: Methane historical levels.	9
Figure 1.7: N ₂ O historical levels.	9
Figure 1.8: The pillars of sustainable development.....	12
Figure 1.9: Renewable energy resources.....	13
Figure 1.10: Biomass to energy technologies.....	15
Figure 1.11: Landfill site.	19
Figure 1.12: Household waste and recycling, England 1996/97 to 2011/12.....	20
Figure 1.13: Overview of the chapters.	22
Figure 2.1: Typical products of thermal conversion.	29
Figure 2.2: Temperature effects on gasification products.	33
Figure 2.3: Moving-bed gasifier.....	35
Figure 2.4: Fluidised-bed gasifier.....	37
Figure 2.5: Entrained-flow gasifier.	38
Figure 2.6: General IGCC block diagram.	43
Figure 3.1: Electromagnetic wave.	52
Figure 3.2: EM propagation around the earth.	55
Figure 3.3: The need of waveguides.....	55
Figure 3.4: Parallel transmission line.	56
Figure 3.5: Coaxial cable.....	56
Figure 3.6: Common waveguide shapes.....	57
Figure 3.7: Potential difference in waveguide.....	59
Figure 3.8: Electric 'E' and magnetic 'H' fields in the waveguide.....	60
Figure 3.9: Mode subscript explanation.	61
Figure 3.10: HFSS design to show different modes in a rectangular waveguide.....	61
Figure 3.11: Transmission line elementary components.....	63
Figure 3.12: Transmission line wave propagation.	64
Figure 3.13: Q-factor curve and bandwidth (Δf).	66
Figure 3.14: Two- port network.	67
Figure 3.15: (a, b) Incident and reflected variables used in S-parameter definition.	67
Figure 3.16: General microwave system setup.....	69

Figure 3.17: Magnetron components.....	71
Figure 3.18: An open magnetron.....	72
Figure 3.19: Microwave circulator.....	73
Figure 3.20: E-H tuner.....	73
Figure 3.21: E-H tuner concept.	74
Figure 3.22: Horn antenna.....	75
Figure 3.23: Flow chart of simulation steps.	79
Figure 3.24: Solution type selection in HFSS.	80
Figure 3.25: Excitation port determination in HFSS.....	80
Figure 3.26: Solution setup in HFSS.....	81
Figure 3.27: Results of simulation in HFSS.....	81
Figure 3.28: States of the matter.....	82
Figure 3.29: Alter NRG plasma system, Courtesy of Alter NRG.....	89
Figure 4.1: Microwave plasma gasification system.	94
Figure 4.2: Alter power supply.....	94
Figure 4.3: WG9A waveguide.....	95
Figure 4.4: Magnetron used for LJMU’s gasification system.....	95
Figure 4.5: The experiment circulator.	97
Figure 4.6: Stopford’s gasification chamber design.	98
Figure 4.7: Gasification chamber from design to implementation.....	99
Figure 4.8: E-field vectors in a rectangular waveguide using HFSS.	100
Figure 4.9: E-field magnitude along centre line of the waveguide using HFSS.	100
Figure 4.10: Tapered cavity.....	101
Figure 4.11: LJMU’s plasma cavity design.....	102
Figure 4.12: E-field magnitude for the plasma cavity prototype.....	102
Figure 4.13: Microwave plasma cavity.	103
Figure 4.14: 3D model of the gasification system.....	104
Figure 4.15: Microwave plasma system simulation.	105
Figure 4.16: 3D representation of E and H arms position sweep for minimum reflected power.....	106
Figure 4.17: Microwave plasma system.	107
Figure 4.18: E-arm position sweep and reflected voltage.	107
Figure 4.19: Reflected power representing the reflected voltage with E-arm sweep.....	108
Figure 4.20: Gasification process flow chart.....	109
Figure 4.21: Block diagram of the system’s control parameters and interfacing method.	111
Figure 4.22: Main components of LabVIEW programme.	112
Figure 4.23: Power control GUI.....	114
Figure 4.24: Front panel of the control system.....	114
Figure 4.25: Quintox analyser control parameters.	115

Figure 4.26: Syngas production representation.	115
Figure 4.27: cDAQ 9172 and C series compatible modules, courtesy of ni.com.	118
Figure 4.28: Diode power detector.	118
Figure 4.29: Power source setup.	119
Figure 4.30: Power control block diagram.	119
Figure 4.31: Relay circuit diagram.	120
Figure 4.32: Relay circuit constructed on a test board.	120
Figure 4.33: Gas setup.	121
Figure 4.34: Gas instruments.	122
Figure 4.35: Brooks mass flow controller.	122
Figure 4.36: Argon flow rate control block diagram.	123
Figure 4.37: 3D model of the tuning arm.	124
Figure 4.38: E-H tuner arm control components.	125
Figure 4.39: The different components of the computerised E-H tuner.	126
Figure 4.40: E-H tuner control block diagram.	127
Figure 4.41: Stepper motor interface with cDAQ.	127
Figure 4.42: N-type thermocouple.	128
Figure 4.43: Temperature control block diagram.	128
Figure 4.44: Gas analysers control block diagram.	129
Figure 4.45: K1550 gas analyser.	130
Figure 4.46: Quintox 9106 Gas Analyser.	131
Figure 4.47: Setup section.	132
Figure 4.48: System's control flow chart.	134
Figure 5.1: Power calibration block diagram.	138
Figure 5.2: Flow rate to voltage conversion value range 1.	140
Figure 5.3: Flow rate to voltage conversion value range 2.	140
Figure 5.4: Flow rate to voltage conversion value range 3.	141
Figure 5.5: Flow rate to voltage conversion value range 4.	141
Figure 5.6: Hydrogen sensor calibration block diagram.	143
Figure 5.7: Planed smooth timber.	144
Figure 5.8: Samples preparation.	145
Figure 5.9: Drying oven.	146
Figure 5.10: Samples microwave analysis setup.	147
Figure 5.11: Palm date seeds samples.	154
Figure 6.1: Voltage to decibel conversion.	158
Figure 6.2: Moisture meter.	163
Figure 6.3: Full range frequency analysis.	164

Figure 6.4: Microwave analysis for the selected frequency range.	164
Figure 6.5: Microwave behaviour with the feedstock.	165
Figure 6.6: Microwave absorption curve for 10 repetitions.	166
Figure 6.7: Microwave absorption characteristic curve.	168
Figure 6.8: Correlated samples curve vs. uncorrelated sample.	169
Figure 6.9: The three different sample states absorption curve.....	170
Figure 6.10: Samples before and after gasification process.	171
Figure 6.11: Plasma's temperature profile at the crucible.....	172
Figure 6.12: Plasma burst length with different power levels.....	173
Figure 6.13: CO levels for 30 g samples.	175
Figure 6.14: CO levels for 10 g samples.	175
Figure 6.15: Plasma temperature at 500 and 600 watts.....	176
Figure 6.16: CO production with 600 watt power level.....	177
Figure 6.17: CO production with 500 watt power level.....	178
Figure 6.18: Pressure effects on CO production.	179
Figure 6.19: Pressure effects on H ₂ production.....	180
Figure 6.20: Syngas production with different pressure levels.	181
Figure 6.21: Four repetitions for CO production at 0 mbar.	182
Figure 6.22: Four repetitions for H ₂ production at 0 mbar.....	183
Figure 6.23: Four repetitions for CO production at 50 mbar.	183
Figure 6.24: Four repetitions for H ₂ production at 50 mbar.....	184
Figure 6.25: Four repetitions for CO production at 100 mbar.	184
Figure 6.26: Four repetitions for H ₂ production at 100 mbar.....	185
Figure 6.27: Argon flow effects on CO production.	186
Figure 6.28: Argon flow effects on H ₂ production.....	186
Figure 6.29: Syngas production with different argon flow rates.....	187
Figure 6.30: Four repetitions for CO production at 0.25 L/min.....	188
Figure 6.31: Four repetitions for H ₂ production at 0.25 L/min.	189
Figure 6.32: Four repetitions for CO production at 0.5 L/min.....	189
Figure 6.33: Four repetitions for H ₂ production at 0.5 L/min.	190
Figure 6.34: Moisture effects on CO production level.....	191
Figure 6.35: Moisture effects on H ₂ production level.....	192
Figure 6.36: Syngas production change with different moisture levels.	193
Figure 6.37: Manually controlled system behaviour.	194
Figure 6.38: Tuned system behaviour.	194
Figure 6.39: Algorithm effects on CO production.	196
Figure 6.40: Algorithm effects on H ₂ production.....	196
Figure 6.41: Comparison between syngas levels with and without applying the algorithm.	197
Figure 6.42: Helium plasma vs. argon plasma for CO levels.....	198

Figure 6.43: Helium plasma vs. argon plasma for H ₂ levels.....	199
Figure 6.44: Palm date seeds samples.....	201
Figure 6.45: Palm date seeds vs. timber for CO levels.	201
Figure 6.46: Palm date seeds vs. timber for H ₂ levels.....	202
Figure 6.47: Syngas levels for the gasification process with and without the control algorithm applied.....	203

List of Tables:

Table 1.1: Renewables Overview.....	14
Table 2.1: Comparison of primary products of gasification and combustion.	29
Table 2.2: Syngas contaminant.....	34
Table 2.3: Biomass classification.	40
Table 2.4: Energos technology gasification plants.....	45
Table 3.1: Electromagnetic spectrum.	53
Table 3.2: Waveguide dimensions and their operating frequencies.....	58
Table 4.1: NI DAQs specification and use.....	117
Table 5.1: K1550 error rates.....	144
Table 6.1: Power calibration experiment.....	157
Table 6.2: Argon flow calibration experiment.	159
Table 6.3: E-H tuner calibration experiment.....	160
Table 6.4: Hydrogen sensor calibration experiment.....	161
Table 6.5: Moisture and ash content calculation.	162
Table 6.6: Correlation factors for microwave absorption for the same sample and 10 repetitions.	167
Table 6.7: Sample size choice.	174
Table 6.8: Power level with different argon flow rates.	177
Table 6.9: Pressure effects on syngas production.	179
Table 6.10: Repetition experiments and error rates.....	182
Table 6.11: Argon flow rate effects on syngas production.	185
Table 6.12: Repetition experiments and error rates.....	188
Table 6.13: Moisture effects on syngas production.....	190
Table 6.14: Improvement effects with different argon flow rates.....	195
Table 6.15: Helium plasma vs. argon plasma experiments.	198
Table 6.16: Helium plasma vs. optimised argon plasma area calculations.	200
Table 6.17: Palm date seeds vs. timber for syngas levels.	200
Table 6.18: Area calculations for syngas production.	204
Table 6.19: Optimal system's parameters.	206

List of Abbreviations:

AC	Alternative Current
APP	Advanced Plasma Power
ASU	Air Separation Unit
AWS	Archimedes Wave Swing
CCL	Climate Change Levy
CCS	Carbon Capture and Storage
cDAQ	Compact Data Acquisition
CHP	Combined Heat and Power
CTE	Complete Thermodynamic Equilibrium
CV	Calorific Value
CSV	Comma Separated Value
DC	Direct Current
DECC	Department of Energy and Climate Change
DEFRA	Department for Environment, Food and Rural Affairs
EfW	Energy from Waste
EM	Electromagnetic
ETS	Emissions Trading Scheme
FEM	Finite Element Method
FT	Fischer Tropsch
GHGs	Greenhouse Gases
GUI	Graphical User Interface
HFSS	High Frequency Structure Simulator
HHV	High Heat Value
HRSG	Heat Recovery Steam Generator

HTU	Hydrothermal Upgrading
IEA	International Energy Agency
IGCC	Integrated Gasification Combined Cycle
IPCC	International Panel on Climate Change
LabVIEW	Laboratory Virtual Instrument Engineering Workbench
LHV	Low Heat Value
LJMU	Liverpool John Moores University
LTE	Local Thermodynamic Equilibrium
MHV	Medium Heat Value
MSW	Municipal Solid Waste
NFFO	Non-Fossil Fuel Obligation
NI	National Instruments
NOAA	National Oceanic and Atmospheric Administration
OECD	Organisation for Economic Co-operation and Development
OFGEM	Office of Gas and Electricity Market
OWC	Oscillating Water Column
PV	Photovoltaic
Q-factor	Quality factor
R&D	Research and Development
REF	Renewable Energy Foundation
REN21	Renewable Energy policy Network for the 21 st century
RF	Radio Frequency
RO	Renewable Obligation
ROC	Renewable Obligation Certificate
Syngas	Synthesis gas

TE	Transverse Electric
TEM	Transverse Electromagnetic
TM	Transverse Magnetic
VI	Virtual Instrument
VSWR	Voltage Standing Wave Ratio
WPC	Westinghouse Plasma Corporation
UNFCCC	United Nations Framework Convention on Climate Change

List of Symbols

B	Magnetic field flux density
C	Carbon
C	Capacitance
c	Speed of light
CH ₄	Methane
CO	Carbon monoxide
CO ₂	Carbon dioxide
D	Electric field flux density
E	Electric field
f	Frequency
f _c	Cut off frequency
G	Conductance
H	Magnetic field
H ₂	Hydrogen
H ₂ O	Water
H ₂ S	Hydrogen sulphide
HFC	Hydro fluorocarbons
J _c	Current density
J _d	Displacement current
L	Inductance
N ₂	Nitrogen
N ₂ O	Nitrous oxide
NH ₃	Ammonia
NO ₂	Nitrogen dioxide

NO_x	Nitrogen oxide
O_2	Oxygen
PFC	Perfluorocarbons
R	Resistance
SF_6	Sulphur hexafluoride
SO_2	Sulphur dioxide
Z_0	Characteristic impedance
Z_L	Load impedance
Γ	Reflection coefficient
ϵ	Permittivity
η	Efficiency
λ	Wave length
λ_g	Waveguide wavelength
μ	Permeability
v	Velocity
ω	Angular frequency
ρ	Charge density

Chapter One: Introduction

1.1. Introduction and Project Scope

A green future in which pollution is dropped to its minimum levels, lands are preserved, waste is fully recycled, and energy is available to all without the need for drilling another oil well. Is this a dream? No, it is not. Governments around the world are planning to make this reality through regulations, research, development, and raising awareness.

Energy production is a major reason for an unsustainable future. The main method used today for our electricity production is burning fossil fuels. It is the 21st century but we still use 20th century technology for our energy needs, which is an unacceptable situation.

The demand of energy certainly differs between developed and developing countries [1]. However, the demand rises with the number of consumers and this number is not decreasing. In 2011 the world's human population reached 7 billion, and is expected to rise to 9 billion by 2030 [1]. More people means increased energy demands. These demands are still mainly satisfied by the unsustainable fossil fuels as reported in the world energy council 2010 [2]. Moreover, environmental concerns [3-5] have been raised in the past decade regarding fossil fuel burning and its greenhouse gas emissions.

Alternative energy sources are vital for a greener and sustainable future. These alternatives can come from the sun, wind and water energy. However, they are not available all of the time and all over the world. Nuclear power is another option for generating energy, but concerns about safety and radiation accidents [6, 7] like the Fukushima incident in Japan

2011 amongst others in addition to the fear of military utilisation of nuclear power [8] does not make it a favourable choice.

Energy from waste (EfW) is an attractive alternative. It is sustainable and available globally and waste increases with the world's population, which makes it the ideal option to meet energy demands and recycle waste at the same time. However, EfW technologies are still in need of further development and optimisation. Gasification is an EfW method; it usually uses carbohydrate materials such as coal and wood to create synthesis gas (or syngas) which is an alternative to natural gas.

This project looks at alternative energy, in particular gasification technologies. The design and the implementation of a state-of-the-art microwave plasma gasification system are discussed throughout this thesis. Improvements of the implemented system is essential for the best performance. These improvements are achieved by applying sensors and algorithms to the system's structure. Performance evaluation of the system is done by using different types of feedstock. Wood pieces are used as initial samples for the system's improvement study. Wood is substituted with palm date seeds and the results gained are promising.

Liverpool John Moores University's microwave plasma gasification system has the potential of being a green and sustainable energy production technology which utilises cutting edge microwave technologies to develop the traditional gasification methods.

1.2. Aims and Objectives

The aim of this project is to understand and develop a microwave plasma gasification technology as a type of thermochemical conversion of bio-waste to energy. Liverpool John Moores University (LJMU) has already built a microwave induced plasma

gasification system. However, this system was a pilot design which needed further development in order to enhance its performance. A full remodelling of the system has been completed in this work to understand the microwave plasma creation and its parameters. From this remodelling and pilot system testing, the idea of developing the system has been thought of. A full automation and control of the system is believed to enhance its performance and increase the efficiency of syngas production. The aim of this project is achieved by dividing it into work packages, each of which focuses on a specific area to ensure the full understanding of the literature and the appropriate development of the system. These work packages are:

Work package 1: Literature review of the necessity of an alternative energy source and the available alternatives. Gasification theory is looked at in this work package along with microwave and plasma technologies. The literature review also looks at the available gasification technologies and research.

Work package 2: HFSS system analysis and development. HFSS is a high frequency system simulator, through which the pilot LJMU's gasification system is simulated and analysed for a further understanding of the system operation.

Work package 3: Instrumentation and LabVIEW interface with the different sensors needed for the automation and the control of the gasification process

Work package 4: Develop an automated monitoring and control system to tackle the complexity of manual control of the gasification process and to improve and maximise syngas production rates.

Work package 5: Interfacing with syngas sensors for monitoring of the gasification procedure and as a proof of the benefits of the control system implemented.

Work package 6: Documentation of the study both in a thesis and in conference and journal papers as a contribution to the knowledge database and for future development and reference.

1.3. Background

1.3.1. The Need for Renewable Energy

Energy is vital and essential for human beings; in every aspect of our life we use energy in some form; electric, transport fuel, heating, etc... However, the source of the energy (i.e. fossil fuel) is diminishing, thus another source is necessary to fulfil our energy needs. According to reports on the status of global energy by the renewable energy policy network for the 21st century (REN21) [9], renewable energy accounts for only 16% of the energy mix as shown in figure 1.1. The dominant energy source is obviously fossil fuel which include coal, petroleum and natural gas. Nuclear power has the lowest share in the energy mix (only 2.8%); USA, France and Japan are the main countries for nuclear power production. Nuclear power can be considered green and efficient. However, the main concerns involved with nuclear power are safety and well-being. The recent earthquake and tsunami in Japan in March 2011 badly affected the Fukushima nuclear plant and may have effects on generations to come.

The process of forming fossil fuels is nature dependent; such a process could take millions of years to complete. Anaerobic decomposition is an example of forming fossil fuel from buried dead organisms.

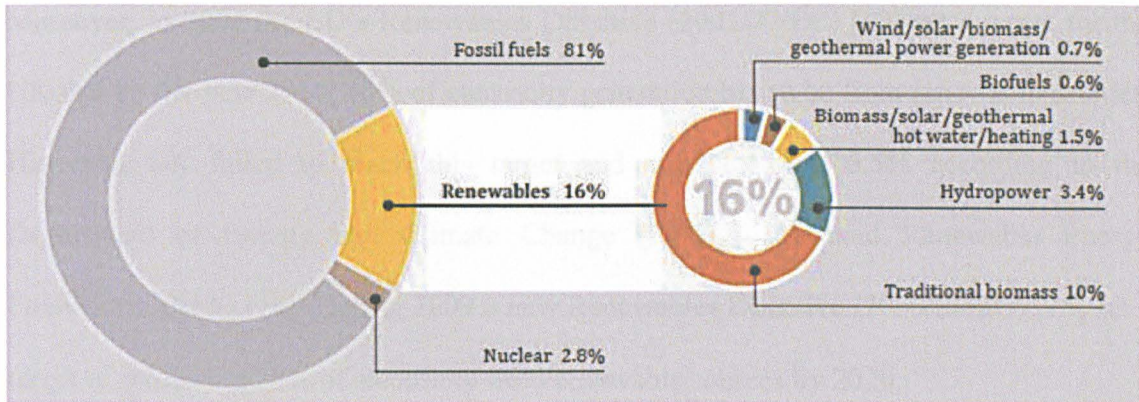


Figure 1.1: Renewables share of global final energy consumption, taken from [9].

Governments around the world, especially in the developed countries, seek to reduce their dependency on fossil fuels. For example, in the United Kingdom the Utilities Act (2000) [10] made significant changes to the regulatory system for electricity. The Act replaced the old Non-Fossil Fuel Obligation Orders (NFFO), which were put in place under the powers of the Electricity Act 1989 [11], with the Renewables Obligation (RO). RO increased the amount of electricity produced from renewable sources and finally came into force in April 2002. The Act basically stated four main key points to follow which are [2]:

- The electricity suppliers must produce a particular percentage (at least 3%) of electricity from renewable sources;
- Electricity generated from all renewable sources (excluding hydro plants over 10 MW) will be exempted from the Climate Change Levy (this is explained in detail in section 1.3.2 market drivers);
- Financial support including capital grants and R&D programmes will be offered for renewable energy development;
- A regional strategic approach will be dedicated to renewable energy planning.

Moreover, in 2001 the EU's Renewables Directive (2001/77/EC) [12] set a target for the UK that by the year 2010, 10% of electricity generation has to be from renewable sources. However, UK failed to reach this target and only achieved 6.5% according to the Department of Energy and Climate Change (DECC) [13] and Renewable Energy Foundation (REF) [14]. During 2009 a new Renewables Directive (2009/28/EC) [15] set a target of producing 20% of electricity from renewable sources by 2020.

So what is the driver behind these Directives and Acts? One can argue that it is due to the many challenges and drawbacks resulting from the use of fossil fuels, both for the environment and mankind's wellbeing.

The environmental effects come from the way energy is produced using fossil fuels. Burning fossil fuels has contributed to the issue of global warming. Global warming occurs when heat is captured in the earth's atmosphere, which leads to the increasing temperature on the surface of earth. The temperature of the earth has increased significantly in the past century, especially after the industrial revolution, according to climate change reports [16-18]; this can be observed in figure 1.2. The reason behind this temperature increase according to the reports is the gases in the atmosphere that trap heat; these gases are called greenhouse gases (GHGs).

Figure 1.3 shows the main contributors of GHG emissions in the US in 2006 [19]. The largest percentage is due to the effects of electricity generation, thus green electricity production technologies are being continually studied and developed.

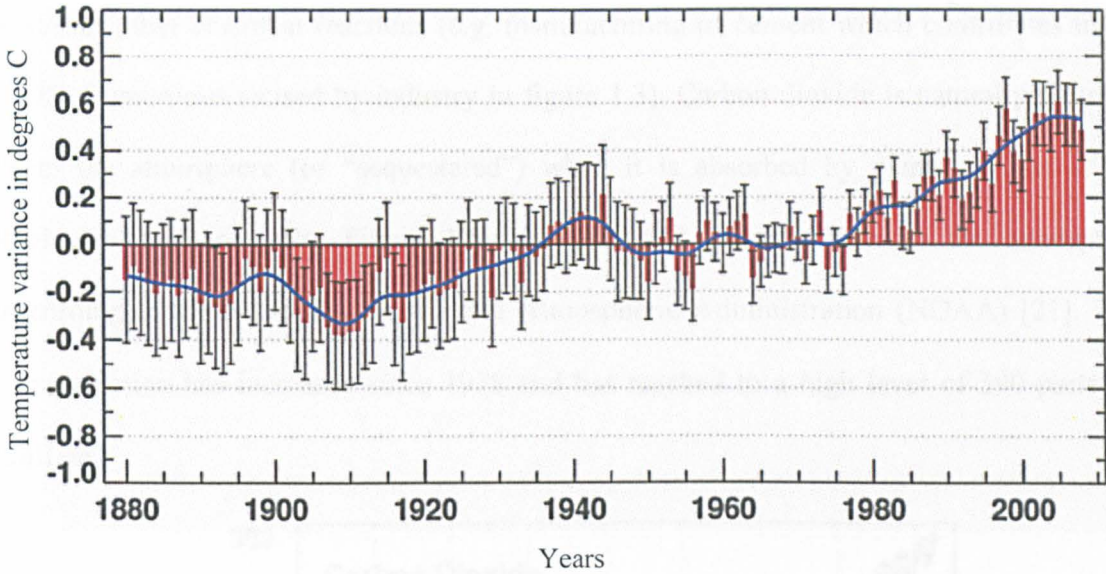


Figure 1.2: Temperature variance in the past 100 years, taken from [17]

The principal greenhouse gases that enter the atmosphere and their percentages are shown in figure 1.4 [20]. These gases are carbon dioxide, methane, nitrous oxide and fluorinated gases.

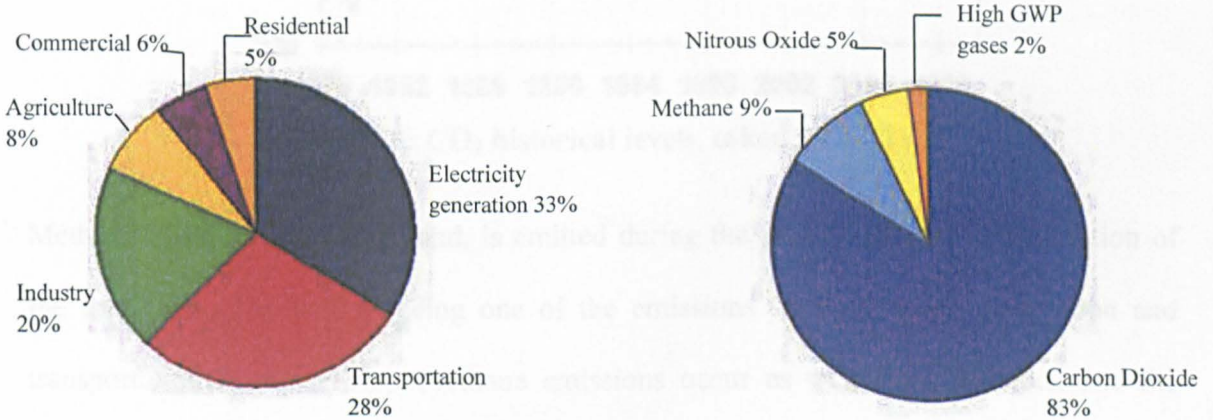


Figure 1.3: GHG sources, taken from [20]. Figure 1.4: GHG emissions, from [20].

Carbon Dioxide (CO₂) enters the atmosphere through the burning process of any material, especially fossil fuels (of the CO₂ from burning fossil fuels 33% comes from electricity generation and 28% from transportation as shown in figure 1.3). It can also be emitted as a

result of other chemical reactions (e.g. manufacturing of cement which contributes to the 20% of emissions caused by industry in figure 1.3). Carbon dioxide is naturally removed from the atmosphere (or “sequestered”) when it is absorbed by plants as part of the biological carbon cycle. Figure 1.5 illustrates CO₂ concentration in the atmosphere according to the National Oceanic and Atmospheric Administration (NOAA) [21]. This concentration has increased since 1978 and has reached to a high level of 390 parts per million.

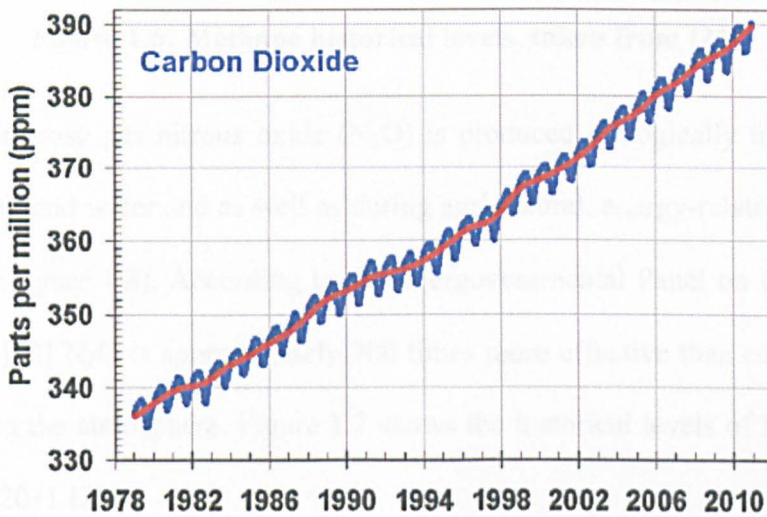


Figure 1.5: CO₂ historical levels, taken from [21].

Methane (CH₄) on the other hand, is emitted during the production and transportation of the fossil fuels (as well as being one of the emissions from electricity generation and transportation in figure 1.3). Methane emissions occur as well from livestock and the decomposition of organic waste in municipal solid waste (MSW) landfills. Figure 1.6 shows the historical records of methane reported in NOAA, 2011[21].

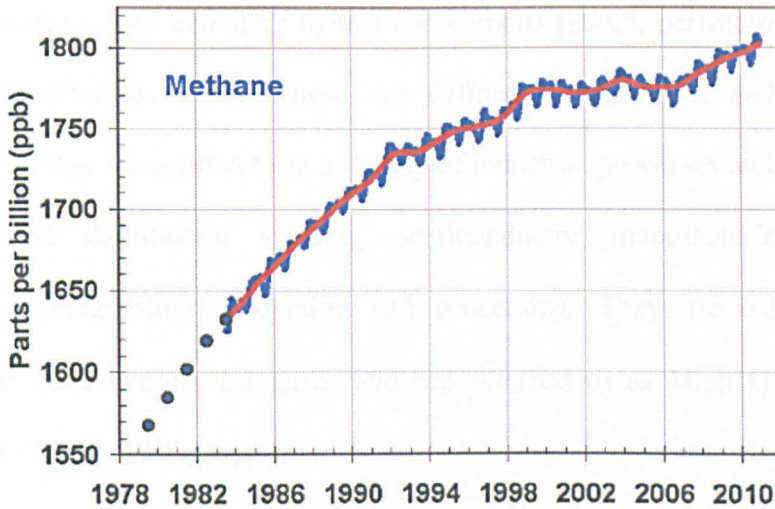


Figure 1.6: Methane historical levels, taken from [21].

The third greenhouse gas nitrous oxide (N_2O) is produced biologically by the processes occurring in soil and water and as well as during agricultural, energy-related and industrial activities (look figure 1.3). According to the Intergovernmental Panel on Climate Change (IPCC) report [22] N_2O is approximately 300 times more effective than carbon dioxide at trapping heat in the atmosphere. Figure 1.7 shows the historical levels of N_2O taken from NOAA report 2011 [21].

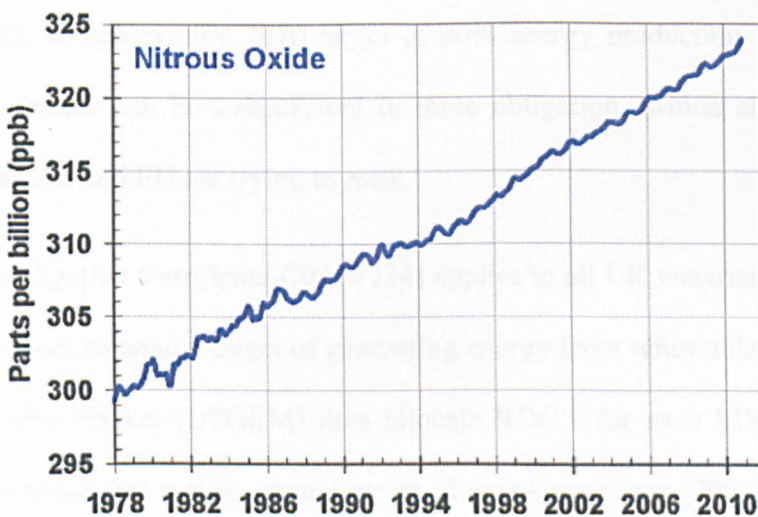


Figure 1.7: N_2O historical levels, taken from [22].

Finally, Fluorinated Gases including hydrofluorocarbons (HFC), perfluorocarbons (PFC), and sulphur hexafluoride (SF_6). These are defined as synthetic, and are powerful greenhouse gases that are emitted from a variety of industrial processes including electrical transmission and distribution systems, semiconductor manufacturing, aluminium production, and magnesium production and processing. They are emitted at lower quantities than other greenhouse gases and are referred to as High Global Warming Potential gases (“High GWP gases”).

From this short analysis of the GHGs and from figures 1.3-1.4 it can be noted that energy production from fossil fuel sources is the main cause of climate change and the associated environmental changes. Moreover, fossil fuels are considered as a finite energy source plus the long term price increase of oil [23] makes it essential to look for other source of energy, a source that is green, renewable and sustainable.

1.3.2. Market Drivers for Renewables

Energy suppliers are being driven to move towards renewables by a set of regulations placed by the EU to achieve the 2020 target of 20% energy production from renewable sources. Those drivers can be summarised in three obligations which all of the energy companies in the UK and EU are trying to meet.

(i) *Renewable Obligation Certificate* (ROC) [24] applies to all UK electricity suppliers and obliges them to meet an annual target of generating energy from renewables. The Office of Gas and Electricity Market (OFGEM) then allocate ROC's for each MWh generated to calculate if a company has met its annual target. For the base year (2002), the target was 3% of the total electricity supplied must be derived from renewable sources, and then it

gradually increased by between 0.5-1% annually to reach to 10.4% in 2011, finally it will be 20% by the year 2020.

(ii) *Emission Trading Scheme* (ETS) was established to set an EU-wide limit on the emission of GHGs. This scheme is regulated under EU Allowances (EUAs). EUAs are equivalent to suppliers' annual limit emissions of CO₂ which is decreasing gradually. Suppliers that exceed the EUAs will be fined a €40 per excess tonne of carbon dioxide (2005-2007); this fine increased to €60/CO₂ tonne (2008-2012).

(iii) *Climate Change Levy* (CCL) is the third market driver toward renewables, and it is a tax on the use of non-renewable energy. It is paid through electricity bills, the tax for UK is set as 0.43p/kWh for electricity as of 2006 [24], and companies are aiming to reduce the tax by moving to renewables.

1.4. Current Renewable Solutions

According to the Oxford dictionary, renewable energy, for short renewables, is defined as "*a source of energy that is not depleted by use, such as water, wind, or solar power*". This simple definition implies that the source of this energy should be available for use in the present and at any point in the future, in other words, the source of renewable energy should be sustainable. Sustainable is also defined by the Oxford dictionary as "*able to be maintained at a certain rate or level*". Having a sustainable green energy helps provide the required energy for the present and future generations without harming the earth, and, with more research, could result in lower energy prices.

Sustainable development can be broadly defined as living, producing and consuming in a manner that meets the needs of the present without compromising the ability of future

generations to meet their own needs [25]. Such a development balance between three pillars is required in order to deliver a long term sustainable growth [26-28]. Figure 1.8 shows these three pillars (i.e. environmental, social and economic). A sustainable development is a development that meets all of these three aspects.

Figure 1.9 shows the different types of renewable energy resources [29] and table 1.1 summarises the available technologies with some related information for each type.

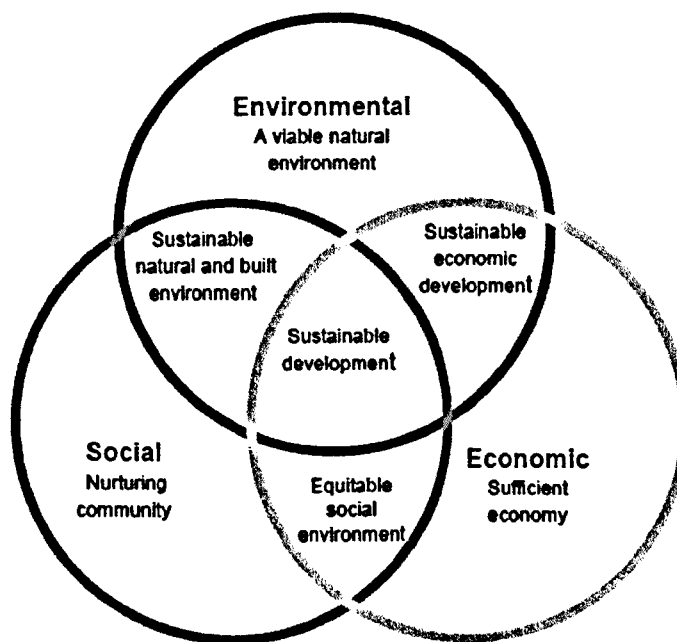


Figure 1.8: The pillars of sustainable development.

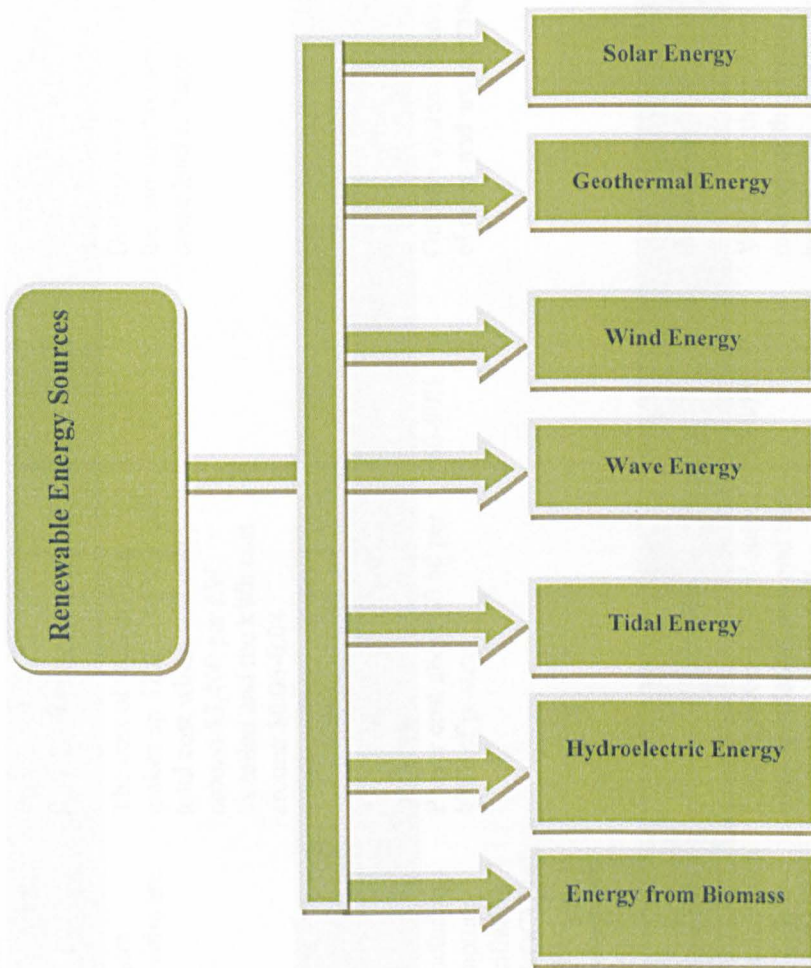


Figure 1.9: Renewable energy resources.

Energy from biomass is what this work is focused on thus is explained in detail in the next section and in chapter 2.

Table 1.1: Renewables Overview

Renewable Source	Location	Types/ Ways of utilisation	Cost/ KWh	Efficiency	Downsides
Solar	Where sun shines	Collectors panels [30] and PV cells [31]	Power cost between \$0.06-0.17 per kWh of power	5-20%	Toxic and hazardous chemical are used during manufacturing
Geothermal	Near an underground water/steam reservoir	Drilled wells where geothermal reservoirs are presented [32]	The cost of well drilling makes up 42% to 95% of the total cost which will cost around \$3,400 per kW installed and the kWh cost around \$0.06-0.08	50-70%	Drilling wells can weaken the surrounding area and cause land collapse
Wind	High windy places	Wind turbines [33]	\$0.04-0.09 per kWh and capital cost range between \$1-2 million per MW of capacity	25-40%	Visually unattractive
Wave	Coastal (onshore/offshore)	Wave turbines including: Tapchan wave capture system [25], Oscillating water column (WOC) [34], and submerged devices such as Archimedes wave swing (AWS) [35]	Power cost about \$0.50 per kWh of power	80-90%	Onshore systems create a lot of noise and are unattractive
Tidal	Coastal/offshore	Tidal barrage [36] Tidal stream [37] Tidal turbine [38]	Cost about \$0.10 per kWh	80%	Can cause damage to fish and the ecosystem
Hydroelectric	Stream, river, or falling water source	Hydroelectric plants with a storage reservoir [39] Run-of-river plants [40] Pumped storage plants [41]	Cost \$1,000 per kW of output plus installation fees and the kWh range \$0.03-0.25	50-80%	Will affect the general makeup of the stream because the water will be diverted to power the turbine
Biomass	Close to an existing landfill	Physical process, thermo-chemical process and bio-chemical process.	Small scale plants cost between \$110,00 and \$140,000 per daily tonne of capacity	About 80%	Metal materials cannot be converted

1.5. Energy from Biomass

Converting biomass into energy falls under three main technologies [42-44]; physical process, thermo-chemical process and bio-chemical process. Figure 1.10 lists the technologies and the different methods of each.

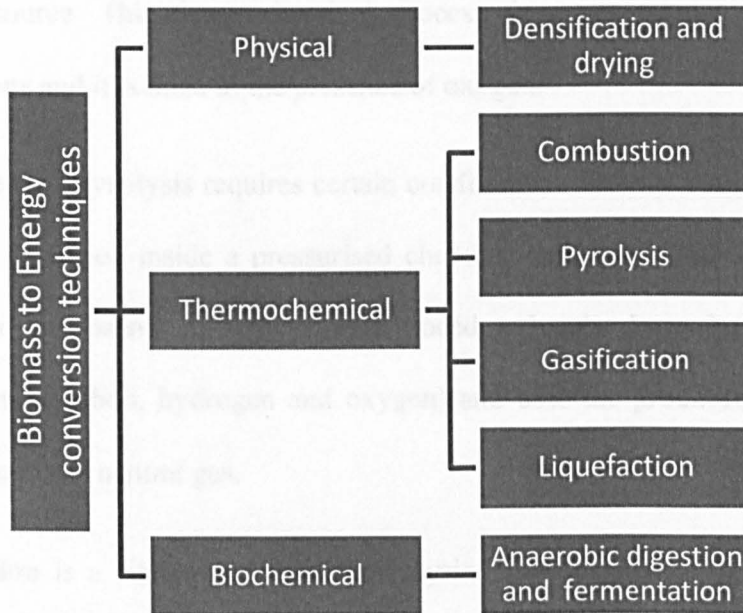


Figure 1.10: Biomass to energy technologies.

1. Physical conversion: Densification and drying process uses biomass (wood by-products like slaps, chips or sawdust) as the feedstock fuel for residential and industrial applications. The wood by-products are processed into uniform sized particles so they can be compressed into fuel wood products. Densification methods are based on shapes and sizes and the most common methods are to create logs, pellets or briquettes. Logs are generally used for residential markets as fireplace and wood stove fuel, while pellets are used more in commercial applications like industrial boilers as they have a higher energy density. Briquettes on the other hand, are mainly produced in the developing countries and they are used as a fuel source for both residential and industrial applications.

2. Thermochemical conversion: this type of conversion includes four main methods; combustion, gasification, pyrolysis and liquefaction.

Combustion is the direct way of using biomass without any pre-processing by simply burning it. The produced heat energy is then used in heating and cooking and even as a lighting source. This thermochemical process does not require any special chemical preparations and it is done in the presence of oxygen.

The process of **pyrolysis** requires certain conditions to turn the biomass into energy as the feedstock is placed inside a pressurised chamber with high temperatures (usually above 430 °C) in the absence of oxygen. This procedure breaks down the biomass into its main components (carbon, hydrogen and oxygen) and uses the produced oils and gases as an alternative to the natural gas.

Gasification is a similar process to pyrolysis and considered to be an extension of the pyrolysis procedure which is improved to give higher yields of carbon and energy in the gas phase [45]. However, in gasification, higher temperatures are required (above 700 °C) and a limited amount of oxygen should be presented in the chamber wherein the process takes place.

Liquefaction process extracts the liquid from the biomass to produce high value chemicals (bio-fuel), thus wet feedstock is used in this process. The liquefaction can take two main routes; direct and indirect liquefaction [46]. The hydrothermal liquefaction is an example of the direct liquefaction and it converts the biomass in water with high temperature and pressure. This method is applied by the Royal Dutch Shell plc, through the Hydrothermal upgrading (HTU). The concept of HTU is to convert biomass into gaseous product and oil

within 5-15 min by heating to temperatures ranging between (300-350) °C and a pressure of 15-20 MPa [47].

3. Biochemical conversion: Anaerobic digestion is a biological process which decomposes the organic materials by anaerobic micro-organisms in the absence of dissolved oxygen [48]. This digestion leads to a nearly complete conversion of the organic material into a high energy gas mixture (biogas) consisting mainly of methane (CH₄) and carbon dioxide (CO₂), with smaller percentage of hydrogen sulphide, ammonia and new bacterial biomass [49, 50]. The biogas produced has energy content of approximately half of the natural gas and this digestion occurs naturally in the buried municipal waste in landfill sites, the gas produced is known as landfill gas. This landfill gas is captured in the new developed landfill sites [51].

Biomass to energy technology is applied worldwide [52]; in the US in late 2009 for example, 8.5GW of electricity was provided from solid biomass, making it the world's largest producer of this form of power. Reports [52] show that electricity generation from solid biomass in Europe has tripled since 2001 and China's capacity rose 14% in 2009 to 3.2GW, the country plans to install up to 30GW by 2020, while India generated 1.9TWh of electricity with solid biomass in 2008. In Brazil there are over 4.8GW of biomass cogeneration plants at sugar mills, which generated more than 14TWh electricity in 2009. Germany passed the USA as the largest biogas-generated electricity producer in 2007, and remained the largest producer in 2009. It is also the largest producer of electricity from liquid biomass, at 2.9TWh in 2007.

1.6. The Waste Issue

Renewables can participate in achieving a greener and a more sustainable future. However, waste harms this future vision. Between 1990 and 1995, the amount of waste generated in Europe increased by 10%, according to the Organisation for Economic Cooperation and Development (OECD) [53]. By 2020, the OECD estimates an increase of 45% in waste generation from 1995.

The methods of managing this waste are by either burning it in incinerators, or dumping it into landfill sites (67% of the waste percentage) [54]. Such a site is shown in figure 1.11. Both of these methods create environmental damage. Burning the waste emits CO₂ to the atmosphere which contributes to GHGs emissions which are controlled and regulated by the EU (see section 2.2 for ETS). Meanwhile, landfill sites can take up valuable land space. Moreover, they cause air, water and soil pollution, discharging carbon dioxide (CO₂) and methane (CH₄) into the atmosphere and chemicals and pesticides into the earth and groundwater [54].

To tackle the waste generation issue, the EU has set a waste framework Directive (2008/98/EC) [55]. This Directive aims to find alternative methods for managing waste, reduce landfill use, and limit GHGs emissions. Instead of burning or dumping the waste, it should be recycled, composted or re-used.



Figure 1.11: Landfill site.

According to this Directive, a target of 50% of the waste from households in the UK, for example, should be recycled, composted or re-used by 2020. The UK government is continuously working to achieve this target. According to the Department for Environment, Food and Rural Affairs (DEFRA) [56], the proportion of household waste sent for recycling, composting or re-use between July 2010 and June 2011 in England was 42 %, increasing from 41.5 % in the period April 2010 to March 2011. Moreover, the generation of household waste continued to decrease between July 2010 and June 2011, with a 0.9 % reduction to 23.2 million tonnes [56].

Figure 1.12 shows DEFRA statistics regarding household waste and recycling for England between 1996/7 and 2011/12.

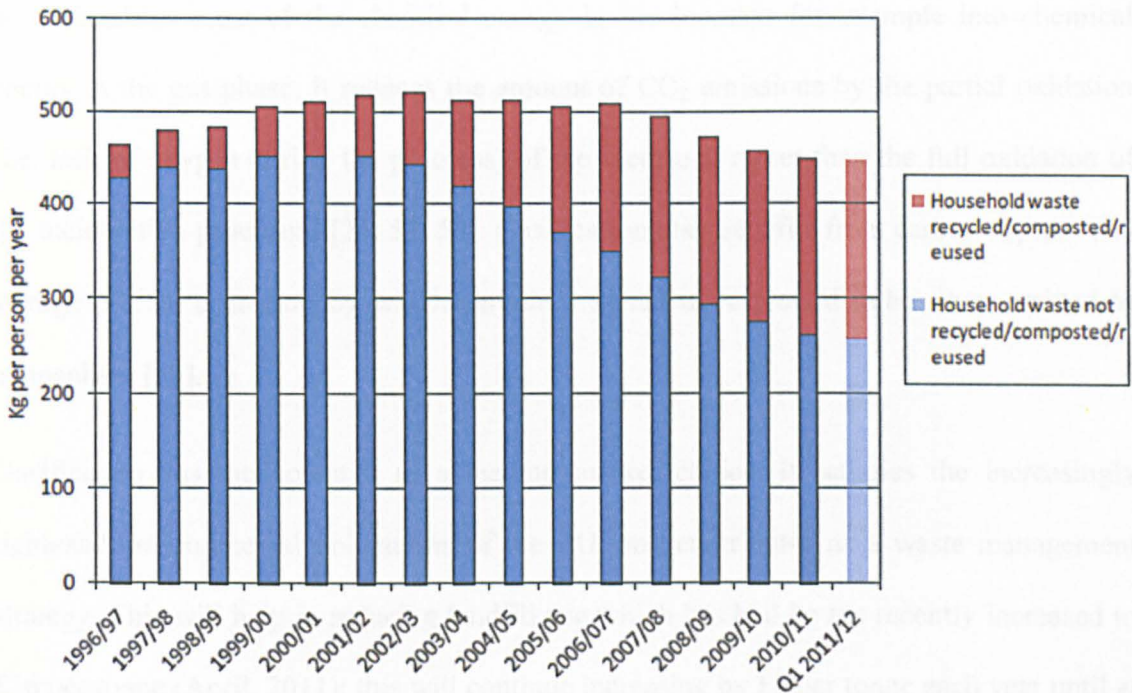


Figure 1.12: Household waste and recycling, England 1996/97 to 2011/12, from [56].

1.7. Gasification for Energy Generation

Gasification could be the potential solution for tackling both sustainable energy demands and waste management issues. It is an Energy from Waste (EfW) method wherein the feedstock (i.e. the fuel of energy production) could be diverted from household waste to be converted into energy for use in thermal or electrical applications. Heat generated from the gasification process can be used to convert water to steam for use in steam engines, while derived synthetic gas can be used to generate electricity via energy conversion technologies like gas engines.

Gasification will help governments' plans for recycling waste. This waste is sustainable as long as humans consume food. Moreover, gasification technologies reduce the volume of GHGs emissions. It has advantages over direct incineration (i.e. burning) of the feedstock

as it translates most of the chemical energy in the biomass for example into chemical energy in the gas phase. It reduces the amount of CO₂ emissions by the partial oxidation (i.e. lack of oxygen during the process) of the feedstock rather than the full oxidation of the incineration procedure [24, 57, 58]. Gasification also benefits from carbon capture and storage (CCS); a method by which carbon is stored underground rather than emitted to atmosphere [59].

Gasification has the potential as a leading market choice. It satisfies the increasingly tightened environmental obligations of the EU, and contributes as a waste management strategy. This will help in reducing landfill use which has had its tax recently increased to £56 per tonne (April, 2011); this will continue increasing by £8 per tonne each year until at least 2014 [60].

1.8. Chapters Overview

This thesis is divided into seven chapters, each of which is dedicated to a certain subject and builds on the previous chapters to create a full understanding of the systems literature and concepts. Figure 1.13 shows an overview of the chapter's progression from introduction to conclusion.

Chapter one is a general introduction of the thesis, it lists the aims and objectives of the work and covers the renewable energy needs and market drivers, then lists each of the available alternatives with more focus on energy from biomass as gasification technologies fall under this category. The waste and landfill problem is also explained in this chapter to conclude that gasification technologies can tackle both energy supply and waste

management issues at the same. Finally, an overview of the thesis's chapters is presented in this chapter which helps in a better understanding of the layout of the thesis.

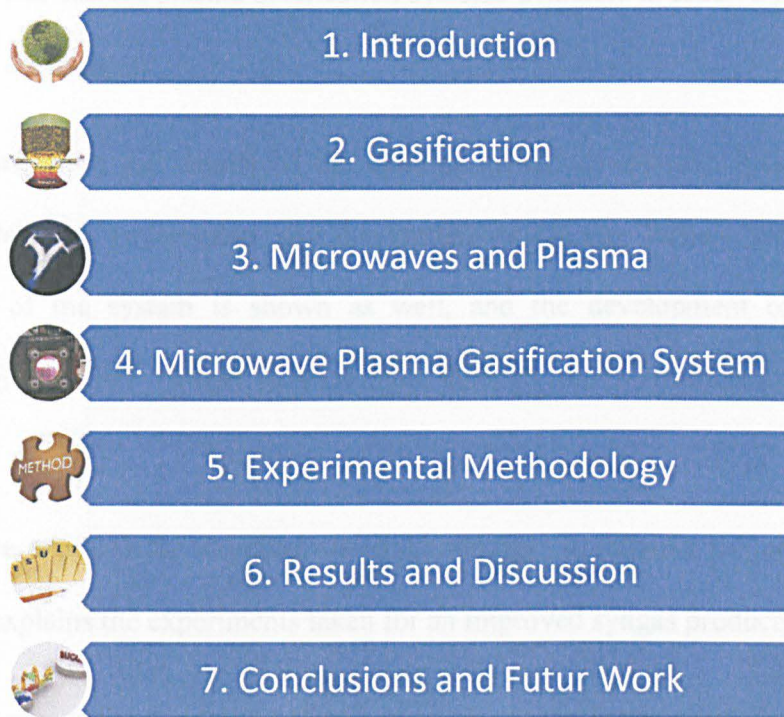


Figure 1.13: Overview of the chapters.

Chapter two explains gasification technology's history and theory then explains the stages and the types of the conventional gasification procedure. The waste stream used in gasification process is also explained here. A brief review of power generation from gasification is mentioned but not in full detail as the main focus of the study is the design and improvements of the system rather than the actual conversion of the syngas into energy. The chapter ends with a summary of the environmental considerations and advantages of biomass gasification for a better and greener future.

Chapter three explains microwaves and plasma theory. It starts with the theory of the electromagnetic radiation and explains the main components of a microwave system, and

then it explains the use of a high frequency structure simulator which is used to model the microwave plasma gasification system. Plasma definition and parameters are presented in this chapter, and current plasma gasification systems available at today's market are listed at the end of the chapter.

Chapter four gives the details of the exciting LJMU microwave plasma gasification system, explains its components and the limitations for any further developments. The remodelling of the system is shown as well, and the development of an automated controlled gasification system is explained through the instrumentation and control algorithm.

Chapter five explains the experimental methodology. It presents the calibration of the system and explains the experiments taken for an improved syngas production.

Chapter six shows the results and the observations of the experiments detailed in chapter five. Discusses the results and ties them to the literature review to see the potential use of the system.

Chapter seven concludes the thesis and shows the key findings of the project and matches them with the aims and objectives. It discusses any potential future work.

1.9. Summary

Renewable energy is the simple answer for our energy needs. It is green and sustainable; it meets the EU obligations and regulations to achieve the 2020 target of 20% of electricity produced from renewable sources. Different kinds of natural sources are available such as solar, geothermal, wind, wave, tidal, and hydroelectric energy. Energy from biomass is the focus of this study and generally has three main categories; physical, thermochemical, and

biochemical. The waste issue was discussed in this chapter. EU regulations requiring recycling 50% of the UK's household by 2020 should be met. Gasification technology as a type of thermochemical energy from waste production is an attractive route to help achieving both EU renewables and waste framework regulations and meeting the targets set by 2020. The aim of this project is to understand and develop a microwave plasma gasification technology. This aim is achieved by dividing the work into 6 different work packages. These work packages include the literature review, HFSS design, instrumentation and LabVIEW interface, develop automated algorithm for system control, syngas gas analysers interface for production rate study, and finally the documentation of the study.

This document is divided into seven different chapters to build up enough knowledge of microwave plasma gasification technology for syngas production.

Chapter Two: Gasification

2.1. Introduction

Gasification can take several routes by which it can be achieved; it can sometimes be a combination of two or more thermochemical processes, for example, the gasification of waste with pyrolysis as the first step of the process. However, the subject of this thesis is microwave plasma gasification, which is a novel thermochemical conversion of different feedstock into energy in the form of synthesis gas (syngas). It is believed to be more efficient and could save in the input power. No commercialised microwave plasma gasification system is available up to the date of completing this thesis, thus developing and analysing such a system would benefit businesses and add to the knowledge base for further development in the future.

Understanding microwave plasma gasification requires knowledge of gasification, plasma, and electromagnetics. This chapter introduces first gasification history and theory along with gasifier types available in the market today, and then it explains methods of energy extraction from gasifiers.

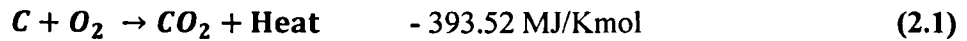
Finally, the environmental considerations and advantages of gasification technology are listed at the end of this chapter.

2.2. History of Gasification

Gasification is a well-known technique for energy production using carbon combustion which dates back to 1788 when Robert Gardner obtained the first patent with regard to gasification [61]. In 1792, the first confirmed use of produced gas was reported; Murdoc [61] used the gas generated from coal to light a room in his house. For many years after

coal gas was used for heating and cooking. The importance of gasification appeared during World War II where a lack of energy emerged and some countries relied heavily on oil imports. After the end of World War II, the importance of gasification decreased due to the availability of diesel and gasoline.

There is an increasing awareness of greenhouse effects and the environmental summits and protocols, such as the Kyoto protocol to the United Nations Framework Convention on Climate Change (UNFCCC or FCCC), that are aimed to protect the earth's atmosphere from gas emissions. This awareness gave back gasification technology its place as a green energy technology. It is believed to have major potential as a clean energy source from waste as it does not refer to fuel combustion or full oxidation anymore. Gasification, among other thermochemical waste conversion methods, is believed to have the potential to provide the world with clean and sustainable energy. Such thermochemical techniques are mainly categorised under three main types; Combustion, Gasification and Pyrolysis. The main differences between these three methods are the presence of oxygen at the conversion process and the temperature wherein the process takes place, thus the products produced from each type (i.e. mainly heat and steam in combustion, oil and gas in pyrolysis and mainly gas in gasification). The first and the oldest method is combustion; in this method a full oxidation reaction is carried out. It has been used since the industrial revolution to operate machines and steam trains by burning fossil fuel to get heat (the main product of combustion). This heat cannot be stored and should be used immediately for power generation. The main reaction of combustion for coal is [62]:



Combustion was widely used before the awareness of greenhouse gas emissions and its effect on climate change. This awareness led to various research and development in order to create a new and cleaner way of creating energy. Instead of the full combustion which emits large amounts of carbon dioxide (i.e. incineration of feedstock), a partial oxidation method has been developed. The general definition of gasification is the conversion of any carbonaceous feedstock “fuel” to gaseous products using partial oxidation. The main product of this partial oxidation is Synthesis Gas or Syngas which consists mainly of Hydrogen (H₂) and Carbon Monoxide (CO). The Syngas is later cleaned and further processed to produce chemicals, fertilisers, liquid fuel and electricity [63]. The feedstock that is converted to Syngas can be derived from hydrocarbon materials. Coal was the first feedstock used in the gasification process, but due to the demand for sustaining the earth’s resources, other types of feedstock are being used; biomass is in use at the moment which includes corn stove, bagasse, sawdust, wood [64], and most importantly food waste which gives the advantage of obtaining energy from a low cost and otherwise useless waste, and recycle it at the same time.

Gasification generally requires high temperature in a pressurised container to break the feedstock’s chemical bonds and generate syngas. In view of that, gasification technologies are categorised in two main methods:

- Conventional heating gasification; it depends on heating the feedstock using high power sources that achieve the high temperatures needed to break down the chemical bonds.

- Plasma heating gasification; in which breaking the chemical bonds depends on the temperature of the plasma. The use of plasma as the heat source has advantages over the conventional gasification process and it is considered to be a faster, better way for obtaining and controlling syngas production. Plasma is generally generated by either AC/DC current or by Microwaves. Microwave plasma gasification is the method used for syngas production in this project.

Pyrolysis is another thermal conversion of the feedstock. However, it is commenced with the absence of oxygen or air. Gasification is considered as an extension of the pyrolysis procedure by the addition of air to it, thus it increases the burn rate, increases the temperature and therefore increases the gas yields. Pyrolysis can be a part of the gasification process, where pyrolysis takes place first then a partial oxidation is presented. It can be used as an independent method as well, it is then categorised as slow or fast pyrolysis; slow pyrolysis can take hours to complete and its target is to collect both gases and liquids from the process. In the process of slow pyrolysis, temperature is raised gradually from 250°C to 750 °C to collect products in the different forms (liquid or gas), while in fast pyrolysis, the goal is to produce liquid fuel from biomass that can be substituted for fuel oil in any application. This is achieved by applying very high heat and heat transfer rates, which often requires a finely ground biomass feed [45].

Table 2.1 below shows a comparison between the thermochemical conversion process parameters and products [63]

Table 2.1: Comparison of primary products of gasification and combustion.

Parameter	Combustion	Gasification	Pyrolysis
Oxygen presence	Excessive	Limited	None
Temperature	Dependent on the amount of oxygen but usually above 300°C	Above 750°C	250°C -750°C
Main product	Heat	Syngas	Pyrolysis oil and gas
Carbon	CO ₂	CO and lower amounts of CO ₂	CO
Hydrogen	H ₂ O	H ₂	H ₂ and H ₂ O
Nitrogen	NO _x	N ₂	N ₂
Sulfur	SO ₂	H ₂ S	H ₂ S
Oxygen	O ₂	-	-

Figure 2.1 shows a comparison between the three thermal conversion methods and the products gained from each of them [65].

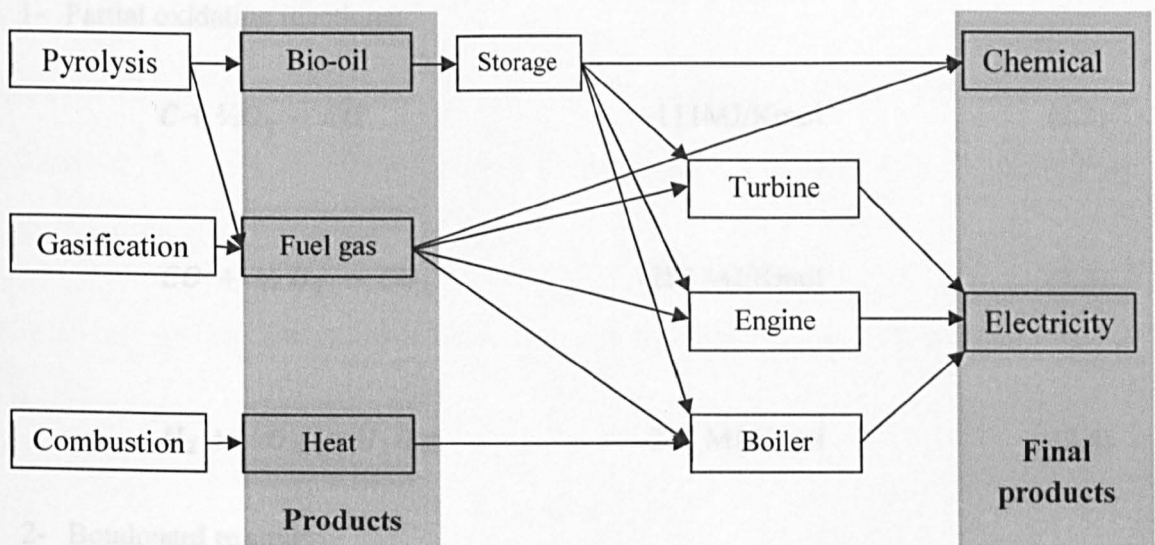


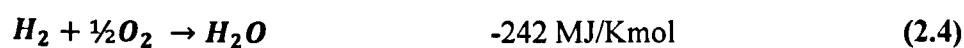
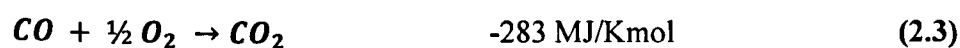
Figure 2.1: Typical products of thermal conversion.

From this figure, it can be noted that the main product from combustion is heat. Gasification and pyrolysis on the other hand, produce energy rich gas (syngas) in addition to the heat produced in combustion.

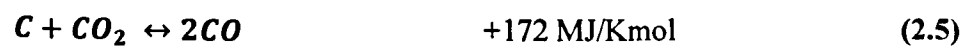
2.3. Gasification Theory

Gasification is a thermal process to break down the chemical bonds of the feedstock presented to a gasifier, thus it is important to understand the thermodynamics of gasification as a first step to having an overall knowledge of gasification. Studies show that the gasification process takes place at temperature range between 800-1800 °C depending on the characteristics of the feedstock [66], mainly the softening and melting temperature of the ash. Feedstock undergoes several chemical reactions, of which some are exothermic and some are endothermic, in order to produce syngas. The principle reactions of solid carbon as an example are as follows [66]:

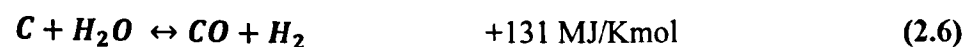
1- Partial oxidation reactions:



2- Boudouard reaction:



3- The water gas reaction:



4- Methanation reaction:

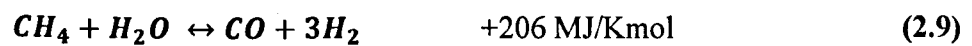


For the complete carbon conversion, the three heterogeneous reactions (2.5, 2.6, and 2.7) can be reduced to the following two equations:

- The CO shift reaction:

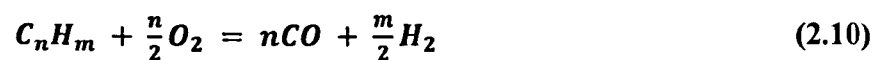


- Steam methane reforming reaction:



Equations (2.2, 2.5, 2.6, and 2.7) describe the four ways in which carbonaceous or hydrocarbon fuel can be gasified, but most gasification processes rely on a balance between reactions (2.2) and (2.6).

For real fuel including coal, which also contains hydrogen, the overall reaction can be written as:



Where:

- For gas as pure methane, $m = 4$ and $n = 1$
- For oil, $m = 2$ and $n = 1$
- For coal, $m = 1$ and $n = 1$

Equations (2.5:2.9) are reversible equations (represented by double arrows) meaning they can proceed both from right to left as well as from left to right. Generally, forward and reverse reactions take place simultaneously at different rates.

In addition to thermodynamics, it is important to understand the kinetics of the gasification process. Kinetic theory studies the effect of temperature rise on the procedure (slow or fast heating of the feedstock), and the temperature value (medium heat value MHV, or low heat value LHV). Thus, temperature is vital to the gasification process as it will eventually affect the syngas purity.

If the heating up is slow, the gasification reaction of both volatiles and char with steam is slow and the concentration of volatiles increases rapidly leading to impurity of the produced syngas. If the rate of heating is high, both pyrolysis and gasification take place simultaneously resulting in low concentration of the volatiles and cleaner gas is obtained. Figure 2.2 shows the effects of MHV and LHV in gasification process [65].

In order to obtain bio-fuel from biomass for example, MHV should be applied in a high speed mechanism. This confirms the target of fast pyrolysis, mentioned before, to be for liquids production. This project is to do with plasma gasification in which rapid temperature rises are applied to the feedstock, thus bio-fuel can be obtained according to this kinetic theory.

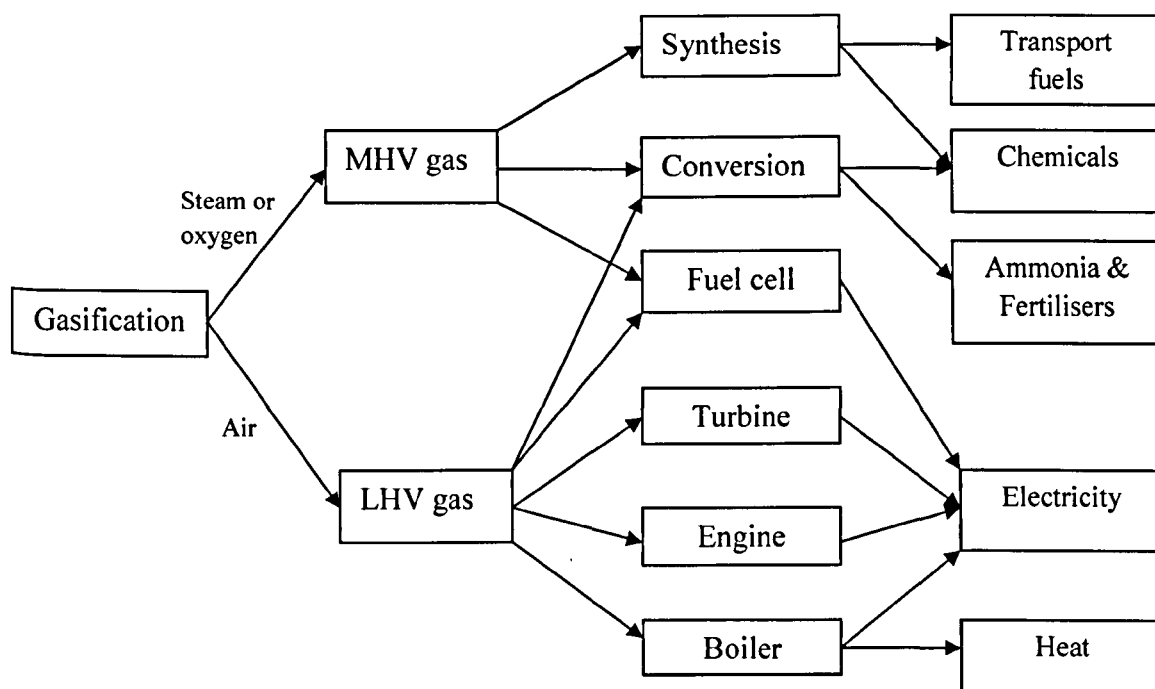


Figure 2.2: Temperature effects on gasification products.

2.4. Stages of Gasification

The gasification process undergoes four stages in general [67]:

- 1- **Preparation of the waste feedstock;** depending on the feedstock form, a pre-treatment might be required before it enters the gasifier. For example, it is necessary to remove metal compounds from the waste by applying a magnetic field to the waste before the gasification process.
- 2- **Heating the waste;** this is the gasification procedure which will produce the syngas and some other residues like ash and slag.
- 3- **Cleaning the produced gas;** to remove some of the particulates.
- 4- **Generating electricity, heat or chemical products;** by using the cleaned gas.

This project deals with syngas production and improvement only and will not deal with the cleaning of gas or generating energy. However, it is important to analyse and know the composition of syngas to be able to determine the outcome gases of the project's gasification system and the syngas percentage of this outcome.

Syngas mainly consists of hydrogen (H_2) and carbon monoxide (CO), with a small amount of carbon dioxide CO_2 , water H_2O , methane CH_4 , and other higher hydrocarbons C_2^+ . In addition to these compounds, there are other pollutants which may accompany the gasification process and syngas production. These contaminants are summarised in Table 2.2 with their effects [68].

Table 2.2: Syngas contaminant.

Contaminant	Example	Potential Problem
Particles	Ash, char, fluid bed material	Erosion
Alkali Metals	Sodium and potassium	Hot corrosion, catalyst poisoning
Nitrogen compounds	NH_3 and HCN	Emissions
Tars	Refractive aromatics	Clogging of filters
Sulfur, Chlorine	H_2S and HCL	Corrosion, emission, catalyst poisoning

2.5. Types of Gasifiers

Traditional gasifiers are generally categorised into three main types [69]; Moving-bed gasifiers, fluidised-bed gasifiers and entrained flow gasifiers. Each type has its own merits.

2.5.1. Moving-bed Gasifiers

Moving-bed gasifiers typically have a grate to support the feed material and maintain a stationary reaction zone. They are relatively easy to design and operate, and are therefore

useful for small and medium scale power and thermal energy uses. It is difficult, however, to maintain uniform operating temperatures and ensure adequate gas mixing in the reaction zone. As a result, gas yields can be unpredictable and are not optimal for large-scale power purposes (i.e. over 1 MW).

Moving-bed gasifiers can take two categories; updraft and downdraft. In the updraft moving-bed gasifier shown in figure 2.3 (a), waste is admitted from the top of the gasifier and air or oxygen enters at the bottom (counter flow). The feedstock falls onto a grate and forms a fuel pile. It is shown in figure 2.3 (b) that the produced gas is at a low temperature and it is laden with condensed tars and oils.

Downdraft or co-flow gasifiers are designed to overcome the condensed tars and oils produced by updrafts [65], since the waste and air both flow in the same direction downward through the gasifier. With the moving bed gasifier, oxygen consumption is very low and they operate on lump coal and waste as feedstock.

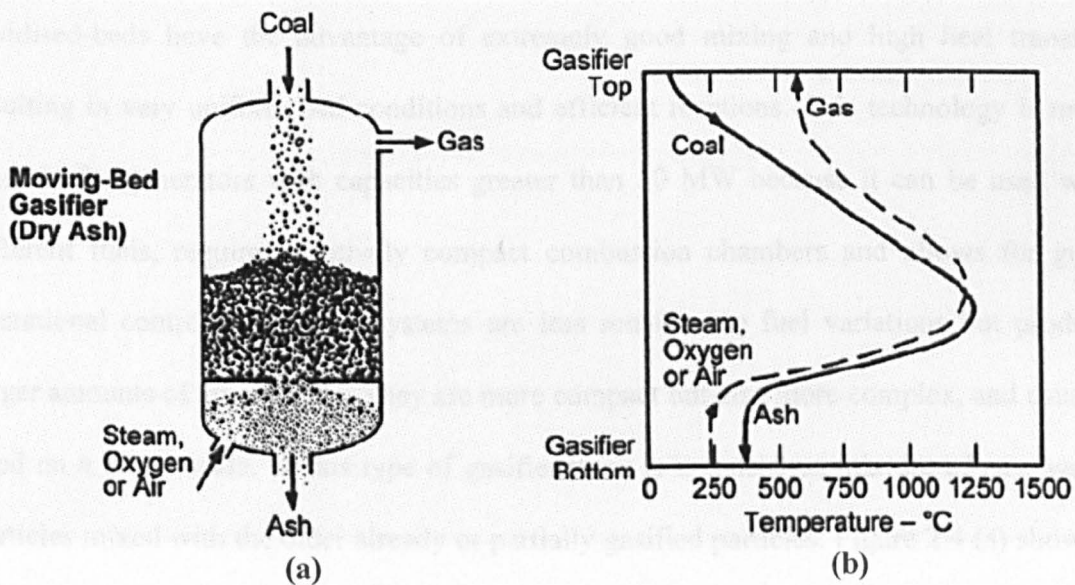


Figure 2.3: Moving-bed gasifier.

Moving-bed gasifiers have the following characteristics:

- Low oxidant requirements.
- Produced gas has relatively high methane content.
- There is production of hydrocarbon liquids such as tars and oils.
- Limited ability to handle fine components.

2.5.2. Fluidised-bed Gasifiers

Fluidised beds offer the best vessel design for the gasification of MSW. In a fluidised bed, inert material and solid fuel are fluidised by means of air distributed below the bed. A stream of gas (typically air or steam) is passed upward through a bed of solid fuel and material (such as coarse sand or limestone). The gas acts as the fluidising medium and also provides the oxidant for combustion and tar cracking. The fluidised bed behaves like a boiling liquid and has some of the physical characteristics of a fluid.

Fluidised-beds have the advantage of extremely good mixing and high heat transfer, resulting in very uniform bed conditions and efficient reactions. This technology is more suitable for generators with capacities greater than 10 MW because it can be used with different fuels, requires relatively compact combustion chambers and allows for good operational control [70]. Such systems are less sensitive to fuel variations but produce larger amounts of tar and dust. They are more compact but also more complex, and usually used on a larger scale. In this type of gasifier there is a consistent mixture of new waste particles mixed with the older already or partially gasified particles. Figure 2.4 (a) shows a

general fluidised-bed gasifier. Figure 2.4 (b) shows the temperature arrangement in the gasifier.

Fluidised-bed gasifiers have the following characteristics:

- Extensive solids recycling
- Moderate oxygen and steam requirements
- Uniform and moderate temperature

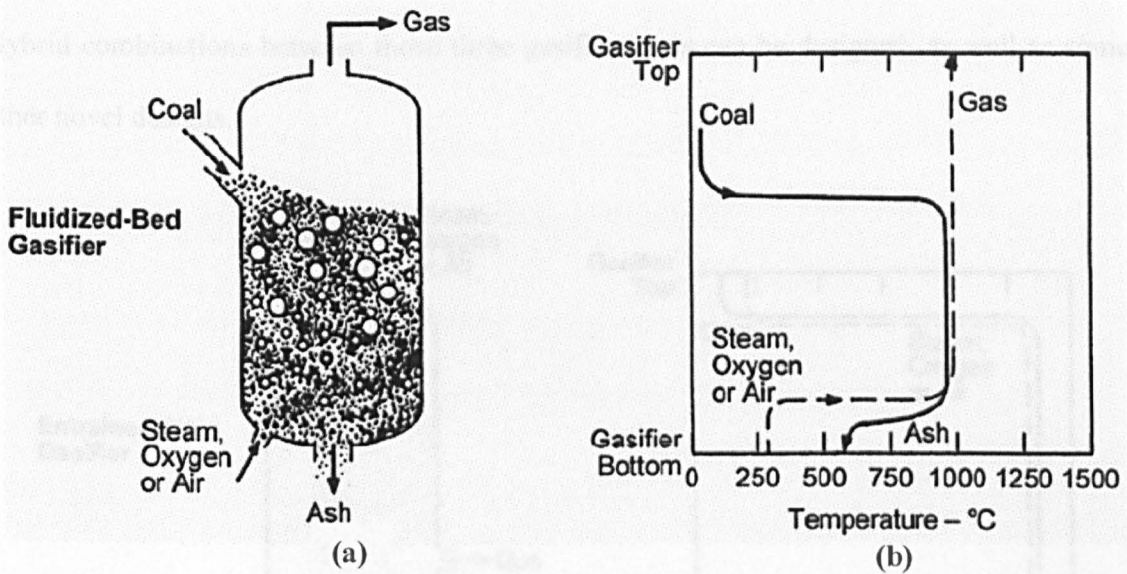


Figure 2.4: Fluidised-bed gasifier.

2.5.3. Entrained-flow Gasifiers

Here, the feedstock is a fine material (from coal or waste) which is introduced to the gasifier along with the flow of the oxidant (co-current flow). This rapidly heats up and reacts with the oxidants. The residence time of an entrained flow gasifier is in the order of seconds, thus it must operate at high temperature to achieve high carbon conversion. Figure

2.5 (a) shows the entrained flow gasifier and its thermal arrangement inside the gasifier (figure 2.5 (b)).

Entrained gasifiers have the following characteristics:

- High temperature operation.
- Raw syngas may have some molten slag.
- Large oxidant and feedstock preparation requirements.
- Wide waste type gasification ability.

Hybrid combinations between those three gasifier types can be designed, as well as some other novel designs.

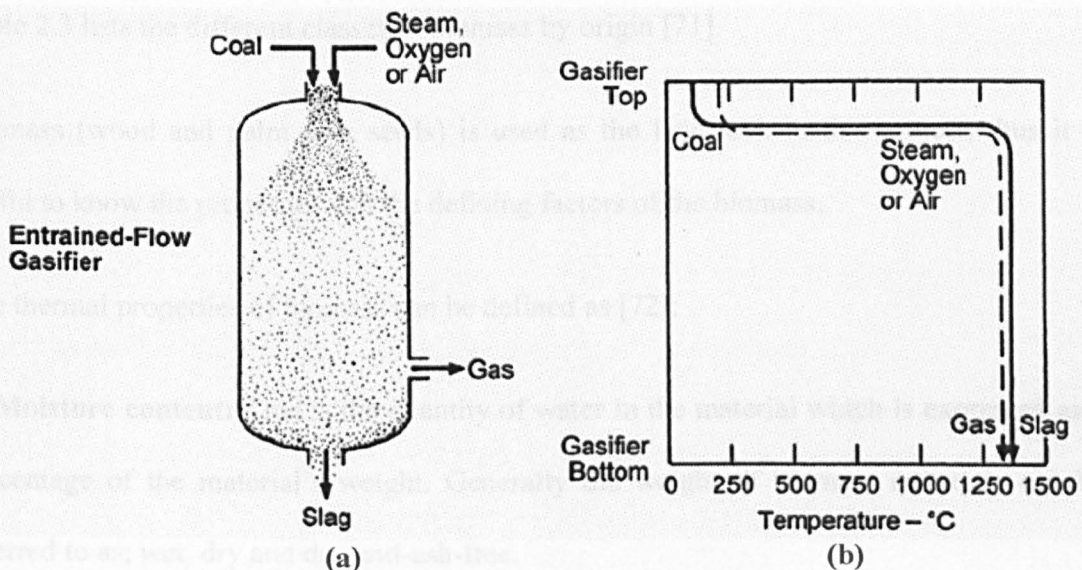


Figure 2.5: Entrained-flow gasifier.

The scope of this project is the gasification of biomass materials and waste. Biomass feedstock is similar to coal, and is considered as a very young coal, thus is treated the same regarding the gasification temperature range. However, there are some noteworthy differences between the two;

- The biomass ash quality has a lower melting point than coal ash, but it is aggressive when in a molten state.
- Biomass has higher reactivity
- Biomass may include vegetables thus some other considerations have to be looked at, such as its fibrous characteristic
- Tar mass in the biomass gasification process is much higher than in coal gasification.

2.6. Waste Streams for Gasification

Biomass can be defined as any living material on earth such as plants, animal or bacteria. Table 2.3 lists the different classes of biomass by origin [71].

Biomass (wood and palm date seeds) is used as the feedstock in this project, thus it is useful to know the properties and the defining factors of the biomass.

The thermal properties of biomass can be defined as [72]:

1- Moisture content: This is the quantity of water in the material which is expressed as a percentage of the material's weight. Generally the weight of biomass materials can be referred to as; wet, dry and dry-and-ash-free.

The moisture content of a sample can be calculated for the mass change during drying according to equation 2.11 [73]:

$$\text{Moisture content} = \frac{\text{Original mass} - \text{oven dry mass}}{\text{Oven dry mass}} \quad (2.11)$$

Table 2.3: Biomass classification.

Biomass group	Biomass sub-groups, varieties and species
Wood and woody biomass	Coniferous or deciduous; soft or hard; stems, branches, foliage, bark, chips, pellets, briquettes, sawdust, sawmill.
Herbaceous and agricultural biomass	Annual or perennial and field-based or processed-based such as: grasses and flowers, straws and other residues (fruit, shells pits, seeds...)
Aquatic biomass	Marine or freshwater algae; macroalgae or microalgae
Animal and human biomass waste	Bones, meat-bones meal, chicken litter, various manures
Contaminated biomass and industrial biomass wastes	Municipal solid waste (MSW), demolition wood, refuse-derived fuel, sewage, sludge, hospital waste, waste papers....
Biomass mixtures	Blends from the above varieties

2- Ash content: Ash is the inorganic component in the biomass and can be expressed in the same way as moisture content, but it is usually expressed on a dry basis. This content is important as it affects the behaviour of gasification and combustion under high temperatures. Melted ash may cause problems in gasification reactors.

The ash content can be calculated according to the equation 2.12 [74]

$$\text{Ash content} = \frac{m_2 \times 100}{m_1} \times \frac{100}{100 - MC} \quad (2.12)$$

Where m_2 is incineration residue mass (g)

m_1 is original mass in analytical moisture content (g)

MC is the analytical moisture content (%)

3- Volatile matter content: This content refers to the part of biomass that is released at high temperatures (400-500 C°) where biomass decomposes into volatile gases and solid char. This content reaches 80% in biomass materials (20% in coal).

4- Elemental composition: The composition of the biomass is usually uniform and mainly consists of carbon, oxygen and hydrogen (which are presented as the heating value of the biomass), a small portion of nitrogen (NO_x and N₂O emissions) and other hydrocarbons and components which are presented as corrosion and ash melting.

5- Calorific value or heating value: Refers to the amount of heat available in a fuel (kJ/kg). This property is very important as it is an indicator of the total amount of energy that is available in the fuels and it is directly related to the fuel chemical composition. This value can be expressed in one of the following methods [75, 76];

- The higher heating value (HHV) or (gross heating value); takes into consideration the total amount of heat energy in the fuel including the energy contained in the water vapour in the exhaust gases.
- The lower heating value (LHV) or (net heating value); this value does not include the energy embodied in the water vapour.

6- Bulk density: Refers to the weight of material per unit of volume and is generally expressed on an oven-dry weight basis (the moisture content MC = 0) or an as-is basis. Biomass bulk densities show extreme variation and are measured in (kg/m³).

Heating value and bulk density determine the energy density in biomass (the potential energy available per unit volume of the biomass). Biomass energy densities in general are lower than the fossil fuel energy density (petroleum or coal).

2.7. Power Generation from Gasification

Power generation equipment options which can be integrated with the gasification process are varied according to application (i.e. electricity production, chemical production, fuels etc.) and generally include steam boilers, reciprocating engines, combined cycle turbines, fuel cells and Fischer-Tropsch process.

Electric power can be produced via the direct combustion of the biomass (i.e. boiler or steam turbine). Combustion boilers have the highest tolerance for tars and other impurities but are also the least efficient (25 %). Moreover, direct combustion suffers from GHGs emissions. Power generation from gasification can be achieved by integrating combustion engine, combustion turbine, steam turbine or fuel cell [77]. These systems can produce both heat and power (CHP- Combined Heat and Power) and have higher efficiencies (up to 40%) [78].

Fischer-Tropsch (FT) process is used when liquid hydrocarbon fuels products are required from the process [79]. The following sections describe combined cycle turbines (Integrated Gasification Combined Cycle IGCC) and FT process as potential components in an integrated MSW gasification system and then an overview of some gasification projects.

2.7.1. Integrated Gasification Combined Cycle IGCC

The concepts of IGCC system is not new, it is a combination of well-known technologies. As its name suggests, an IGCC system integrates the gasification process with the energy

production process (i.e. gas turbine and steam turbine) at the same location hence saving the cost of transferring the syngas. Moreover, IGCC maximises the use of syngas to produce electricity. Figure 2.6 shows a general set for IGCC system.

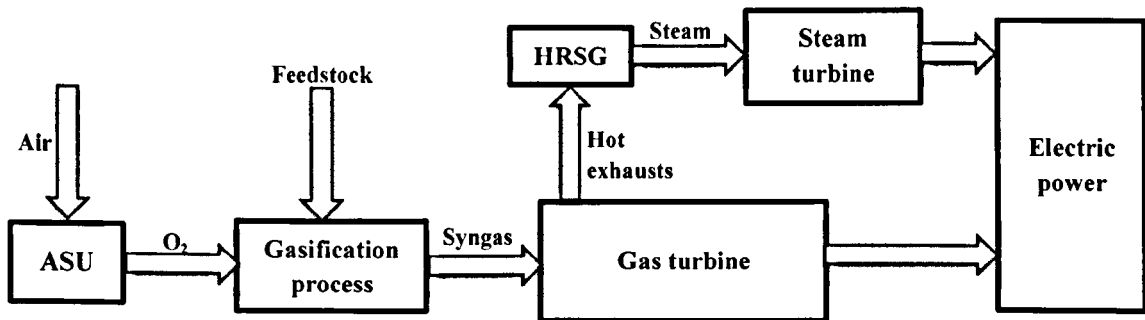


Figure 2.6: General IGCC block diagram.

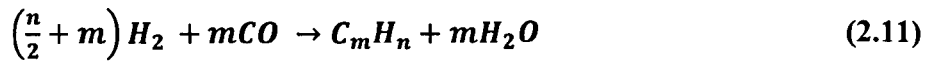
The system utilises an air separation unit (ASU) to separate air components and only uses O₂ as the gasification reactance. This O₂ is fed to the gasifier along with the feedstock to form syngas which is then used, after cooling, in a gas turbine to produce electricity. The hot exhaust from the gas turbine is passed through a heat recovery steam generator (HRSG) where it produces steam to drive a steam turbine. This combined cycle of gas and steam turbine maximises the electricity production from the syngas [80].

2.7.2. Fischer Tropsch Process

FT process is a well-used technology for producing oil-like liquids (i.e. gasoline and diesel). FT liquids are totally free of sulphur and contain very few aromatics compared to gasoline and diesel [79]. However FT process is more utilised in coal based (Sasol, South Africa) or natural gas based (Shell, Malaysia) gasification process, but it is used now for liquids production from biomass gasification [81]. FT process involves the catalytic

reaction of H_2 and CO to form hydrocarbon chains of various lengths (i.e. CH_4 , C_2H_6 , etc.).

The general reaction of this process can be written as in equation (2.13) [68]:



where m is the average chain length of the hydrocarbons formed, and n takes one of two values according to what kind of hydrocarbons are wanted. If paraffins are formed (i.e. methane CH_4) then $n = 2m + 2$, and if olefins are formed (i.e. ethylene C_2H_4) n takes the value of $2m$.

2.7.3. Conventional Heating Gasification Projects

Gasification as mentioned before is not a new technology. However, gasification plants and companies began to be popular in late 1990s. A list of global gasification companies and technologies is listed in the appendix to give an overview of options available and the scale of production.

ENER-G is one of the main gasification technology providers. Its headquarters are in Norway and it has offices in 17 countries. ENER-G developed and provided its technology (energos) to many regional gasification plants. Table 2.4 compares between three plants using energos technology around Europe.

Table 2.4: Energos technology gasification plants.

Plant location	Generation capacity	Foot print	Waste stream	Fuel capacity	Project cost	Commis sion date	Owner
Isle of Wight/ UK	13.5 GWh/year (electrical)	400 m ²	Pre-treated Refuse Derived Fuel (RDF) from the island	30,000 tonnes/year	£8m	2009	Waste Gas Technology
Hurum/ Norway	90GWh/year	1200 m ²	MSW, Commercial and industrial waste	36,000 tonnes/year	N/A	2001	Daimyo AS
Sarpsborg/ Norway	230GWh/year (steam energy)	2500 m ²	Commercial and industrial waste	78,000 tonnes/year	£45m	2010	Hafslund Heat and Power AS

From the table above it can be noted that the gasification plants can be either on small or large scale (i.e. the foot print and the fuel capacity).

Gasification can also be in home use scale and some companies have already started to commercialise their home use gasification systems, for example Gasifier Experience Kit (GEK) offers home scale gasification systems goes up to 20KW [82].

New research and development projects moved gasification from the conventional heat to the use of plasma as the heat source.

2.8. Environmental Consideration and Advantages of Biomass Gasification

Biomass gasification is reported to have many environmental advantages in comparison to oil and coal fuels. Producer gas from the gasification of biomass has much lower sulphur content, for instance, which reduces SO₂ emissions and lowers the risk of soil and water acidification [78]. Producer gas can be a good alternative to fossil fuels, and help many developing countries to improve their industries and lower their debts from oil imports. One of the most attractive features of the gasification power generation technology is its potential to effectively dispose of biomass and wood waste while meeting the strict EU

regulations (shown in chapter 1 section 1.3.1 and 1.3.2) at a lower cost than current systems (i.e. incineration of fossil fuel).

Biomass gasification technology brings many advantages to energy production industry and to the environment, these advantages can be summarised from Allied Environmental Technologies report on integrated biomass gasification combined cycle [78] as follows:

1. Cleaner Environment; biomass gasification can meet the environmental permitting constraints for energy generation. NO_x is reduced by over 90%, and CO_2 is cut by 35%. This environmental performance matches and even exceeds that of alternative energy sources.

2. Low-Cost Electricity; the electricity produced from biomass gasification is claimed to be competitive with the electricity produced by a conventional coal plant and further developments of gasification claim to drop this cost to 75%.

3. Low Water Use; water quantity requirements for the purpose of cooling of the gasification plant are only 50 to 70 % of the quantity required to run a conventional coal plant.

4. Low CO_2 Emissions; significant reductions in CO_2 emissions per unit of power produced can be achieved using biomass gasification plants, this is due to the oxygen starvation inside the gasifiers (gasification not incineration) and to some CO_2 reduction strategies applied such as CO_2 capture and storage (CCS) technology [83].

5. Continuous Product Improvement; gasification technologies are subject of on-going advanced research and development. This development follows a planned progression

toward a more efficient performance by the technology. These researches achieved by LJMU along with others all over the world are proof of this continuous improvement.

6. Marketable By-Products; commercial gasification plants claim to market gasification process by-products (i.e. ENER-G energos technology [84]). Ash and any trace elements are melted, and when cooled, become an environmentally safe, glass-like slag that can be used in the construction or cement industries.

7. Sustainability; gasification technology offers a sustainable energy when feedstock is derived from waste materials and food waste.

8. Public Acceptability; gasification sites offer an acceptable electric power generation option to a public concerned about environmental hazards and waste. Negligible plant emissions, little or no waste, and low-cost electricity for their homes are factors that result in acceptance by the general public.

2.9. Summary

In this chapter, gasification technology was explained. Gasification steps and gasifier types have been overviewed with a discussion of the waste streams that can be used with gasification technology. The characteristics of the waste defining its worthiness are defined. Moisture content, ash content, and calorific value are going to be looked at for the feedstock used in this work.

The power generation from the gasification is briefly explained in this chapter. two main methods are usually used for this purpose; integrated gasification combined cycle and Fischer Tropsch process.

Some conventional heating gasification projects are listed in this project, and finally the environmental considerations and advantages of gasification are discussed. Sustainability, low cost electricity, and a cleaner environment are amongst the advantages of gasification technology.

Chapter Three: Microwaves and Plasma

3.1. Introduction

Gasification technology, as discussed in the previous chapter, has been under continuous development to achieve efficient, environmental and more flexible systems which can produce higher amounts of syngas in a shorter time and less pollutant emissions (i.e. greenhouse gases). These developments moved gasification from being a forgotten technology to a potential EfW innovation. Conventional gasification systems use conventional heating systems to break down the feedstock (which is generally coal). Coal has been substituted with more sustainable feedstock such as waste, saw-wood and sugar canes. Moreover, the core of technology has changed as well; the conventional heating systems are replaced with plasma systems. AC/DC plasma gasification systems are available in today's market. However, microwave plasma gasification is still under development. This chapter is focused on microwave theory and components which make plasma gasification through a microwave source possible. Electromagnetic theory and microwave components are presented first in this chapter, followed by an explanation of high frequency structures simulator as the first step of designing the microwave plasma gasification system, then Plasma theory and key parameters. The benefits of using microwave plasma gasification rather than plasma gasification is discussed at the end of this chapter.

3.2. Electromagnetics

Electromagnetic (EM) phenomenon is perhaps one of the greatest discoveries of 19th century physics. Four great scientists are responsible for much of our understanding of electromagnetics today; Gauss, Faraday, Ampere and Maxwell. However, James Clerk Maxwell was the one who connected the previous work of scientists and added new terms (i.e. the displacement current field in Ampere's law). As a result, this allowed us to understand EM phenomena through Maxwell's four equations for EM wave propagation. A brief explanation of the basic concepts is outlined in this chapter to aid understanding of the necessary EM concepts.

Naturally, positive and negative magnetic forces attract each other and two positives or two negatives repulse each other. This natural law can be applied to electric charges; the attraction and repulsion between the electric charges is the electrical force. The electric charge was first noticed and studied by Charles-Augustin de Coulomb and was given the symbol (Q) and the unit coulomb. Gauss studied this electric force between electric charges and defined the electric flux density (D) in differential form as

$$\nabla \cdot \mathbf{D} = \rho \quad (3.1)$$

This equation states that the divergence ($\nabla \cdot$) of the flux density (D) is equal to the charge density (ρ) in the volume from which D originates. This means that the total number of electric field lines departing (positive) or entering (negative) any volume is equivalent to the total charge enclosed by the same volume [85]. This equation (3.1) is considered to be Maxwell's first equation and implies an electric force between electric charges.

Further to this, Ampere developed the definition of electric current. He defined electric current as a the flow of electric charge through a medium and then stated that an electric current in a straight wire would attract a similar current in a parallel wire, 1 meter away, with a force of unit strength for every meter of the wire's length. This electric field will also create a magnetic field around the wire. This is mathematically explained in equation (3.2) wherein ($\nabla \times$) is the rotation function, (H) is the magnetic field, and (J_c) is the current density in the wire.

$$\nabla \times H = J_c \quad (3.2)$$

Maxwell added the displacement current (J_d) to this equation which explained the spread of electromagnetic waves through empty space, when he stated that light is a form of EM wave and all EM waves travel with the speed of light in a vacuum (speed of light $c = 3 \times 10^8$ meter per second). This displacement current J_d is defined as the rate of change of electric flux with respect to time ($\frac{\partial D}{\partial t}$), thus leading to Maxwell's second equation (3.3)

$$\nabla \times H = J_c + \frac{\partial D}{\partial t} \quad (3.3)$$

Gauss studied the magnetic field as well and explored Gauss's law for magnetism. He noticed that the magnetic field lines in any given volume are continuous throughout the space and always close in a circle. This can be explained by equation (3.4), which states that the divergence ($\nabla \cdot$) of the flux density of magnetic field (B) is zero [86]. This equation is Maxwell's third equation for explaining EM wave behaviour.

$$\nabla \cdot B = 0 \quad (3.4)$$

Finally, Maxwell adopted the work of Faraday on magnetic fields stated in the equation below (3.5)

$$\nabla \times \mathbf{E} = -\frac{\partial \mathbf{B}}{\partial t} \quad (3.5)$$

The meaning of this equation is that the changing in \mathbf{B} field provokes an electric field (\mathbf{E}) perpendicular to it. The \mathbf{E} field closes on itself in a closed loop. This equation is the same as Faraday's law, which states that the voltage induced in a loop is proportional to the rate of change of the magnetic field within the loop with respect to time.

From the aforementioned equations we can define EM as a combination of magnetic and electric fields travelling perpendicular to each other and the propagation direction.

The classification of EM waves is made according to their length and oscillation frequency. Microwaves are part of the EM spectrum and are the type of radiation used in this project to help create the environment for plasma, which in turn interact with our feedstock, thus gasifying it and creating energy. In this section, EM radiation is discussed along with the EM radiation's conveyors (waveguides) and finally the microwave hardware that is used to create the plasma burst.

3.2.1. Electromagnetic Radiation and Spectrum

EM waves are typically illustrated as in figure 3.1.

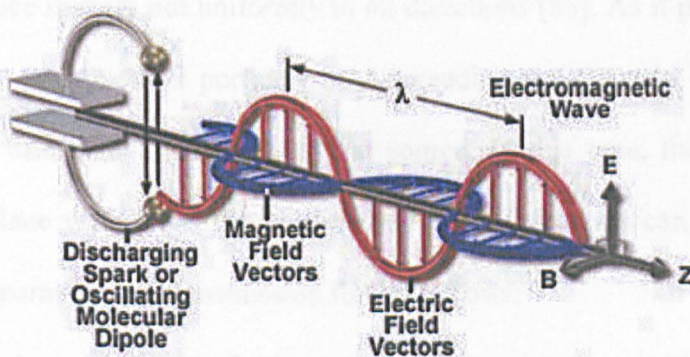


Figure 3.1: Electromagnetic wave.

The EM radiation is emitted by charged particles (i.e. electrons). The radiation occurs when these particles are accelerated or when they change direction. A magnetron is used to

produce microwaves in laboratory systems. However, generally EM radiation is emitted in nature by two means; thermal or non-thermal mechanisms [87]. All hot objects above absolute zero (i.e. 0 K on the Kelvin scale or $-273.15\text{ }^{\circ}\text{C}$) emit EM waves. These waves are categorised according to their frequency and wavelength in table 3.1 [88].

Table 3.1: Electromagnetic spectrum.

Region	Frequency (Hz)	Wavelength (m)	Common Use
Radio	$< 3 \times 10^9$	$> 10^{-1}$	TV and Radio signals
Microwaves	$3 \times 10^9 - 3 \times 10^{12}$	$1 \times 10^{-1} - 1 \times 10^{-3}$	Communication and navigation
Infrared	$3 \times 10^{12} - 4.3 \times 10^{14}$	$1 \times 10^{-3} - 7 \times 10^{-7}$	Fibre optics communication
Visible	$4.3 \times 10^{14} - 7.5 \times 10^{14}$	$7 \times 10^{-7} - 4 \times 10^{-7}$	Human eyes seeing
Ultraviolet	$7.5 \times 10^{14} - 3 \times 10^{17}$	$4 \times 10^{-7} - 1 \times 10^{-9}$	Detecting forged bank notes by fluorescence
X-Rays	$3 \times 10^{17} - 5 \times 10^{19}$	$1 \times 10^{-9} - 1 \times 10^{-11}$	Medical images of bones
Gamma Rays	$> 5 \times 10^{19}$	$< 1 \times 10^{-11}$	Killing cancer cells

It is noted from the table above the importance of EM waves in our daily life. This project proves that EM waves, in particular microwaves, have application potential in production of energy via gasification technology.

EM energy in space spreads out uniformly in all directions [88]. As it propagates, it forms a spherical wave. Only a small portion of the spreading wave would be “seen” from an outside observer at a great distance from the source. In this case, the EM wave would appear to be a plane wave, thus the characteristics of EM waves can be summarised as plane waves in a parallel strip transmission line as follows:

- Electric and magnetic fields oscillate in planes orthogonal to each other and to the direction of the propagation.

- The frequency of a wave is its rate of oscillation and it is measured in hertz (Hz).
- The velocity (v) of propagation of EM waves in free space is

$$v = \frac{1}{\sqrt{(\epsilon_0\mu_0)}} \text{ meters/sec} \quad (3.6)$$

Where (ϵ_0) is the permittivity of free space and (μ_0) is the permeability of free space.

The value for these constants is:

$$\epsilon_0 = 8.85 \times 10^{-12} \text{ C}^2/\text{N.m}^2 \quad \mu_0 = 4\pi \times 10^{-7} \text{ N/A}^2$$

Inserting the values in equation (3.6) we get $v = 2.998 \times 10^8$ m/s, this is the speed of light [89]. This speed differs according to the medium of propagation as each medium has different permittivity and permeability properties, which in turn will affect the wavelength (λ) and the frequency (f) of a wave (3.7)

$$\lambda = \frac{v}{f} \quad (3.7)$$

EM propagation has a number of requirements to ensure minimum loss of energy. Such conditions are the sensitivity of receiver, the signal to noise ratio and the path that EM waves takes in their propagation; for example the line-of-sight requirement is important in microwave communication. However, this line-of-sight condition can be overcome by receiving the wave from its reflected path (an example of communication types is shown in figure 3.2). The earth's atmosphere in figure 3.2 reflects EM waves emitted in a specific angle range. However, if the waves fall outside that specific range then they are transmitted to outer space which then is called satellite communication. This is how EM waves are transmitted all over the globe even if there is no line-of-sight between the transmitter and the receiver, but how can we control the waves (i.e. convey them in a system for example)

before they are propagated? This is answered in the next sections which discuss waveguide transmission lines.

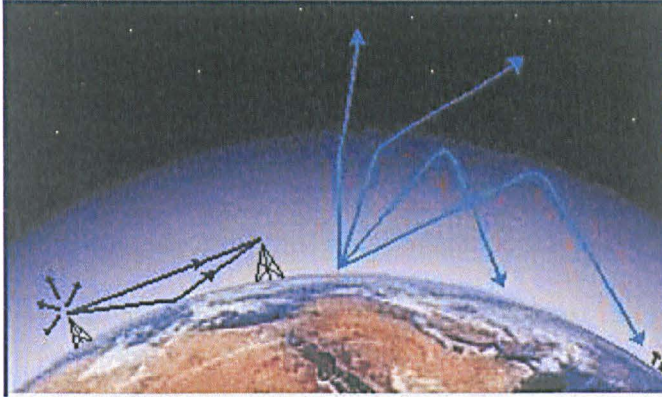


Figure 3.2: EM propagation around the earth.

3.3. Waveguides

EM waves can be propagated in free space, but when transmitting from a source and receiving in a particular application, we need a low loss method of transmission (figure 3.3).



Figure 3.3: The need of waveguides.

The simplest method to convey EM waves is to use a parallel transmission line as shown in figure 3.4. However, this method is suitable only for low frequency applications (i.e. old television aerial cables) due to the amount of loss that parallel cables suffer and the fact that the loss increases with the frequency, thus it is suitable for applications up to 200 MHz.

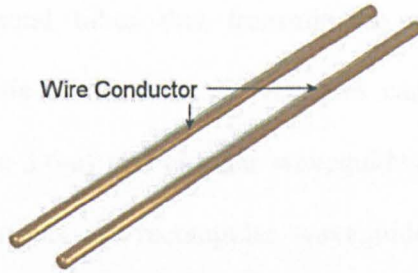


Figure 3.4: Parallel transmission line.

The second method of conveying electromagnetic waves is the coaxial cables (figure 3.5). In these cables, the radiation is guided along the space between the two conductors only and there is no radiation outside the outer conductor. However, these cables suffer from loss as well due to the cable resistance and therefore are only suitable for applications using frequencies up to 3000 MHz (i.e. for video and radio frequencies with low power signals) [90]. Nevertheless, there are coaxial cables on the market that operate at higher frequency ranges such as RG142 which can operate at a maximum frequency of 8GHz [91] and RG304 which operates at a maximum frequency of 12GHz [92], but they are rather expensive.

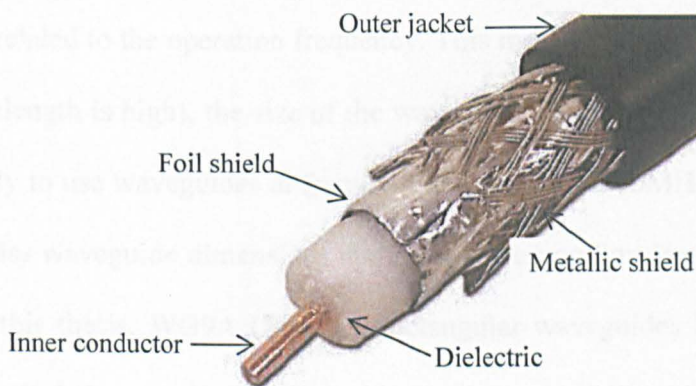


Figure 3.5: Coaxial cable.

The most common method of conveying higher frequency waves is using waveguides.

Waveguides are hollow metal tubes that transmit the electromagnetic radiation by containing it inside the walls of the tube. Waveguides can come in many shapes, but generally rectangular (figure 3.6-a) and circular waveguides (figure 3.6-b) are used. The waveguides used in this project are rectangular waveguides due to their flexibility in connecting magnetrons and applications.

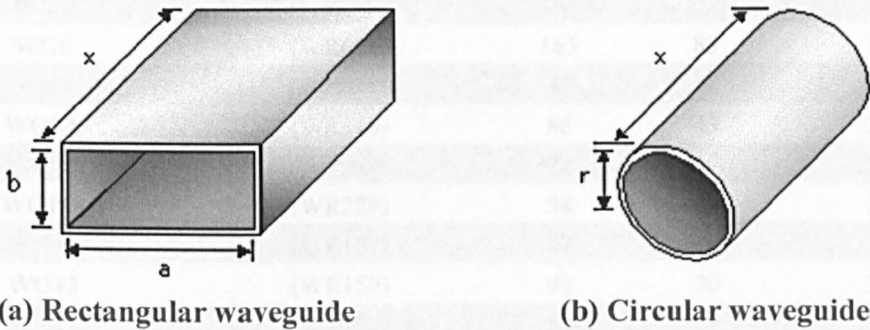


Figure 3.6: Common waveguide shapes.

Waveguides can theoretically be used to convey EM waves at any frequency. However, they are typically used for higher frequencies (above 300MHz). The reason for this is that a waveguide's dimensions (a and b dimensions in a rectangular waveguide for example) are directly related to the operation frequency. This means that when the frequency is low (and the wavelength is high), the size of the waveguide is large [93]. Therefore it is impractical and costly to use waveguides at frequencies lower than 300MHz. Table 3.2 shows a list of rectangular waveguide dimensions and their corresponding frequencies [94]. For the work done in this thesis, WG9A (WR340) rectangular waveguides have been used because of their practical shape and suitability with the frequency utilised (2.45 GHz).

Table 3.2: Waveguide dimensions and their operating frequencies.

UK standard Designation	US standard Designation	Dimension a (mm)	Dimension b (mm)	Frequency Range (GHz)
WG00	(WR2300)	584	292	0.32 – 0.49
WG0	(WR2100)	533	267	0.35 – 0.53
WG1	(WR1800)	457	229	0.41 – 0.625
WG2	(WR1500)	381	191	0.49 – 0.75
WG3	(WR1150)	292	146	0.64 – 0.96
WG4	(WR975)	248	124	0.75 – 1.12
WG5	(WR770)	196	98	1.96 – 1.45
WG6	(WR650)	165	83	1.12 – 1.70
WG8	(WR430)	109	55	1.70 – 2.60
WG9A	(WR340)	86	43	2.10 – 3.00
WG10	(WR284)	72	34	2.60 – 3.95
WG11a	(WR229)	58	29	3.30 – 4.90
WG12	(WR187)	47	22	3.95 – 5.85
WG13	(WR159)	40	20	7.90 – 7.05
WG14	(WR137)	34	15	5.85 – 8.20
WG15	(WR112)	28	12	7.05 – 10.0
WG16	(WR90)	22	10	8.20 – 12.4
WG17	(WR75)	19	9.5	10.0 – 15.0
WG18	(WR62)	15.8	7.9	12.4 – 18.0
WG19	(WR51)	13	6.5	15.0 – 22.0
WG20	(WR42)	10.7	4.3	18.0 – 26.5
WG22	(WR28)	7.1	3.5	26.5 – 40.0
WG23	(WR22)	5.7	2.8	33.0 – 50.0
WG24	(WR19)	4.8	2.4	40.0 – 60.0
WG25	(WR15)	3.8	1.9	50.0 – 75.0
WG26	(WR12)	3.1	1.6	60.0 – 90.0
WG27	(WR10)	2.5	1.3	75.0 – 110.0
WG28	(WR8)	2	1	90 – 140
WG29	(WR7)	1.7	0.82	110 – 170
WG30	(WR5)	1.3	0.65	140 – 220
WG31	(WR4)	1.1	0.55	170 – 260
WG32	(WR3)	0.87	0.44	220 – 325

3.3.1. Waveguide Transmission Modes

To understand how EM waves are transmitted through waveguides, we consider that the rectangular waveguide in figure 3.7 is connected to a microwave source which produces alternating current. This electrical variation across the waveguide's wall will cause an electron excess on the top wall and correspondingly a shortage of electrons on the bottom wall. This in turn will cause a potential difference between both walls (this is represented by the vector E in figure 3.7).

The result of this potential is electrical current flow, which according to Maxwell's equations will result in magnetic fields that will circle around the current. However, due to the metallic walls of the waveguide, the magnetic and electric fields are contained and therefore the magnetic field forms a closed loop around the electric field in the perpendicular plane.

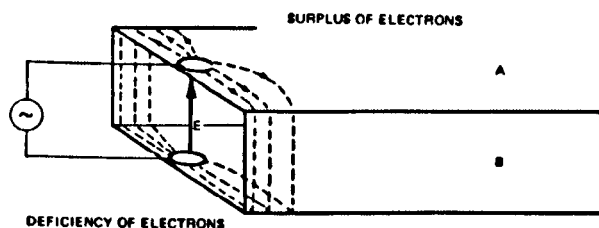


Figure 3.7: Potential difference in waveguide.

More electric and magnetic fields are created along the waveguide with the continuing alternating current from the microwave source. An example of these fields is presented in figure 3.8.

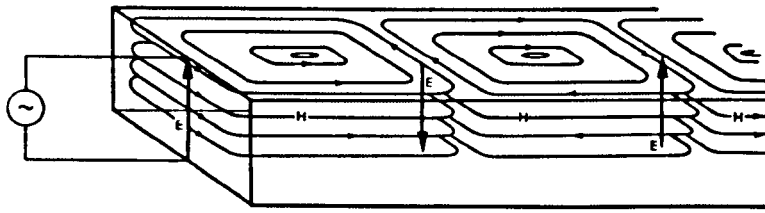


Figure 3.8: Electric ‘E’ and magnetic ‘H’ fields in the waveguide.

These fields propagate inside the waveguide, satisfying Maxwell equations, and are called modes. This EM field distribution can be expressed as a superposition of plane waves and is generally termed as transverse electric (TE) modes, transverse magnetic (TM) modes or transverse electromagnetic (TEM) modes. These terms indicate that, in the direction of propagation, the TE modes have no electric field component, TM modes have no magnetic field component, and TEM modes have neither electric nor magnetic field components [95].

Any EM propagation in a guiding structure can be expressed as a linear combination of these modes. However, there is a fundamental difference between TE, TM on one hand and TEM on the other; TE and TM modes have a cut-off frequency below which they cannot propagate. This cut-off frequency depends on the cross-sectional dimension of the waveguide as will be explained in the next section. TEM modes cannot propagate in waveguides. However, they can be propagated in transmission lines which can support TE, TM, and TEM modes. In addition to these three transverse modes, there are hybrid modes which have electric and magnetic fields in the direction of propagation. Waveguides have a dominant propagation mode which is defined by the cut-off frequency. For example, the rectangular waveguide’s dominant mode is TE_{10} .

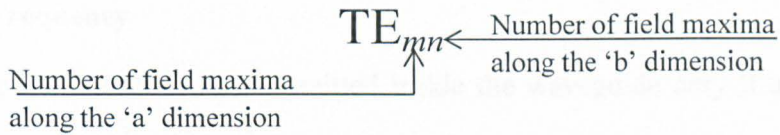


Figure 3.9: Mode subscript explanation.

The two indexes of the mode symbol in figure 3.9 indicate the number of the half waves which form across the dimensions of the wave guide. The first index is across the width of the waveguide 'a' and the second index is across the height of the waveguide 'b'. Some propagation modes are shown in figure 3.10 using a 3D simulation program.

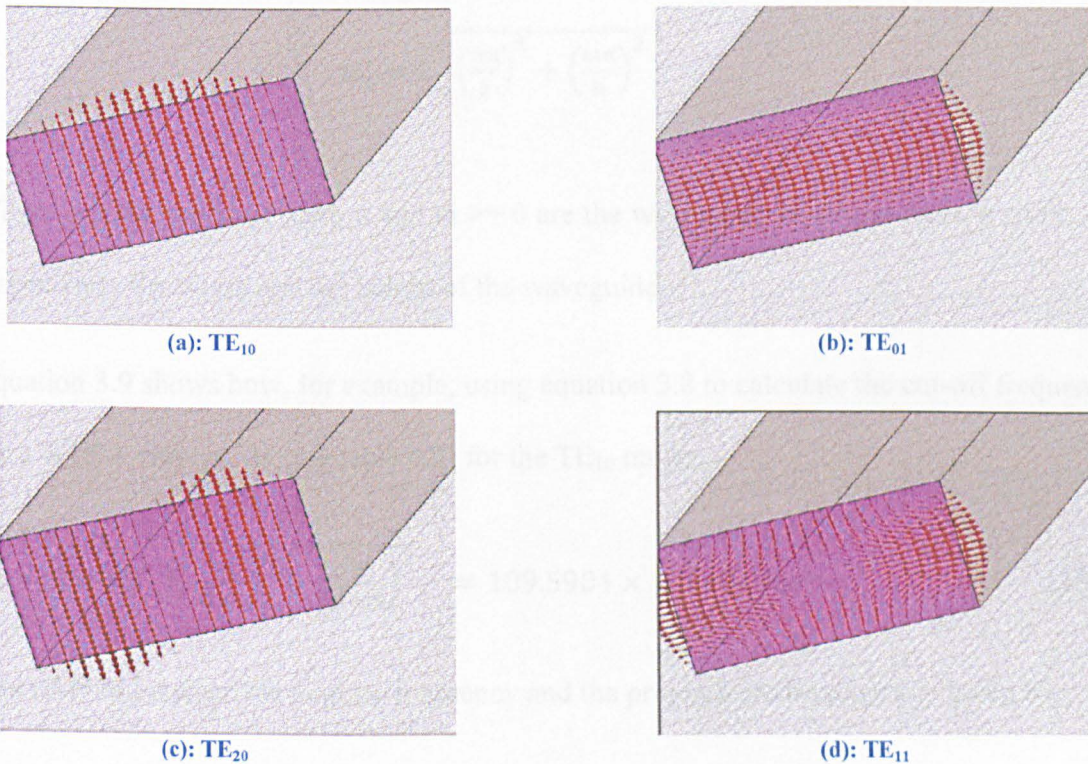


Figure 3.10: HFSS design to show different modes in a rectangular waveguide.

3.3.2. Cut-off Frequency

Electromagnetic radiation can be transmitted inside the waveguide only if a fundamental rule is satisfied. This rule states that the free space wavelength should be less than twice the width of the wave guide. The frequency that corresponds with this wavelength is called the cut-off frequency, f_c . Any EM wave with a frequency below the cut-off frequency will attenuate or reflect instead of being transmitted, and therefore waveguides are considered to be a type of high pass filter.

For a rectangular wave guide (TE_{mn}), we can calculate the cut-off frequency using the angular frequency (ω_c (*rad/sec*)) equation [96]:

$$\omega_c = c \sqrt{\left(\frac{n\pi}{a}\right)^2 + \left(\frac{m\pi}{b}\right)^2} \quad (3.8)$$

Where c is the speed of light, n and $m \geq 0$ are the waveguide mode numbers, a and b are respectively the width and the height of the waveguide.

Equation 3.9 shows how, for example, using equation 3.8 to calculate the cut-off frequency for a WG9A waveguide (see table 4.2) for the TE_{10} mode:

$$\omega_c = 3 \times 10^8 \sqrt{\left(\frac{1\pi}{0.086}\right)^2 + \left(\frac{0\pi}{0.034}\right)^2} = 109.5904 \times 10^8 \text{ rad/sec} \quad (3.9)$$

The relation between the angular frequency and the propagation frequency is given by:

$$f = \frac{\omega}{2\pi} \quad (3.10)$$

Substituting (3.9) in (3.10) gives us $f_c = 1.74 \text{ GHz}$. Under the frequency of 1.74GHz the WG9A cannot be used without significant loss.

3.3.3. Impedance of Transmission Lines

All transmission lines have characteristic impedance Z_0 which is defined by the representation of its elementary components. Figure 3.11 illustrates a schematic of a transmission line's components.

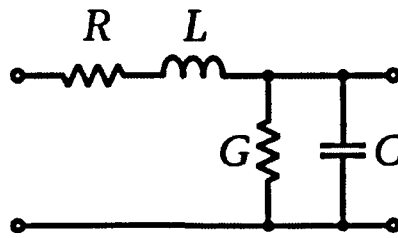


Figure 3.11: Transmission line elementary components.

This impedance is given by equation (3.11)

$$Z_0 = \sqrt{\frac{R+j\omega L}{G+j\omega C}} \quad (3.11)$$

Where R is the resistance per unit length, L is the inductance per unit length, G is the conductance of the dielectric per unit length, C is the capacitance per unit length, and ω is the angular frequency.

For a lossless line, R and G are both equal to zero and the characteristic impedance is given as equation (3.12)

$$Z_0 = \sqrt{\frac{L}{C}} \quad (3.12)$$

A load connected to a transmission line also has impedance Z_L which depends on the type of load. To ensure an optimised power transfer from the line to the load, impedance should be matched (i.e. $Z_0 = Z_L$).

3.3.4. Voltage Standing Wave Ratio (VSWR), Reflection Coefficient and Q factor

A standing wave is a concept to describe the behaviour of wave propagation. When the waves encounter a reflective boundary (e.g. a difference in the medium's impedance), part of its energy is sent towards the source (figure 3.12). These reflected waves collide with the other transmitted waves that have the same frequency, and in effect this collision produces the combination of opposing amplitudes (constructive interference); if waves are at maximum amplitude for both direct and reflected waves, then the amplitudes combine, conversely, if the two waves are at zero amplitude then they cancel each other out (destructive interference).

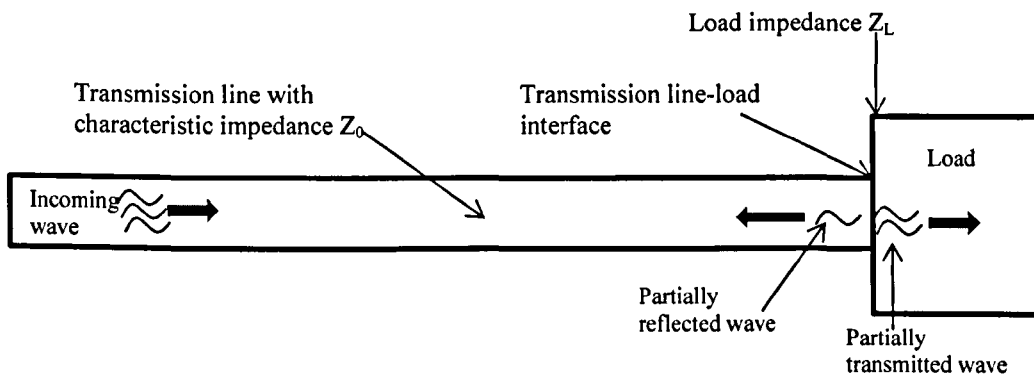


Figure 3.12: Transmission line wave propagation.

VSWR is defined as the ratio of maximum voltage to minimum voltage on a transmission line. The values of VSWR are scalar measurements and represent how well a load's impedance is matched with the source's impedance. For example, if both impedances are matched at the junction, then there will be no reflection and all the energy gets transmitted (ratio 1:1). If there is total reflection of the wave, the ratio would be $\infty:1$.

Reflection coefficient (Γ) describes the impedance mismatch in a way similar to VSWR. However, it can also distinguish between short and open circuits. A short circuit has a value of -1, while an open circuit has a value of 1. Γ is a complex number describing both the magnitude and the phase of the reflected signal and is given by the equation (3.13):

$$\Gamma = \frac{Z_L - Z_0}{Z_L + Z_0} \quad (3.13)$$

where Z_L is the load impedance, Z_0 is the characteristic impedance of the line. However and quite often, only the magnitude of the reflection coefficient is given and has a symbol $|\Gamma|$. The relationship between VSWR and reflected coefficient is given by equation (3.14):

$$|\Gamma| = \frac{\text{VSWR} - 1}{\text{VSWR} + 1} \quad (3.14)$$

Another useful parameter to study the microwave system behaviour is the quality (Q) factor. This is a dimensionless measure of the oscillation inside a microwave waveguide. This parameter represents the comparison between the frequency at which a system oscillates (resonant frequency f_r) and the rate at which it dissipates its energy (the bandwidth around the resonant frequency Δf). In another words Q-factor is a measure of the frequency selectivity of a cavity [97] and high Q means that the cavity is highly frequency selective. This factor is given by equation 3.15 or the good approximation equation 3.16.

$$Q = \omega \times \frac{\text{Energy Stored}}{\text{Power Loss}} \quad (3.15)$$

$$Q = \frac{f_r}{\Delta f} \quad (3.16)$$

Where ω is the angular frequency of the system and the energy stored and power loss are derived from the properties of the system studied.

A typical Q-factor curve is shown in figure 3.13. It is possible to determine the bandwidth of a transmission line from this curve by calculating the frequencies (f_1 and f_2) that relate to half the maximum energy (or by deducting 3 dB from it). This bandwidth gives the ranges of frequencies that a transmission line can pass with no significant power loss.

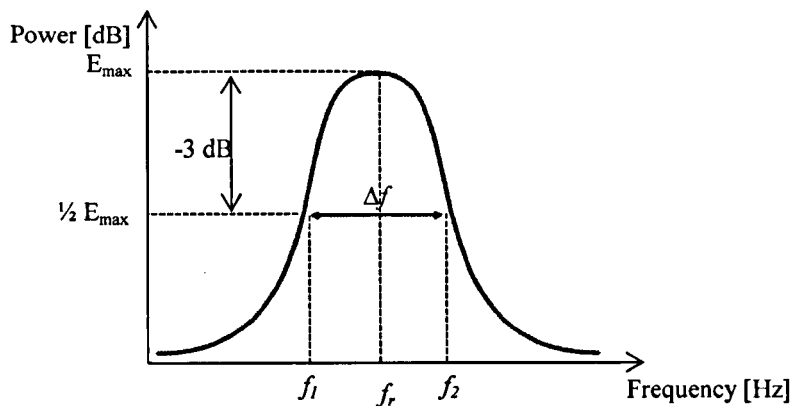


Figure 3.13: Q-factor curve and bandwidth (Δf).

3.3.5. S-Parameters

Any network (i.e. microwave circuit in this project case) operates with small signals, and can be easily characterised and analysed by parameters measured at the network ports regardless of the contents of the network. These parameters determine the network behaviour and properties.

The easiest parameters to measure and calculate in microwave domain are the scattering parameters or S-parameters. Let us consider a two-port network as shown in figure 3.14

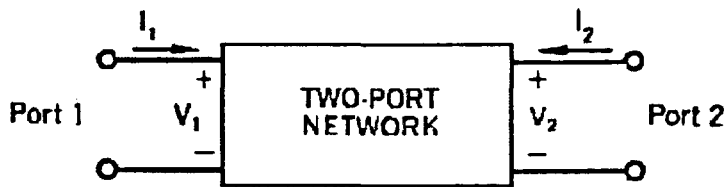


Figure 3.14: Two- port network.

S-parameters measurements are obtained without the need of the input and the output to be successively opened and short circuited. They are usually measured with the device imbedded between a 50Ω load and source. S-parameters describe the interrelationship of a set of variables (a_i , b_i) [98]. These variables are normalised complex voltage waves incident on and reflected from the index “i” port of the network and they are defined in terms of the terminal voltage V_i , the terminal current I_i and an arbitrary reference impedance Z_i as shown in figure 3.15.

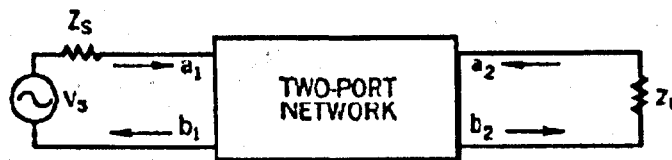


Figure 3.15: (a, b) Incident and reflected variables used in S-parameter definition.

Z_i in most measurements is positive and real, so it takes the name Z_0 in the variable equations as follow:

$$a_i = \frac{V_i + I_i Z_0}{2\sqrt{Z_0}} = \frac{\text{Voltage wave incident on port } i}{\sqrt{Z_0}} \quad (3.17)$$

$$b_i = \frac{V_i - I_i Z_0}{2\sqrt{Z_0}} = \frac{\text{Voltage wave reflected from port } i}{\sqrt{Z_0}} \quad (3.18)$$

The linear equations which describe the two-port network are [98]:

$$b_1 = s_{11}a_1 + s_{12}a_2 \quad (3.19)$$

$$b_2 = s_{21}a_1 + s_{22}a_2 \quad (3.20)$$

And the s-parameters are:

$$s_{11} = \left. \frac{b_1}{a_1} \right|_{a_2=0} = \text{input reflection coefficient} \quad (3.21)$$

$$s_{22} = \left. \frac{b_2}{a_2} \right|_{a_1=0} = \text{output reflection coefficient} \quad (3.22)$$

$$s_{21} = \left. \frac{b_2}{a_1} \right|_{a_2=0} = \text{forward transmission gain} \quad (3.23)$$

$$s_{12} = \left. \frac{b_1}{a_2} \right|_{a_1=0} = \text{reverse transmission gain} \quad (3.24)$$

S-parameters are gains and reflection coefficients which represent the power level of incident and reflected waves.

These parameters are used as measurements of the reflected power from any microwave system, and it is used in this study as a part of the microwave analysis of the feedstock used for the gasification process.

3.4. Microwave components

A description of the microwave hardware used in LJMU microwave plasma gasification system is presented here. Figure 3.16 shows a general configuration for a microwave system to use in any application; we use it for gasification in this case.

Microwave energy as aforementioned is used in order to create plasma that gasifies the feedstock.

The following components are needed in order to be able to transmit the microwave signal from the source to the application:

- Microwave power source to power the magnetron with sufficient energy
- Waveguide system
- Magnetron which creates the microwave signal
- Circulator to protect the magnetron and power source from reflected waves
- Tuning system for impedance matching between the application and the waveguide system.

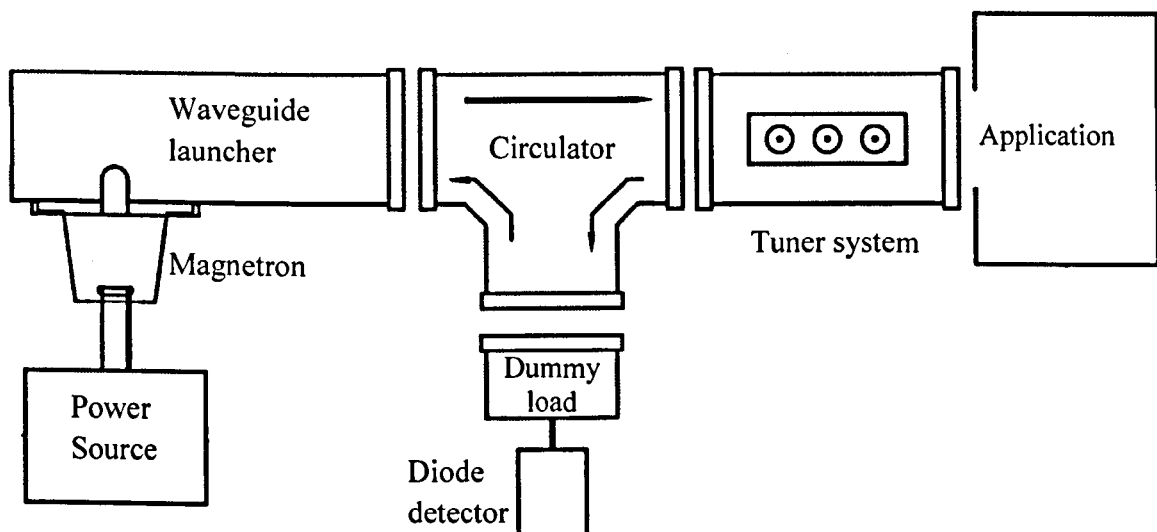


Figure 3.16: General microwave system setup.

Power sources can come with different power capabilities to satisfy the different applications. The type of waveguide used in this work is rectangular waveguides. They are used to convey the microwave energy from the magnetron to the application (the gasification chamber), and to link between the different parts of the microwave system. In

the following section, a brief explanation of the magnetron, circulator and the tuning system is shown to help the reader to identify these pieces of hardware when reading the experimental setup of the gasification system.

3.4.1. Magnetrons

A magnetron is a high power microwave oscillator. This oscillator converts the potential energy of an electron cloud into microwaves [99]. It consists of an electron tube (cathode) inside a resonant vacuum chamber (anode). The anode consists of a hollow copper tube which can be found in different designs but all of which are in essence a metal cylinder with an even number of concentric hollow cavities around a central void where the cathode is located (see figure 3.17). When DC current is applied via a power source, the cathode heats up and the electrons accelerate. The presence of a strong magnetic field in the region between the cathode and the anode produces a force on the electrons which is perpendicular to the DC field. This magnetic field causes the electrons to spiral away from the cathode in paths of varying curves. When the electron cloud approaches an anode hollow, it induces a positive charge in one side of the vane.

The outcome of this continuous cloud movement is an AC field. The produced electric field from the magnetron is a combination of the DC field applied by the power supply and this AC field.

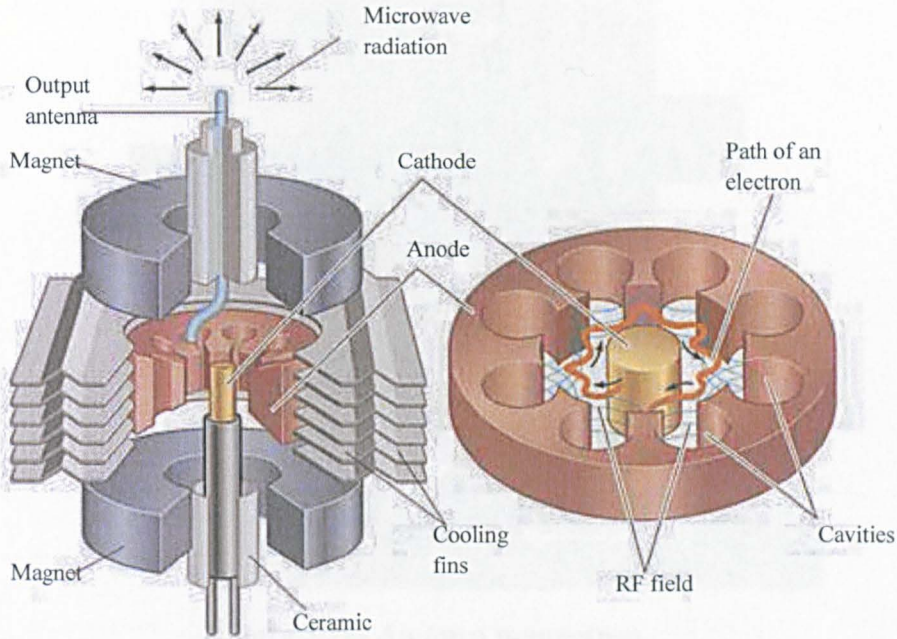


Figure 3.17: Magnetron components.

From this point on, the accelerated electrons are transmitted from the magnetron into the waveguide by the means of an antenna, which is a probe connected to the anode in one of the magnetron's cavities and coupled into the waveguide making the transmission of the microwaves.

Figure 3.18 shows an open magnetron where we can notice a copper wire where the input power is connected to the bottom. Above the copper wire there is a ceramic insulating piece and a circular ring magnet, and above that we find the open cavity where the connection between the cathode and the antenna can be seen. Further up we notice another ring magnet with another ceramic piece which contains the antenna that delivers the microwave to the waveguide.

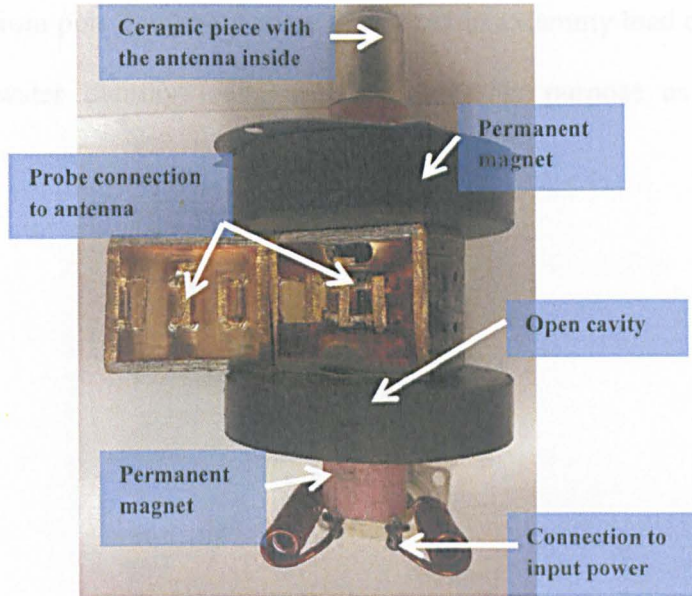


Figure 3.18: An open magnetron.

3.4.2. Circulators

A circulator is a three-port ferromagnetic passive device used to control the direction of signal flow in a circuit. The three ports are linked at a junction containing a ferrite component, which forces energy to circulate in one direction only. To understand the concept of a circulator operation, one can imagine a cup of water. Stirring the water inside the cup in clockwise direction for example, and then adding pepper to the water, we notice that the pepper flow would follow the water direction only because the water field is too strong to move against. The ferrite inside the circulator has similar effect. It produces a strong magnetic field that drives the signal inside it in a specific direction. This device is referred to as a non-reciprocal symmetrical junction [100]. Typically one port is an input port, the second is an output port and the third is a decoupled port which is connected to a dummy load to dissipate any reflected power (Figure 3.19). If port 1 and port 2 are well matched then the signal exits port 2 with little loss only. If there is a mismatch then the

power reflects back from port 2 to port 3 to be dissipated in a dummy load connected to it. Usually circulated water dummy loads are used for this purpose as they provide appropriate cooling.

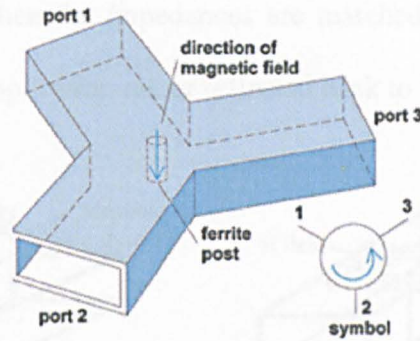


Figure 3.19: Microwave circulator, taken from [101].

3.4.3. Tuning system

A tuning section is added to the microwave system to optimise its performance. This means maximising the amount of energy delivered to the load and increasing the total efficiency of the system. The tuner shown in figure 3.20 is called an EH tuner; this consists of vertical (E) and horizontal (H) waveguides (arms).

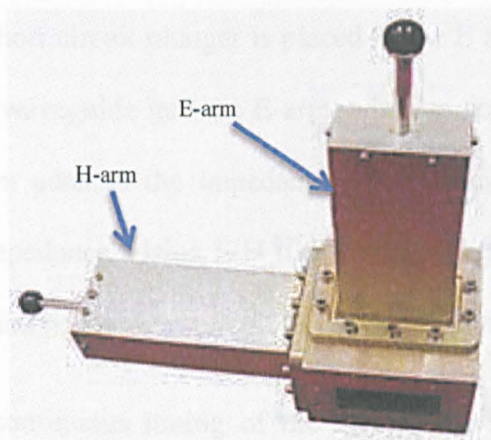


Figure 3.20: E-H tuner.

Figure 3.21 shows a detailed schematic of an E-H tuner. The arm contains a movable short circuit plunger, which acts like a stub in the main path of the microwave.

The effect of this stub is a change in the characteristic impedance Z_0 of the line to match the load impedance Z_L . When the impedances are matched, then maximised microwave energy is delivered to the application rather reflected back to the system and wasted.

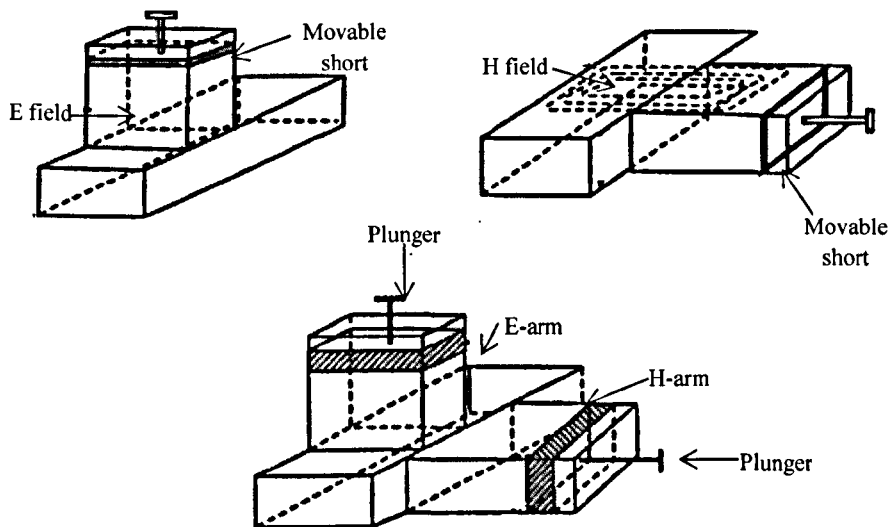


Figure 3.21: E-H tuner concept, taken from [102].

For an E-H tuner, a short circuit plunger is placed in the E and H plane. The electric field enters from the main waveguide into the E-arm, whereas, in the H-arm the magnetic field penetrates. The E-arm adds to the impedance of the transmission line and the H-arm subtracts from this impedance. Using E-H tuner matches a wide range of load impedance by changing the position of the short circuit plungers of E and H arms [102].

In this project, the continuous tuning of the microwave plasma gasification system is required throughout the process as the load impedance (i.e. gasification chamber) changes. This change is due to the different gases produced inside the gasifier in different periods.

For example, the start of the microwave gasification process needs enough power to ionise argon gas into plasma. The tuner changes the line impedance to match with the load impedance and achieve the minimum reflected power (i.e. maximum transmitted power). Henceforth, gases start to build up inside the gasifier, and there is a mismatch in impedances. E-H tuner tries to overcome this mismatch by changing the arms positions.

3.5. Horn Antenna

Horn antennae are a type of antennae which can support the smooth transition of microwaves from waveguides to free space [103]. They provide high gain, low VSWR wide bandwidth and they are easy to operate [104]. Horn antennae are constructed from rectangular waveguide as shown in figure 3.22.

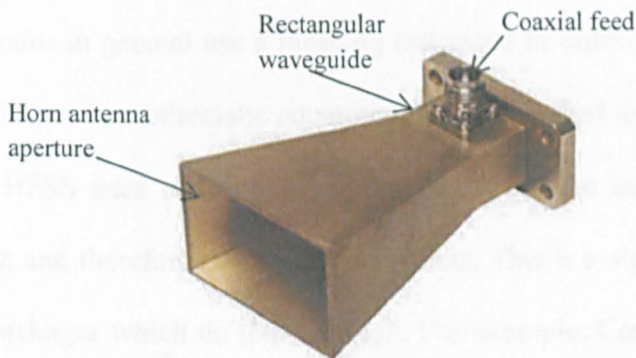


Figure 3.22: Horn antenna.

The operation of horn antennae can be compared to the operation of megaphones, which, in turn, are acoustic horn radiators. These megaphones are used for sound waves directivity in the same way horn antennae are used for microwave directivity.

This directivity is important when microwaves are needed to be applied on a specific area. This is the case in this project wherein the properties of the feedstock are examined. Horn antennae, with aperture of the same size of the samples analysed, are used in the project to

determine the microwave absorption inside the samples. This determination is done by comparing S_{21} parameters for different samples (i.e. reflected power). This will be discussed in the methodology and result chapters.

3.6. High Frequency Structure Simulator HFSS

HFSS is a high-performance full-wave electromagnetic field simulator for arbitrary 3D volumetric passive device modelling [105]. The main use of the software is for the antenna design, electronic circuits, RF and Microwave components, transmission lines and IC packaging. It uses finite element method (FEM) to solve the very complex mathematical model of electromagnetic structures by finding approximate solutions to partial differential equations as well as to integral equations.

Simulation programs in general use a meshing technique in order to simplify the structure under study and solve the mathematic equations in these meshed areas instead of in the full structure scale. HFSS uses adaptive triangular meshing. The use of triangles provides better tessellation and therefore more accurate results. This is a significant advantage over other software packages which do the same job. For example, Concerto [106] generates a rectangular mesh which remains constant in size unless it is overridden by the user.

A significant reduction in simulation time is achieved using adaptive triangular meshing, because less time and resources are used in simulating a relatively simple area while maintaining accuracy in the more complicated areas. The mesh applied to the structure is automatically adapted to apply a higher resolution mesh to areas of interest such as wave ports and holes. When a simulation run is completed, it is possible to create an overlay on

the 3D model displayed on the design window. Parameters such as E-Field, H-Field, and Specific Absorption Rate can be viewed on any 2D plane, or as a 3D representation.

The simulation plays an important role in system design process. It has considerable advantages by giving a prior knowledge of how a structure will behave under certain conditions. Perhaps the greatest advantage of simulation is the fact that one is able to gain practical feedback when designing real world systems, gaining valuable knowledge on the relationship between cause and effect (for example, the location of a segment or section within a structure). This allows investigating the correctness or efficiency of the design before the production step. Similarly, one could study the behaviour of alternative designs without having to physically build them. Examining the effects of design decisions or features before construction allows a great reduction in the cost of implementation. Using simulation software allows the investigation of the relative advantages and disadvantages of individual designs giving the designer the invaluable knowledge of at least an approximate behaviour.

Simulations can be an important way of saving money and time, but it is not free from flaws. One should not rely exclusively on a simulation in order to make decisions. There might be simulation errors either because there was an incorrect keystroke or because the calculations performed have been made with incorrect assumptions.

Simulation programs are programmed using real world laws and rules. However, in real life these rules and laws interact with an infinite number of variables which are generally simplified in a virtual world. When using HFSS, there are some necessary and elemental steps that need to be followed in order to create a usable simulation.

Figure 3.23 shows a flow chart of the steps that a designer should take for a correct simulation design and the solution loop where the adaptive meshing mechanism takes place in HFSS. The first step a designer should take to create a model for simulation using HFSS is to select the solution type. The solution type defines the type of results, the excitation description and the convergence. There are three solution types available in HFSS:

- **Driven Modal:** this type is used when a designer is calculating the modal-based S-parameters. S-parameters are microwave parameters describing the reflected and the incident powers of waveguide modes
- **Driven Terminal:** this type differs from the driven mode as it calculates the terminal-based S-parameters of multi-conductor transmission line ports. These parameters will be expressed as terminal voltages and currents.
- **Eigenmode:** designer uses this mode when the resonant frequencies of the structure and the fields at those resonant frequencies are being calculated.

After setting the solution type shown in figure 3.24, the designer can start structuring his model and defines the materials contained in the modal, here some microwave theory should be considered; for example the boundaries and the excitation ports are set in this step (figure 3.25). The final step a designer should follow is setting the frequency sweep and other solution setup as shown in figure 3.26. HFSS then can commence the analysis which might take some time if the structure is complex and many parameters are being studied. After this analysis, the results are available to be presented like in figure 3.27

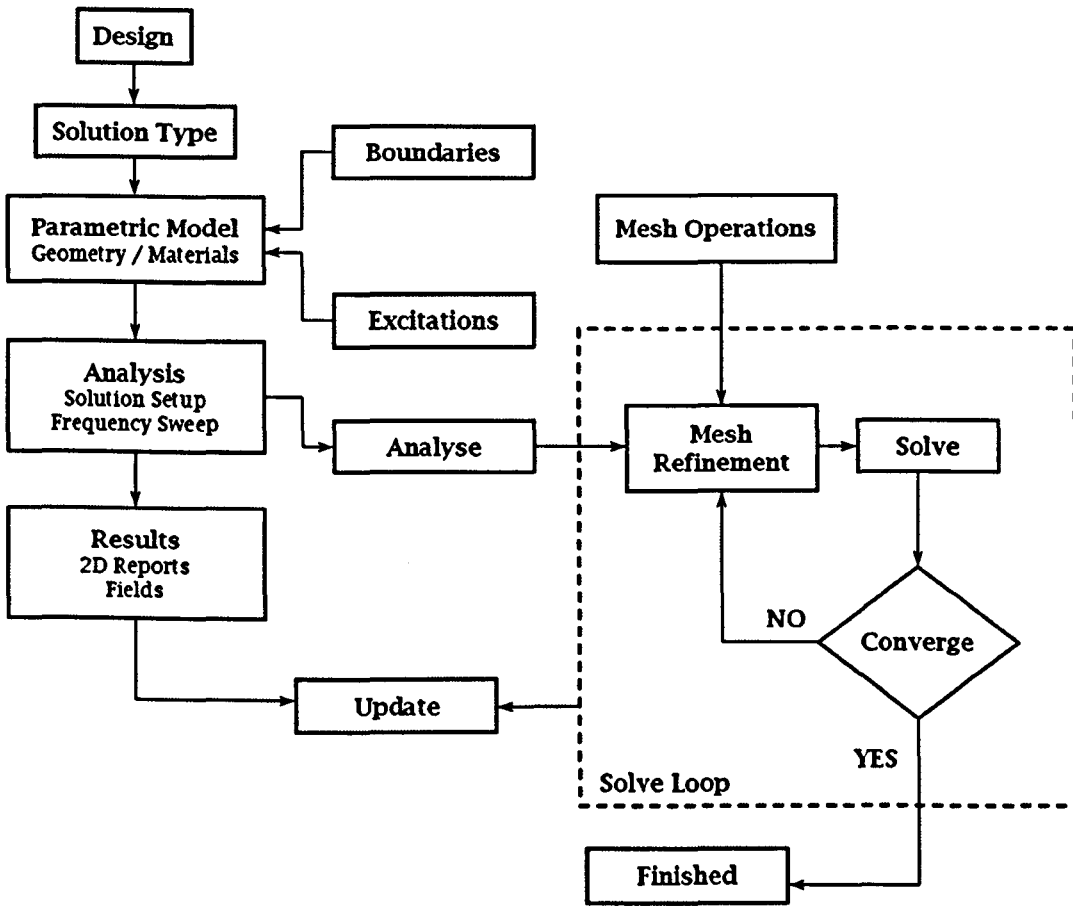


Figure 3.23: Flow chart of simulation steps.

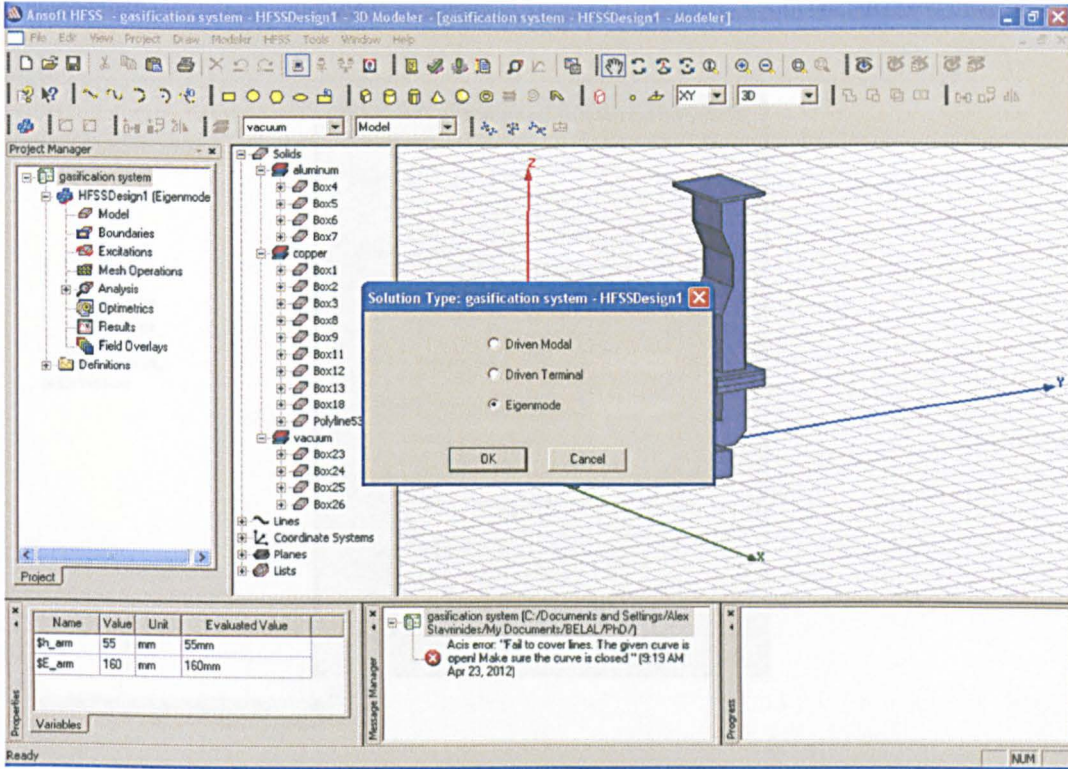


Figure 3.24: Solution type selection in HFSS.

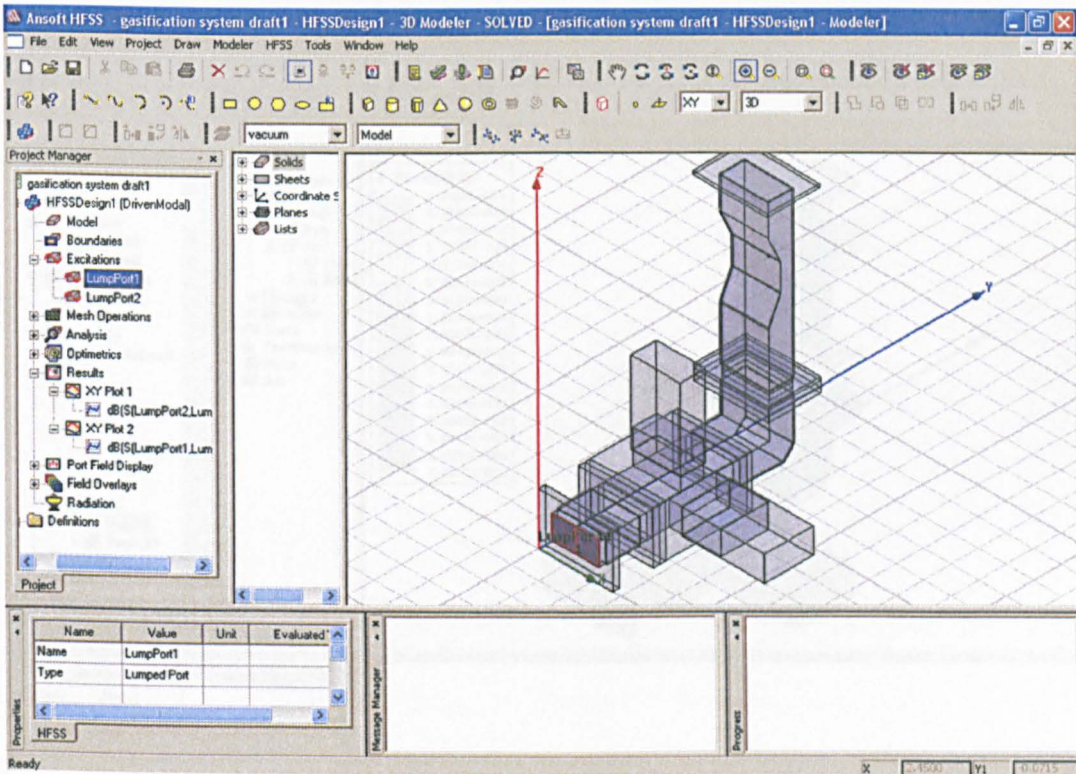


Figure 3.25: Excitation port determination in HFSS.

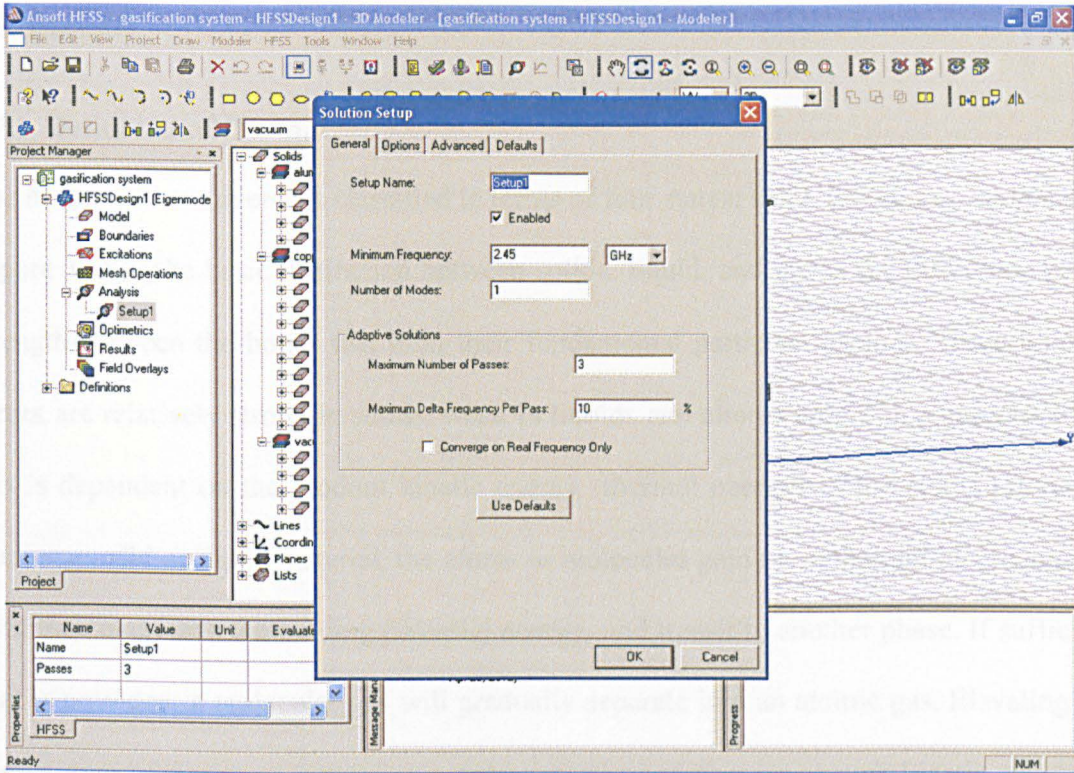


Figure 3.26: Solution setup in HFSS.

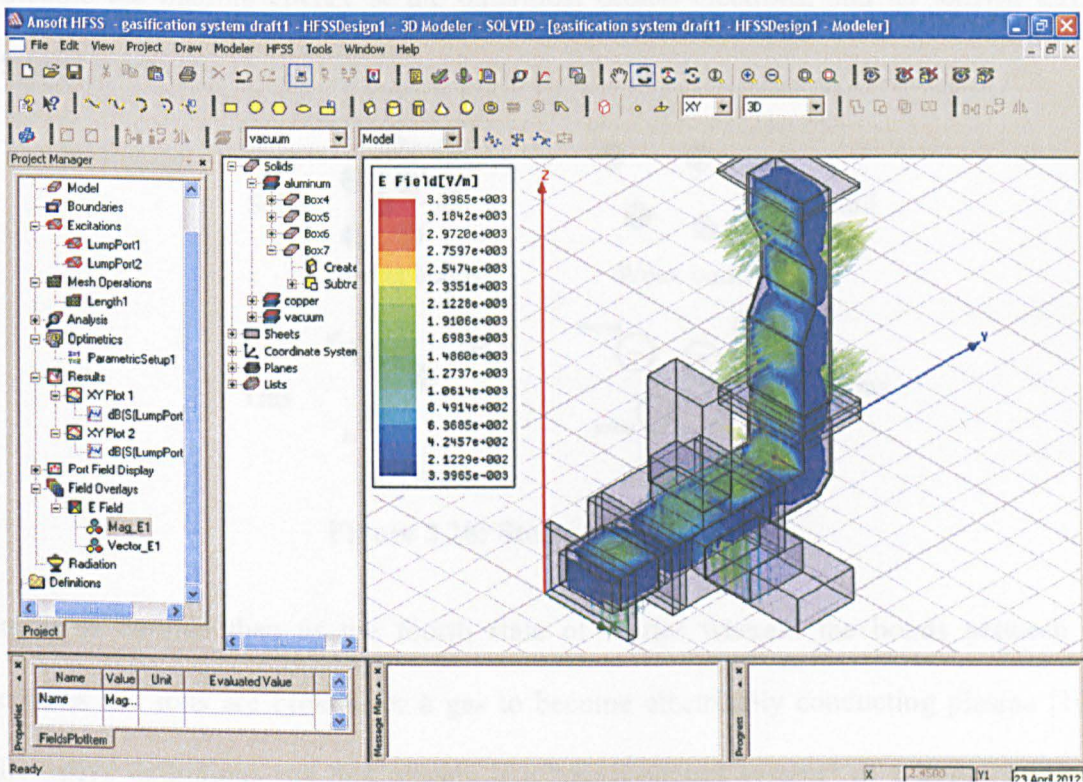


Figure 3.27: Results of simulation in HFSS.

3.7. Plasma

3.7.1. Definition of Plasma

The matter in the universe is classified in terms of four states: solid, liquid, gas, and plasma (figure 3.28). The basic distinction between solids, liquid, and gas is the difference in the strength between the bonds that hold their fundamental particles together. These binding forces are relatively strong in solids, weak in liquids and almost absent in a gaseous state; this is dependent on the random kinetic energy (thermal energy) of the atoms [107]. By heating a solid or liquid material, the atoms or molecules gain more thermal kinetic energy until they overcome the binding potential energy, and transit to another phase. If sufficient heat is provided, a molecular gas will gradually separate into an atomic gas. Elevating the temperature will give an increasing number of atoms to possess enough kinetic energy to overcome the binding energy at the outermost orbital electrons, and an ionised gas or ‘Plasma’ results.

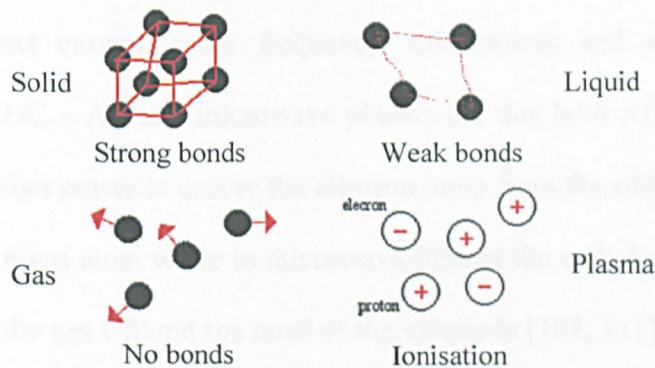


Figure 3.28: States of the matter.

Plasma is defined then as the fourth state of matter wherein the bonds between the electrons and ions are broken for a gas to become electrically conducting plasma [108].

Alternative definitions say that plasma is a “quasi-neutral system” of a large number of

charged particles which exhibit collective behaviour. It can be said that it is quasi-neutral because electrons can escape resulting in an overall slightly positive charge, but generally the positive and negatively charged particles balance gives the plasma its electrical neutrality [109]. It is also said that it is a collective system because the charged particles inside the plasma behave collectively in an orderly manner moving in what can be described as plasma waves. In these waves, the electrons will have a much higher frequency than the ions due to their much smaller mass. Examples of naturally occurring plasmas can be seen in lightning and the stars (e.g. the sun).

3.7.2. Plasma Excitation Sources

Reading the plasma literature, one finds that the study of plasma parameters is a complex and vast study. This fact is because the plasma itself is a complicated physical phenomenon and not fully understood yet.

In a gas, plasma is usually excited and sustained by providing an electromagnetic field in different forms: direct current, radio frequency, microwaves and so on [110]. The differences between DC – AC and microwave plasma are that both AC and DC plasmas need electrodes and high power to ensure the electron jump from the cathode surface to the anode, thus ionising a gas atom while in microwave plasma the technique is different, the electric field ionises the gas without the need of the electrode [108, 111]. This microwave plasma has advantages over typical DC plasma [112] as listed below;

- The plasma jet properties and quality is stable comparing to the DC plasma, as it has no electrode and therefore no electrode vapour contamination.

- The nozzle electrode erosion is ignored as the nozzle stays relatively cold since the plasma is operated in the open air at the tip of the nozzle.
- Cheaper requirements to create the plasma; the magnetron power supply is robust and cheap (any commercial microwave oven would do).

3.7.3. Gas Interaction with Microwaves

The electrons in plasma system are the main element that controls the energy transfer from the external electric field (i.e. in microwave field) to the discharge gas (i.e. the plasma gas). However, both ions and electrons interact with the applied external electric field and are accelerated by absorbing energy from it. Electrons are the lightest particles in the plasma, so they are the easiest to be accelerated and absorb the most of the microwave energy. A higher microwave field will then result in more electrons and atoms acceleration and higher rates of gas turning to plasma. The accelerated electrons transfer the energy to the molecules of the gas through collisions and cause their ionisation and dissociation.

Particles in plasma, as in any other gaseous system, are in continuous motion. This motion results in collisions between the particles, and is categorised into two types; elastic and inelastic. The collisions between the electrons and the relatively heavy targets (neutral or charged particles) that do not result in an excitation of the target are called elastic collisions. Inelastic collisions on the other hand are the collisions wherein the target is excited after the collision with the electron. Literature shows [110] that the energy transfer of the inelastic collision between the electron and the heavy targets determine the excitation or the ionisation rate wherein the electron can almost transfer all its energy to the heavy particles to ionise it and create plasma. Hence the inelastic energy transfer is the key for ionisation, elastic energy transfer should be as little as possible to obtain efficiency.

For example, Argon gas, which is used in this project as the plasma gas, its elastic energy transfer is very low compared to its inelastic energy transfer [113], this makes argon a good and a cheap source for plasma creation.

The flow rate of the plasma gas also effects its interaction with microwaves [114]. The increase of gas flow rate provides more gas particles at a given period of time. However, the residence time of atoms in the plasma becomes short, which in turn will result in lower plasma density if the microwave power level is not sufficient to ionise all of the gas particles in this shorter residence time.

Helium is another noble gas has the potential for plasma discharge applications. Helium is considered to be a better substitute for argon for plasma creation [115-117]. These claims of helium being a better plasma gas are built upon the fact that helium has a greater thermal conductivity (He $1.520 \text{ mW cm}^{-1} \text{ K}^{-1}$ versus Ar $0.1772 \text{ mW cm}^{-1} \text{ K}^{-1}$) and a lower mass (helium is the lightest atomic gas). The greater thermal conductivity accelerates the rate of ionisation. This acceleration is related as well to the lower mass of helium. The comparison between these two plasma gases for syngas production is studied later in this project.

3.8. The Potential Benefits of Microwave Plasma Gasification

Using a microwave power source, in this work, instead of AC/DC source to create the plasma for a gasification system is believed to have some further advantages than those in general gasification (mentioned in chapter two, sections 2.9).

Microwave plasma gasification advantages can be listed as:

- 1- It can be generated using significantly less energy (in kW range) compared to that of conventional technologies (in MW range). This results in a much reduced load requirement

on the system, serving as a real opportunity to improve the efficiency of advanced gasification processes.

2- The technology has a significantly lower capital expenditure compared to conventional DC plasma torches and as such makes plasma gasification a commercially viable option for smaller scale systems.

3- The torches have a significantly longer operational lifespan compared to that of conventional DC plasma torches, resulting in extended periods between plant shutdown and maintenance.

4- The application of microwave plasma significantly reduces the footprint of such high-temperature gasification systems making the technology suitable for smaller regional based projects and specialist field deployment.

3.9. Key Microwave Plasma Gasification Parameters

Microwave plasma gasification procedure has some key parameters which affect syngas production. These parameters relate to the plasma capability to gasify the feedstock. Hence this project uses microwave induced plasma; a parameter such as microwave power level is one of the most important factors increasing this capability. The reflected power from the microwave system plays a major part. It should be at a minimum level which maximise the delivered power to the gas-microwave interaction region (i.e. the application in figure 3.16).

Plasma gas flow rate also plays an important role in the determination of the plasma burst strength (see section 3.7.3). The gas flow rate and the power level actually determine the strength of the plasma burst, thus its temperature.

Other key parameters of the gasification process are the pressure inside the gasification chamber and the type and properties of the sample used. All of these parameters are studied in this project and can be listed as follows:

- The effects of the automation of the E-H tuner,
- The effects of the pressure inside the gasification chamber,
- The effects of the plasma temperature which is related to both argon flow rate and the power source level,
- The effects of argon flow rate as a part of plasma temperature parameter,
- The effects of power source level as a part of plasma temperature parameter,
- The effects of the sample's moisture.

3.10. Current Plasma Gasification Technologies

The use of plasma technologies in waste-to-energy industry is relatively new. However, plasmas have been used for over 30 years to decompose and destroy hazardous wastes and to melt ash from mass-burn incinerators into safe non-leachable slag [118-120].

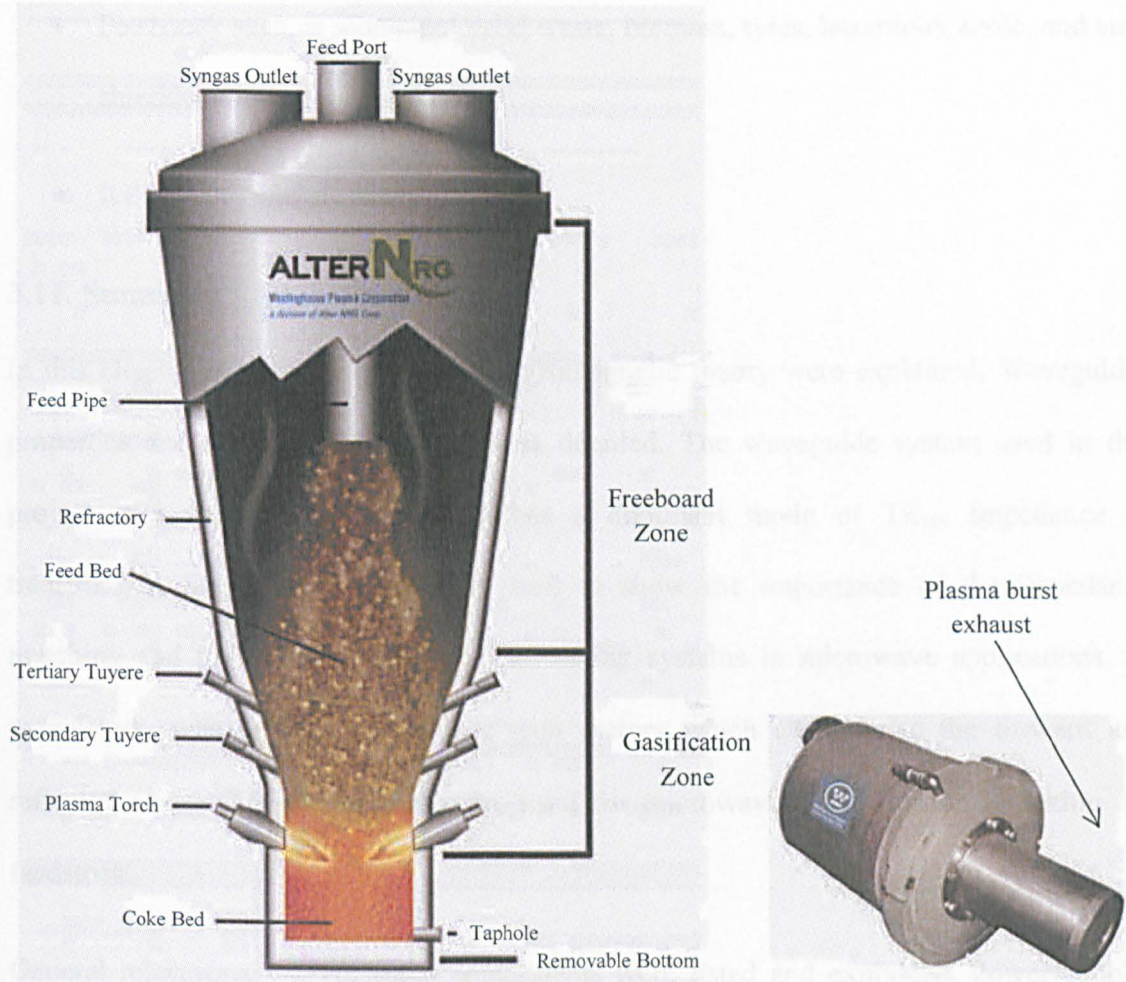
The gasification technology council has stated in their latest report [121] that there are plasma gasification plants operating in Japan, Canada and India. The USA has proposed a number of plasma gasification plants to be commissioned in 2015 and one plasma gasification plant was commissioned in 2011 in Hurlburt Field, Florida.

UK has one operating plasma gasification plant in Swindon since 2008 treating a wide variety of feedstock including a range of refuse derived fuels, tyre-crumb, auto-shredder residue, food waste and other biomass [122]. This plant is based on Gasplasma® technology which is developed by Advanced Plasma Power (APP). The plasma created is

DC plasma and the company claims to have the capacity to treat 150,000 tonnes per year of municipal solid waste which produces power and heat capable of powering 15,000 homes and giving heat to 700 homes. However, this plasma plant uses the plasma as a tool to clean the produced syngas from the fluid bed gasifier, and has the plasma as a separate second stage after the syngas has been produced.

Another project operating since 2010 in the USA is in Madison, Pennsylvania [123]. This project is developed by Alter NRG, a major Canadian alternative and sustainable energy developer. Unlike the UK plant, Alter NRG has developed a plasma gasifier in which plasma interacts with the feedstock and create syngas (shown in figure 3.8 (a)). The core of this gasifier is the plasma torch (figure 3.8 (b)) owned and designed by Westinghouse Plasma Corporation (WPC is a subsidiary of Alter NRG). WPC torch is a DC plasma torch with power input requirements in the range of 80kW - 2,400kW depending on the torch model [124]. The company claims to convert all kind of organic materials into syngas. Any material that cannot be gasified is melted and flows out as molten slag.

Microwave induced plasma gasification is under research and development and there are a number of papers reporting microwave plasma gasification technologies [125-128]. These papers study the gasification of different feedstock with microwave plasma source. However, none of them studies the effects of automation and the control of the different key parameters on the syngas production (i.e. the topic of this work).



(a): Plasma gasifier

(b): WPC plasma torch

Figure 3.29: Alter NRG plasma system, Courtesy of Alter NRG.

Reviewing the plasma gasification literature, one can summarise a number of key benefits [129-131]:

- It unlocks the greatest amount of energy from waste
- Thermal efficiency
- Minimal pre-treatment of feedstock

- Feedstock such as municipal solid waste, biomass, tyres, hazardous waste, and auto shredder waste, can be mixed
- It does not generate methane

3.11. Summary

In this chapter, the fundamentals of electromagnetic theory were explained. Waveguides properties and mode of propagation was detailed. The waveguide system used in this project is a rectangular one which has a dominant mode of TE_{10} . Impedance of transmission lines was explained as well to show the importance of the impedance matching and the vital utilisation of the tuning systems in microwave applications. S-parameters were explained as power gain factors which characterise the forward and reflected power. These parameters are used for microwave absorption study within the feedstock.

General microwave system setup components were listed and explained. Power supply, magnetron, circulator, waveguides, and tuner section are the main components for any microwave system and are used in the microwave plasma gasification system. The simulation of microwave systems can be done by HFSS. This simulation can save time and effort by studying the system behaviour even before the implementation. This gives the possibility to study the effects of design change on the system performance.

Plasma theory was briefly explored in this chapter as it is used for the gasification process. The main definition of the plasma as the fourth state of matter, with the main excitation sources, are looked at, along with the gas interaction with microwave and the ionisation of the gas to plasma state.

Some potential benefits of microwave plasma gasification were listed including, the producing of energy from waste with a lower input power and the lower capital cost of the project in comparison with the conventional gasification processes.

Key microwave plasma gasification parameters were specified in this chapter. These parameters are microwave power and reflected power, plasma gas flow rate, sample properties, the temperature of the procedure. These parameters are studied further in the methodology and the result chapter later.

Finally, current plasma gasification projects were presented. Although there are a number of researches about microwave plasma gasification process, they do not deal with the **effects of the different key parameters and the automation of the system**. These two points give this PhD project its novelty as a new and a complete research subject.

Chapter Four: Microwave Plasma Gasification System

4.1. Introduction

The original LJMU microwave plasma system is presented in this chapter. This system utilises microwaves to create plasma. A previous figure (figure 3.16) shows the general setup of microwave hardware to achieve its utilisation. The ‘Plasma Cavity’ is the application part of the system. It is basically a short-circuited waveguide, hence the term cavity instead of waveguide. This cavity contains a nozzle through which argon gas is passed and interacts with the electric field for ionisation. The aim of this original system was to create self-striking plasma, thus the electric field has to be in a maximum magnitude at the point where the nozzle is placed. The design of the gasification chamber is discussed as a part of the original microwave plasma gasification system, the description of system’s limitations are discussed with the development of an improved system. The original system was modelled using HFSS to understand the plasma creation using microwaves. This modelling includes the design of the plasma cavity and then a general system behaviour analysis.

After the explanation of the original system’s design and limitations, this chapter discusses the instrumentation needed to develop the system into a fully controlled one which will help in experimenting different parameters and determine the best operating values.

4.2. Initial LJMU’s Gasification System

The original system was designed in Built Environment and Sustainable Technologies (BEST) laboratories. This system was the foundation stone of the work included in this

project. An overview of the system's components is explained in this chapter, along with the steps taken for the plasma cavity design. This design is re-modelled using HFSS for further understanding of the system's construction. The design of the gasification chamber was done by Stopford Projects. Stopford Projects¹.

Understanding the initial LJMU's system design and components led us to the automation and optimisation ideas which potentially increase the productivity of syngas.

4.2.1. Microwave Components

Figure 4.1 shows the LJMU system setup where all parts are connected in a similar way to figure 3.16, page 69. The power source is not shown in the image due to size limitation of the picture. The magnetron, generating 2.45 GHz microwaves, is connected to the circulator for isolation; this circulator is then coupled to the tuner section through waveguides, and the tuner is manually controlled for impedance matching and connected to the plasma cavity through waveguides as well. This cavity is sealed to the gasification chamber and fed with argon gas which will react with the microwave power to be ionised and to gasify the feedstock inside the chamber.

¹ Stopford Projects is located in the north west of England and initially provided engineering services to the nearby petrochemical industry. Over the past three decades the company has broadened its portfolio to also include bulk chemical, pharmaceutical, fine chemical and the nuclear sector. More recently an in-house environmental research & development department has allowed them to provide engineering support to the renewable energy sector

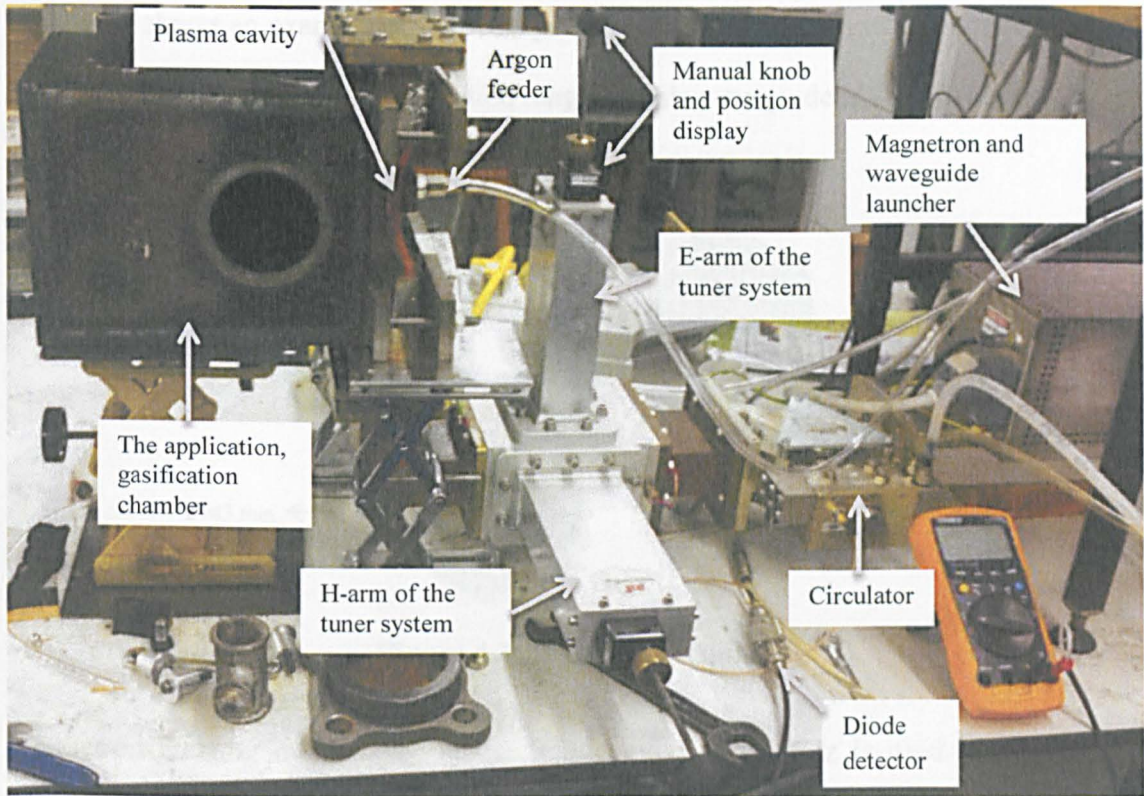


Figure 4.1: Microwave plasma gasification system.

The power source used is manufactured by Alter, model number SM745G (figure 4.2). This model power range is 0-1000 watts and it supplies the magnetron with power to create the microwaves.



Figure 4.2: Alter power supply.

Figure 4.3 shows an example of the waveguide used (WG9A) with its dimensions (W×H= 86mm×43mm). The frequency operation range for this waveguide is 2.1-3 GHz.

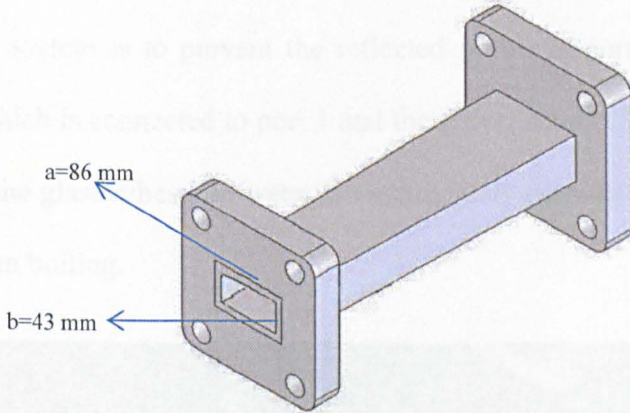


Figure 4.3: WG9A waveguide.

Magnetron creating microwaves at the frequency of 2.45 GHz is used in this project. Figure 4.4 shows this magnetron. It is contained within a metallic box from which it connects to the power source and launches the microwave signal.

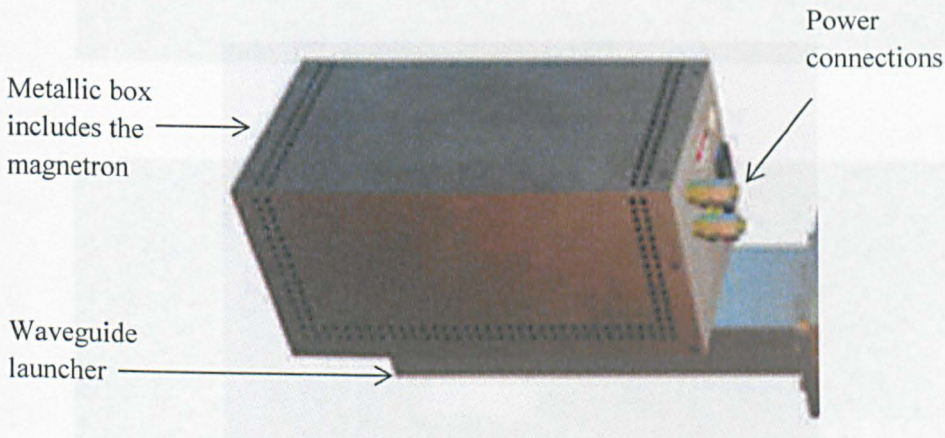
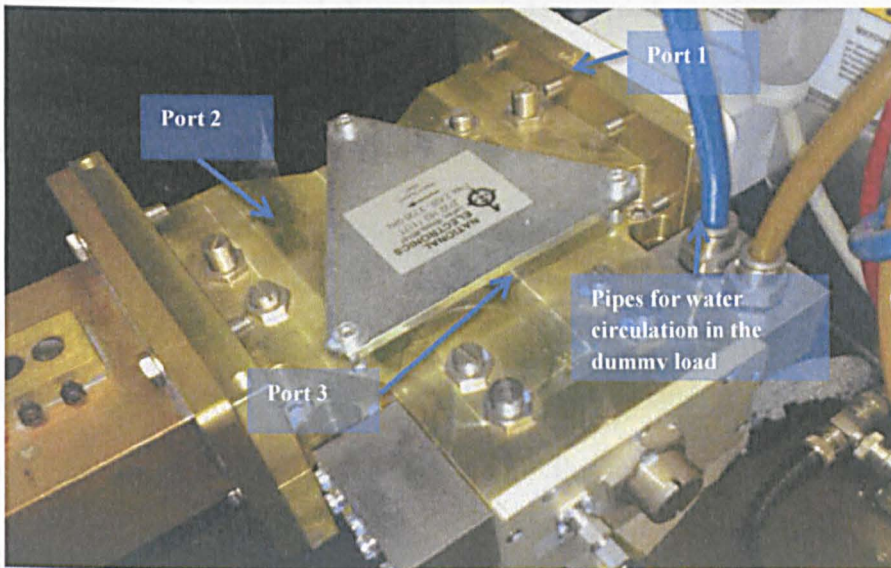


Figure 4.4: Magnetron used for LJMU’s gasification system.

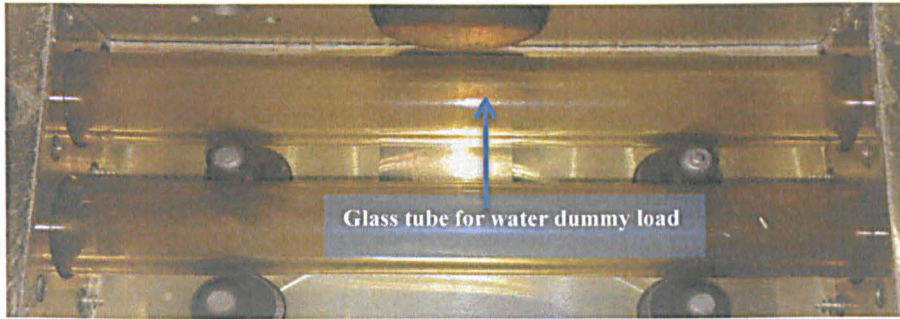
Circulator used in the system is shown in figure 4.5 below. The manufacturers are National electronics [132], and it is for use with the frequency of 2.45GHz. The dummy load is water running through a glass tube (figure 4.5-c). The importance of having a circulator in a microwave system is to prevent the reflected power at port 2 from going back to the magnetron which is connected to port 1 and the power source. The microwave power heats the water in the glass tubes; the water is continuously running through the dummy load to prevent it from boiling.



(a): An overview of the circulator



(b): Bottom view showing the ferrite core



(c): An open circulator showing the glass tubes

Figure 4.5: The experiment circulator.

The system impedance is matched through the E-H tuner shown in the system setup in figure 4.1. This tuner is manually controlled via the two knobs fixed on the top of E and H arms. The knob is connected to the arm’s shaft and moves it up and down. The position of the shaft is displayed on a small counter pointed at in figure 4.1.

4.2.2. Gasification Chamber

The gasification chamber was made to fit the plasma cavity produced in LJMU’s workshops. Figure 4.6 shows the design offered to fit this purpose.

This gasification chamber or ‘gasifier’ is where the feedstock is placed for syngas production. The chamber is sealed to maintain the pressure inside which can be controlled manually using the pressure relief valve. Syngas produced from the gasification process is exhausted from the system for analysis from the gas exhaust pipe (see figure 4.7). The gasification process can be observed from the window glass on the front side of the chamber.

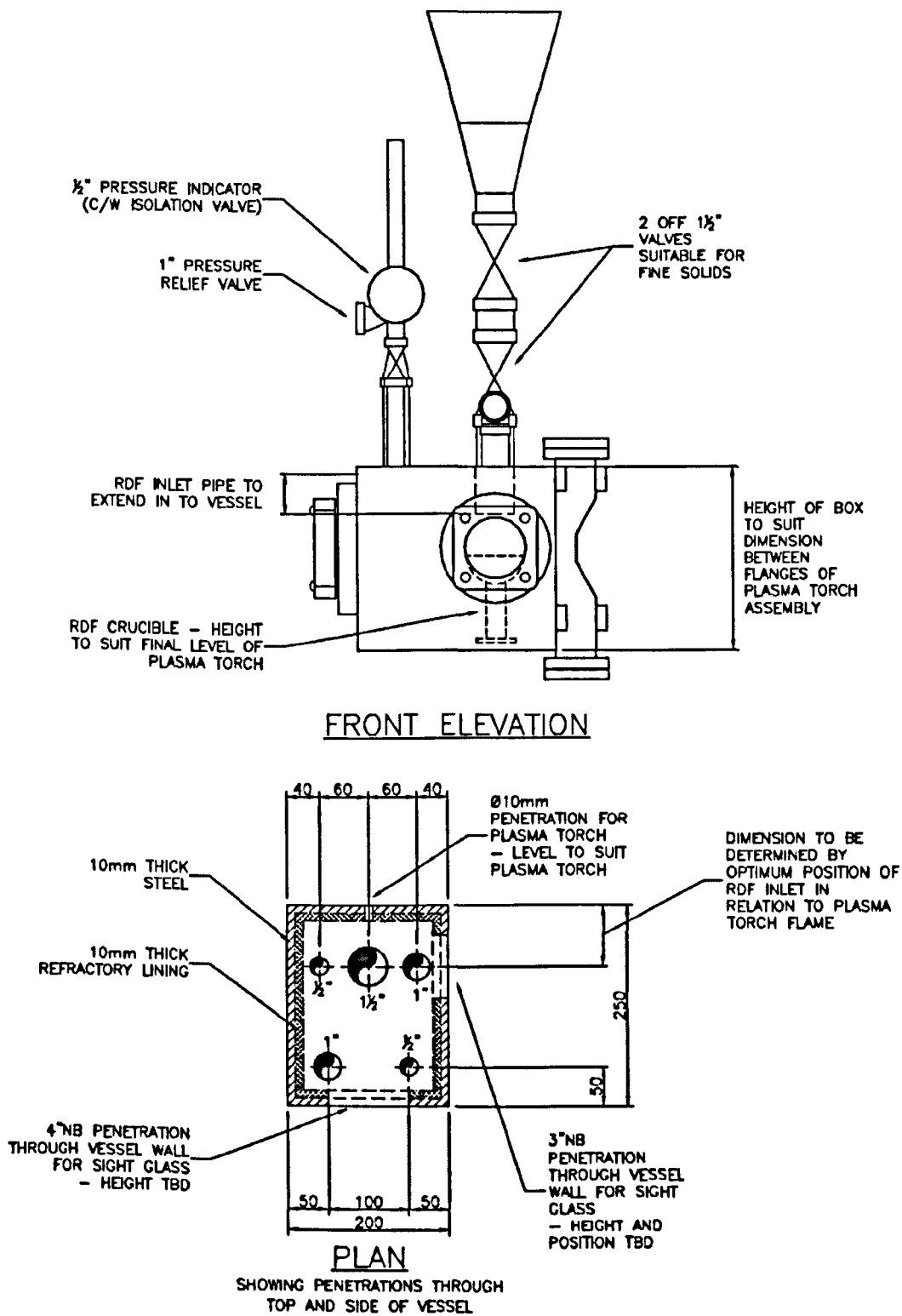
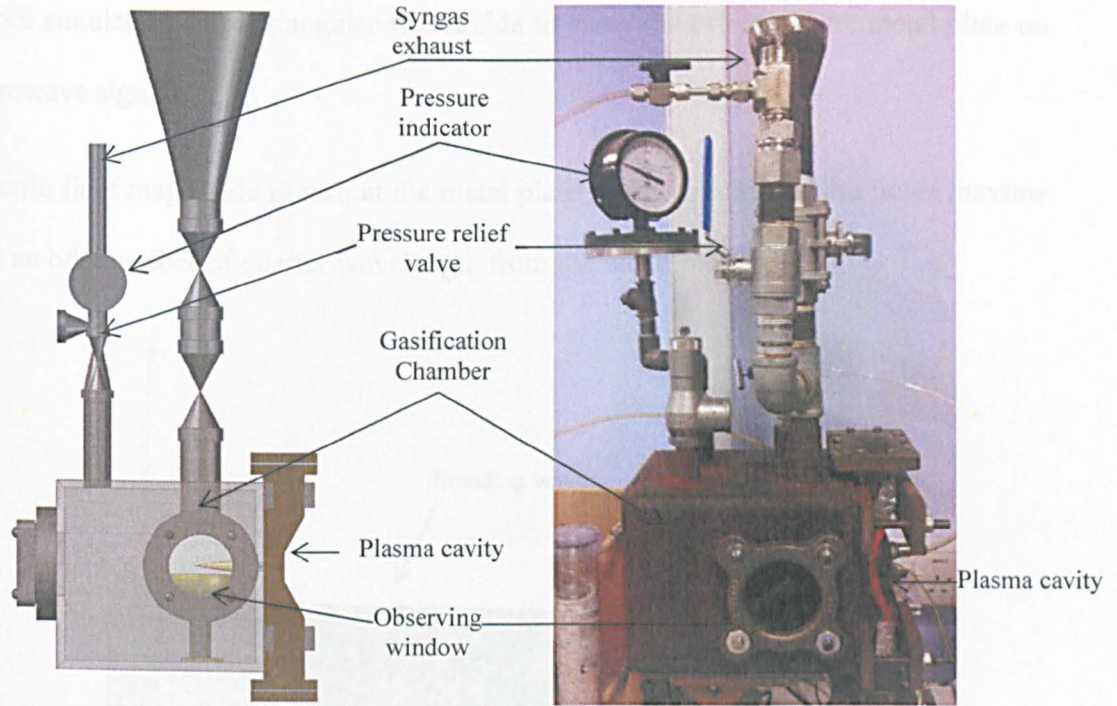


Figure 4.6: Stopford's gasification chamber design.



(a): Schematic diagram.

(b): Final experimental setup.

Figure 4.7: Gasification chamber from design to implementation.

4.2.3 Microwave Plasma Cavity Modelling

The creation of microwave plasma was achieved by using a plasma cavity. This cavity as mentioned before in the introduction is a waveguide (WG9A) terminated by a metal plate. This metal plate causes waves to form standing waves; any incident wave will be reflected back toward the source, thus interfering with other travelling waves towards the metal plate and resulting in field maxima at fixed points along the waveguide. If sufficient microwave power is applied, then the higher fields at one of these points can be used as the basis for the plasma torch.

The standing waves are shown by the electric field vectors in figure 4.8 and the electric field magnitude along the centre of the waveguide in figure 4.9. The waveguide chosen for

this HFSS simulation is a rectangular waveguide to show the effects of the metal plate on the microwave signal.

The electric field magnitude is zero at the metal plate (short circuit) and the fields maxima occur at an odd number of quarter wavelength from the metal plate.

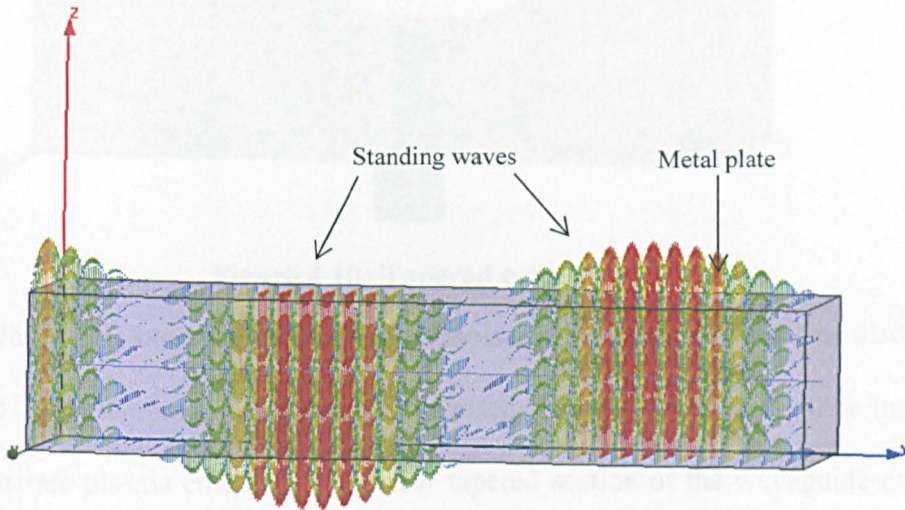


Figure 4.8: E-field vectors in a rectangular waveguide using HFSS.

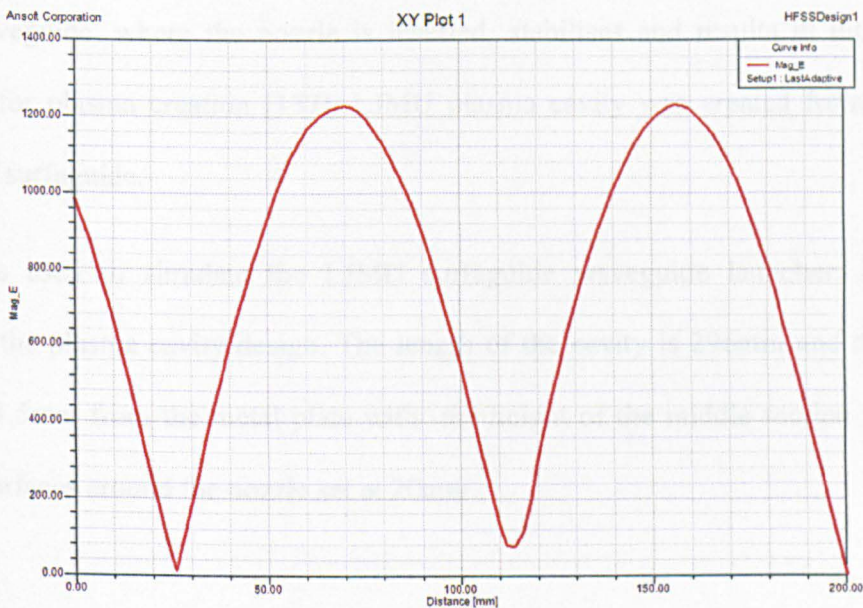


Figure 4.9: E-field magnitude along centre line of the waveguide using HFSS.

The design of the plasma cavity has been inspired from the study of a tapered cavity (figure 4.10) wherein the plasma gas can be inserted from a nozzle placed in the middle of the tapered surface.

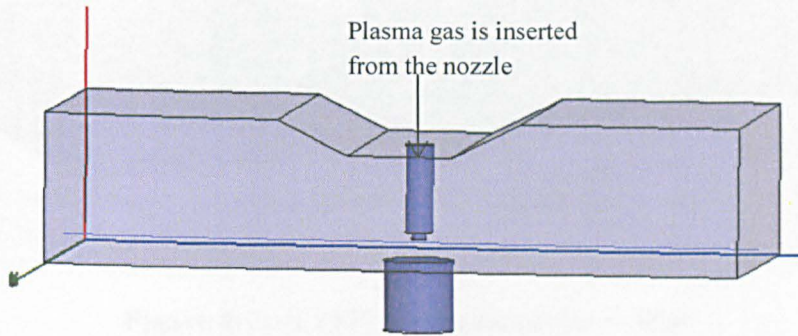


Figure 4.10: Tapered cavity.

This tapered design has been studied mainly by Moisan [133, 134] and was first discussed in his work in 1984. He presented a waveguide-based launcher called surfaguide that can efficiently generate plasma columns. The linear tapered section of the waveguide ensures the continuous and gradual transition to the waveguide to feed and tune the system thus enhancing the performance of a typical rectangular waveguide [135, 136]. The reduced height waveguide, where the nozzle is inserted, stabilises and results in more efficient operation for plasma creation [137]. LJMU plasma cavity was created from the design concept of surfaguide.

HFSS was used to simulate the LJMU surfaguide waveguide launcher. Figure 4.11 illustrates the plasma cavity design. The length of the cavity is 296mm and the nozzle is placed 131.5mm from the metal plate with the height of the middle section between the cavity's surfaces around the nozzle set at 20mm.

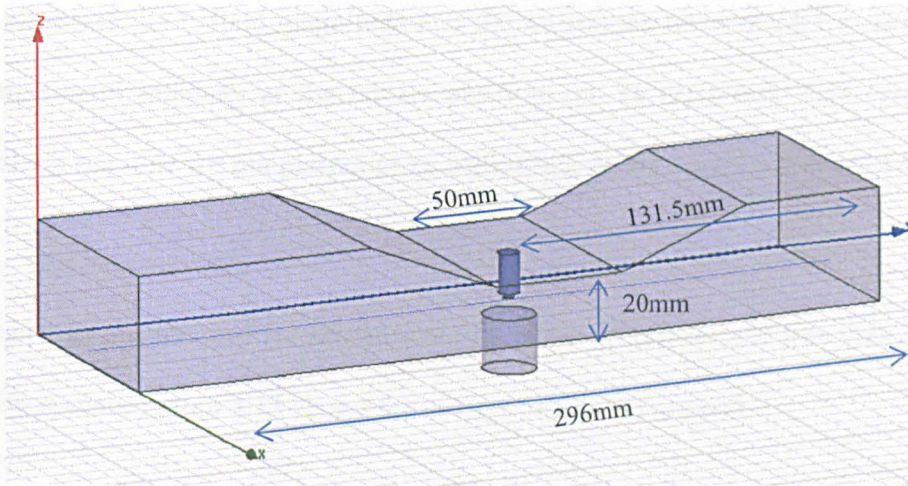


Figure 4.11: LJMU’s plasma cavity design.

The total length of the cavity (the waveguide) is set to 296mm for the convenience of the design as it does not affect the operation because it is connected to the tuner system for impedance matching. The slope angle is set to 29° which satisfies the smooth change in the height of the cavity walls and further enhances the performance of the E-field.

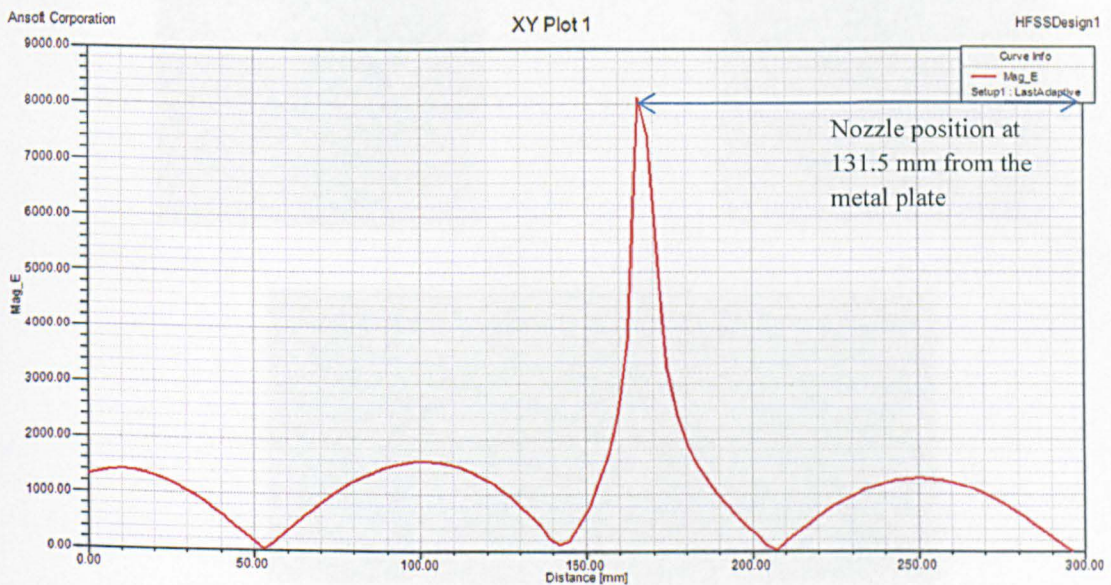


Figure 4.12: E-field magnitude for the plasma cavity prototype.

Figure 4.12 shows the E-field magnitude and the magnitude trend along the cavity length and the maximum intensity at the nozzle position can be observed. This enhancement would make it possible for the plasma to be self-struck as the maximum E-field magnitude achieved.

This design was put forward for production in LJMU workshops and was ready to test in the real life system. Figure 4.13 shows the cavity used in this project.

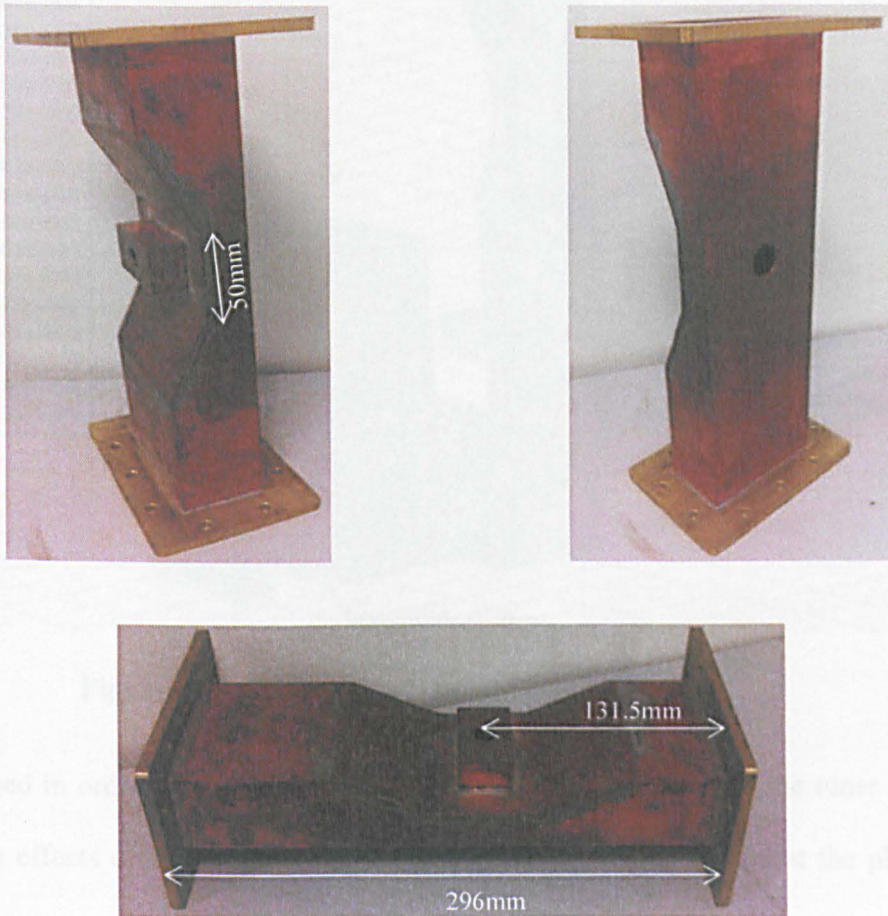


Figure 4.13: Microwave plasma cavity.

The cavity material is copper and the argon gas is fed to the system through the nozzle hole where the E-field is maximised to turn it into plasma.

4.3. Microwave Plasma System Simulation

The plasma cavity simulated in the last section was used in the full system’s simulation to predict the behaviour of the cavity when it is connected to the rest of the microwave’s equipment.

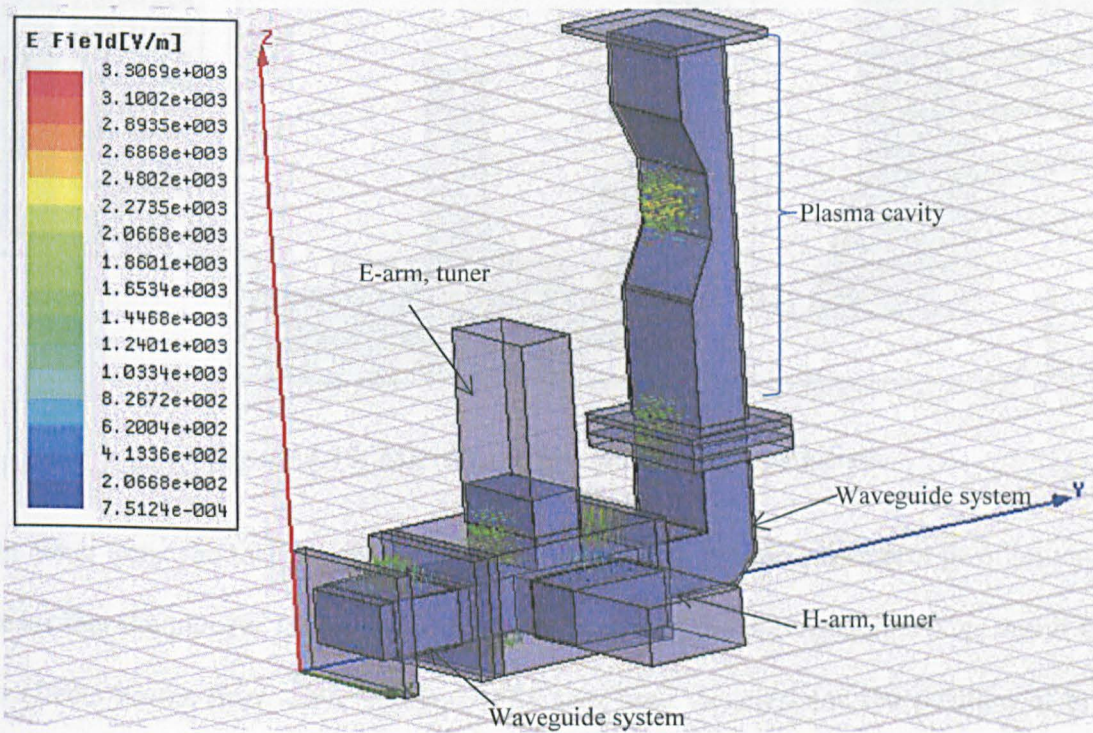


Figure 4.14: 3D model of the gasification system.

HFSS was used in order to simulate the microwave plasma system with the tuner section and study the effects of changing the tuner arm’s position on the E-field at the plasma’s nozzle. The tuner, as mentioned before, is a mean for load matching between the microwave system and the load; when the matching is achieved, the E-field at the load is

maximised and the microwave power is efficiently used. Figures 4.14 and 4.15 show the simulation and zooms to the E-field at the nozzle.

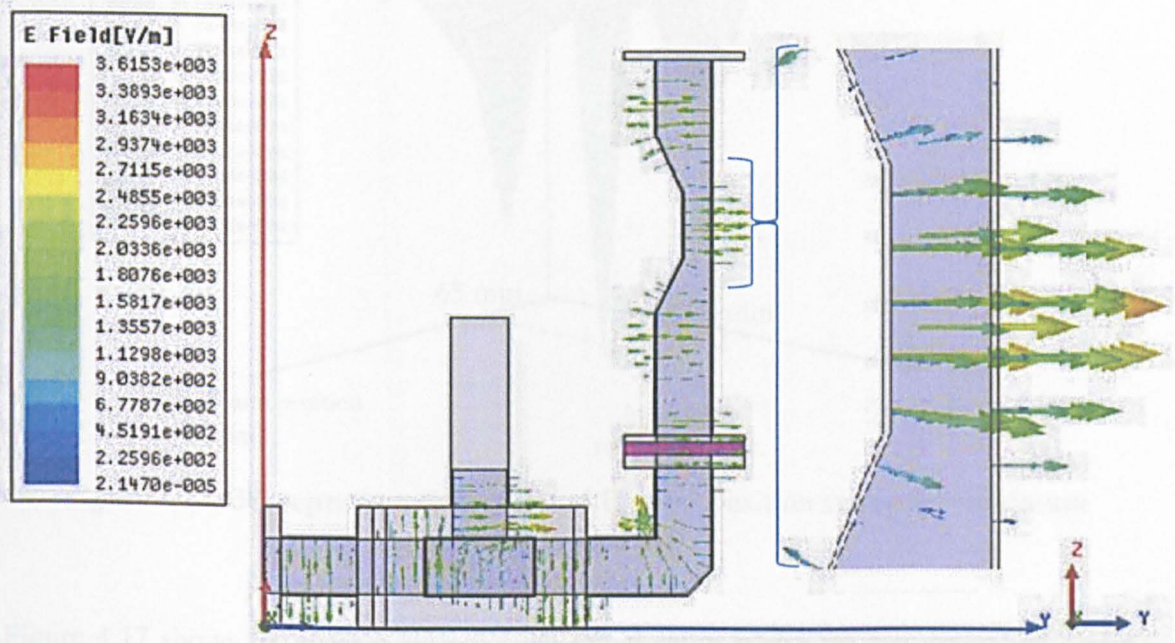


Figure 4.15: Microwave plasma system simulation.

The tuner arms can take a position value varied from 0-100 mm; zero arm position value means that the plunger inside the arm is in contact with the waveguide passage and it has no effects on the microwave system. HFSS was used to determine the position of both arms where the reflected power from the system is minimum. Figure 4.16 shows a 3D representation of E and H arms' full range sweep (from 0-100 mm) in relation with the reflected power. The simulation of all the possible arm positions has given us a value of 65 mm for E-arm and 90 mm for H-arm at which the reflected power is minimum (the lowest peak in figure 4.16). At these values, the transmitted power to the plasma cavity is maximised and self-striking plasma is possible and sustained.

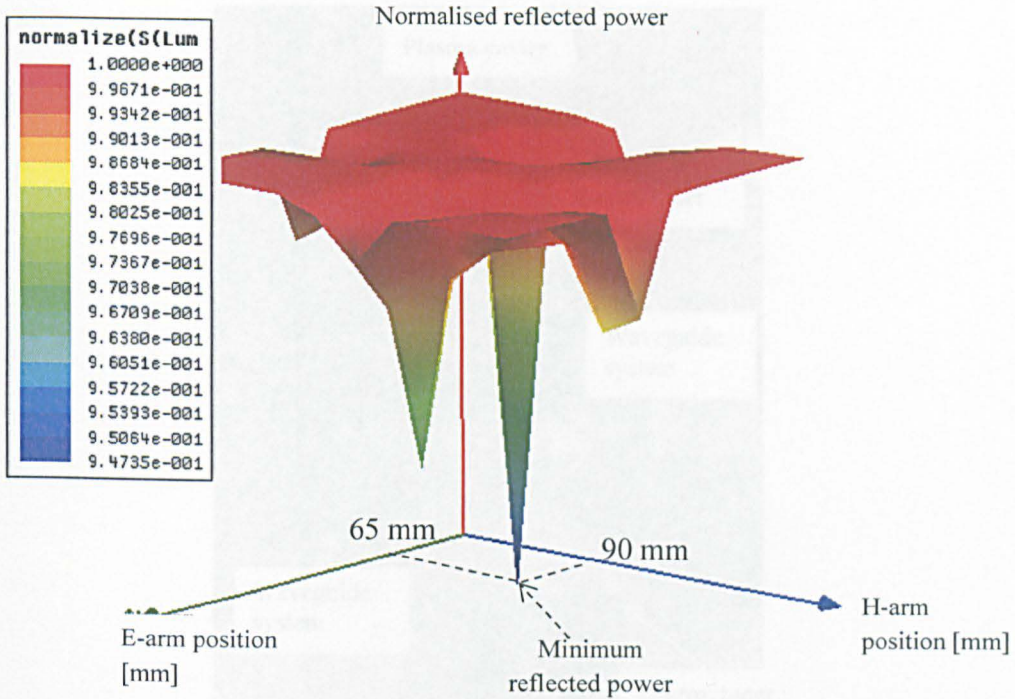


Figure 4.16: 3D representation of E and H arms position sweep for minimum reflected power

Figure 4.17 shows the plasma system’s lab initial setup where we can notice the plasma cavity attached to the microwave system and the tuning system (still manually controlled in this stage). To determine whether HFSS simulation for E-arm value is correct or not in the real system, the same experiment was held. An E-arm position sweep between 0-100 mm was done while recording the reflected power (represented by reflected voltage in figure 4.18). This experiment shows that minimum reflected power for plasma strike is achieved at the same range of 80mm. After striking the plasma, the reflected power is increased due to impedance mismatch. E-arm plays the role to match the system again and reduce this power (the plasma optimised point in figure 4.18).

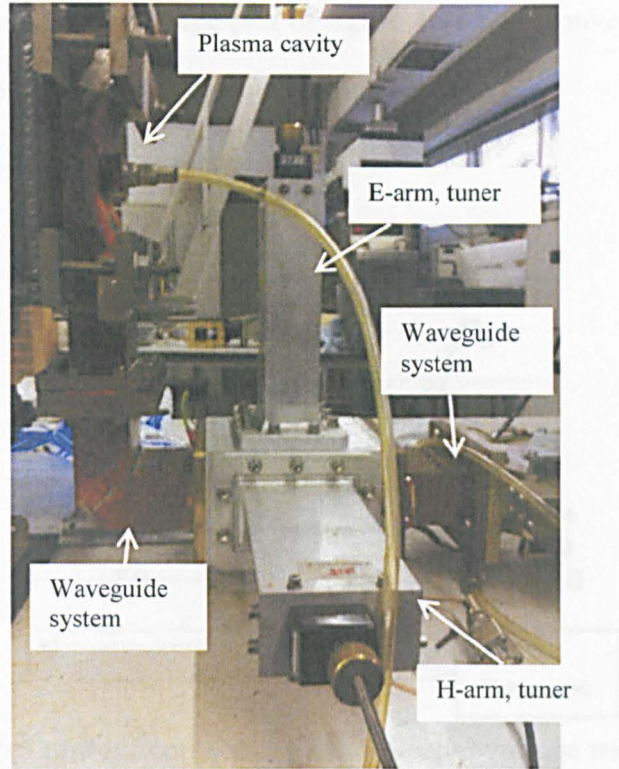


Figure 4.17: Microwave plasma system.

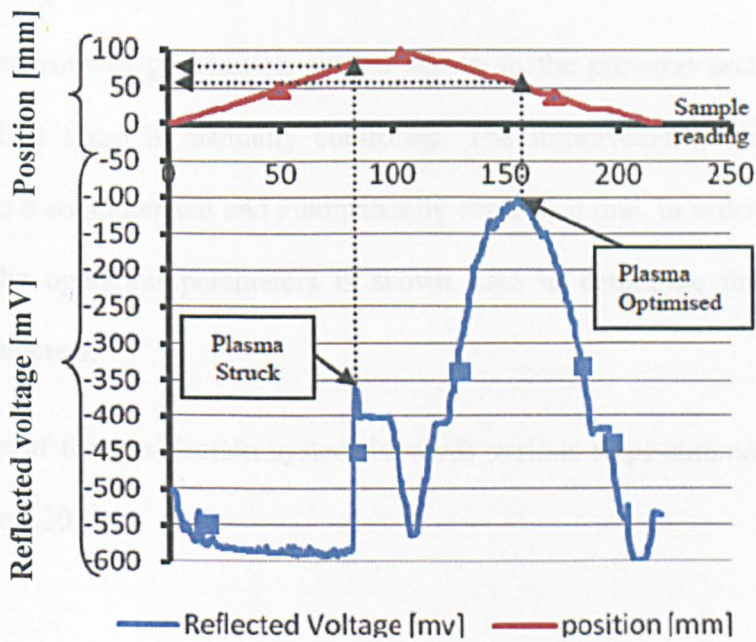


Figure 4.18: E-arm position sweep and reflected voltage.

Figure 4.19 shows the reflected voltage part of figure 4.18 after converting to power unit (dBm) (this will be explained later in the methodology chapter).

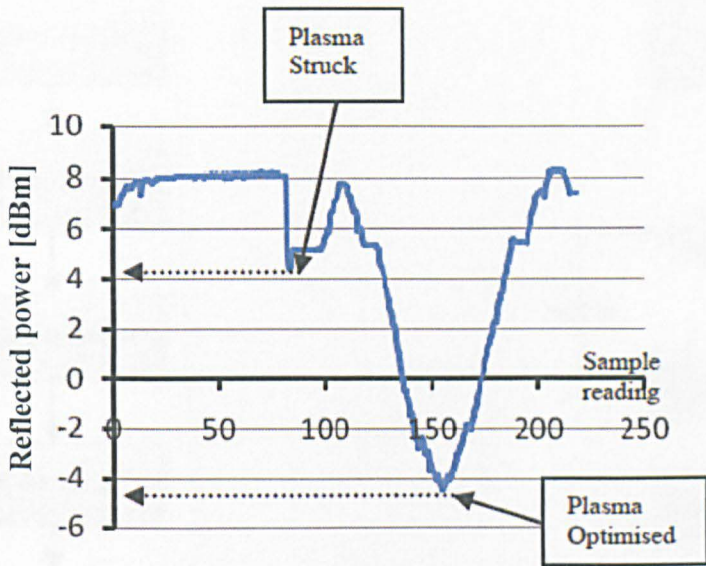


Figure 4.19: Reflected power representing the reflected voltage with E-arm sweep.

4.4. System Improvements

The plasma microwave gasification system shown in the previous sections is the initial one. This initial setup is manually controlled. The improvements on the system will transfer it into a computerised and automatically controlled one. In order to do so, a quick analysis of the operation parameters is shown here to determine the control and the feedback parameters.

The operation of the gasification system involves various steps summarised by the flow chart in figure 4.20

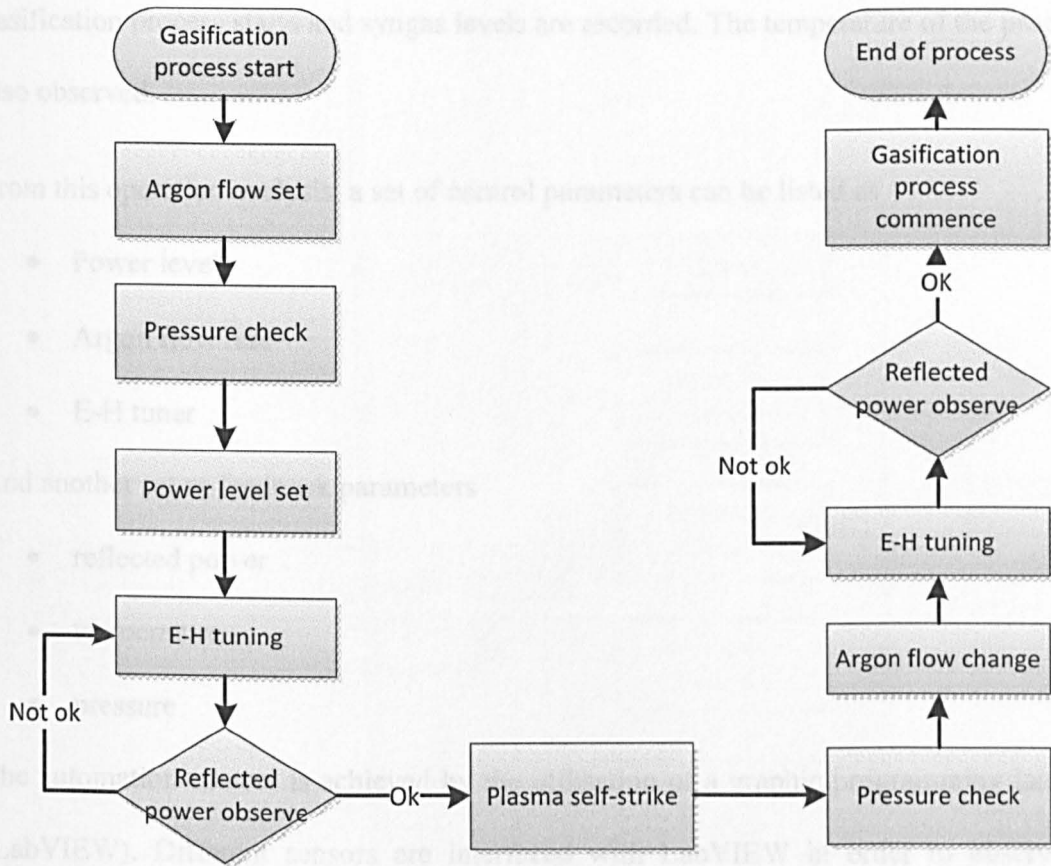


Figure 4.20: Gasification process flow chart.

The start of the procedure needs the set of the argon flow rate first and check of the pressure inside the gasification chamber to be less than 300 mbar. After that, the power is set on 1 kW to drive the magnetron. To strike the plasma, an impedance matching process through the E-H tuner is manually done. During this process, reflected power is observed through a diode detector attached to the circulator which shows it in voltage unit (as reflected voltage). The plasma strikes when the reflected voltage is around 350 mV (see figure 4.18). Argon flow is manually decreased after the plasma is struck to intensify the microwave power on fewer argon molecules. The system needs impedance re-matching to achieve the minimum reflected power and for the optimisation of the plasma, then the

gasification process starts and syngas levels are recorded. The temperature of the process is also observed.

From this operation analysis, a set of control parameters can be listed as

- Power level
- Argon flow rate
- E-H tuner

And another set as feedback parameters

- reflected power
- temperature
- pressure

The automation control is achieved by the utilisation of a graphic programming language (LabVIEW). Different sensors are interfaced with LabVIEW in order to observe and achieve the optimal control.

4.5. Instrumentation and LabVIEW Interface

The improvements of the system operation procedure illustrated in figure 4.20 are achieved by following the block diagram shown in figure 4.21. The control parameters are identified by arrows towards the microwave plasma gasification system (i.e. pointing to the right), while the feedback parameters are the measured parameters coming from the system (i.e. pointing to the left). Pressure control is kept manual in this stage hence it is not shown in the block diagram (figure 4.21). It can be noticed from the same figure that the devices (apart from Quintox gas analyser) are connected to the control PC (LabVIEW) through NI cDAQ.

LabVIEW, cDAQ and the other instrumentations used in this project are explained in this section.

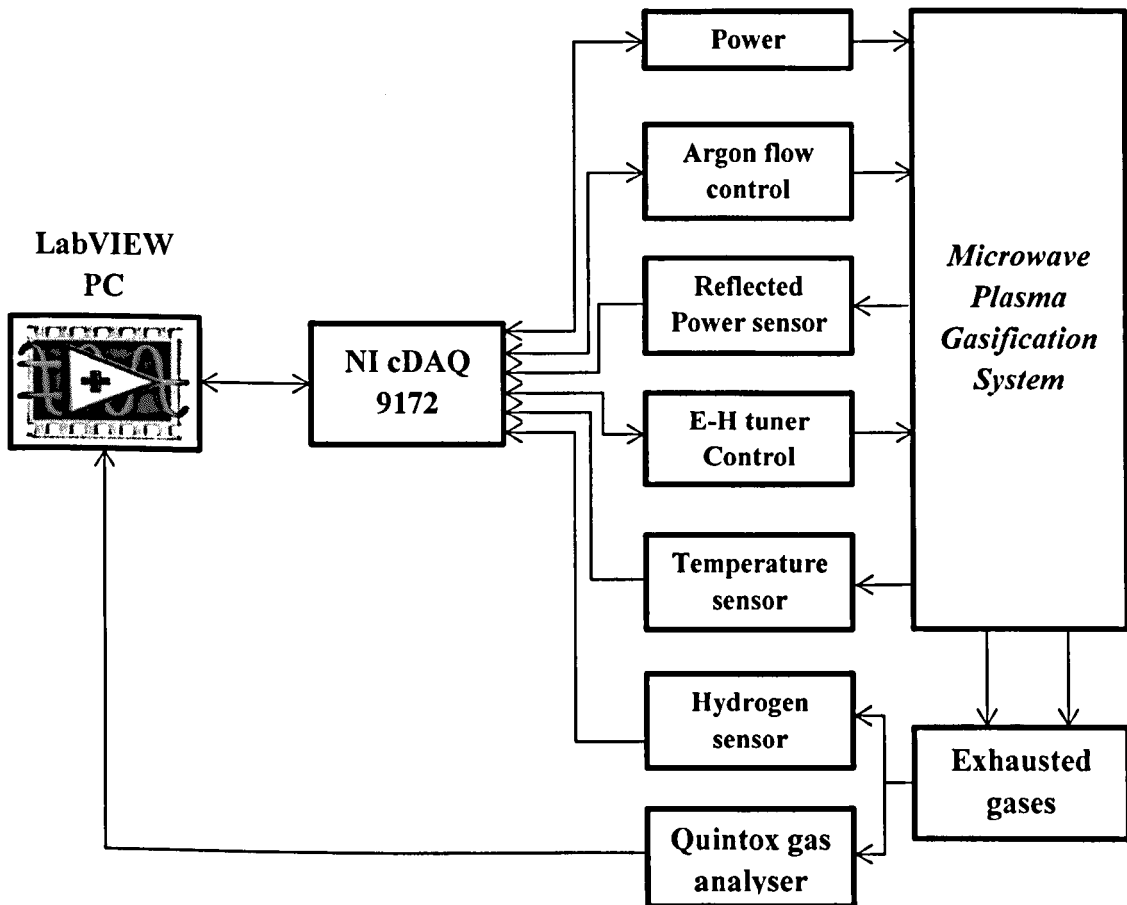


Figure 4.21: Block diagram of the system's control parameters and interfacing method.

4.5.1. The Use of LabVIEW

LabVIEW stands for Laboratory Virtual Instrument Engineering Workbench, and it is a graphic programming language developed by National Instruments (NI). Since its launch, LabVIEW has become an essential tool in industry for the development of test, measurement and controls for instrumentation [138].

As a programming language, LabVIEW uses something called a virtual instrument or VI. A VI is where the program code goes, and it consists of a front panel, a block diagram and an icon that represents the program. Depending on the functionality, a VI can be used as a standalone instrument or as part of a more complex application (as a sub-VI or sub-program).

Figure 4.22 shows most of the important elements of a LabVIEW front panel as well as the block diagram.

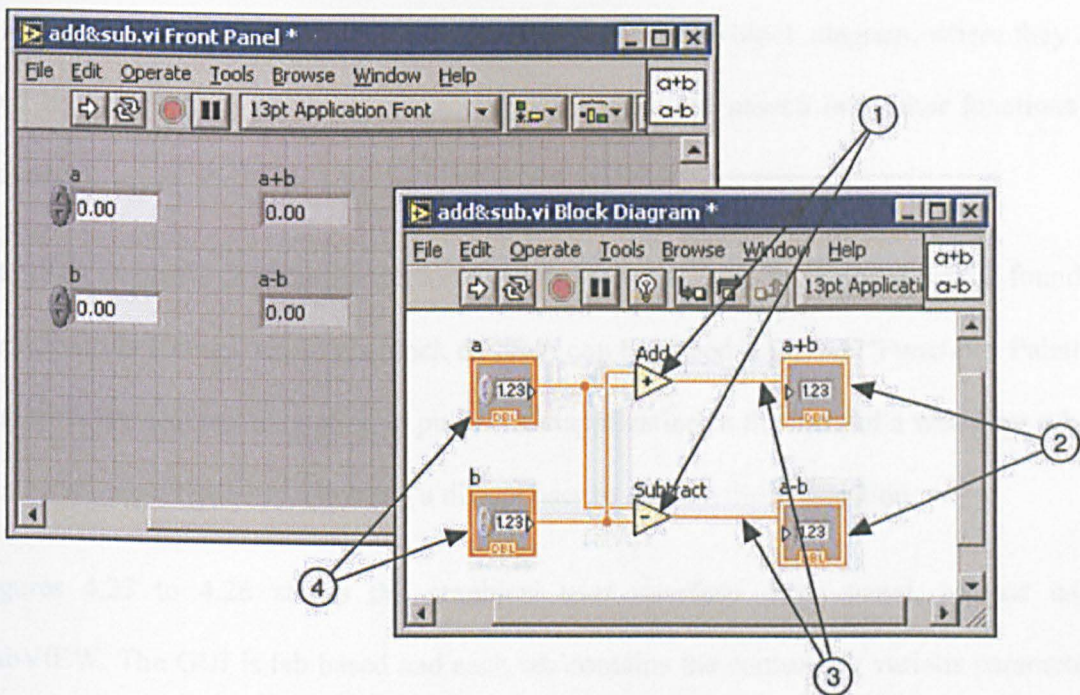


Figure 4.22: Main components of LabVIEW programme.

A front panel is used to display the controls with which the user interacts with the program or virtual device. It consists of controls (e.g. buttons and switches) and indicators (e.g. charts and meters) for the user. Controls are the inputs the user employs to communicate with the program while indicators are the outputs of processes, calculations and measurements performed by the program.

By interacting with the tools available in the front panel, users can control the program, change inputs, and see data updated in real time.

The block diagram is the “code” of the program. If speaking in terms of an instrument, this can be seen as a representation of the circuitry and paths the data takes in the functions and the calculations it performs. Figure 4.22 shows: (1) Nodes, (2) Indicator terminals, (3) Wires and (4) Control Terminals.

Every front panel control or indicator has a corresponding terminal on the block diagram. When a VI executes, values from controls flow through the block diagram, where they are used in the functions on the diagram, and the results are passed into other functions or indicators.

The tools available to program the look and functionality of a front panel can be found in the “Controls Palette” while the block diagram can be coded using the “Functions Palette”. The software also has the option to publish the application in the form of a web page which can be accessed remotely, allowing a distant user to operate the application.

Figures 4.23 to 4.26 shows the graphical user interface, front panel, created using LabVIEW. The GUI is tab based and each tab contains the controls of various parameters. Figure 4.23 shows the power control where users can enable the power source and set the wanted power level. Figure 4.24 shows the control of E-H tuner arms and argon flow rate. It also contains the measurements of feedback parameters such as temperature and reflected power.

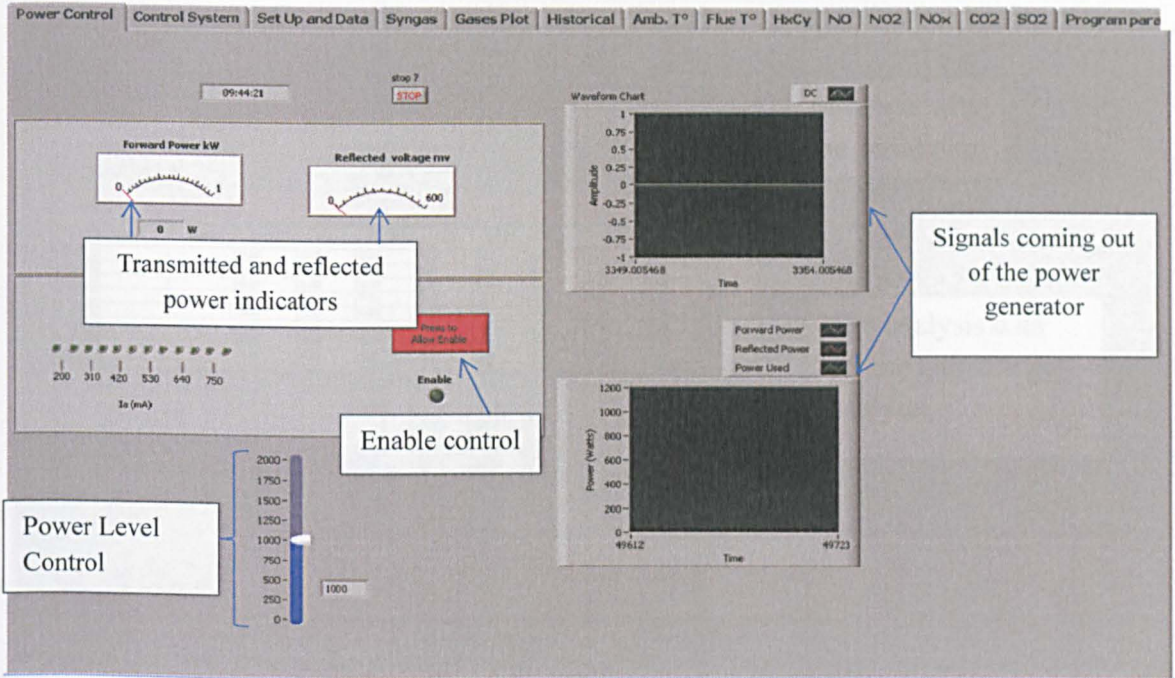


Figure 4.23: Power control GUI.

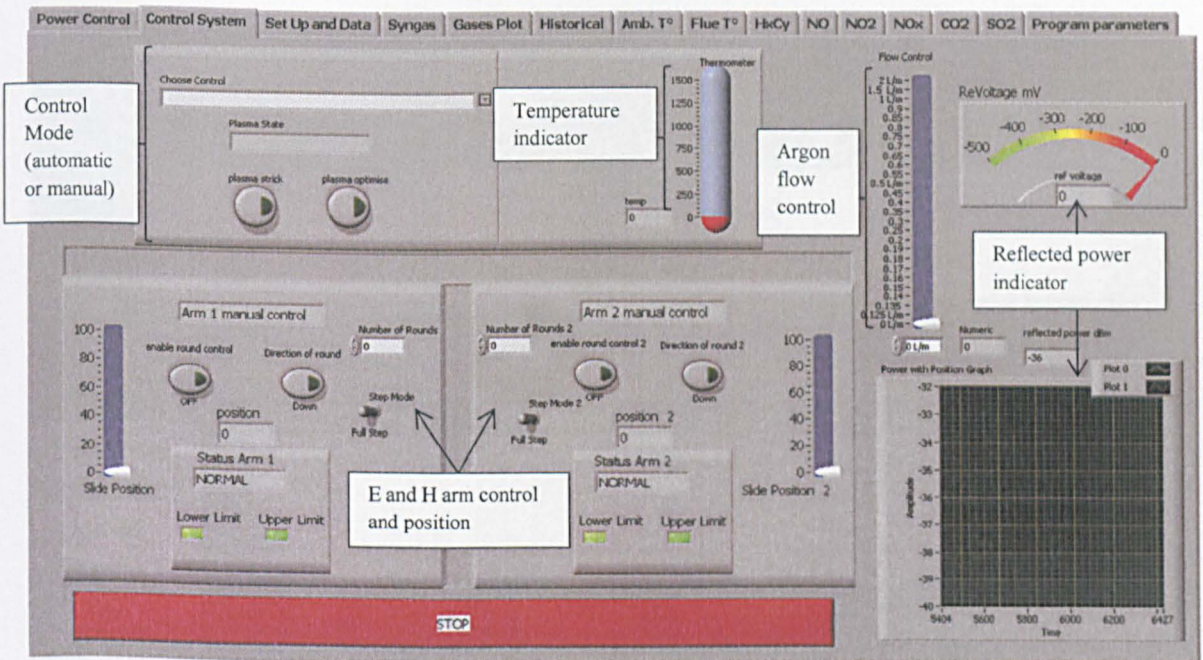


Figure 4.24: Front panel of the control system.

Figure 4.25 shows the GUI's tab of gas measurements from Quintox gas analyser and

figures 4.26 shows the graphical representation of CO and H₂ percentage.

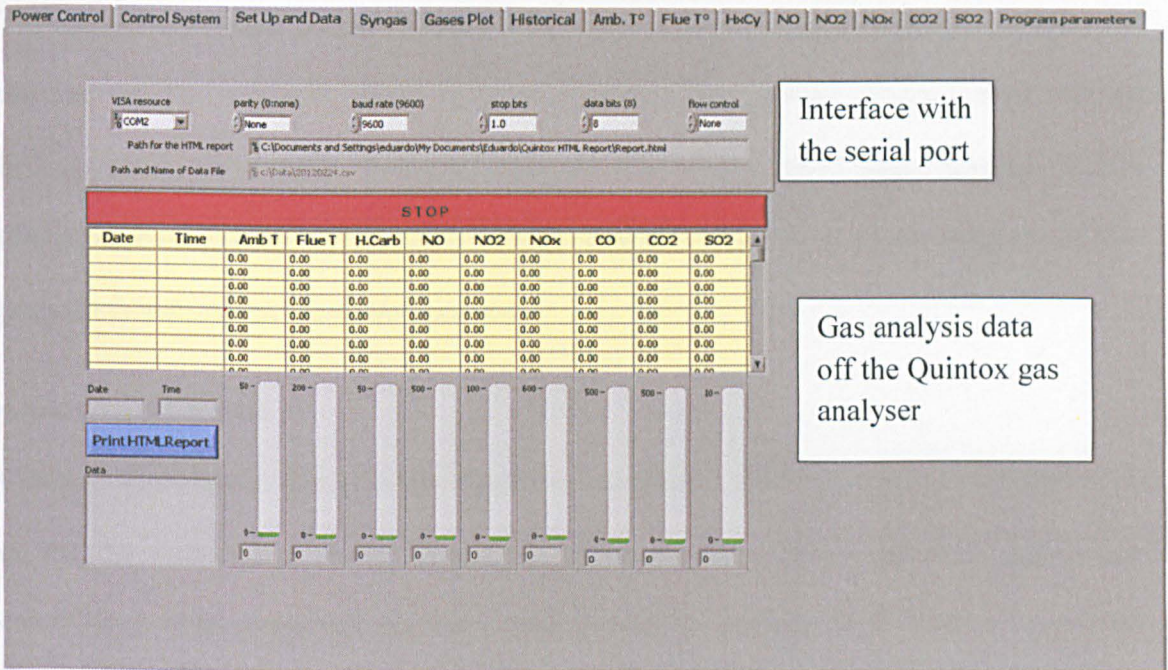


Figure 4.25: Quintox analyser control parameters.

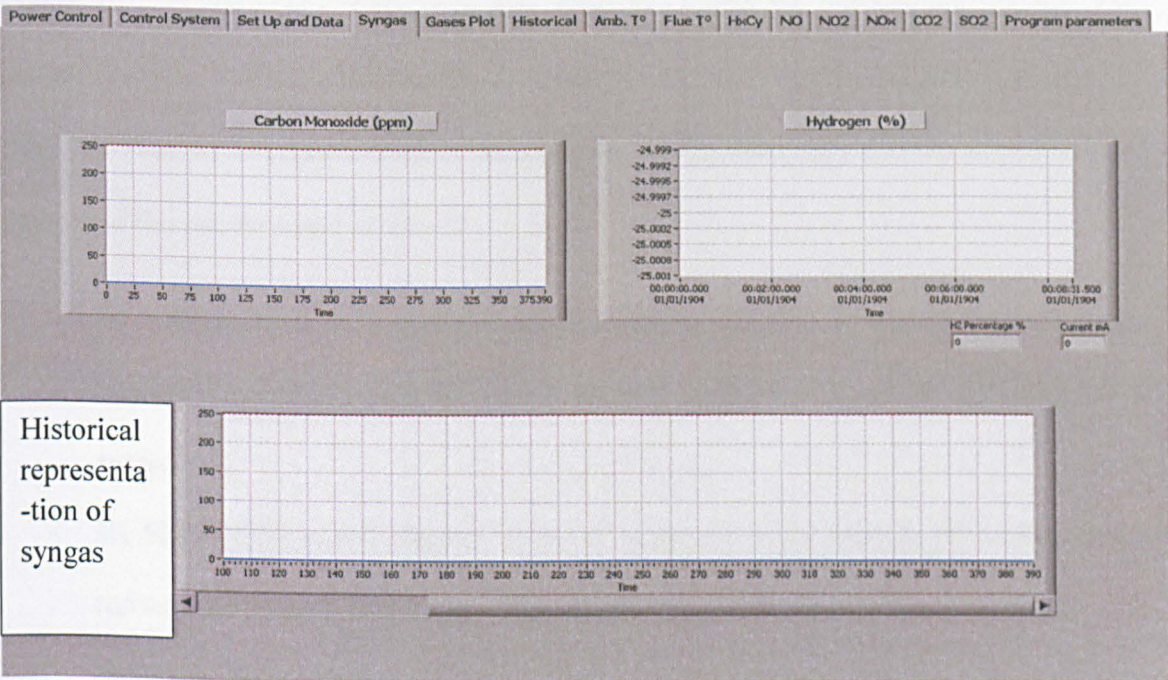


Figure 4.26: Syngas production representation.

The rest of the tabs are similar to figure 4.26 where it shows the graphical representation of the rest of the outcome gases from the gasification process. These gases include hydrocarbons, nitric oxide (NO), nitrogen dioxide (NO₂), other mono-nitrogen oxides (NO_x), carbon dioxide (CO₂), and sulphur dioxide (SO₂). The block diagram of the program is included in the thesis appendix.

4.5.2. cDAQ Chassis

Compact Data Acquisition (cDAQ) chassis are developed by NI to combine and control all of the NI instruments (DAQ modules). Through these DAQ modules, signals are conditioned to be interfaced correctly with LabVIEW installed PCs. They are used for measuring, testing and generating the required control signals in a system.

Figure 4.27 shows cDAQ 9172 which is used to control the gasification system. This chassis contains 8 module slots and is compatible with all of the available DAQs modules from NI. Four NI DAQs are used in our control system. The name and the use of each of these modules can be listed as follow:

- **NI 9264 [139]** is a 16-channel analogue output module. It is used for parameters control. Signals are sent for power control, argon flow control, and E-H tuner control
- **NI 9219 [140]** is a 4-channel universal analogue input module for multipurpose testing and signal measuring. This module is used for feedback parameters. It measures and represent reflected power, E-H tuner arms position and hydrogen yields levels.

- **NI 9401** [141] is an 8-channel, 100 ns bidirectional digital module. It is used for the control of E-H tuner arm movements through stepper motors (explained later on).
- **NI 9211** [142] is a thermocouple input module. It is used for temperature measurement (feedback parameter).

Table 4.1 summarises the use of these DAQs with the signals used to control and measure the procedure's parameters. The parameters included in this table are explained in detail in next sections and in chapters.

Table 4.1: NI DAQs specification and use.

NI device	Parameters type	Connection with	Signals sent (control) / received (feedback)
9264	Control	1- Power source	1- 0-10 V for power enable and level set control
		2- Argon flow	2- 0-5 V for argon flow rate level control
		3- E-H tuner	3- signals to control the stepper motors (E-H tuner): - Enable arm movement - Direction of arm movement - Type of steps (half/full step)
9219	Feedback	1- Reflected power	1- Volt measures from the detector diode
		2- E-H tuner	2- E-H arms position reading and arms limits
		3- Hydrogen sensor reading	3- 4-20 mA current reading from the hydrogen sensor
9401	Control	E-H tuner	Stepper motor clock signal
9211	Feedback	Temperature	Thermocouple readings



Figure 4.27: cDAQ 9172 and C series compatible modules, courtesy of ni.com.

4.5.3. Power Control

The power source is the cornerstone of the system. It feeds the magnetron with the required power for the appropriate operation. The power generator used in this system is situated in a rack setup along with the forward power detector, reflected power detector and control circuit as shown in figure 4.29. The reflected power is detected through a diode detector (figure 4.28). It converts the power readings to voltage reading, thus a calculation to convert it back to power is done and will be shown in the calibration section in chapter five. This power generator can be operated both manually and through a control program (i.e. LabVIEW).



Figure 4.28: Diode power detector.

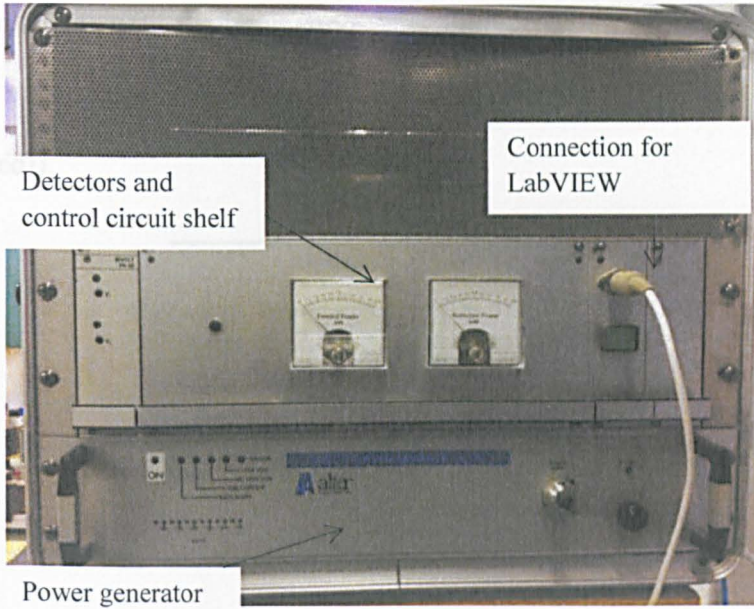


Figure 4.29: Power source setup.

The control and feedback signals used for power control are shown in the block diagram below (figure 4.30). The power generator control was achieved via two main connections; one to enable the power supply and the second to set the power level [143].

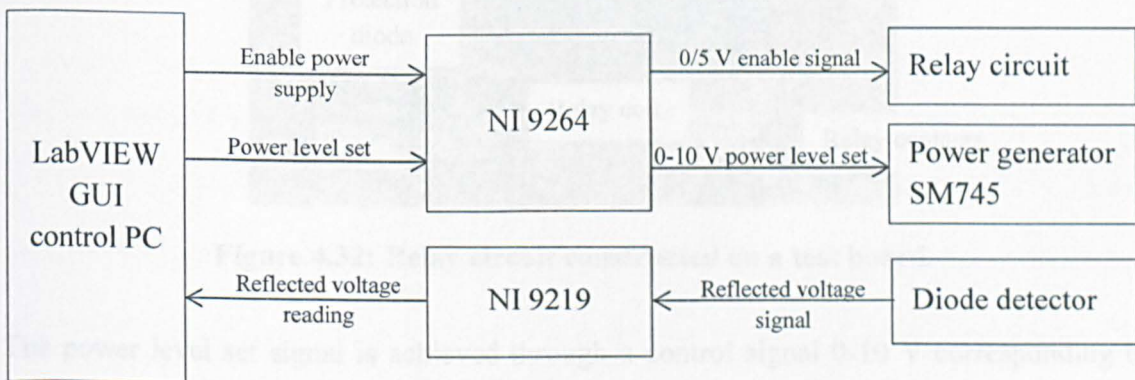


Figure 4.30: Power control block diagram.

The enable signal is the on/off signal for the power device, which can be controlled by connecting or disconnecting two contacts in the power supply. This was realised through a relay circuit (figure 4.31 and the constructed circuit figure 4.32) by connecting the power

device enable contacts with the relay contacts. This relay [144] is controlled via a control signal (0/5 V) which control the position of the contacts (i.e.NO (normally open) or NC (normally closed)).

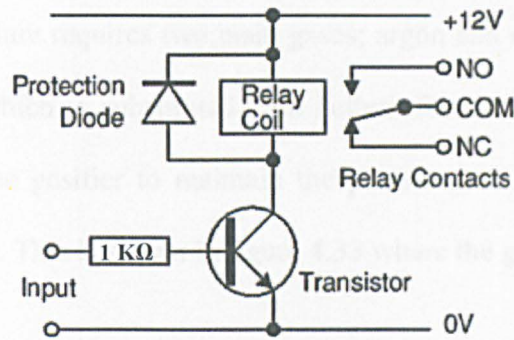


Figure 4.31: Relay circuit diagram.

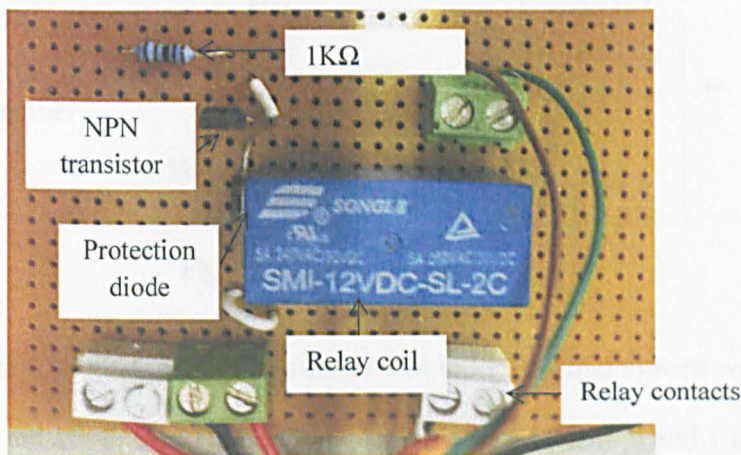


Figure 4.32: Relay circuit constructed on a test board.

The power level set signal is achieved through a control signal 0-10 V corresponding to power level 0-1000 watts. The calibration of this signal is discussed in the calibration section in chapter five.

The reflected power from the gasification chamber is detected through a diode detector (figure 4.28) which is connected to NI 9219 to read the measurements. The conversion

between voltage readings and power readings is also discussed in the calibration section later.

4.5.4. Gas Feed Control

The Gasification procedure requires two main gases; argon and nitrogen. Argon is used as the main plasma gas which is substituted with helium for comparison. Nitrogen, on the other hand, is fed to the gasifier to maintain the pressure and to create an oxygen free environment inside of it. This is shown in figure 4.33 where the gas setup can be noticed.

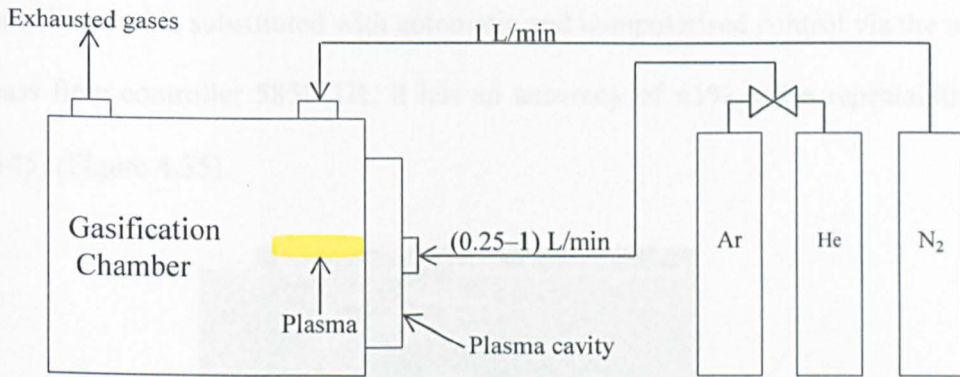
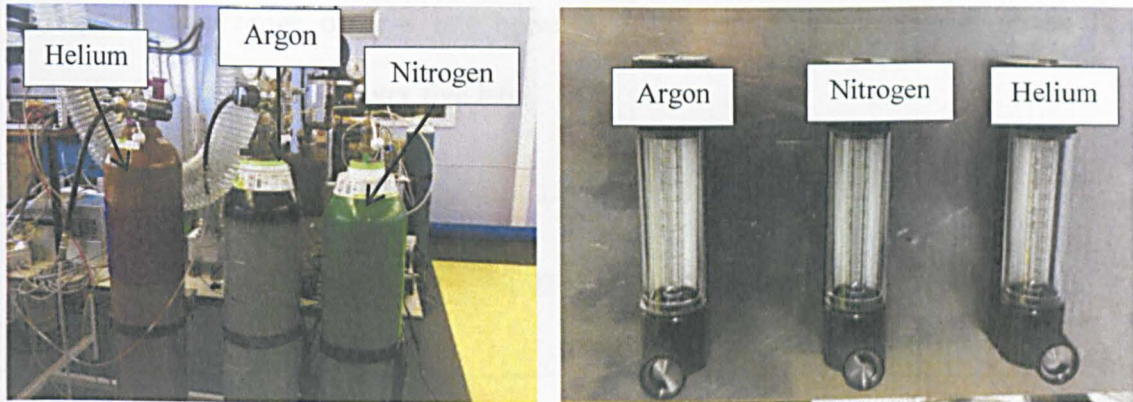


Figure 4.33: Gas setup.

The flow rates of these gases are manually controlled in the original system where nitrogen is fixed on 1L/min and argon flow rate is changed between 0.25 L/min and 1 L/min. This is because the striking of the plasma needs a higher flow rate to commence then a lower rate to concentrate the microwave radiation on a smaller number of argon molecules, thus ionising more of it into plasma. Figure 4.34 (a) shows the gas bottles (argon, nitrogen, helium) and figure 4.34 (b) shows the manual control of the gases.



(a): Gas cylinders

(b): Manual flow meters

Figure 4.34: Gas instruments.

Argon manual control is substituted with automatic and computerised control via the use of Brooks mass flow controller 5850 TR. It has an accuracy of $\pm 1\%$ and a repeatability of $\pm 0.25\%$ [145] (Figure 4.35).



Figure 4.35: Brooks mass flow controller.

The control was achieved through interfacing the unit (5850 TR) with LabVIEW via NI 9264 (figure 4.36). The unit needs a voltage signal in the range of 0-5 V which linearly

corresponds to a range of flow rate between 0-20 L/min. The calibration of the flow controller is discussed in chapter five later.

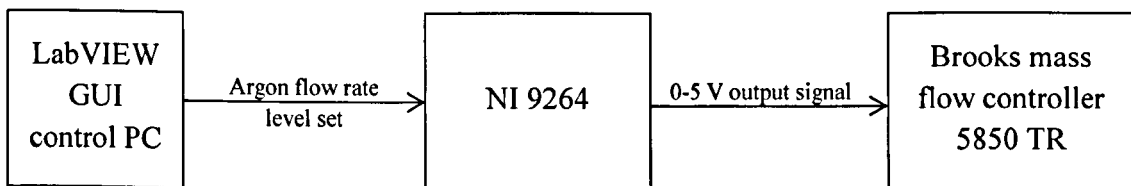


Figure 4.36: Argon flow rate control block diagram.

The output of the control unit is contacted then to the plasma cavity through the manual flow meter to make sure that the flow rate level set from LabVIEW is the realised output to the plasma cavity.

4.5.5. E-H Tuner Control

The E-H tuner is the heart of the control system. Its job is to match the impedance between the load (i.e. the gasification chamber) and the waveguide system. This match is needed in two scenarios. The first scenario is when striking the plasma, and the second is when improving the procedure (i.e. minimising the reflected power and stabilising the plasma burst). These two scenarios are needed as the load impedance changes when the plasma is struck and the feedstock starts to gasify.

In the original system setup, the E-H tuner is manually controlled to change the position of the arms. The realisation of a computerised E-H tuner is thought to be achieved by mounting a stepper motor [146] on each of the tuner arms to control the movement of the shafts up and down. Figure 4.37 shows a 3D illustration of how this control is achieved.

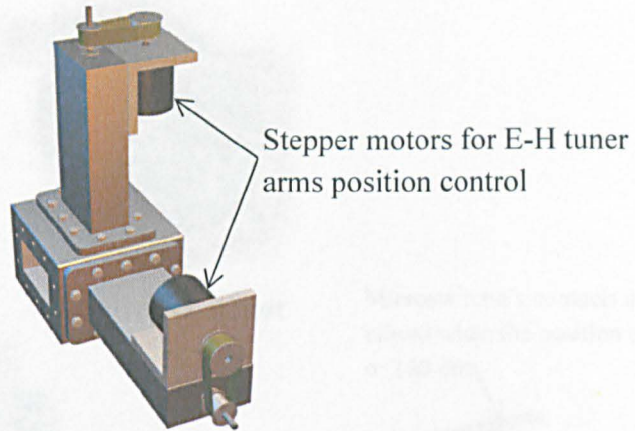


Figure 4.37: 3D model of the tuning arm.

The position of the shafts is also an important parameter to computerise as it is used as a feedback parameter for the system. This was possible by using a linear slide potentiometer 0-10000 Ω [147]. The potentiometer is attached to the arm shaft and slides up or down with it. This changes the resistance output of the potentiometer which corresponds to the position of the arm (this will be discussed at the calibration section). Finally, for safety reasons, microswitches [148] were situated at the both ends of the potentiometer. The microswitches serve as an alarm mechanism. When the position is 0 or 100mm the microswitch is activated (i.e. microswitches contacts are closed) and an alarm is shown in the user graphical interface to immediately stop the stepper motor from further moving the arm up (if the position is 100mm) or down (if the position is 0mm). The stepper motor, slide potentiometer and the microswitch are shown in figure 4.38.

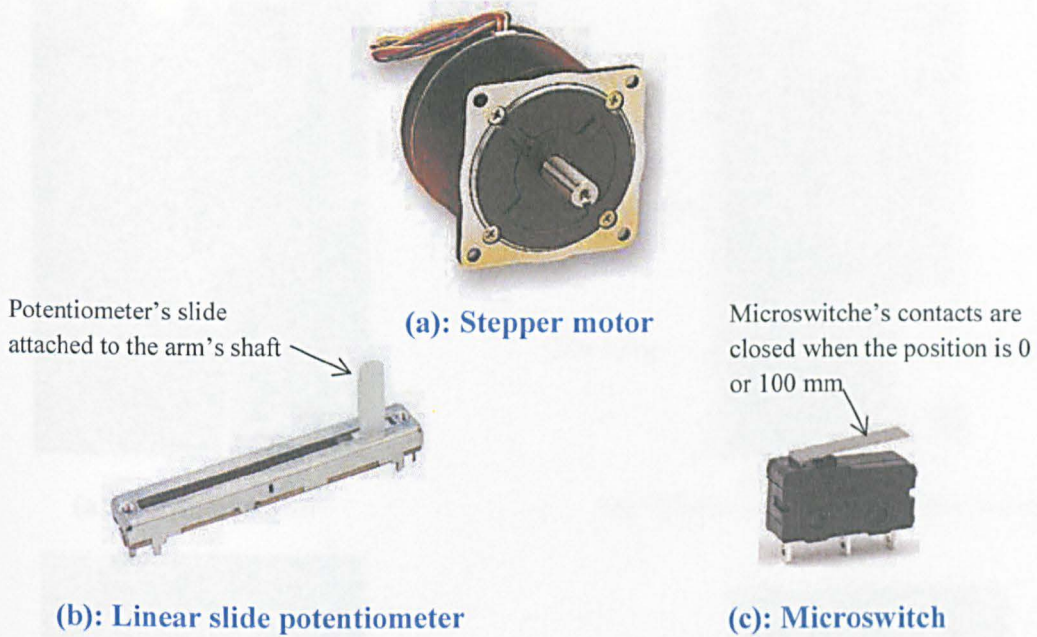
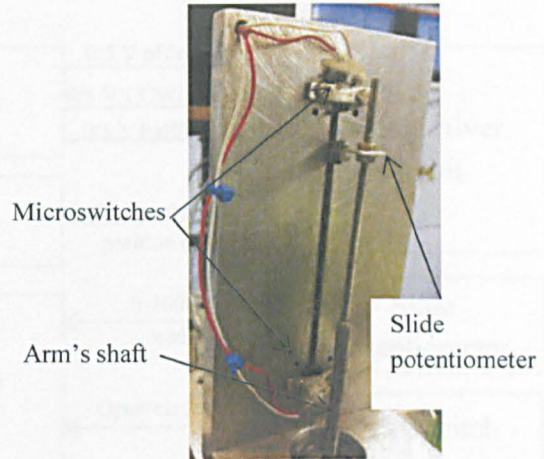


Figure 4.38: E-H tuner arm control components.

The mounting of the components on the arm are shown in figure 4.39. The stepper motor requires a driver circuit to be controlled [149]. This driver circuit conditions signals sent to the motor such as direction of rotation, type of steps (half or full steps), and clock pulse which triggers the motor. Each clock pulse sent rotates the motor one step angle (degree). The stepper motor used (figure 4.38-a) has a step angle of 1.8° [146], thus to rotate the motor 360° , 200 clock pulses are needed. This full rotation corresponds to 1mm E-H tuner shaft change position. The direction of rotation is controlled by sending digital signals ('0' for counter clock wise and '1' for clock wise). Half/full step is also controlled by sending '0'/'1' signals to the motor driver circuit.



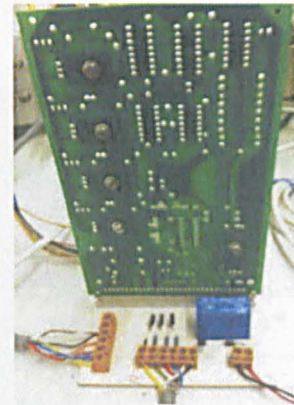
(a): Stepper motor



(b): Microswitch & potentiometer



(c): E-arm view



(d): Stepper motor's driver circuit

Figure 4.39: The different components of the computerised E-H tuner.

The signals communication between the control program and the E-H tuner arm can be seen in the block diagram below (figure 4.40). This block diagram is replicated for both E and H arm.

The interface with LabVIEW of the E-H tuner is illustrated in figure 4.41.

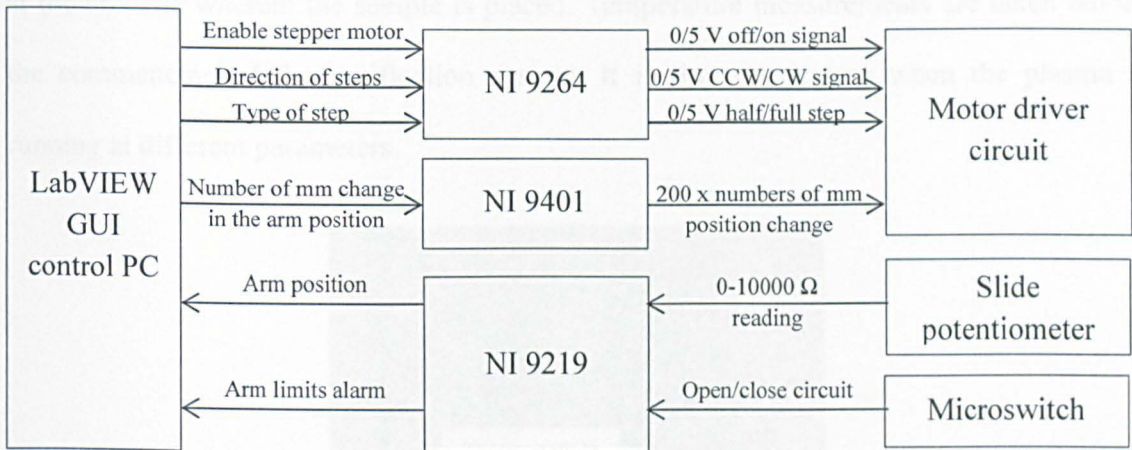


Figure 4.40: E-H tuner control block diagram.

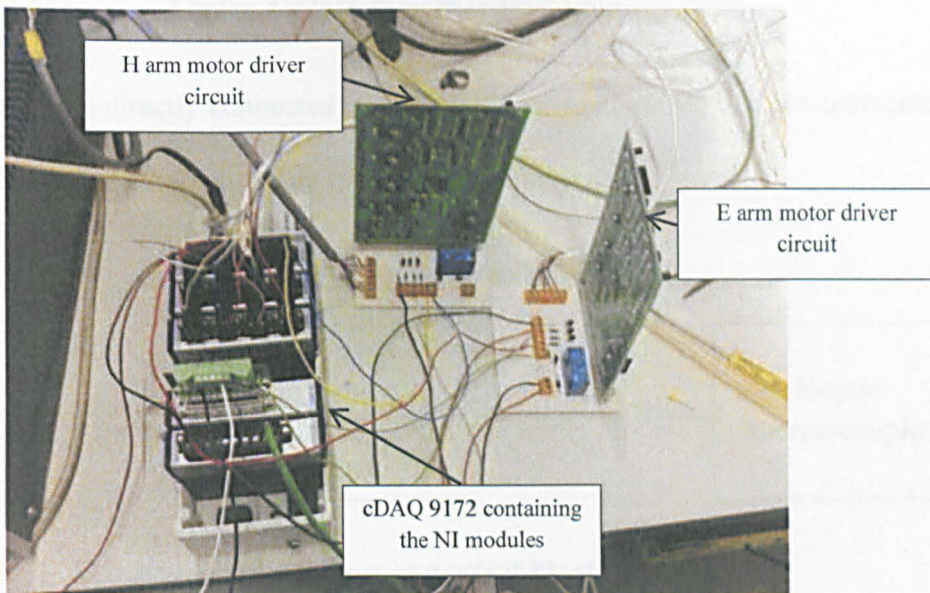


Figure 4.41: Stepper motor interface with cDAQ.

4.5.6. Temperature

The temperature of the plasma is measured using an N-type thermocouple [150] (figure 4.42) which is able to measure temperature in the range of 0-1200 C°. This sensor is placed directly inside the gasification chamber, on the crucible, to measure the temperature

at the crucible wherein the sample is placed. Temperature measurements are taken before the commencing of the gasification system. It is the temperature when the plasma is running at different parameters.

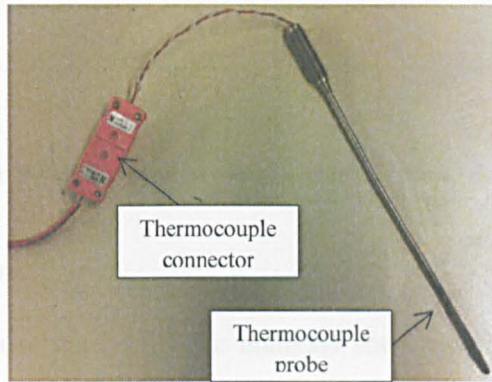


Figure 4.42: N-type thermocouple.

This thermocouple is directly connected to LabVIEW through cDAQ and the temperature measured is shown in the user interface without any conditioning.

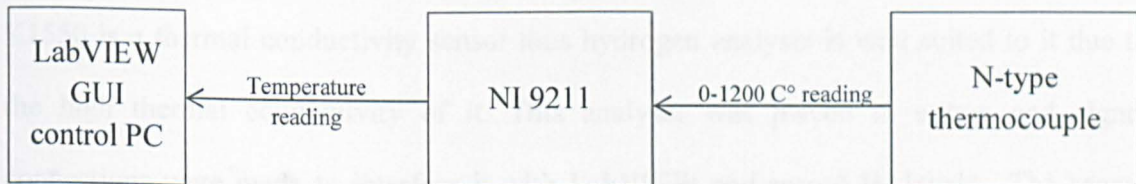


Figure 4.43: Temperature control block diagram.

4.5.7. Gas Analyser

The improvement of the system is proven through syngas production rate, thus gas analysers should be attached to the system in order to measure H_2 and CO . Two different sensors are used for this purpose; hydrogen sensor and Quintox gas analyser. The interface between the gas analysers and LabVIEW is illustrated in the block diagram below (figure 4.44)

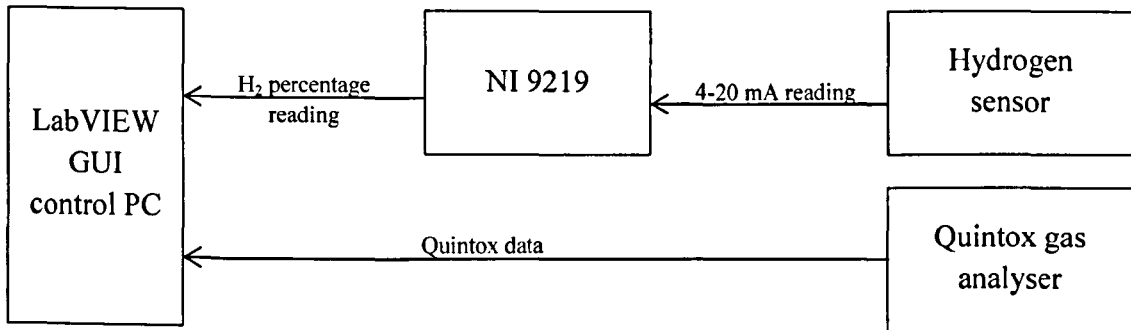


Figure 4.44: Gas analysers control block diagram.

4.5.7.1. Hydrogen Sensor

Hydrogen was measured using a K1550 gas analyser shown in figure 4.45. These analysers are ideal for measuring % levels of one gas in a binary or pseudo-binary mixture. For example, air is composed of many gases but in known, fixed ratio, therefore hydrogen in air is a pseudo-binary mixture and can be measured at % levels with a K1550 noble gas analyser. K1550 has an accuracy of $\pm 2\%$ and repeatability of $< \pm 1\%$ [151]. The same concept is used to measure hydrogen in syngas mixture coming out of the gasifier. The K1550 is a thermal conductivity sensor thus hydrogen analysis is well suited to it due to the high thermal conductivity of it. This analyser was placed in a box and signal connections were made to interface it with LabVIEW and record H_2 levels. The sensor shows the $H_2\%$ on an LED screen as well as in the user interface.

The analyser readings of the thermal conductivity of the gas measured are represented with current reading in the range of 4-20 mA corresponding to gas percentage range of 0-100 %.

The calibration of the sensor is discussed in chapter five later.

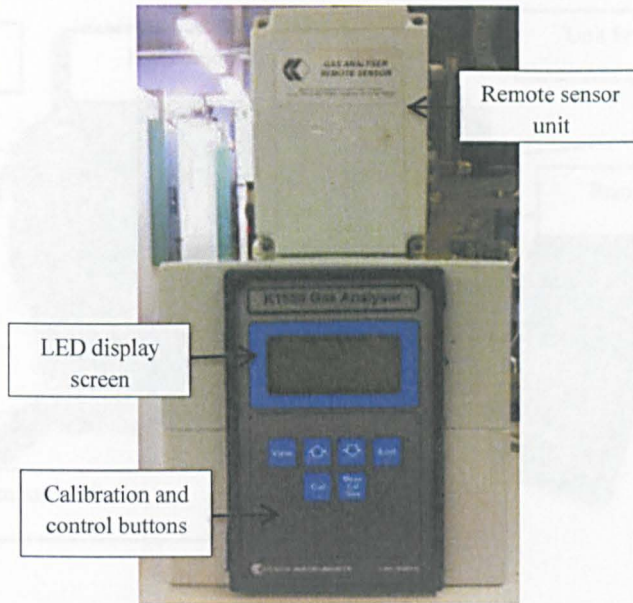


Figure 4.45: K1550 gas analyser.

4.5.7.2. Quintox Gas Analyser

The measurement of carbon monoxide is achieved by using Quintox gas analyser (KM 9106) shown in figure 4.46. It is an electro-chemical portable gas analyser manufactured by Kane-May under the model of Quintox 9106 [152], it is a versatile portable analyser suitable for exhaust emission monitoring. The unit includes a particulate trap and a water vapour condenser. Depending on the number and type of sensors fitted to the unit, it measures a series of 33 parameters.

The Quintox 9106 includes a remote handset which can be used to store up to 1926 parameter sets in its battery powered internal memory. From here data can be directly downloaded to a PC. It can display present pages as well as personally configured screens using the incorporated keypad.

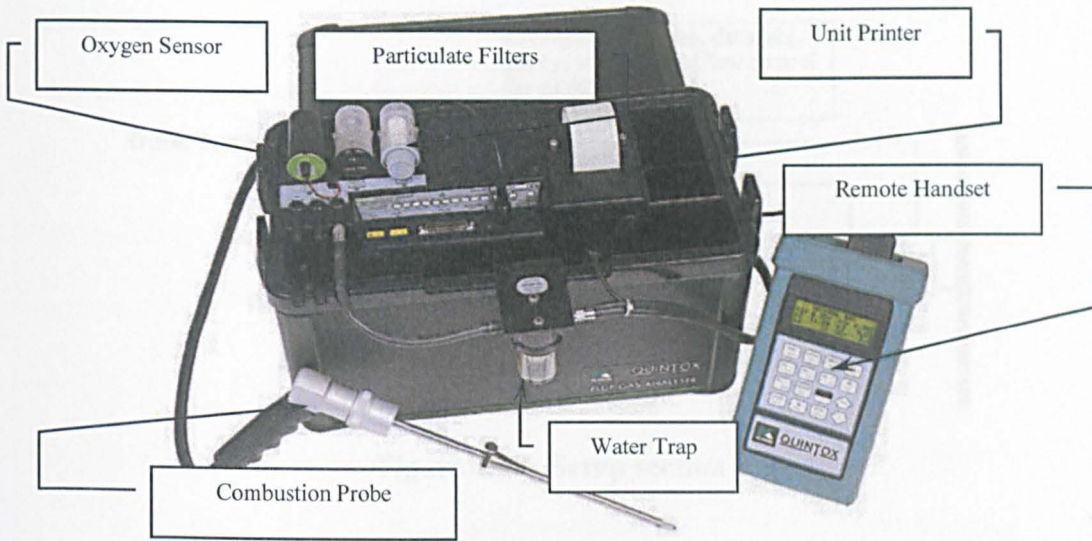


Figure 4.46: Quintox 9106 Gas Analyser.

The unit has an auto print function which can be set to perform readings at predetermined intervals. The shortest interval available is 1 reading every 10 seconds.

All measurements are done in real time and can be transferred to a PC via an RS232 serial port connector built in to the main unit. The data line consists of 33 data items either in binary or as a comma separated value (CSV) output. Once the unit is connected to a PC, the data can be analysed and/or stored for later study.

Although Kane-May (the supplier) offers the possibility of buying its own Fireworks Software [153], we used an LJMU developed LabVIEW code to connect the unit to PC and record data.

Interfacing with the LabVIEW PC is possible through the setting up of a communications port. This port has been set using LabVIEW as figure 4.47 illustrates, wherein the necessary communication parameters are specified to enable the transfer of data from the electrochemical sensor Quintox 9106 and the PC.

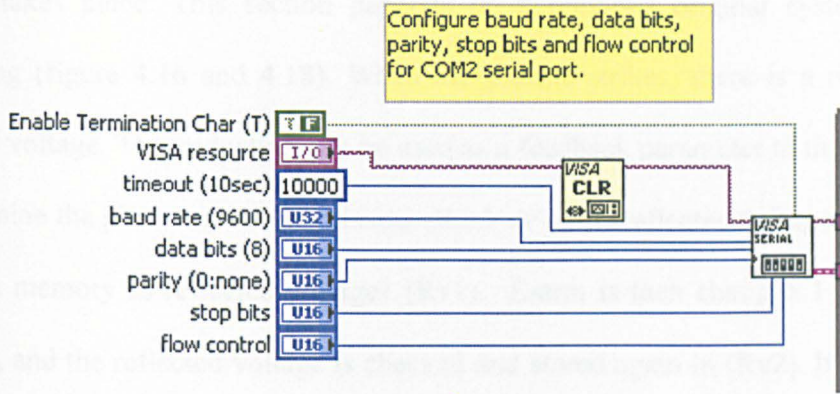


Figure 4.47: Setup section

4.6. Gasification System Control

The control of the gasification system is possible after the automation of power, argon flow rate, E-H tuner, temperature, and gas analysers. This control follows the two scenarios of striking then optimising the plasma burst. Figure 4.48 shows the flow chart of the system control which is an extended version of the gasification process flow chart discussed in figure 4.20.

The control algorithm is divided into three main sections; initial setup, plasma strike, and plasma optimisation. The values of power, pressure, and argon flow rate in the flow chart are the values obtained from the system performance analysis in chapter 6. Systems' parameters are saved to disk throughout the process for feedback (i.e. reflected voltage, arms positions and argon flow) and for results analysis (i.e. CO and H₂).

At the start of the algorithm, an initial setup is required to set argon flow rate, the power, and to check the pressure inside the gasification chamber. Power and argon flow rate are controlled through LabVIEW. However, pressure is controlled manually by releasing the pressure valve to achieve the 50 mbar level. After the initial setup, the plasma strike

process takes place. This section depends on a previous original system testing and simulating (figure 4.16 and 4.18). When the plasma strikes, there is a reduction in the reflected voltage. This reduction can be used as a feedback parameter to the control system to determine the plasma state (i.e. plasma struck or not). Reflected voltage is recorded and stored in memory as reflected voltage1 (Rv1). E-arm is then changed 1 mm in position upwards, and the reflected voltage is checked and stored again in (Rv2). It is noticed from the original system performance that the reflected voltage is reduced by at least 60 mV when the plasma is struck. This is used as a decision box in the flow chart ($Rv1-Rv2 < 60$) to decide when the plasma is struck.

After the plasma has struck, the system needs stabilising and the reflected power needs to be minimised. This is achieved in the third section of the control algorithm. Argon flow rate is changed in this section and the E-H tuner arm positions are changed to find the lowest reflected voltage. The positions of the arms which satisfy this condition (i.e. the minimum reflected voltage) are taken from the system simulation analysis (figure 4.16).

Once the reflected voltage is minimised, the gasification process takes place and gas yields are analysed and recorded through the gas analysers.

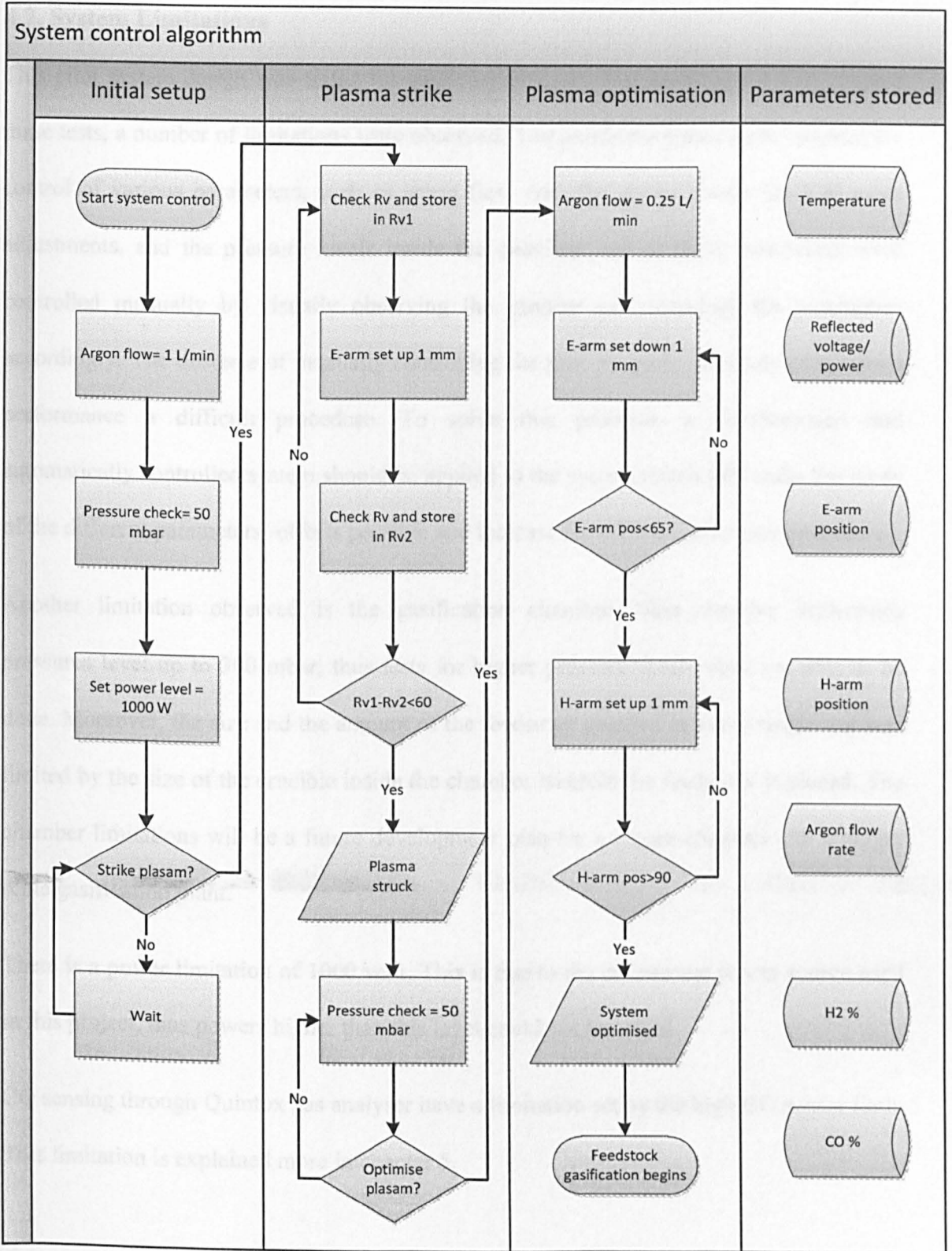


Figure 4.48: System’s control flow chart.

4.7. System Limitations

This pilot system design was tested for gasifying different feedstock (e.g. wood). During these tests, a number of limitations were observed. The gasification procedure requires the control of various parameters, such as argon flow rate, the power levels, the E-H tuner adjustments, and the pressure levels inside the chamber. All of these parameters were controlled manually by visually observing the process and changing the parameters accordingly. The obstacle of manually controlling the process made the study of system's performance a difficult procedure. To solve this problem, a computerised and automatically controlled system should be applied to the system which will make the study of the different parameters' effects possible and increase the efficacy of syngas procedure.

Another limitation observed is the gasification chamber. This chamber withstands pressures level up to 300 mbar, thus tests for higher pressure levels were not able to be done. Moreover, the size and the amount of the feedstock gasified in every single test was limited by the size of the crucible inside the chamber wherein the feedstock is placed. The chamber limitations will be a future development plan for a bigger chamber and a bigger scale gasification plant.

There is a power limitation of 1000 watt. This is due to the microwave power source used in this project, thus powers higher than this level could not be tested.

CO sensing through Quintox gas analyser have a limitation set by the high CO sensor limit.

This limitation is explained more in chapter 5.

4.8. Summary

Throughout this chapter we have explored the original microwave plasma gasification system setup and limitations. All of the original system's parameters were controlled manually by visually observing the process and changing the parameters accordingly. The time ceasing of manually controlling the process made the study of the system's performance a difficult procedure. The automation control of the system was the solution to this particular problem. System modelling has been illustrated to show the design of the plasma cavity and to study the effects of the E-H tuner arm position on reflected voltage. This modelling has given us the arm positions wherein the reflected voltage is minimised. These values are used in the control algorithm.

System improvements are discussed in this chapter through understanding the steps of the gasification process. The instrumentations needed for these improvements are identified and explained. These instruments are: NI DAQs for interfacing with LabVIEW, power control, argon flow rate control, E-H tuner control, temperature, and gas analysis sensors.

Finally in this chapter, the gasification system's control algorithm was explained. This algorithm is divided into three sections; initial setup, plasma strike and plasma optimisation. The system's parameters are saved to disk throughout the control process for feedback (i.e. reflected voltage, arms positions and argon flow) and for results analysis (i.e. CO and H₂).

Chapter Five: Experimental Methodology

5.1. Introduction

The control system's instrumentations were presented in the previous chapter. The calibration of these instrumentations is needed in order to give accurate readings to the program. The system calibration is explained in this chapter for the different sensors used in the control algorithm. Experimentation methodology is detailed in this chapter to understand the steps taken for each experiment set to eventually obtain the final results which determine the system performance.

5.2. System Calibration

5.2.1. Power

Power control in this system consists of two parts, the power generator and the reflected power detector. Both of these parts are calibrated after interfacing with cDAQ. Figure 4.32 in chapter 4 shows the control signals communication between the power devices and cDAQ.

The power source generates power in the range of 0-1000 W. This range is linearly mapped with a voltage control signal range of 0-10 V [143]. This means for every 1 V increment in control signal there is 100 W increment in power generated. This mapping is programmed according to the block diagram shown in figure 5.1. The function of box 1 in this block diagram is to round the power level to the nearest integer. This is done for accurate power to voltage signal conversion. Box 2 is a signal limitation box. It compares

the power level with the power limit of the generator (1000 W) and chooses the level set value if the comparison returned true (T) or 1000 if the comparison returned false (F). Finally the signal is divided by 100 to map it to the correct voltage control signal, which is then sent to the power source. This calibration is shown in the LabVIEW's block diagram appended at the end of the thesis.

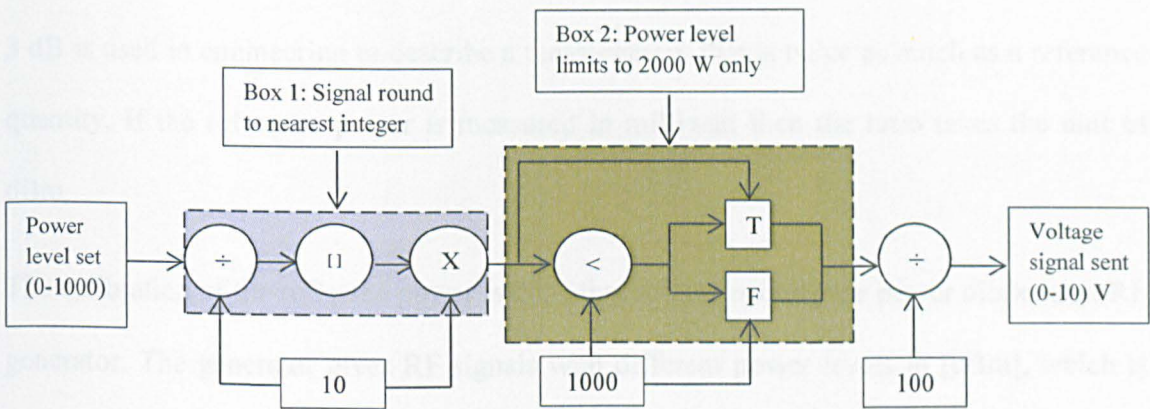


Figure 5.1: Power calibration block diagram.

The validation of this calibration is tested by changing the power level from the LabVIEW controller and compares it to the actual power level shown on the power device as will be shown in results chapter. This experiment is shown in the results chapter with the calculation of the error rate. The second part of the power control calibration is the reflected power calibration. The diode detector illustrated in figure 4.31 measures the reflected power in volts. However the power level is usually calculated in decibel [dB]. Thus calibration is needed to convert from V to dB readings.

Decibel is a standard unit which expresses the ratio between physical quantities relative to a specified or implied reference level ($\frac{P_1}{P_0}$) [154]. It is often used to describe sound levels, power gain and power loss. The decibel is expressed as equation 5.1:

$$dB = 10 \log_{10} \frac{P_1}{P_0} \quad (5.1)$$

This equation indicates that decibel is a logarithmic unit. For example if the measured power (P_1) is double the value of the reference power (P_0) then equation (5.1) gives:

$$dB = 10 \log_{10} \frac{2}{1} = 3 \quad (5.2)$$

3 dB is used in engineering to describe a measurement that is twice as much as a reference quantity. If the reference power is measured in milliwatt then the ratio takes the unit of dBm.

The calibration of the reflected power is done through connecting the power diode to an RF generator. The generator gives RF signals with different power levels in [dBm], which is measured using the power diode to determine the conversion curve between decibel and volts for this diode. The readings are represented in the results chapter along with the relation between the voltage and the power.

5.2.2. Argon Flow

The mass flow controller unit 5850TR (figure 4.37) is controlled by converting flow rate level 0-20 L/min to voltage control signals 0-5 V [145]. However, this mapping between flow rate and voltage signal is not linear, so a manual mapping between the two had to be done to assign a voltage output signal for every flow rate value in the range 0-2 L/min as this is the range our system works in and there was no need to calibrate more values. These values are shown in figures 5.2-5.5. The argon flow control slide in the programme front panel is calibrated according to these values, which in turn sends the mapped voltage control signals to the unit.

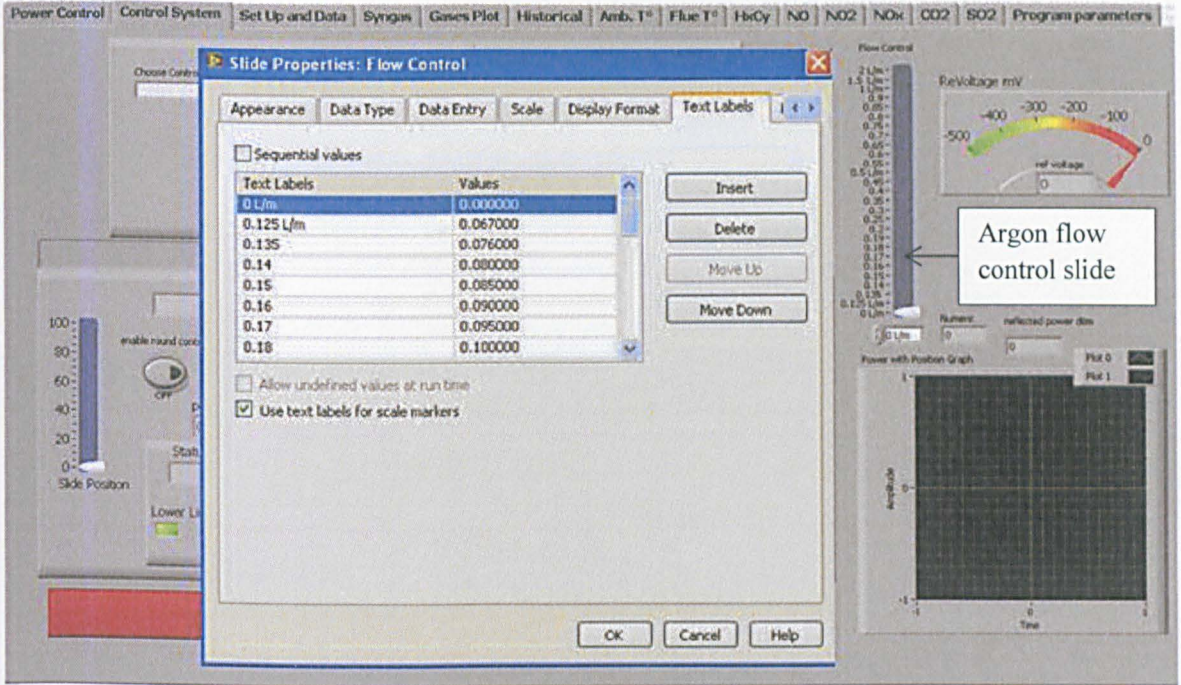


Figure 5.2: Flow rate to voltage conversion value range 1.

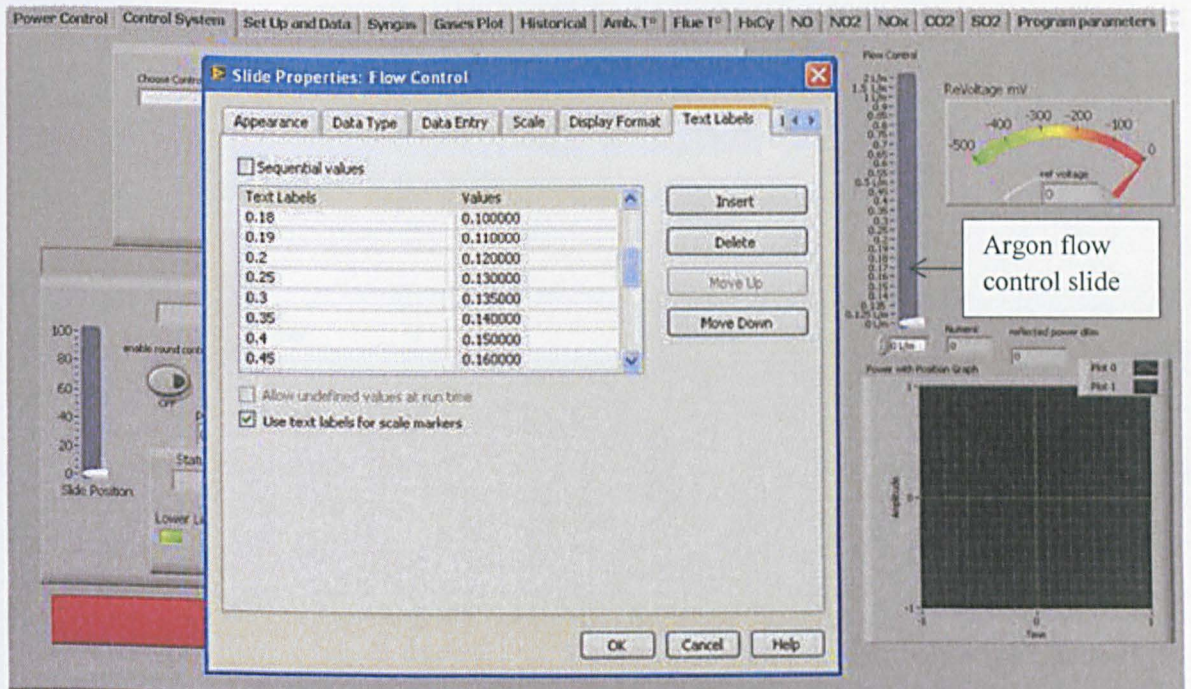


Figure 5.3: Flow rate to voltage conversion value range 2.

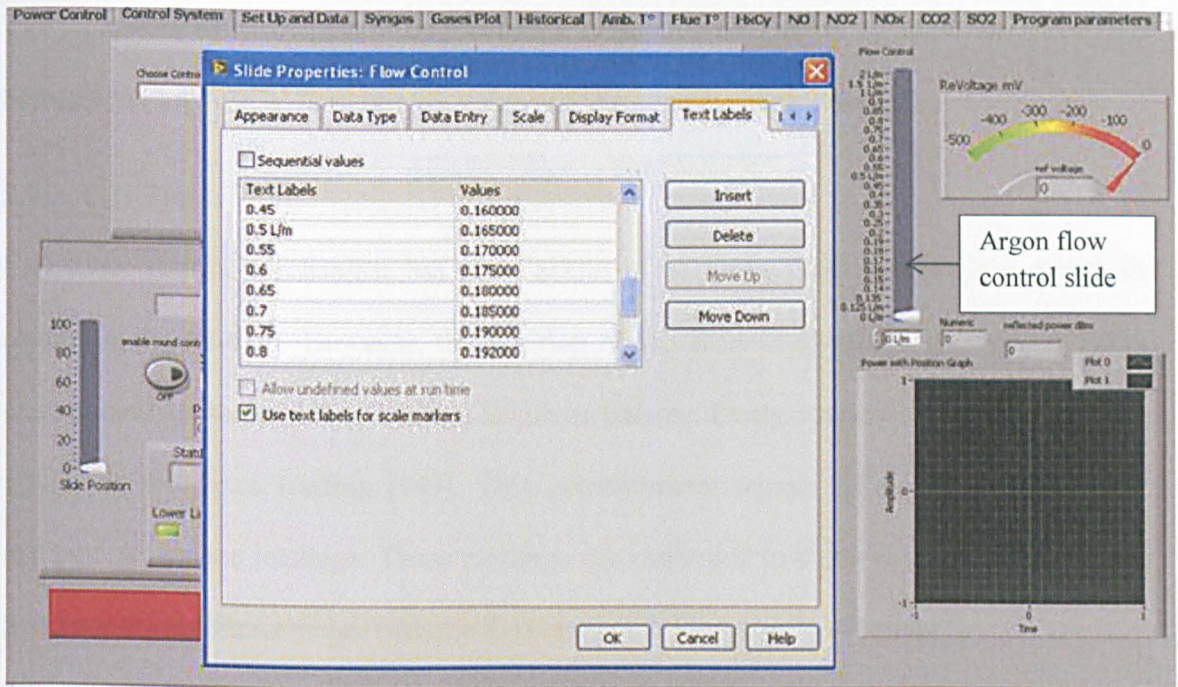


Figure 5.4: Flow rate to voltage conversion value range 3.

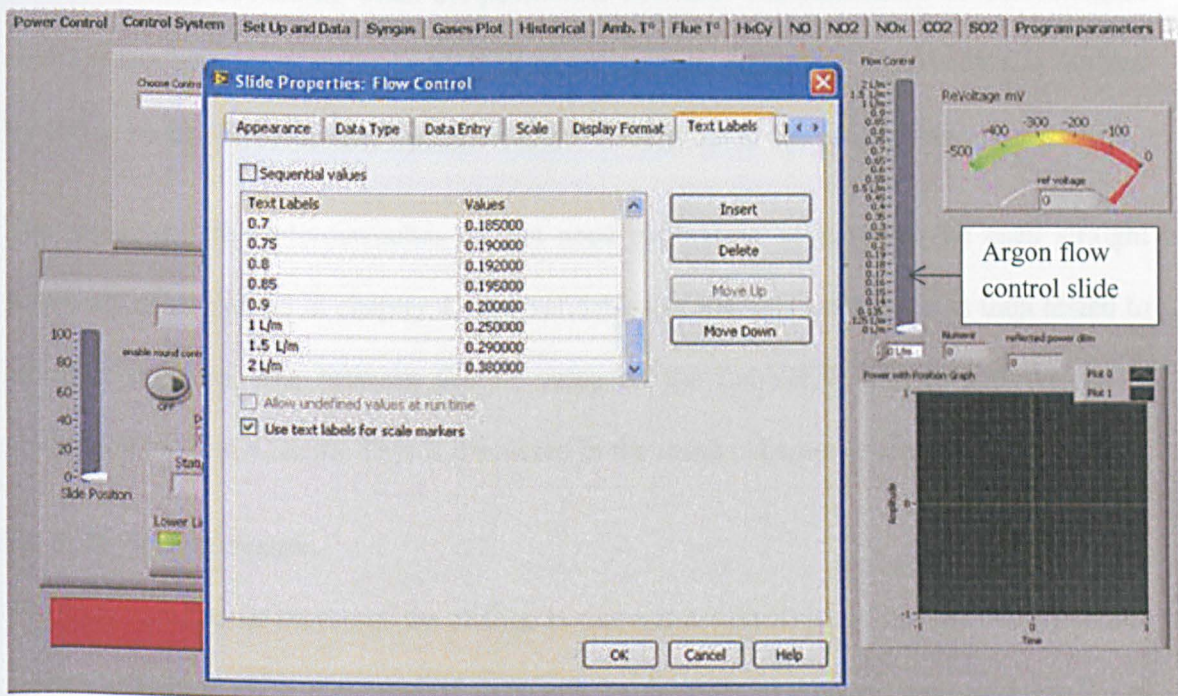


Figure 5.5: Flow rate to voltage conversion value range 4.

The validation of this mapping is examined in the results chapter to show the error rate between the LabVIEW flow rate set value and the actual readout value.

5.2.3. E-H Tuner

E-H tuner control mechanism has been achieved by using three instruments shown in chapter 4, figure 4.40. However, the position of the arms is identified by using a linear slide potentiometer 0-10000 Ω with a length of 100mm. Every 1mm in length change maps 100 Ω in resistance reading [147]. This potentiometer moves up and down and gives different resistance readings. These readings are calibrated to show the arm's position by mapping the resistance range with the E-H arms position range 0-100 mm.

The potentiometer is attached on the arm shafts to give 0 Ω reading when the position is 0mm and 10000 Ω reading when the position is 100 mm. The calibration of the resistance readings can be noticed in the LabVIEW block diagram appended. The reading is divided by 100 to be displayed as arm's position in the front panel of the programme.

The motor and the microswitches do not need calibration as they can be used straight forwardly as explained in chapter 4. The validation of the E-H calibration is then tested to calculate the error rate between the set value on the LabVIEW control and the actual reading on the arm's shafts. This is discussed in the results chapter (chapter 6).

5.2.4. Hydrogen Sensor

The hydrogen sensor measures the change in thermal conductivity of the gas measured and sends current signals in the range of 4-20 mA for the full range of gas concentration 0-100 % [151]. This gives a change of 0.16 mA for every 1% change in the gas measured.

The current reading is measured using NI 9219 DAQ which gives current reading to the LabVIEW program in ampere unit.

The calibration of the signals sent from the hydrogen sensor to represent gas percentage can be done by applying equation 5.3 to the reading

$$Y = \frac{(X \times 1000) - 4}{0.16} \quad (5.3)$$

Where Y is the gas percentage, X is current reading in ampere, which is converted to mA by multiplying by 1000 then subtracted by 4 to suite the range of 4-20 mA.

Equation (5.3) is realised in LabVIEW by following the block diagram shown in figure 5.6. An example of 20 mA reading (0.02 A) is illustrated in red in the same figure which represents 100 % gas concentration.

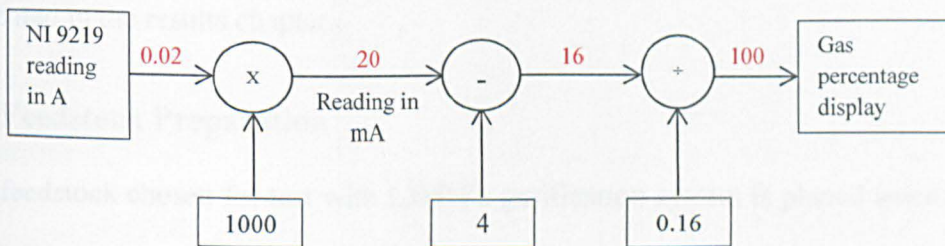


Figure 5.6: Hydrogen sensor calibration block diagram.

However, as mentioned in chapter 4, the hydrogen is measured using the K1550 sensor, which is a non-specific gas sensor. It gives the measurements of one gas (H_2 in this case) with the presence of a background gas (nitrogen). Nevertheless, the background gas in the gasification chamber is not only composed of nitrogen. It is a mixture of argon, nitrogen, and the outcome gases from the gasification process, which include carbon monoxide, carbon dioxide, methane, and other hydrocarbon chains. These gases will affect the H_2 readings and an error rate should be calculated. In order to do so, the manufacturers of the

sensor have been contacted and they have advised the following error rate for the background gas:

Table 5.1: K1550 error rates

Background gas	H ₂ reading error %
Argon (5%)	-0.36
Methane (5%)	+0.46
Carbon monoxide (5%)	-0.05
Carbon dioxide (5%)	-0.35

However, it is not known to us the exact percentage of argon inside the chamber, thus experiments need to be done to specify hydrogen reading error rate accurately. This will be presented in the results chapter.

5.3. Feedstock Preparation

The feedstock chosen for test with LJMU's gasification system is planed smoothed timber (3000×70×44) mm which is bought from a department DIY store in Liverpool figure 5.7.

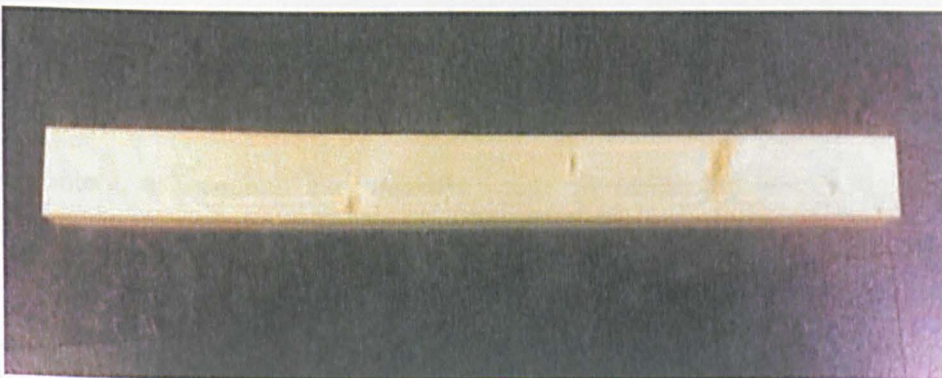
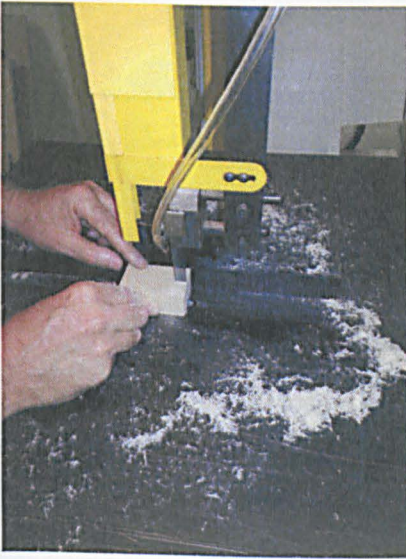


Figure 5.7: Planed smooth timber

This timber was chosen as it is widely available, easy to cut and affordable. As the samples need to be gasified inside the gasification chamber, they need to be cut to a suitable size in order to fit inside the crucible. Samples are cut to different sizes representing different mass of approximately 30g, 15g and 10g, and then are stored in plastic zip bags for labelling and environment control. Figure 5.8-a shows sample cutting and figure 5.8-b shows the different size stored samples.



(a) Samples cutting.



(b): Samples storing.

Figure 5.8: Samples preparation.

5.3.1. Samples Properties Determination

Biomass, as explained in chapter 2 section 2.6, has some key properties which define it. Moisture content, ash content and calorific value are calculated before the gasification process takes place.

Moisture content can be calculated according to equation 2.11 where the mass of the samples are recorded then samples are dried using a laboratory oven shown in figure 5.9 at

100° C. Ash content is calculated according to equation 2.12 by recording samples' weight after the gasification process takes place. Calorific value on the other hand can be calculated by using a bomb calorimeter device.

The calculations of these parameters are shown in the result chapter 6.

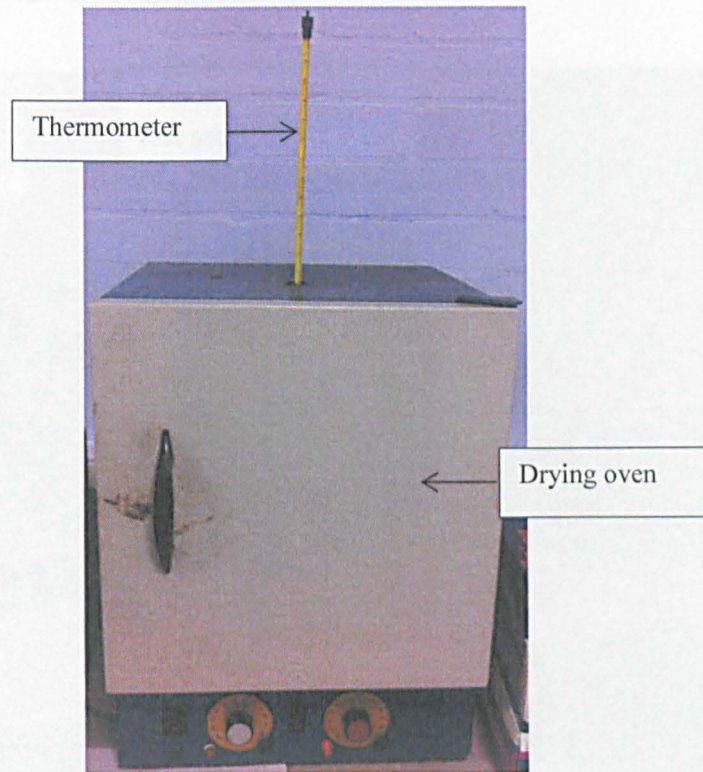


Figure 5.9: Drying oven.

5.3.2. Samples Analysis Using Microwave Sensor

Determining the moisture content, ash content and calorific value is good practice to compare this work with other gasification studies. However, for the purpose of repeatability of this work, another test should be done to determine the similarity between the timber feedstock used for the different experiments. This test is aimed to study the microwave absorption within the feedstock. The absorption characteristics might differ

between two samples even if they were cut from the same log as wood contains knots along with other impurities or defects. Thus studying the microwave absorption can be a method to determine feedstock's homogeneity.

Marconi microwave test set 6200 and a horn antenna with a similar dimension to the feedstock are used for this study (figure 5.10).

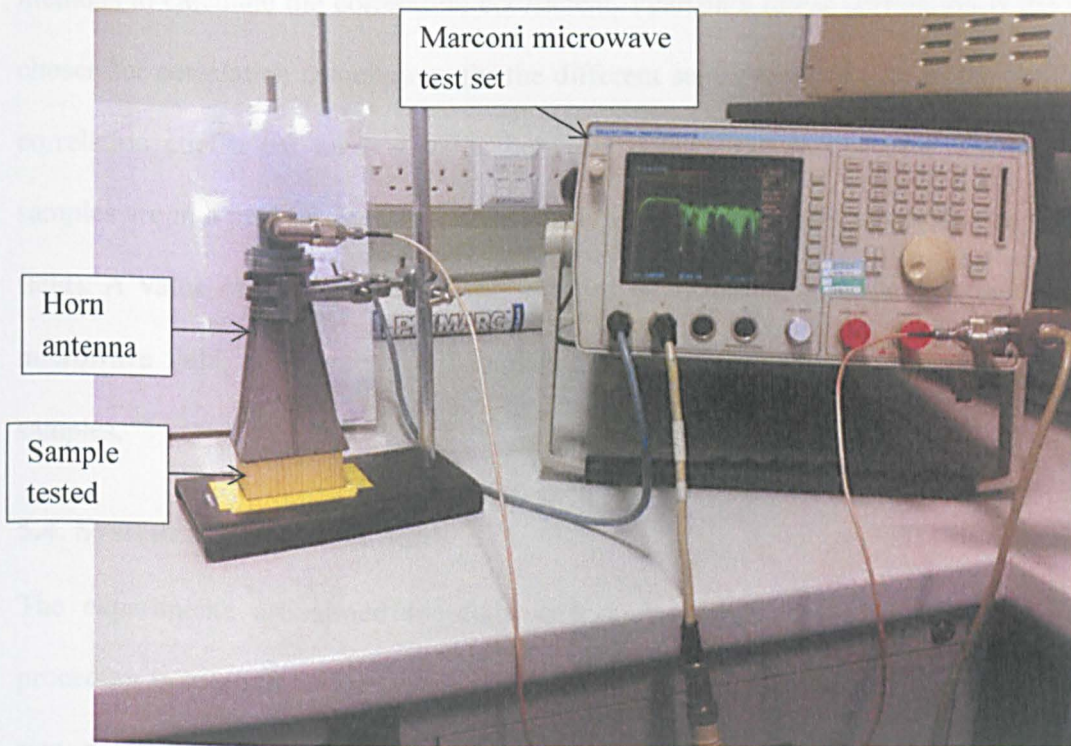


Figure 5.10: Samples microwave analysis setup.

Microwave signals are sent to the horn antenna and the reflected power is recorded (S_{21} parameter). The characteristic curve of the reflected power for each sample is stored and a correlation formula is applied to compare between different samples.

Samples with a correlation coefficient greater than 0.9, are chosen for the gasification experiments. Microwave analysis and the correlation study are presented in the result chapter.

Correlation is the measure of the degree of relationship between different variables under test. This measure is realised by the correlation coefficient [155]. There are different methods to calculate the correlation coefficient. Pearson's linear correlation is the method chosen for correlation calculations for the different samples under test. In this method, the correlation coefficient takes a value between -1 and +1. A +1 value implies that the samples are in a perfect linear relation (i.e. samples behaves similarly with the microwave field). A value of -1 implies that the samples have totally opposite behaviour with the microwave field, and a value of 0 implies that there is no linear correlation between the samples.

5.4. System Experimentation

The experiments are aimed to study and analyse the behaviour of the gasification procedure in relation to the system's various parameters such as sample size, argon flow rate, pressure, power level and sample moisture. The benefit of such experiments is to determine the optimum values of the system parameters which give a better syngas production.

Each set of experiment is done by changing one parameter and fixing the rest. For example testing pressure effects on gasification is done by changing the pressure level in a certain range while setting sample size, argon flow rate, power and moisture on a certain value.

After specifying system best parameters' values, the effect of improvement through the control algorithm is studied.

The initial experiment is analysing the temperature of the plasma burst to give a temperature profile with different power levels and argon flow rates.

CO and H₂ levels for each set of experiments are measured through the gas sensors. However, Quintox gas analyser has a limit for high CO levels of 170000 ppm. To overcome this limitation, different sample sizes are gasified with different power levels, between 400- 1000 watts, for the determination of the size and power within which the gasification process does not produce saturated levels of CO. By doing this, the improvement effects of the gasification procedure can be shown and analysed.

In addition to wood pieces, palm date seed samples were gasified for comparison.

5.4.1. Plasma Temperature Profile

Plasma temperature is affected by two main parameters; power level and argon flow rate. Temperature dependency on these parameters is proven experimentally and can be justified according to plasma literature in chapter 3, section 3.6.

The Temperature sensor is placed on the crucible inside the gasification chamber throughout this experiment, and temperature readings are recorded via the LabVIEW control program. Each temperature reading is taken at a fixed power level value while changing argon flow rate between 0.25-1 L/min. The experiment is repeated for power values in the range of 400-1000 watts

The power range is chosen after experimenting the minimum power which makes the plasma burst powerful enough to reach to the crucible where the sample will be placed.

Argon flow rate range is experimentally chosen as flow rates under 0.25 L/min result in a weak plasma burst which does not reach the sample's surface in the crucible. This is because of the lack of argon molecules interacting with the microwave power. On the other hand, flow rates greater than 1 L/min results in an excess in argon molecules. The microwave power source limit of 1000 watts does not allow the ionisation of the fast passing argon molecules which also result in a weak plasma burst.

5.4.2. Quintox Limitation

Carbon monoxide quantities exceeding 170000 ppm limit will saturate the sensor and a straight line presentation of CO percentage is shown in measurements' figures. Two sets of experiments are needed in order to tackle this problem to decide the sample size and the operational power for the gasification procedure.

5.4.2.1. Sample Size

In this set of experiments, sample size is put under test. Samples in the range of 30g are gasified initially with a power level range of 400-1000 watts. Other system parameters are fixed. Argon flow rate is set on 0.5 L/min, pressure is set on 50 mbar and feedstock has not been dried.

After this initial test with 30g samples, another similar test with smaller samples is under study. 10g timber blocks are gasified with the same power range. The outcome of this experiment helps to specify the suitable sample size which will not give CO saturation levels.

5.4.2.2. Power Choice

The sample size is selected from the previous test. However, further investigations are needed to select a power level that will not result in high CO levels saturating the sensor.

At this point, and from the previous experiment of selecting the sample's size, the analysis of CO production with different power levels (400 watts to 1000 watts) is known. From this analysis, a smaller power range is chosen for a further study with different argon flow rates.

From this study, the power level that does not give CO saturation level with the full argon flow rate can be selected to commence the analysis of the gasification procedure.

5.4.3. Pressure Effects on Gasification Process

This study is aimed to analyse syngas production with different pressure levels inside the gasification chamber. Sample size and power levels are chosen according to Quintox limitation study which does not give saturation levels to be able to compare results. Argon flow rate is set to 0.5 L/min, and the sample is not dried.

Pressure is studied for six samples where it is manually set to a fixed value for each study case (0-50-100-150-200-250 mbar). The pressure level inside the chamber is maintained at the required value by two means. Pressure valve release is used to reduce high pressure levels, while nitrogen gas is pumped into the chamber to raise the pressure level if low.

For repeatability reasons, pressure cases are repeated four different times and experiment error rates are recorded. This study is presented and discussed in the results chapter.

5.4.4. Argon Flow Rate Effects on Gasification Process

Similar to pressure study, the argon flow rate study is aimed to analyse the effects of argon flow on syngas production. The experiment's conditions are the same as the pressure experiment, but the pressure is fixed at 50 mbar where the flow is changed between four values (0.25-0.5-0.75-1 L/min).

For repeatability reasons, flow rate cases are repeated four times and experiment's error rates are recorded. This study is presented and discussed in the result chapter.

5.4.5. Sample Moisture Effects on Gasification Process

This study is aimed to see the difference in syngas production with different moisture content in the samples. Six different case studies are taken into consideration in this experiment. The experiment's conditions are again the same as the previous tests but both pressure level and flow rate are set at 50 mbar and 0.5 L/min respectively.

The first case is the gasification of the sample without any drying of the sample taking place. The second test is the gasification of the sample after soaking it in water. The four remaining cases are done after drying the samples using the laboratory oven for 1, 2, 3, and 4 hours.

5.4.6. Improvements of the Gasification Process

At this point, system parameters are all studied and the best values giving higher syngas production are known. This experiment is aimed to prove the use and benefit of the improvements of the system through the control algorithm explained in chapter 4.

The gasification system experiment conditions are set according to the previous analysis and the gasification system is run but with the automatically controlled algorithm applied on the system.

Here as well, this automatically controlled gasification process is repeated four different times to prove the repeatability and the result is shown in chapter 6.

5.4.7. Argon Plasma versus Helium Plasma

The plasma generated in this project is argon plasma. Argon has been chosen because it is commonly and commercially used for plasma applications, it is widely available and it is cheap in comparison with other noble gases (i.e. helium or neon). However, and for experimental and comparison reasons, helium is tested as the plasma gas. Helium has better properties than argon. It has a higher ionisation potential (24.59 eV compared with 15.76 eV for argon) [156]. This means helium plasma is more efficient than argon plasma. Moreover, helium has a higher thermal conductivity compared to argon [157], which is beneficial for heat transfer from the plasma to the sample. However, helium is much more expensive than argon which makes argon the first option for plasma generation.

The timber sample is gasified using helium plasma to compare CO yields against argon plasma at specified systems' parameters that give higher syngas production according to the previous tests.

5.4.8. Different Feedstock Study

The sample used in all of the experiments above is the same piece of wood. However, wood is a valuable material and supplying wood will obviously mean bringing trees down and affecting the green scenery of our earth.

The samples used for this section's experiments are considered as waste; disposal of such waste could be expensive and affect the earth's atmosphere. Gasification as aforementioned is examined in this project's scope to create energy from cheap and sustainable resources.

Palm dates are produced in large quantities annually in the Middle East and North Africa generally. Date seeds consist of many chemical compositions such as: protein 5.59%, oil 10.19%, total carbohydrate 83.1%, and ash (1.15%). The possibility of using this waste as a source for generating a clean and renewable energy is tested using microwave plasma gasification technology. 10 g samples of palm date seeds (figure 5.11) are used to compare with the timber samples.



Figure 5.11: Palm date seeds samples.

5.5. Summary

This chapter explained the methods taken for the calibration of the instruments used to improve the gasification procedure. The calibration includes; power level, reflected power, argon flow rate controller, E-H tuner, and hydrogen sensor. The calibration is done by conditioning the electric signals to/from the instruments to map the change in the

parameters they control. The validation of this calibration is presented in the results chapter.

Sample preparation is the next step taken in order to start the gasification procedure analysis. The timber feedstock was cut to different sizes to be suitable to place on the crucible inside the gasification chamber. The key parameters of the feedstock such as moisture content, ash content and calorific value are considered in this study.

Systems experimentation methodology is also discussed in this chapter. The experiments are divided into eight different sections. In each section a different parameter was under study and the result of this study will be shown in the results chapter

Finally, this chapter illustrates the use of palm date seeds as a substitute for the timber samples to evaluate the possibility of turning waste into energy.

Chapter Six: Results and Discussion

6.1. Introduction

The importance of the work done in this project can be realised from looking at the results achieved. These results are shown in this chapter and follow the same order of the experiment methodology.

The chapter starts with the validation of the system's control instruments calibration. These instruments include; the power control, argon flow control, E-H tuner control, and hydrogen sensor. After calibration validation, this chapter shows the results of feedstock preparation and discusses the system experimentation for the various parameters.

6.2. System Calibration

6.2.1. Power

The mapping of the power is explained in chapter 5 section 5.2.1. However, an experiment is needed to make sure that the power set thorough LabVIEW control program and the actual readout from the power source are the same. In this experiment, a power level is set from LabVIEW control program, and then compared with the power source output.

Tale 6.1 shows that there is no difference between LabVIEW and the readout power output. This is because of the power source remote control capability and the mapping linearity with the voltage signal (as explained in 5.2.1).

Table 6.1: Power calibration experiment.

LabVIEW Power Set (Watt)	Readout Power (Watt)	Error
0	0	0
100	100	0
200	200	0
300	300	0
400	400	0
500	500	0
600	600	0
700	700	0
800	800	0
900	900	0
1000	1000	0

The second part of the power calibration is the calibration of the reflected power. This includes converting the reflected measurements from mV to dBm. This can be experimentally achieved by connecting the power diode to a power source. The power source is set on different power levels in dBm which is measured with the power diode in mV. The relation between voltage and power is represented in figure 6.1 in a logarithmic scale.

This relation between voltage and power can be put in a function relation presented in equation (6.1) where in X is the input in mV and Y is the output in dBm:

$$Y = \frac{-357.642 + 75X^{0.295}}{9.99 + X^{0.295}} \quad (6.1)$$

This function is used in LabVIEW block diagram to show the reflected power in dBm unit.

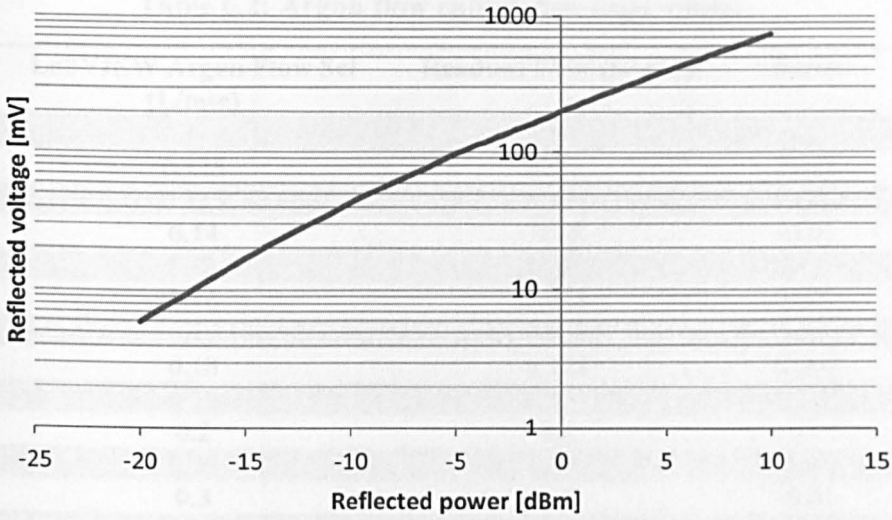


Figure 6.1: Voltage to decibel conversion.

6.2.2. Argon Flow

Argon flow controller calibration experiment is aimed to validate the calibration of the controller and calculate the error rate between the set values and the actual values.

Table 6.2 shows a number of argon flow values set through LabVIEW control program and the actual flow rate value measured.

According to the calibration table below, the error for flow rate is between -0.1 and 0.01. The flow rate values that are used in our gasification process are 0.25-0.5-0.75 and 1 L/min. At these flow rates the maximum error is small and can be neglected as different in the gas amount has in that range has no effect on plasma burst. The error rate shown in the table is acceptable and the flow rate controller can be used accurately with LabVIEW control program.

Table 6.2: Argon flow calibration experiment.

LabVIEW Argon Flow Set (L/min)	Readout Flow (L/min)	Error
0	0	0
0.125	0.12	0.005
0.135	0.132	0.003
0.14	0.15	-0.01
0.15	0.152	-0.002
0.16	0.158	0.002
0.17	0.171	-0.001
0.18	0.178	0.002
0.19	0.191	-0.001
0.2	0.2	0
0.25	0.24	0.01
0.3	0.31	-0.01
0.35	0.35	0
0.4	0.41	-0.01
0.45	0.46	-0.01
0.5	0.51	-0.01
0.55	0.54	0.01
0.6	0.62	-0.02
0.65	0.67	-0.02
0.7	0.72	-0.02
0.75	0.78	-0.03
0.8	0.84	-0.04
0.85	0.88	-0.03
0.9	0.91	-0.01
0.95	0.98	-0.03
1	1.1	-0.1
1.5	1.6	-0.1
2	2.1	-0.1

6.2.3. E-H Tuner

E-H tuner arm positions are controlled by LabVIEW. To make sure that the actual arm position is the same as the set one on LabVIEW, a validation experiment has to be done. This experiment is divided into two sections as table 6.3 show. Firstly the arm is set on 0 mm position and taken up to 100 mm with 5mm increments. Then the position is setdown back to 0 mm.

Table 6.3: E-H tuner calibration experiment.

LabVIEW Position setup (mm)	Readout E-arm Position (mm)	Readout H-arm Position (mm)	LabVIEW Position setdown (mm)	Readout E-arm Position (mm)	Readout H-arm Position (mm)
0	0	0	100	99.7	99.9
5	5.2	5.1	95	94.6	94.4
10	10.3	10.2	90	89.7	89.8
15	15.4	15.3	85	84.8	84.4
20	20.1	20.1	80	79.8	79.5
25	25.3	25.4	75	74.5	74.7
30	30.2	30.2	70	69.7	69.6
35	35.2	35.4	65	64.6	64.8
40	40.3	40.1	60	59.8	59.4
45	45.1	45.3	55	54.7	54.5
50	50.4	50.1	50	49.8	49.6
55	55.3	55.2	45	44.8	44.7
60	60.2	60	40	39.6	39.6
65	65.3	65.3	35	34.7	34.6
70	70.2	70.2	30	29.7	29.4
75	75.3	75.4	25	24.8	24.8
80	80.4	80.1	20	19.7	19.6
85	85.3	85.2	15	14.8	14.8
90	90.2	90.3	10	9.8	9.7
95	95.2	95.1	5	4.7	4.2
100	99.7	99.9	0	0.2	0.2

This arm position change is applied on both E and H arms and the actual position of the arm shaft can be seen on the arms. The actual arm position (readout position) is read from the display on the arm shafts and a note of the position is taken and compared with the LabVIEW set one to calculate the error.

Table 6.3 shows the error for both arms when the position is setup and then setdown. The maximum difference between LabVIEW position and actual position is 0.8mm.

6.2.4. Hydrogen Sensor

Hydrogen sensor is tested for different gasification situations without placing a sample inside the crucible to study the background gases effects on H₂ measurements.

Table 6.4 shows the four states that the gasification chamber can be in. When only nitrogen is present in the chamber then the sensor picks up 0 % hydrogen reading. This verifies the sensor settings of measuring hydrogen in nitrogen background gas. The next chamber states are flooding it with argon and then mixing argon and nitrogen to set the environment for plasma striking.

When the plasma is struck without the presence of the feedstock, K1550 picks up -2.5% hydrogen. This value should be added to all of the gasification's hydrogen measurements to compensate for this error.

Table 6.4: Hydrogen sensor calibration experiment.

Gasification Chamber State	H₂ percentage (%)
Nitrogen flooded	0
Argon flooded	-7
Argon and nitrogen mix	-5
Plasma running	-2.5

6.3. Feedstock Preparation

6.3.1. Samples Properties Determination

For the purpose of defining the moisture content and the ash content of the samples used. A number of random samples were selected as in table 6.5. The sample weight has been measured first. Using the laboratory oven, samples have been dried and their weight after drying is taken. Finally, we gasified the samples and measured their weight after gasification. After recording the original, dried and after gasification weights, we can apply equations 2.11 and 2.12 in chapter 2 section 2.7 to determine the moisture and the ash content of the timber.

Table 6.5: Moisture and ash content calculation.

Sample Number	Original mass (g)	Dried mass (g)	Mass after gasification (g)	Moisture Content (%)	Ash Content (%)
1	32.7	29.13	12.7	12.2	44.2
2	31.42	27.8	11.27	13	41.2
3	7.74	6.78	4.53	14.1	47.1
4	8.65	7.71	3.53	12.1	46.4
5	15.27	13.62	5.82	12.1	43.3

The moisture content calculated for the samples was between 12 and 14 %. To make sure that the calculations are right, a moisture meter with a measuring range of 6-44 % for wood and $\pm 1\%$ accuracy was used [158]. Figure 6.2 shows the measurement device of the sample's moisture content. Using this meter has confirmed the calculations as the moisture content according to the meter was between 12 and 14 %.

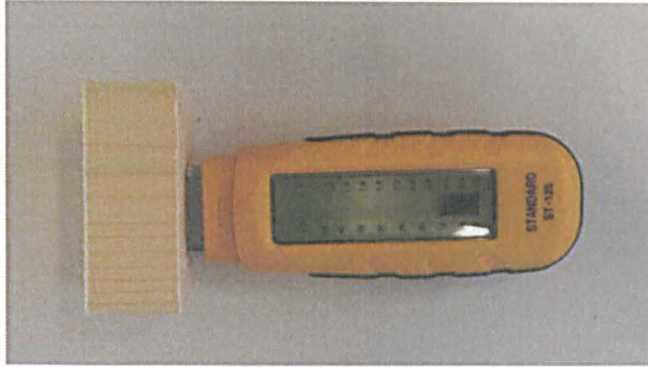


Figure 6.2: Moisture meter.

The calorific value of the samples was taken from a previous study of wood fuels done by the Italian Agriforestry Energy Association [159]. This study analyses the properties of a vast number of wood types. For planed smooth timber, the calorific value is 19 MJ/Kg.

6.3.2. Sample Analysis Using Microwave Sensor

The analysis of the similarity between the feedstock samples is done through microwave absorption study using Marconi test set and a horn antenna (see section 5.3.2). The Marconi device has a frequency range of 10 MHz to 20 GHz. Thus a specific range (the resonance frequency of the horn antenna) should be selected first to commence the feedstock microwave analysis. To do so, a full range frequency display is tested without the presence of the feedstock under the horn antenna (see figure 5.10 for experiment setup). From this full range analysis, a specific frequency range is chosen to analyse the feedstock. Figure 6.3 illustrates this analysis where we can notice the reflected power peaks. The first two peaks are chosen to do the analysis in their range. This range is between 7000 MHz and 8000 MHz.

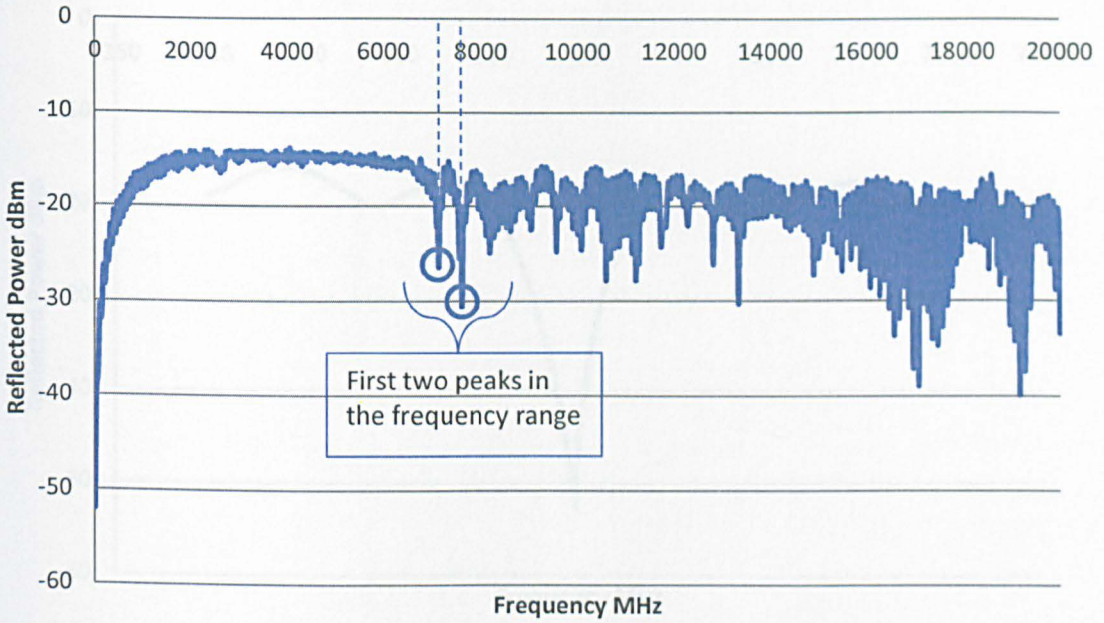


Figure 6.3: Full range frequency analysis.

Figure 6.4 shows the microwave behaviour within the frequency range selected, and figure 6.5 shows the characteristic curve for microwave absorption in the feedstock.

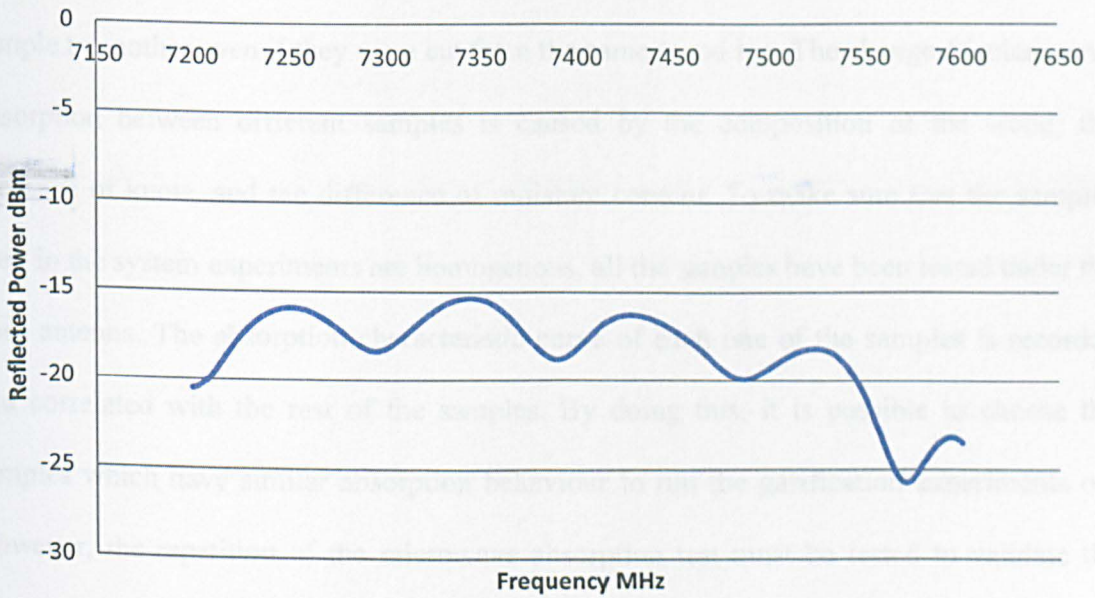


Figure 6.4: Microwave analysis for the selected frequency range.

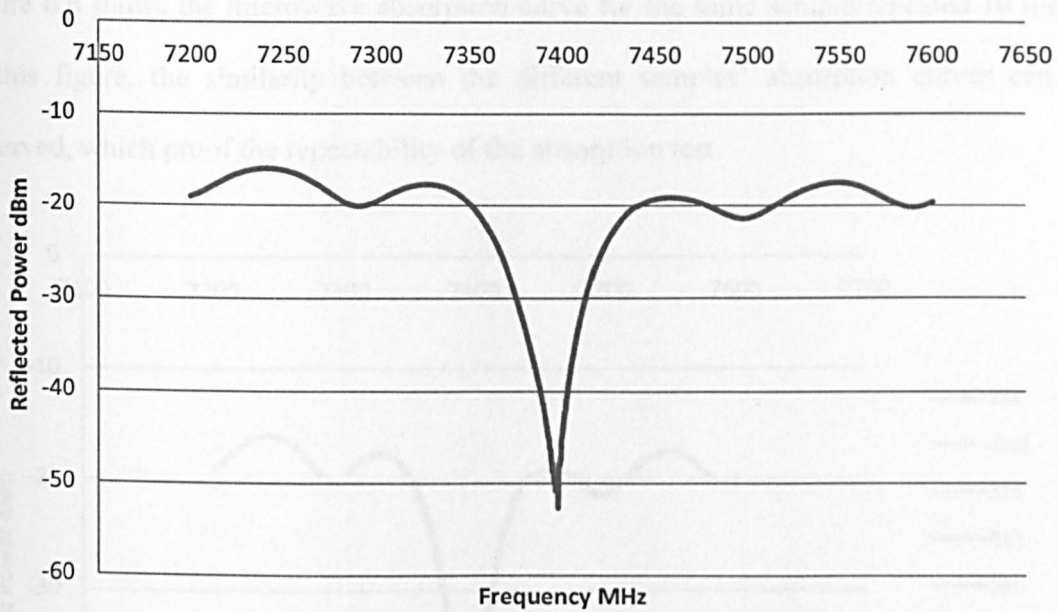


Figure 6.5: Microwave behaviour with the feedstock.

From figure 6.5 it can be noticed that the microwave signal reflected when the sample is under the horn antenna is weaker than the signal reflected when there is no feedstock. This is because of the absorption of the signal inside the sample, which might change from one sample to another even if they were cut from the same wood log. The change of microwave absorption between different samples is caused by the composition of the wood, the presence of knots, and the difference of moisture content. To make sure that the samples used in the system experiments are homogenous, all the samples have been tested under the horn antenna. The absorption characteristic curve of each one of the samples is recorded and correlated with the rest of the samples. By doing this, it is possible to choose the samples which have similar absorption behaviour to run the gasification experiments on. However, the repetition of the microwave absorption test must be tested to validate the readings. This is done by repeating the experiment 10 different times for the same sample and compares the absorption curve then correlates the readings.

Figure 6.6 shows the microwave absorption curve for the same sample repeated 10 times. In this figure, the similarity between the different samples' absorption curves can be observed, which proof the repeatability of the absorption test.

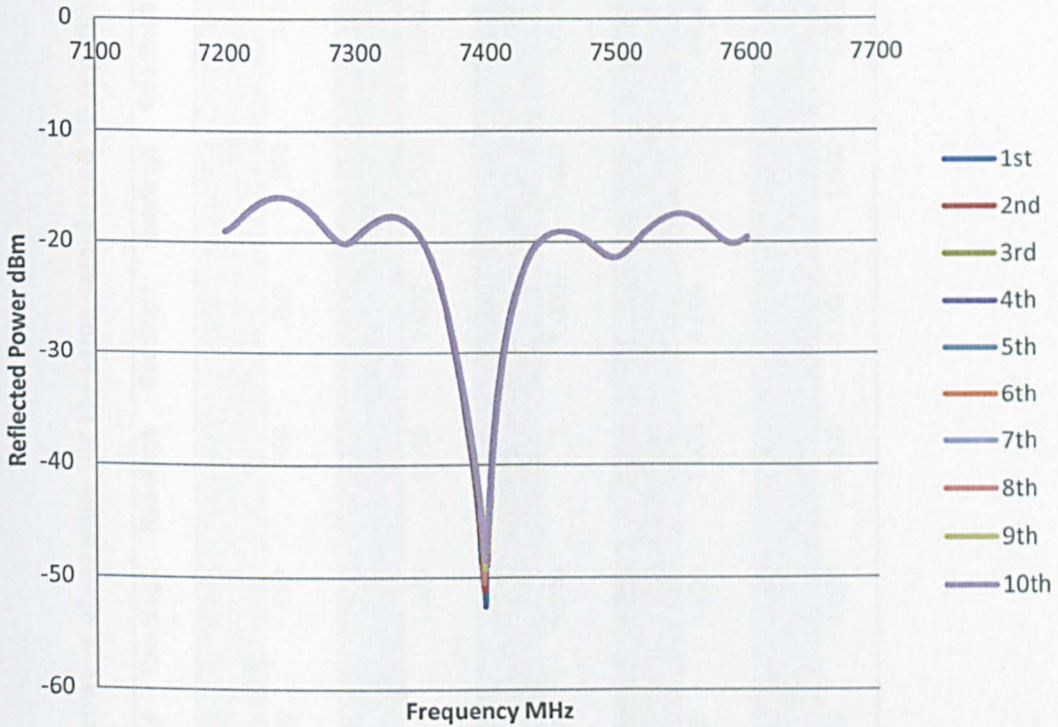


Figure 6.6: Microwave absorption curve for 10 repetitions.

These curves are correlated and table 6.6 shows the correlation factors of each pair of readings. This factor is between 0.99 and 1 which represent a very high similarity in the test readings.

Table 6.6: Correlation factors for microwave absorption for the same sample and 10 repetitions.

	Reading1	Reading2	Reading3	Reading4	Reading5	Reading6	Reading7	Reading8	Reading9	Reading10
Reading1	1	.999	.998	.998	.998	.997	.998	.998	.998	.997
Reading2	.999	1	1.000	1.000	.999	.999	.999	.999	.999	.999
Reading3	.998	1.000	1	1.000	1.000	.999	1.000	1.000	1.000	1.000
Reading4	.998	1.000	1.000	1	1.000	1.000	1.000	1.000	1.000	1.000
Reading5	.998	.999	1.000	1.000	1	1.000	1.000	1.000	1.000	1.000
Reading6	.997	.999	.999	1.000	1.000	1	1.000	1.000	1.000	1.000
Reading7	.998	.999	1.000	1.000	1.000	1.000	1	1.000	1.000	1.000
Reading8	.998	.999	1.000	1.000	1.000	1.000	1.000	1	1.000	1.000
Reading9	.998	.999	1.000	1.000	1.000	1.000	1.000	1.000	1	1.000
Reading10	.997	.999	1.000	1.000	1.000	1.000	1.000	1.000	1.000	1

Microwave absorption characteristics test is applied on all of the samples that are going to be used in the system experiments. Only the samples which have correlation factor equal to or greater than 0.98 are chosen for the experiments. Figure 6.7 shows the microwave absorption curves for 10 random samples. It is noticed that these samples have different reaction with microwave power; some of the samples absorb microwave power more than other samples. This is because of the different moisture level each of the samples might have, or because of existence of knots inside the sample.

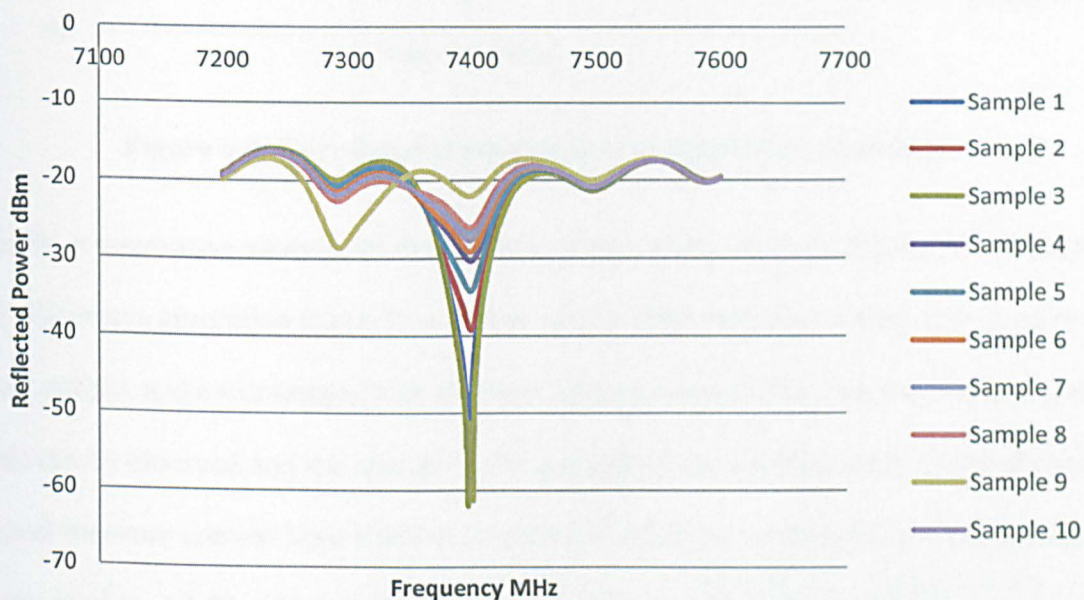


Figure 6.7: Microwave absorption characteristic curve.

Figure 6.8 shows 9 similar samples and one different. Sample 1 has a totally different behaviour from the rest of the samples, 2 to 10. In this case for example, samples 2 to 10 are chosen for the system experiments as they will give repeatable study cases for the experiments.

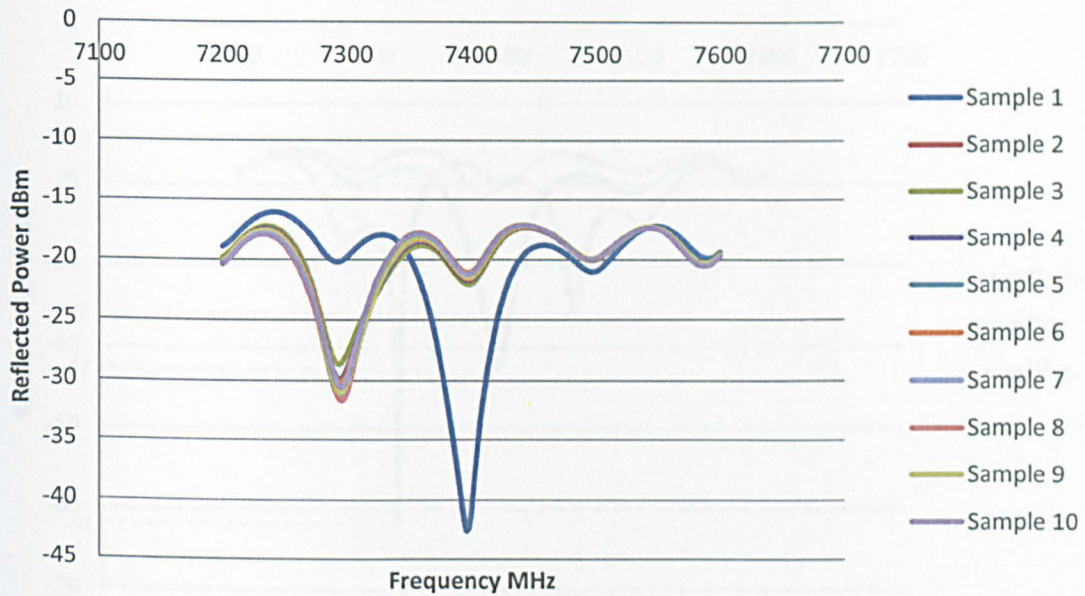


Figure 6.8: Correlated samples curve vs. uncorrelated sample.

Finally, a microwave analysis of the different sample states is done. Figure 6.9 illustrates the microwave absorption curve for a sample with normal moisture content (14%), an oven dried sample, and a wet sample with moisture content around 35%. The shift in the curve's peak can be observed and the change in the strength of the reflected power. Samples with normal moisture content have a reflected power of -42 dBm, while dried samples reflected power rises to -37 dBm. On the other hand, wet samples reflected power drops down to -61 dBm. This means that dry samples reflect more power than both normal and wet samples.

The effect of moisture is studied in the system experiments to specify the sample state which gives higher syngas production.

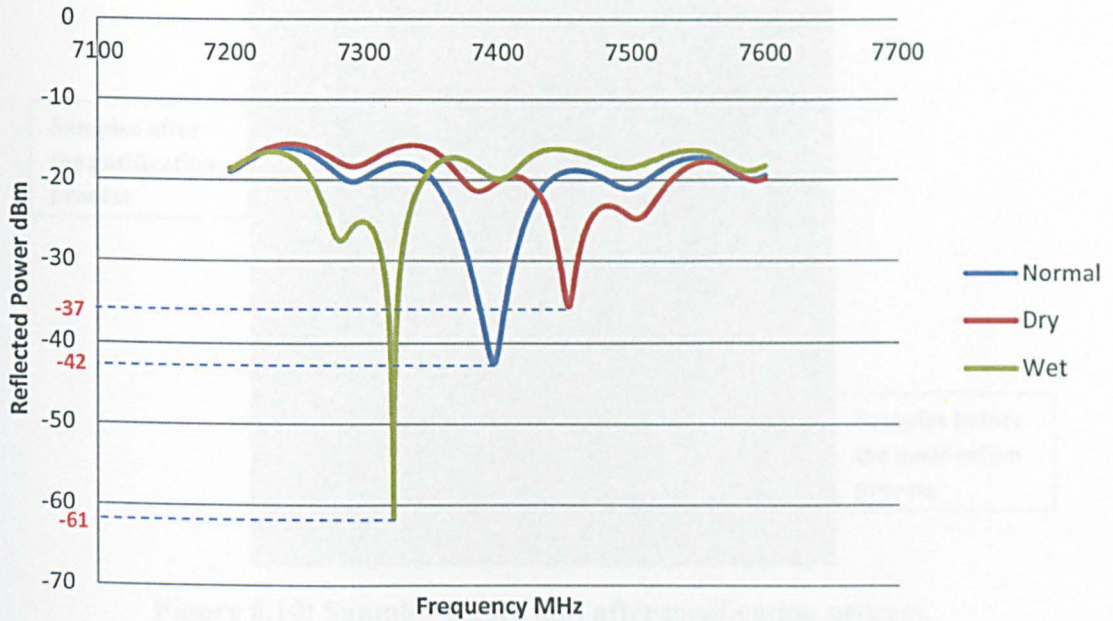


Figure 6.9: The three different sample states absorption curve.

6.4. System Experimentation

System experimentations are done with the timber samples prepared and analysed before. Figure 6.10 shows the different sizes of the samples before and after the gasification process. It is noticed from the figure the shrinkage of the samples. However, the samples after gasification remain in one solid piece rather than turning into ash. The black carbon like colour is due to the lack of oxygen when burning the feedstock (i.e. gasifying it). These residues can be used in fire places for example for residential heating.



Figure 6.10: Samples before and after gasification process.

6.4.1. Plasma Temperature Profile

The first analysis of the microwave plasma gasification system is the study of the plasma's temperature. The temperature is dependent on two factors; power and argon flow rate. Figure 6.11 illustrates the plasma temperature on the crucible in the gasification chamber (i.e. where the samples are placed). The temperature curve is measured for each argon flow rate with different power levels. It can be noted that at 0.25 L/min argon flow rate temperature behaviour is out of trend. For power levels equal to or less than 600 watt, the plasma burst for 0.25 L/min argon is not strong enough and it does not reach the crucible, thus its temperature is lower than the other flow rates. However, power levels higher than 600 watts are sufficient to empower the plasma burst to reach the crucible.

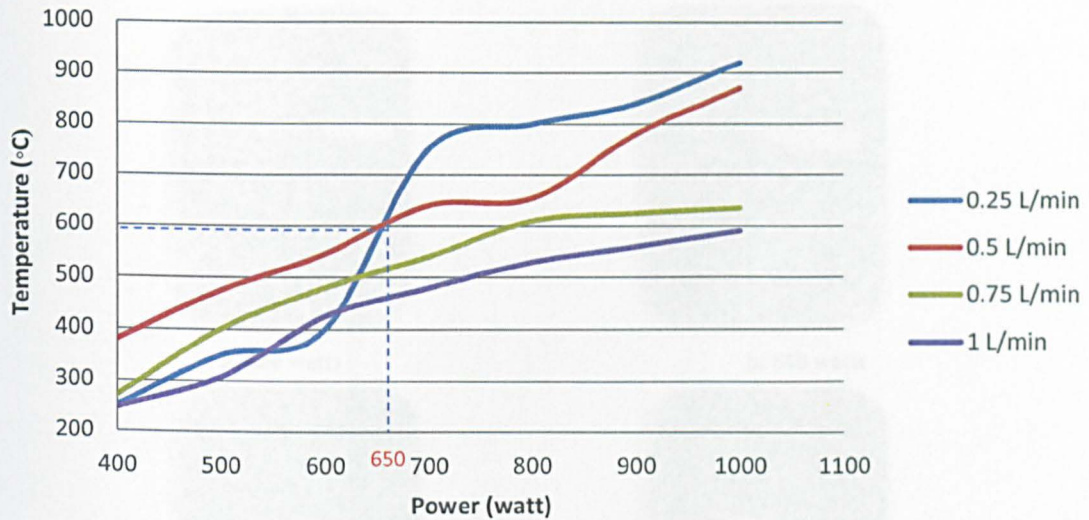


Figure 6.11: Plasma's temperature profile at the crucible.

This means, at the crucible where the feedstock is situated, flow rate of 0.25L/min gives hotter plasma than the other flow rates. However, with low power levels, the plasma with this flow rate does not reach the crucible, but plasmas with 0.5 L/min flow rate can reach and the temperature recorded is higher.

Flow rate of 0.5 L/min is used throughout the system experiments with lower power levels. Figure 6.12 shows the different plasma lengths with different power levels at 0.5 L/min argon flow rate. It is noticed that at lower power level, the plasma burst is shorter than when higher power level is used. This is logical as higher power levels will results in more dense plasma as more argon molecules will be ionised and converted to the plasma state.

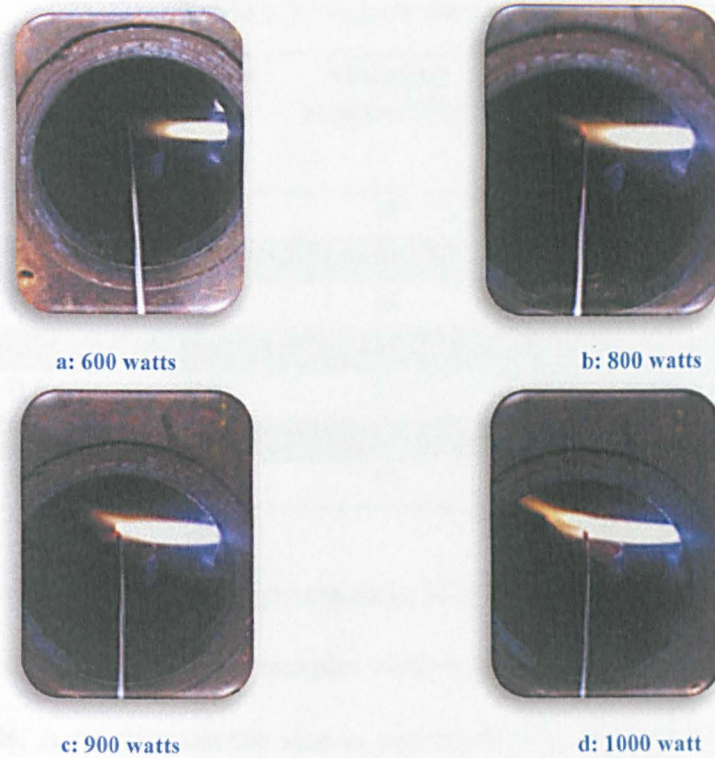


Figure 6.12: Plasma burst length with different power levels.

6.4.2. Quintox Limitation

6.4.2.1. Sample Size

Two different sample sizes are used to determine the appropriate sample size that overcomes the saturation limit in CO levels.

Table 6.7 summarises the experiments taken to determine sample's size. The experiments are repeated at the same systems parameters with different power levels.

Table 6.7: Sample size choice.

Power (watts)	Argon flow rate (L/min)	Pressure (mbar)	Moisture content (%)	CO level (ppm)	
				30 g (appx.)	10 g (appx.)
400	0.5	50	14	Saturation	80000
500	0.5	50	14	Saturation	Saturation
600	0.5	50	14	Saturation	Saturation
700	0.5	50	14	Saturation	Saturation
800	0.5	50	14	Saturation	Saturation
900	0.5	50	14	Saturation	Saturation
1000	0.5	50	14	Saturation	Saturation

Figure 6.13 shows CO levels for approximately 30 g samples with different power levels. It can be noticed that this range of samples always give a CO saturation level with all of the power levels. A smaller sample size is needed then to overcome Quintox limitation issue. This is shown in figure 6.14. Approximately 10 g samples are used in this case. At 400 watts, CO has given 80000 ppm (8%). This indicates that it is possible to use this range of sample's size with a power level of 400 watts as the gasification experiment initial parameters. However, and because plasma's strength depends on argon flow rate as well as power level, it is important to test the 10 g samples with power levels higher than 400 watt but with different argon flow rates. These tests will show the behaviour of CO production in relation to power and flow rate.



Figure 6.14: CO levels for 10 g samples.

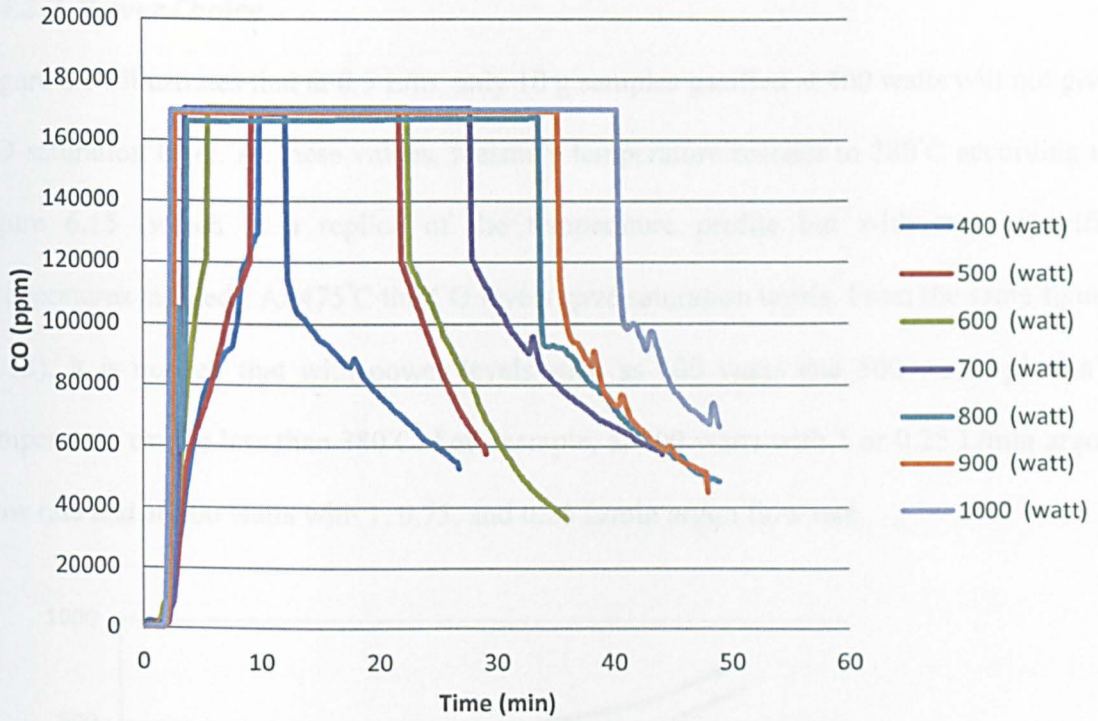


Figure 6.13: CO levels for 30 g samples.

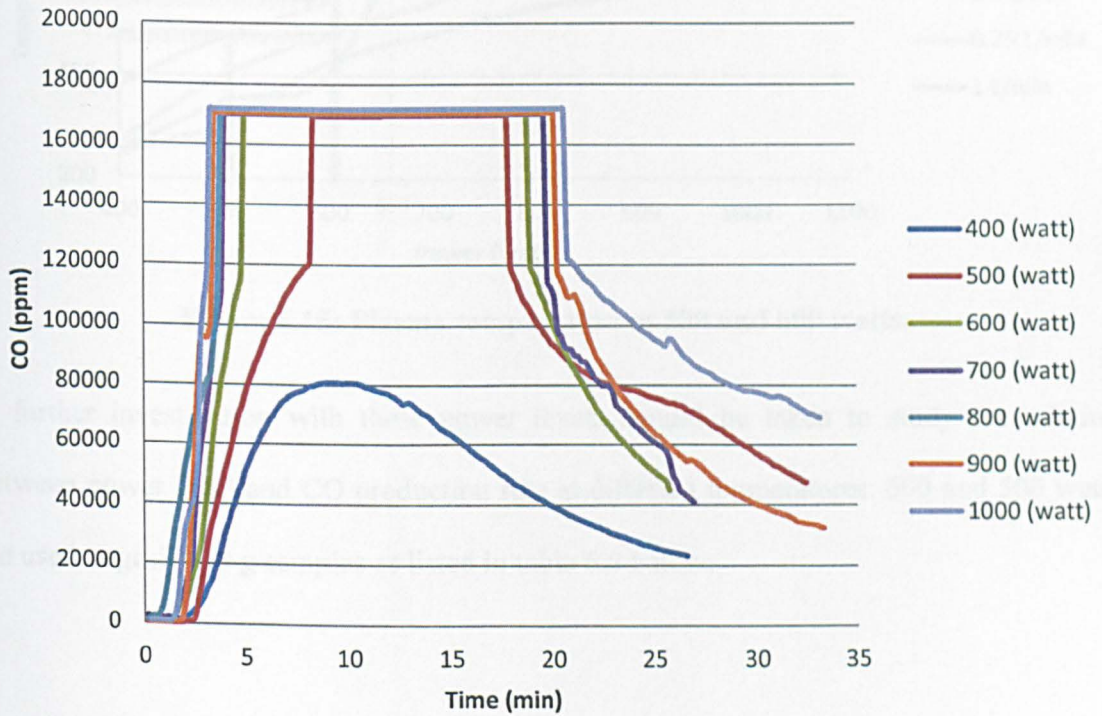


Figure 6.14: CO levels for 10 g samples.

6.4.2.2. Power Choice

Figure 6.14 illustrates that at 0.5 L/m, only 10 g samples gasified at 400 watts will not give CO saturation level. At these values, plasma's temperature reaches to 380°C according to figure 6.15 (which is a replica of the temperature profile but with more specific temperatures marked). At 475°C the CO levels gave saturation levels. From the same figure (6.13), it is noticed that with power levels such as 600 watts and 500 watts, plasma's temperature can be less than 380°C. For example, at 600 watts with 1 or 0.25 L/min argon flow rate and at 500 watts with 1, 0.75, and 0.25 L/min argon flow rate.

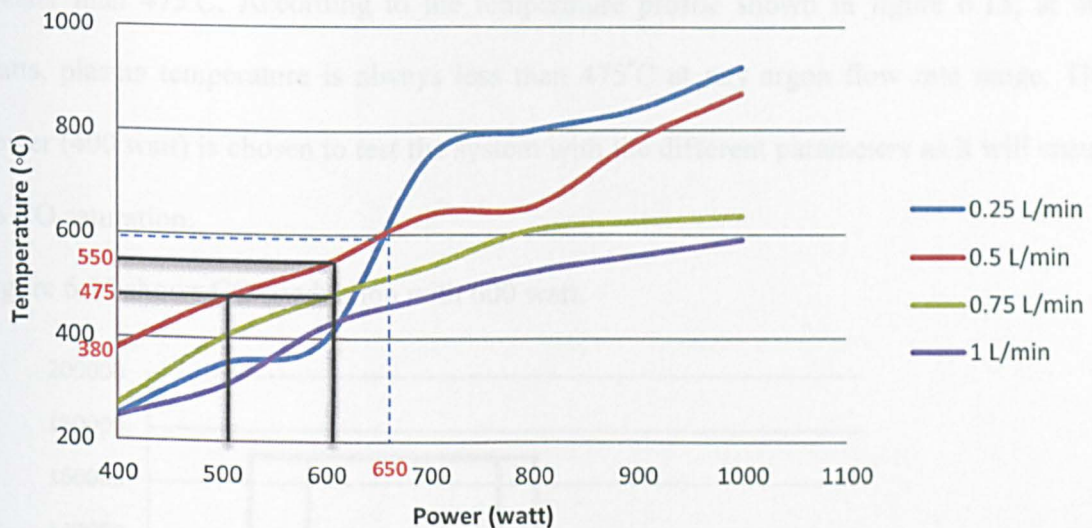


Figure 6.15: Plasma temperature at 500 and 600 watts.

A further investigation with these power levels should be taken to study the relation between power level and CO production rate at different temperatures. 600 and 500 watts are used to gasify 10 g samples as listed in table 6.8 below.

Table 6.8: Power level with different argon flow rates.

Power (watts)	Argon flow rate (L/min)	Temperature (°C)	Pressure (mbar)	Sample's moisture content (%)	CO level (ppm)
500	0.25	350	50	14	72000
	0.5	475	50	14	Saturation
	0.75	400	50	14	12000
	1	307	50	14	90000
600	0.25	400	50	14	95000
	0.5	550	50	14	Saturation
	0.75	480	50	14	Saturation
	1	425	50	14	80000

It is noticed from table 6.8 that CO levels reach saturation at temperatures equal to or greater than 475°C. According to the temperature profile shown in figure 6.15, at 400 watts, plasma temperature is always less than 475°C at any argon flow rate range. This power (400 watt) is chosen to test the system with the different parameters as it will ensure no CO saturation.

Figure 6.16 shows CO production with 600 watt.

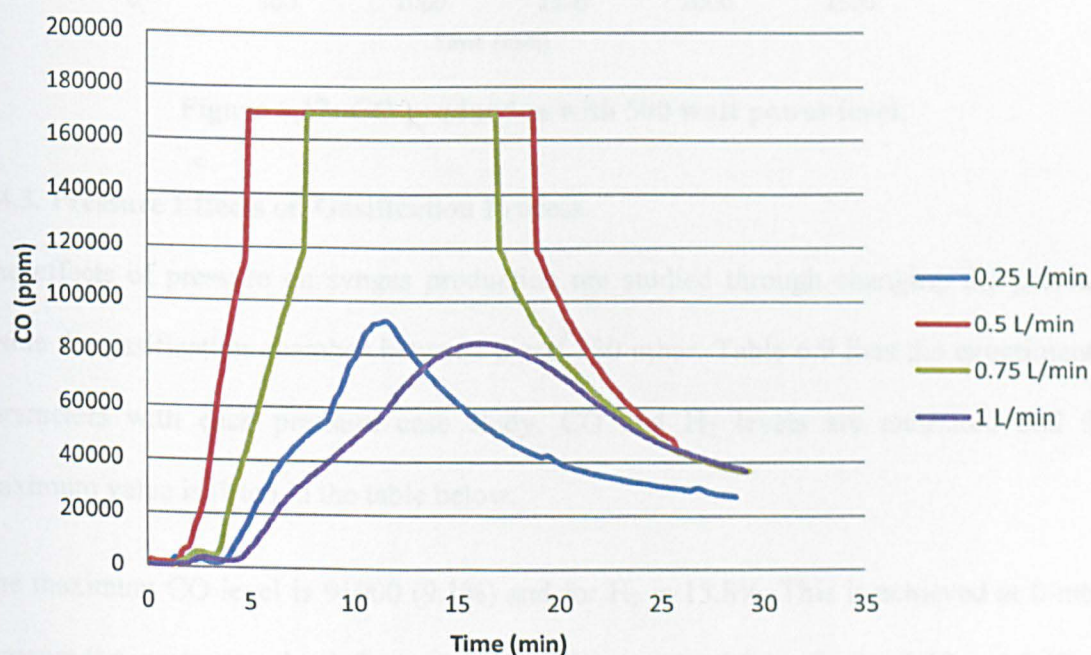


Figure 6.16: CO production with 600 watt power level.

CO saturation levels can be noticed at argon flow rates of 0.5 and 0.75 L/min. Figure 6.17 shows CO production with 500 watt power level. Only with flow rate of 0.5 L/min, CO reaches the saturation level. This is because of the higher plasma temperature with this flow rate.

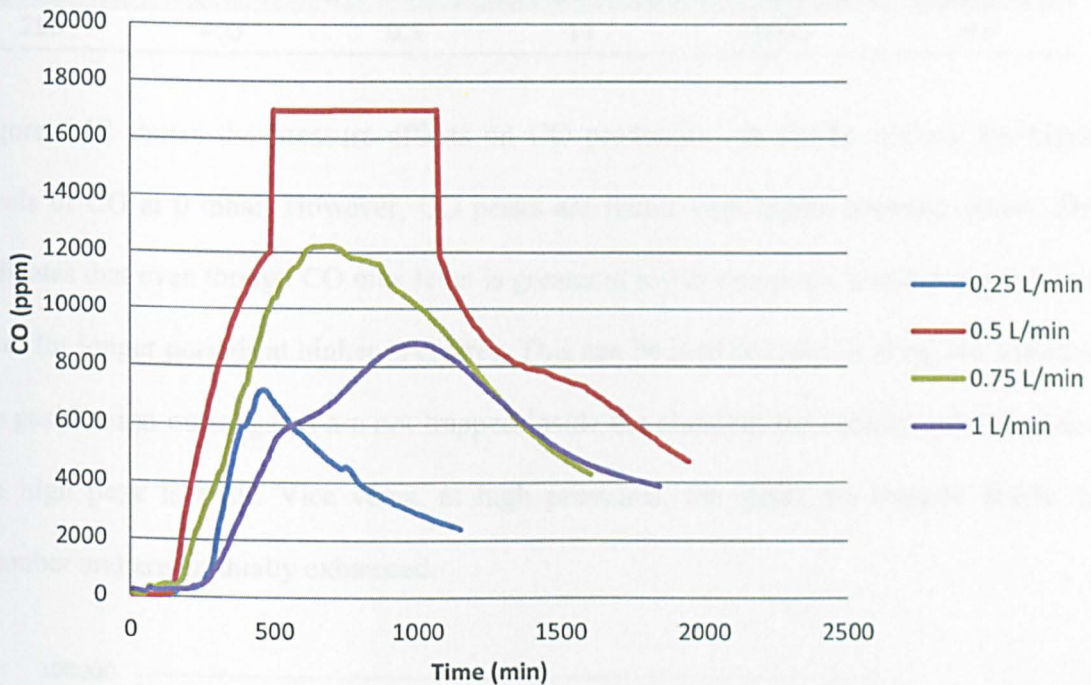


Figure 6.17: CO production with 500 watt power level.

6.4.3. Pressure Effects on Gasification Process

The effects of pressure on syngas production are studied through changing the pressure inside the gasification chamber between 0 and 250 mbar. Table 6.9 lists the experiments' parameters with each pressure case study. CO and H₂ levels are measured and the maximum value is listed in the table below.

The maximum CO level is 91000 (9.1%) and for H₂ is 15.8%. This is achieved at 0 mbar pressure (i.e. pressure valve left open), and can be explained from figures 6.18 and 6.19.

Table 6.9: Pressure effects on syngas production.

Pressure (mbar)	Power (watt)	Argon flow rate (L/min)	Moisture content (%)	CO max level (ppm)	H ₂ max level (%)
0	400	0.5	14	91000	15.8
50	400	0.5	14	80000	14
100	400	0.5	14	62000	12
150	400	0.5	14	55000	10.7
200	400	0.5	14	51000	10
250	400	0.5	14	50000	8.6

Figure 6.18 shows the pressure effects on CO production. It can be noticed the higher levels of CO at 0 mbar. However, CO peaks are flatter with higher pressure levels. This indicates that even though CO max level is greater at lower pressures, it maintains this max level for longer periods at higher pressures. This can be justified as at 0 mbar, for example, the gasification outlet gases are not trapped inside the chamber but rapidly exhausted thus the high peak is built. Vice versa, at high pressures, the gases are trapped inside the chamber and are gradually exhausted.

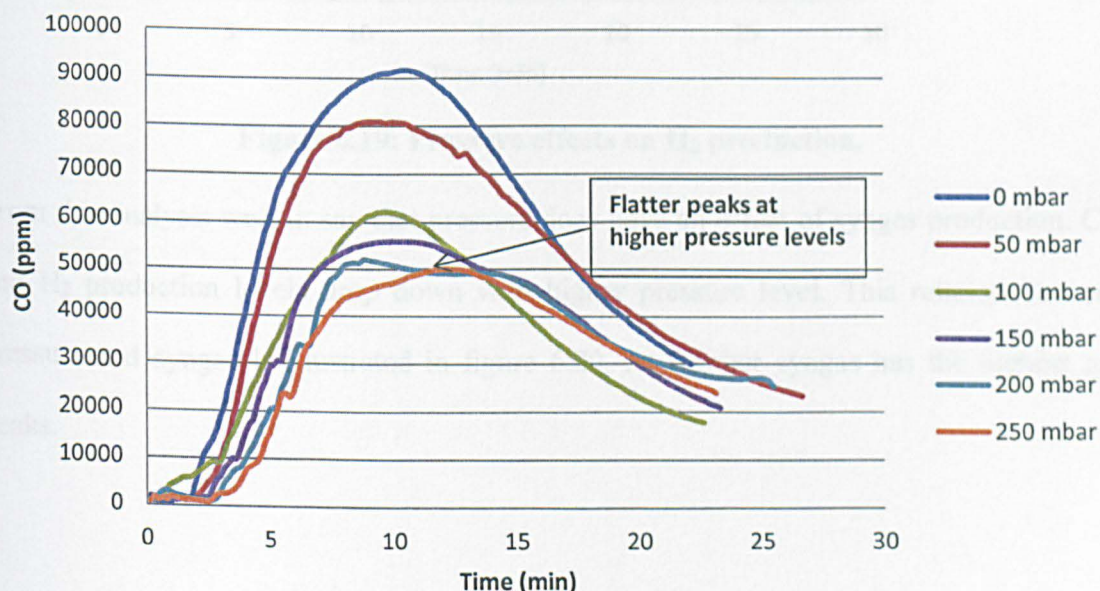


Figure 6.18: Pressure effects on CO production.

These flatter peaks are clearly noticed in H_2 production curves. Figure 6.19 shows the effects of pressure on H_2 production. At 0 mbar, hydrogen reached a maximum level of 15.8 %. However, this peak quickly declined to lower levels. On the other hand, at 50 mbar, hydrogen maximum peak is at 14 %. Hydrogen at this pressure maintains higher levels for a longer period compared with the rest of the pressure rates. As a result, 50 mbar is chosen as the optimal value to run the gasification process on.

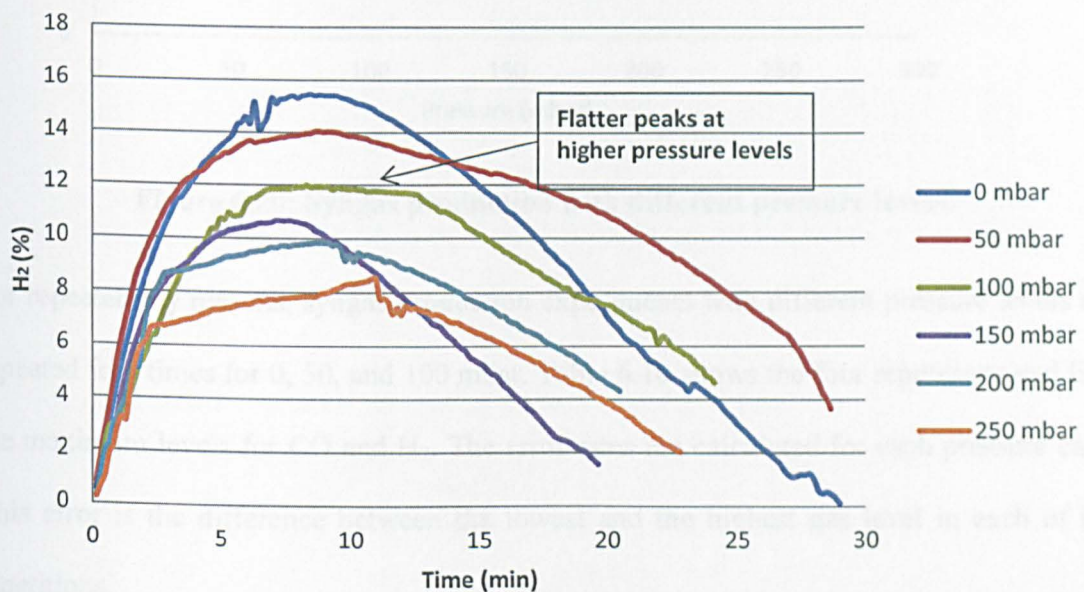


Figure 6.19: Pressure effects on H_2 production.

From this analysis we can say that pressure does have an effect of syngas production. CO and H_2 production levels drop down with higher pressure level. This relation between pressure and syngas is illustrated in figure 6.20. At 0 mbar syngas has the highest gas peaks.

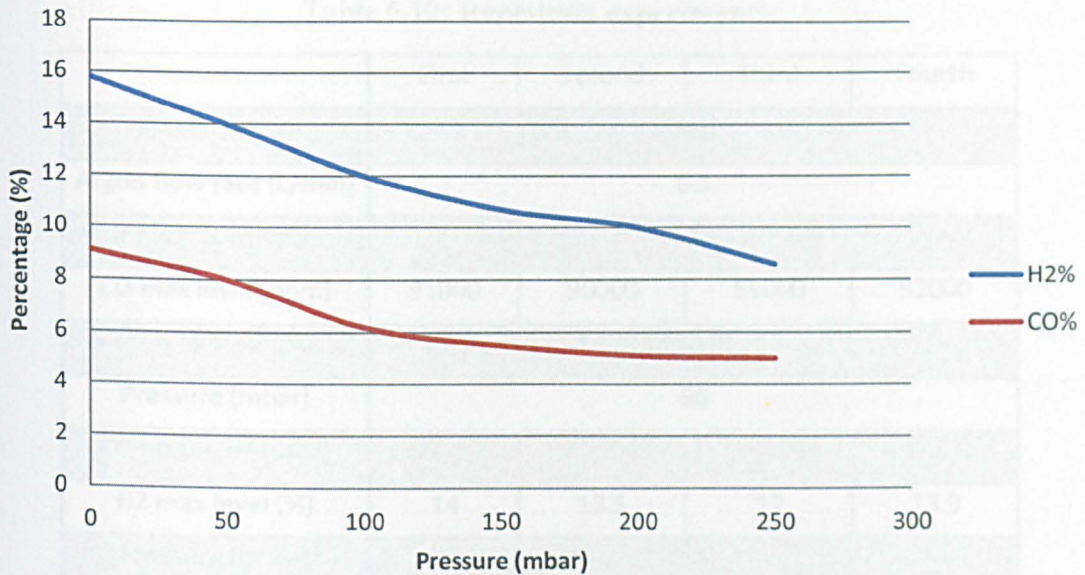


Figure 6.20: Syngas production with different pressure levels.

For repeatability reasons, syngas production experiments with different pressure levels are repeated four times for 0, 50, and 100 mbar. Table 6.10 shows the four repetitions and lists the maximum levels for CO and H₂. The error rates are calculated for each pressure case. This error is the difference between the lowest and the highest gas level in each of the repetitions.

Figures 6.21 to 6.26 shows the repetition experiments where the small deviation between the curves in each of the cases analysed can be observed.

Table 6.10: Repetition experiments.

	First	Second	Third	Fourth
Power (watt)	400			
Argon flow rate (L/min)	0.5			
Pressure (mbar)	0			
CO max level (ppm)	91000	90000	89000	92000
H2 max level (%)	15.8	16.8	17	16
Pressure (mbar)	50			
CO max level (ppm)	80000	82000	94000	90000
H2 max level (%)	14	13.5	12	13.9
Pressure (mbar)	100			
CO max level (ppm)	62000	60000	55000	51000
H2 max level (%)	12	12.7	12.4	13

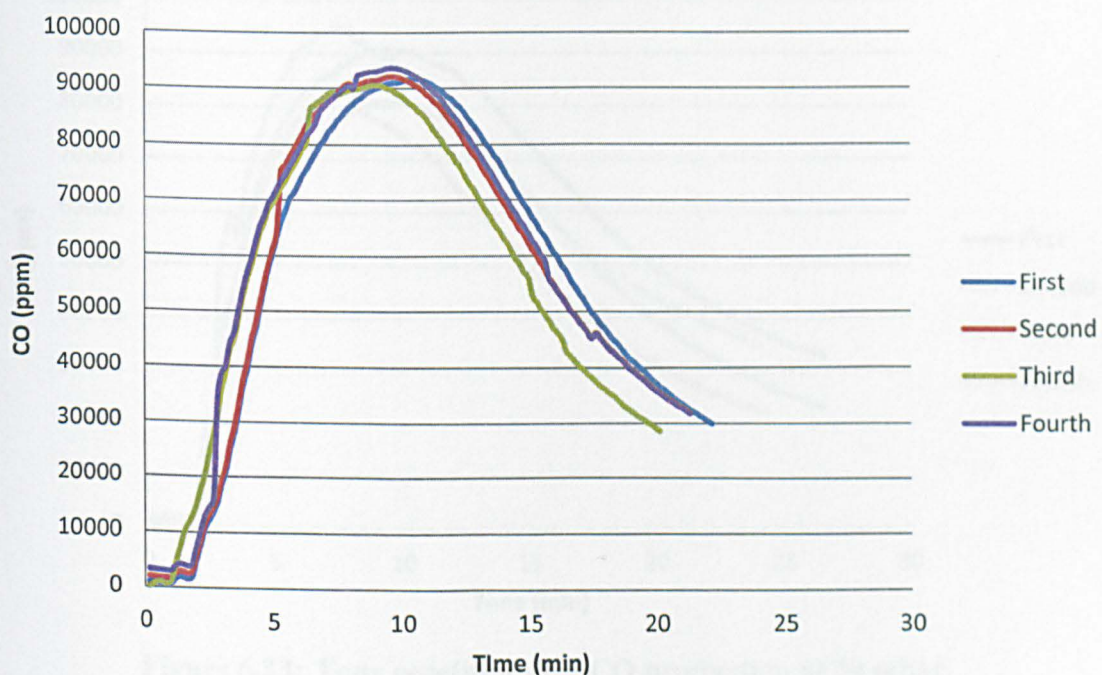


Figure 6.21: Four repetitions for CO production at 0 mbar.

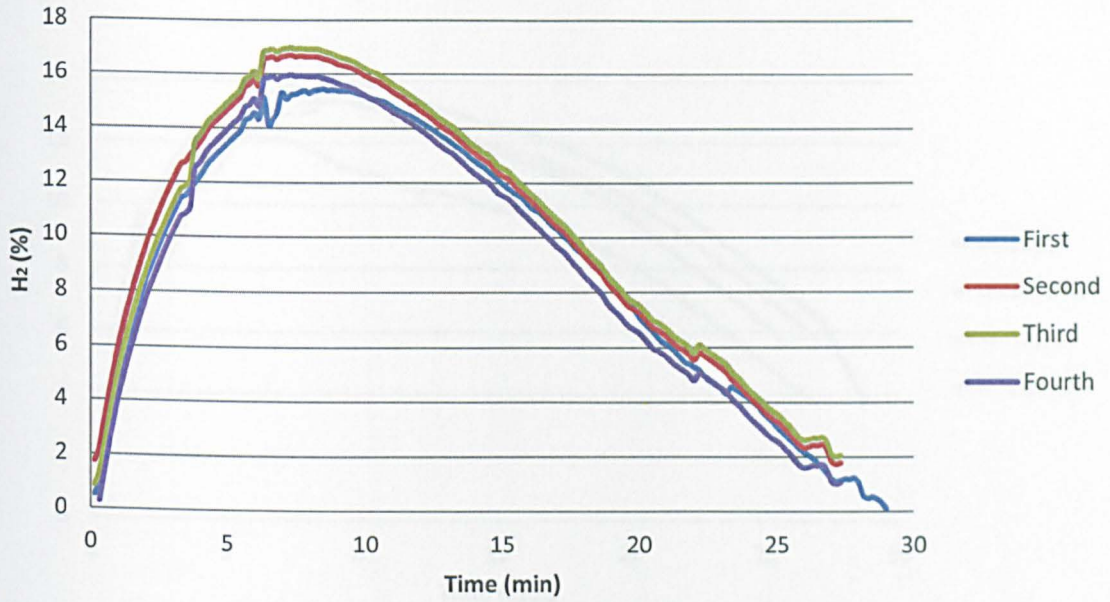


Figure 6.22: Four repetitions for H₂ production at 0 mbar.

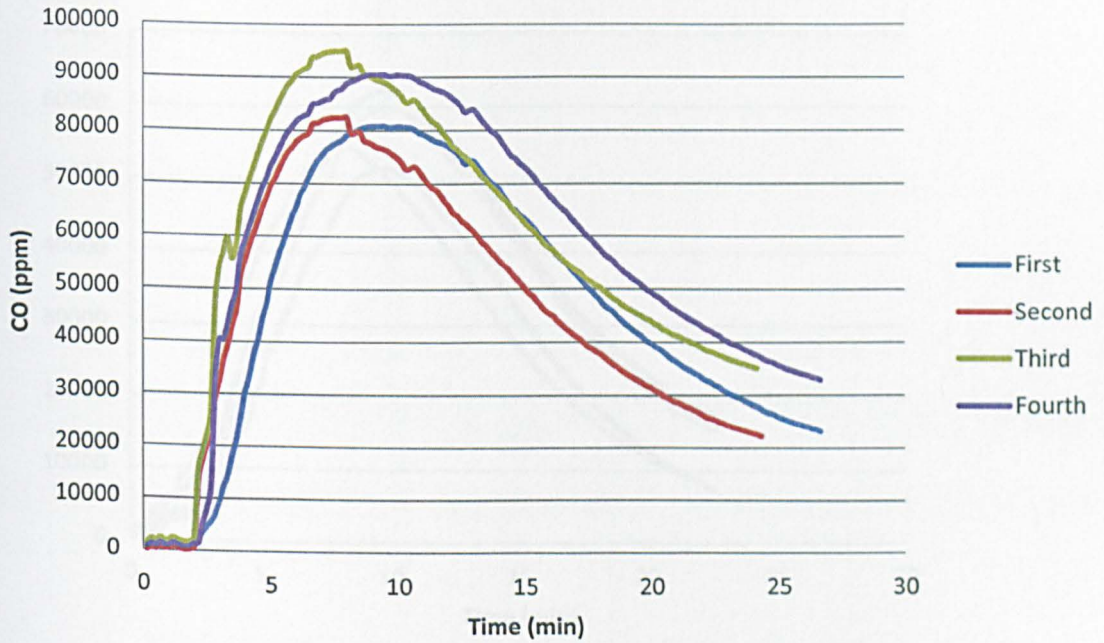


Figure 6.23: Four repetitions for CO production at 50 mbar.

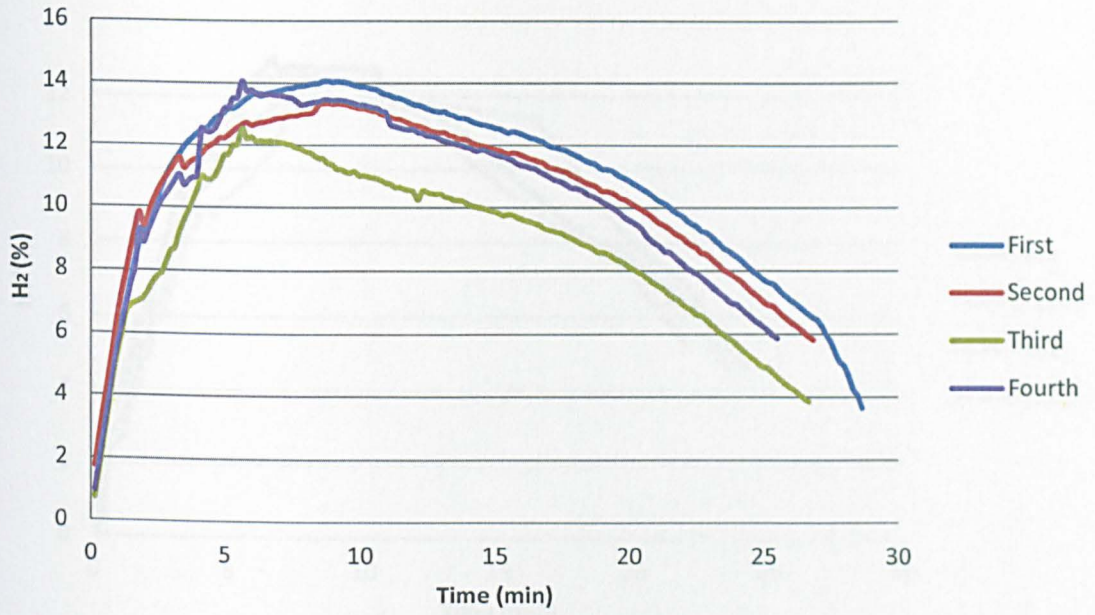


Figure 6.24: Four repetitions for H₂ production at 50 mbar.

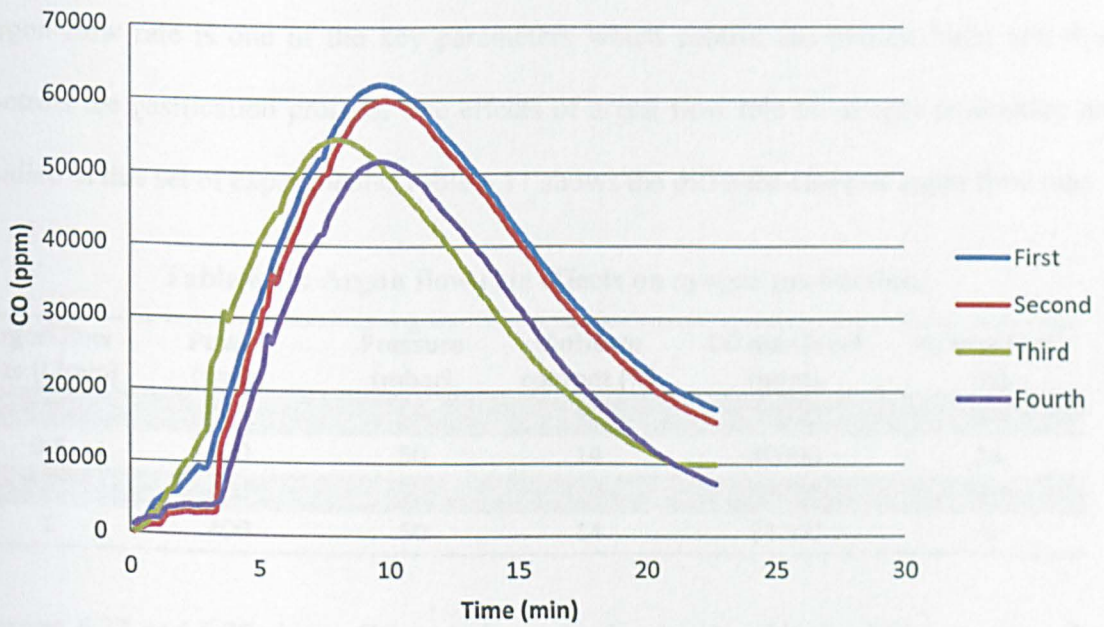


Figure 6.25: Four repetitions for CO production at 100 mbar.

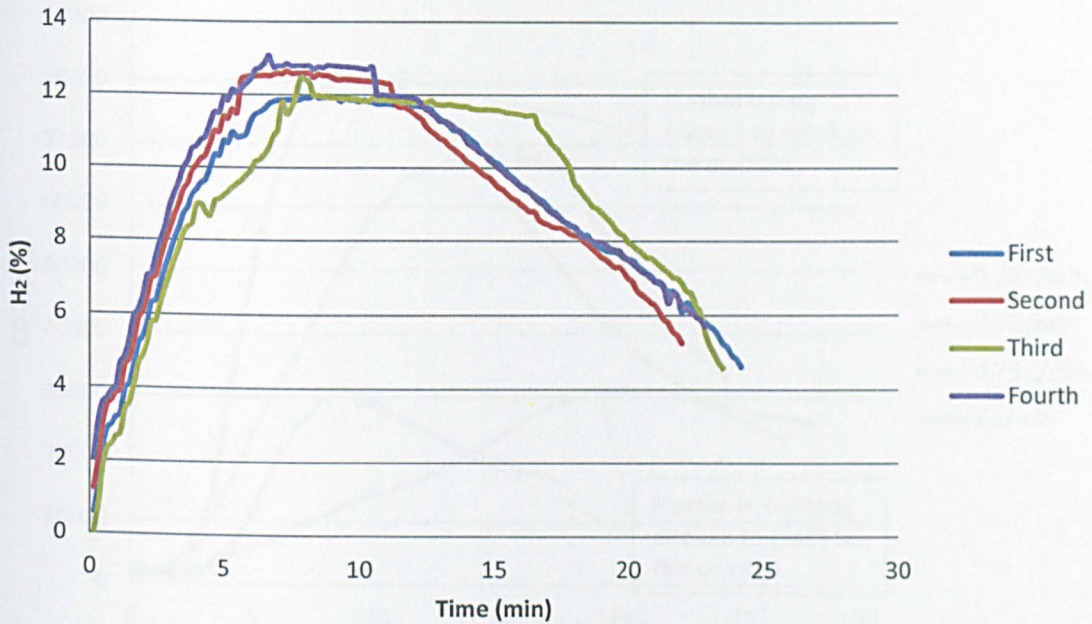


Figure 6.26: Four repetitions for H₂ production at 100 mbar.

6.4.4. Argon Flow Rate Effects on Gasification Process

Argon flow rate is one of the key parameters which control the plasma burst and thus controls the gasification process. The effects of argon flow rate on syngas production are studied in this set of experiments. Table 6.11 shows the different cases of argon flow rate.

Table 6.11: Argon flow rate effects on syngas production.

Argon flow rate (L/min)	Power (watt)	Pressure (mbar)	Moisture content (%)	CO max level (ppm)	H ₂ max level (%)
0.25	400	50	14	31000	5.6
0.5	400	50	14	80000	14
0.75	400	50	14	67000	12.9
1	400	50	14	31000	6

Figures 6.27 and 6.28 shows CO and H₂ production levels with the different argon flow rates.

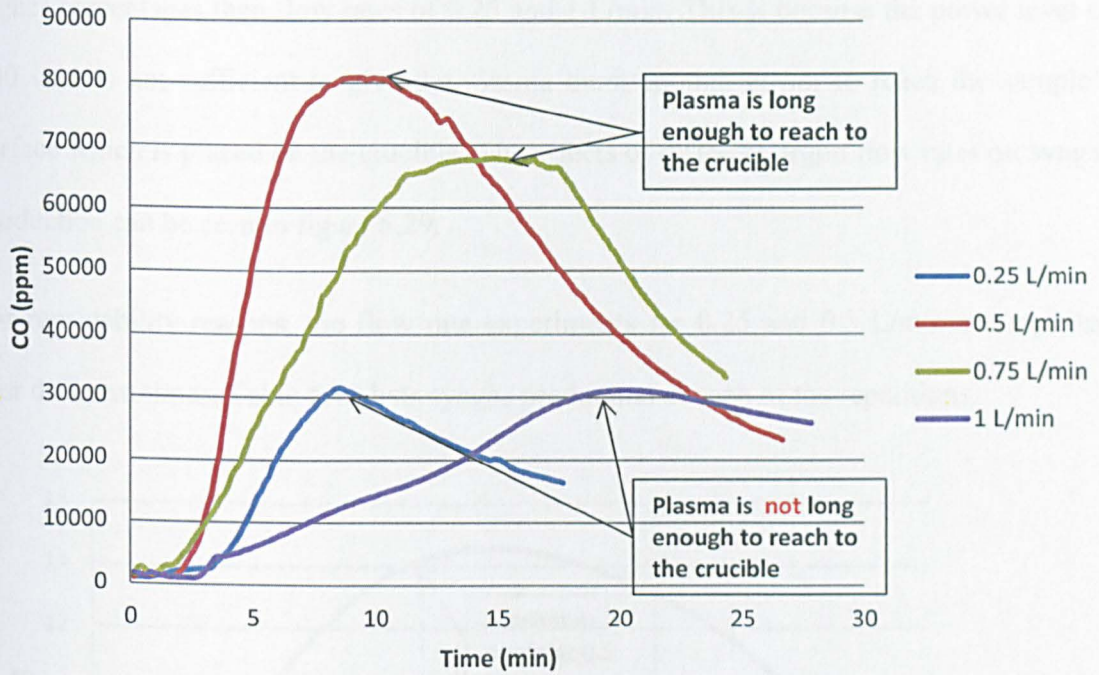


Figure 6.27: Argon flow effects on CO production.

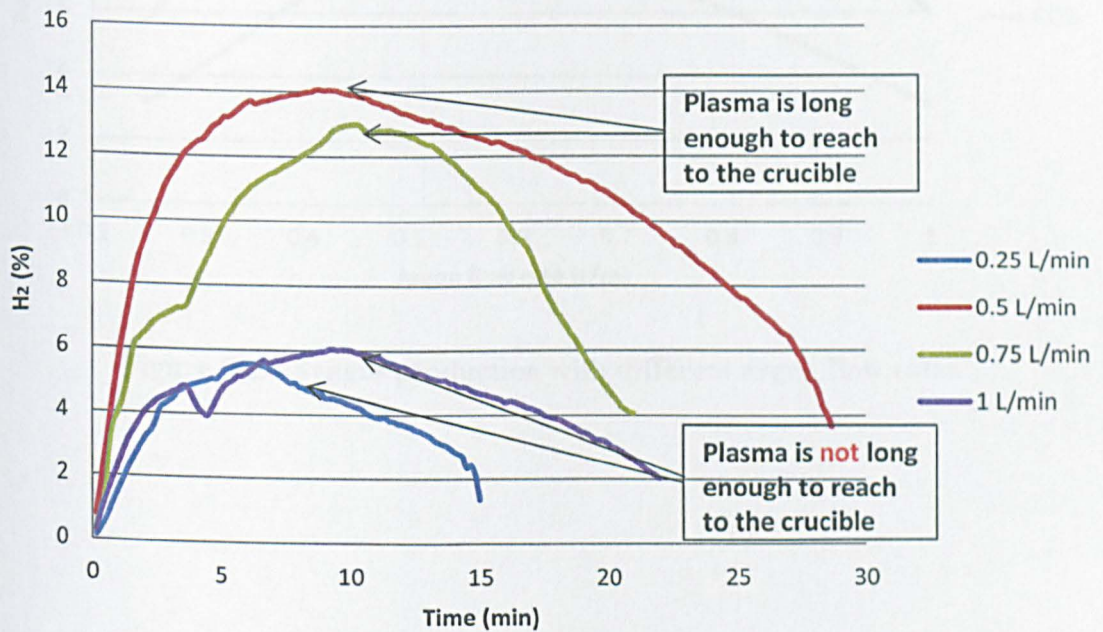


Figure 6.28: Argon flow effects on H₂ production.

It is noticed from the figures that the production level of syngas dramatically differs between different flow rates. For flow rates of 0.5 and 0.75 L/min, CO and H₂ levels reach

higher percentages than flow rates of 0.25 and 1 L/min. This is because the power level of 400 watt is not sufficient to give the plasma burst enough power to reach the sample's surface which is placed on the crucible. The effects of different argon flow rates on syngas production can be seen in figure 6.29.

For repeatability reasons, the flow rate experiments for 0.25 and 0.5 L/min are repeated four different times. Table 6.12 lists syngas production at each of the repetitions.

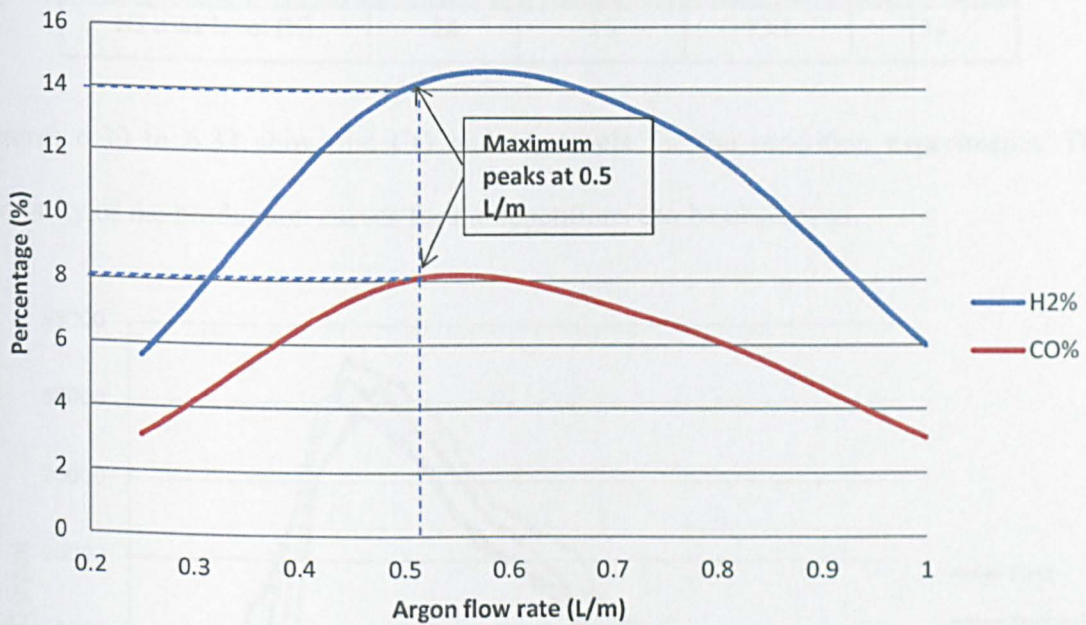


Figure 6.29: Syngas production with different argon flow rates.

Table 6.12: Repetition experiment.

	First	Second	Third	Fourth
Power (watt)	400			
Pressure (mbar)	50			
Argon flow rate (L/min)	0.25			
CO max level (ppm)	31000	31000	33000	30000
H2 max level (%)	5.6	5.4	5.1	5.7
Argon flow rate (L/min)	0.5			
CO max level (ppm)	80000	80000	81000	78000
H2 max level (%)	14	16	13.1	14

Figures 6.30 to 6.33 show the CO and H₂ levels for the repetition experiments. The similarity of the production curves for the repetitions can be observed.

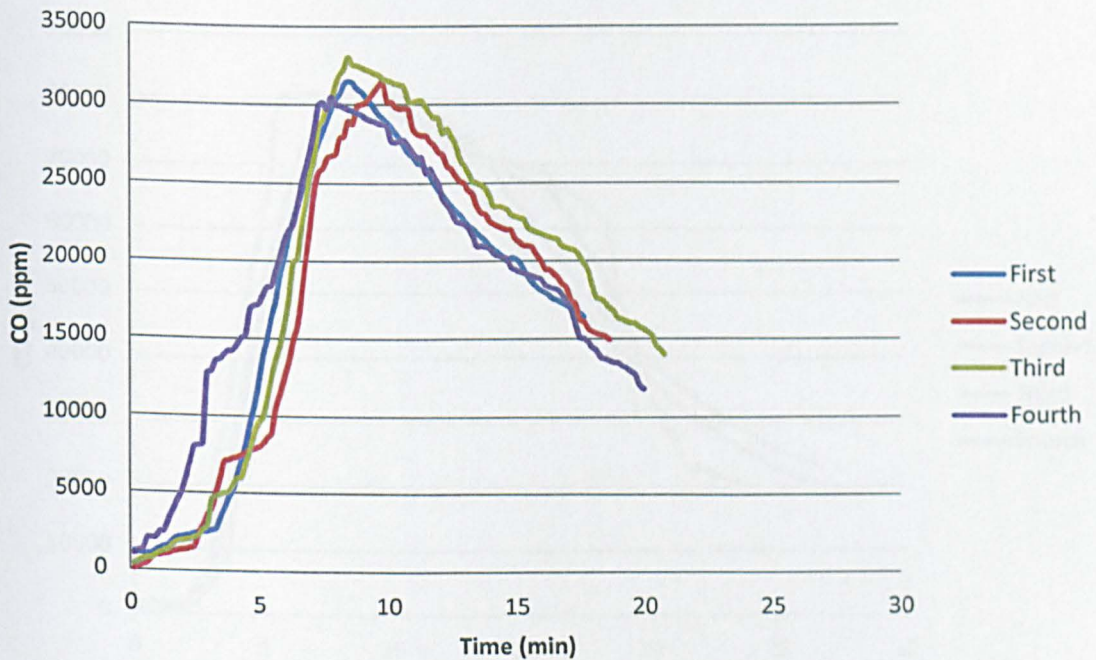


Figure 6.30: Four repetitions for CO production at 0.25 L/min.

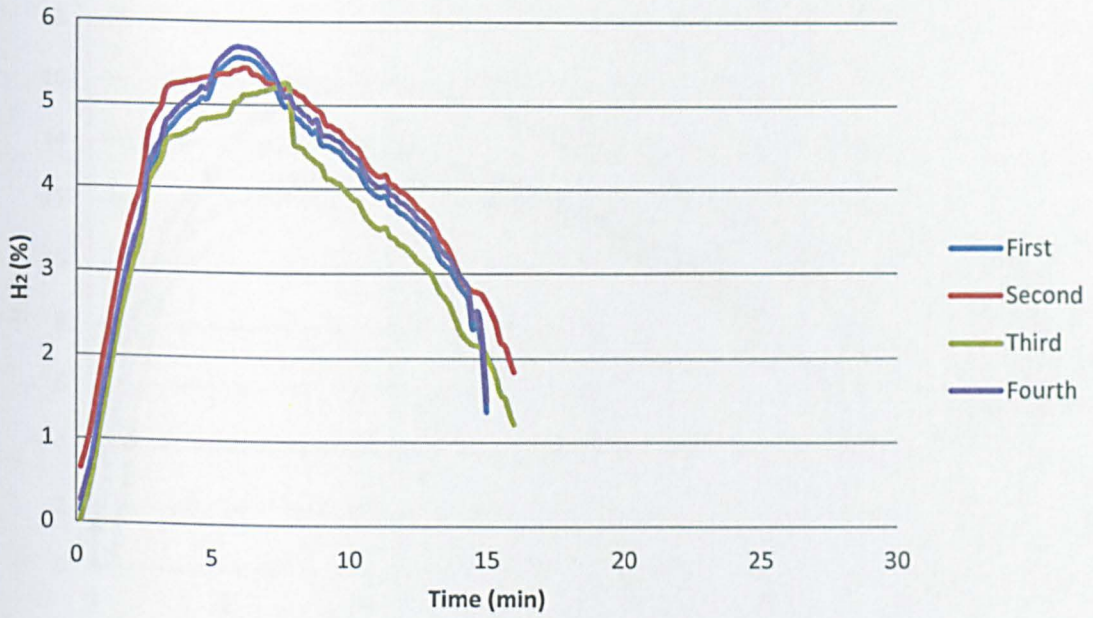


Figure 6.31: Four repetitions for H₂ production at 0.25 L/min.

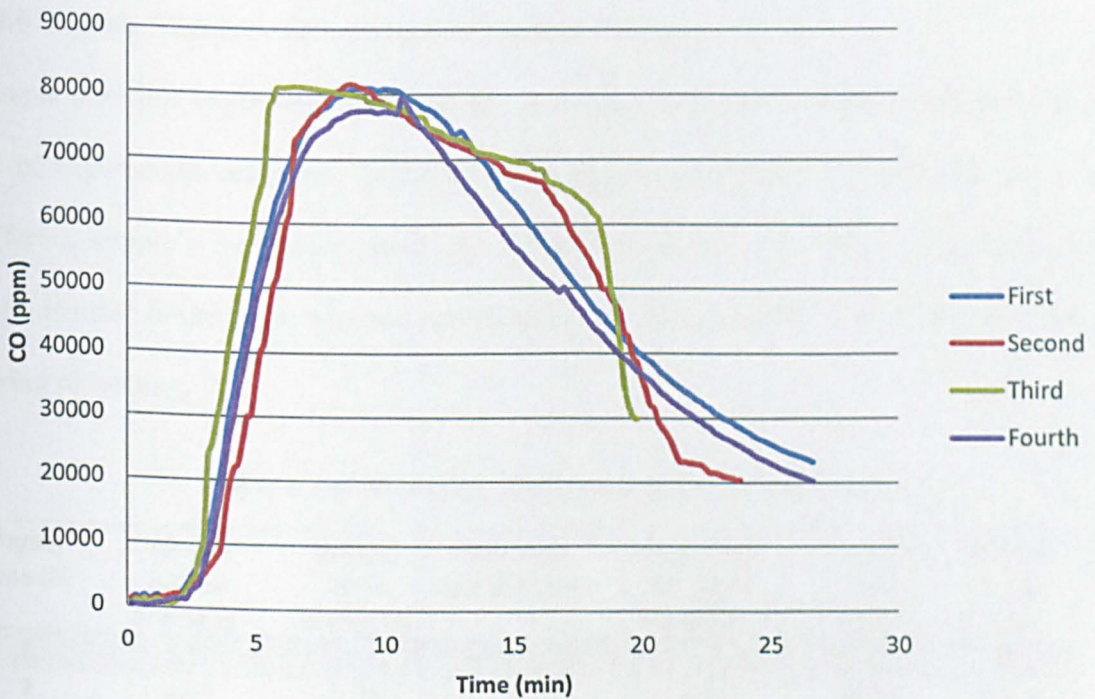


Figure 6.32: Four repetitions for CO production at 0.5 L/min.

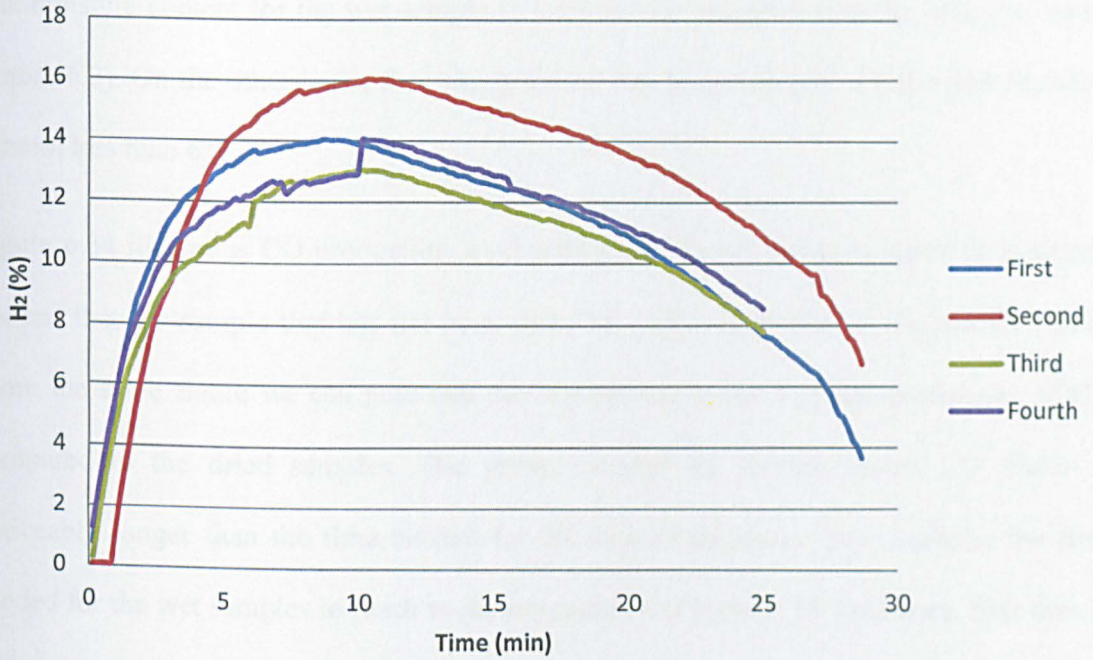


Figure 6.33: Four repetitions for H₂ production at 0.5 L/min.

6.4.5. Sample Moisture Effects on Gasification Process

Sample moisture might have some effects on syngas production. To study these effects, a set of experiments are done. Table 6.13 lists these experiments. Six different cases for different sample’s moisture content are prepared. 4 samples are dried in the laboratory oven as listed in the table, whereas one sample is soaked in water and the last kept with no drying or wetting.

Table 6.13: Moisture effects on syngas production.

Drying time (h)	Weight before drying (g)	Weight after drying (g)	Moisture content (%)	Weight loss for dried sample (%)	CO max level (ppm)	H ₂ max level (%)
1	7.98	7.12	10	10.77	62000	11
2	8.65	7.71	8	10.86	60000	10.2
2	8.34	7.38	6	11.51	58000	9.1
4	7.74	6.78	<6	12.40	50000	5.9
no drying	8.1	-	14	-	80000	14
wet	9.82	-	35	-	66000	16.2

The moisture content for the wet sample is 35% and is measured with the moisture meter (figure 6.2). On the other hand, the sample which has been dried for 4 hours has moisture content less than 6%.

Figure 6.34 illustrates CO production level with the different moisture cases. It is clearly noticed that the sample that has not been dried or wetted is giving the highest CO level. From the same figure we can note that the wet sample gives a robust production of CO compared to the dried samples. The period needed for the maximum CO yields is noticeably longer than the time needed for the rest of the cases. For example, the time needed for the wet samples to reach to the maximum CO level is 18.5 minutes. This time is equal to 9.8 minutes for the not dried sample.

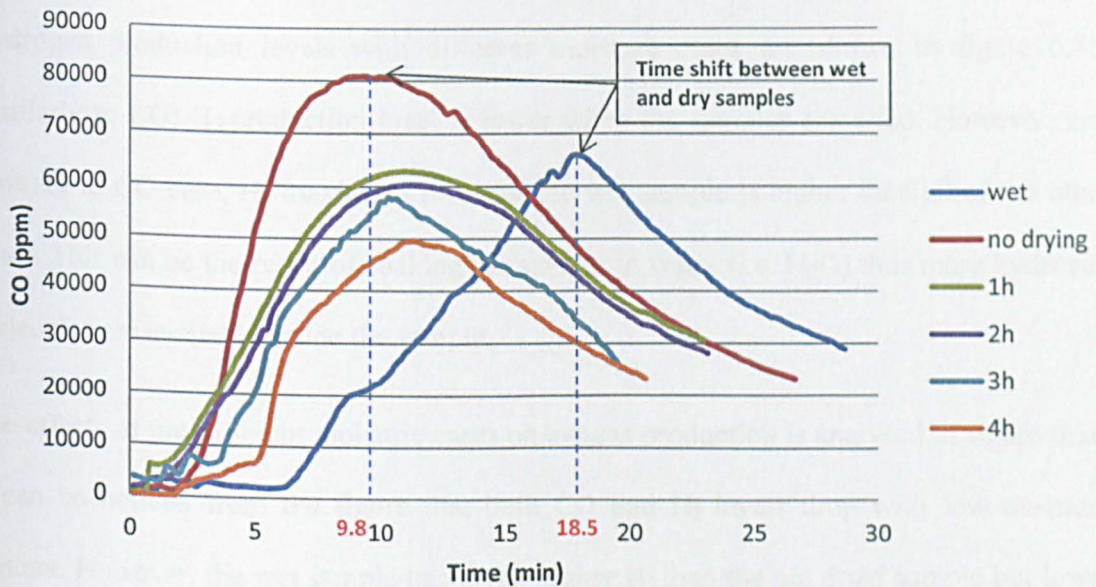


Figure 6.34: Moisture effects on CO production level.

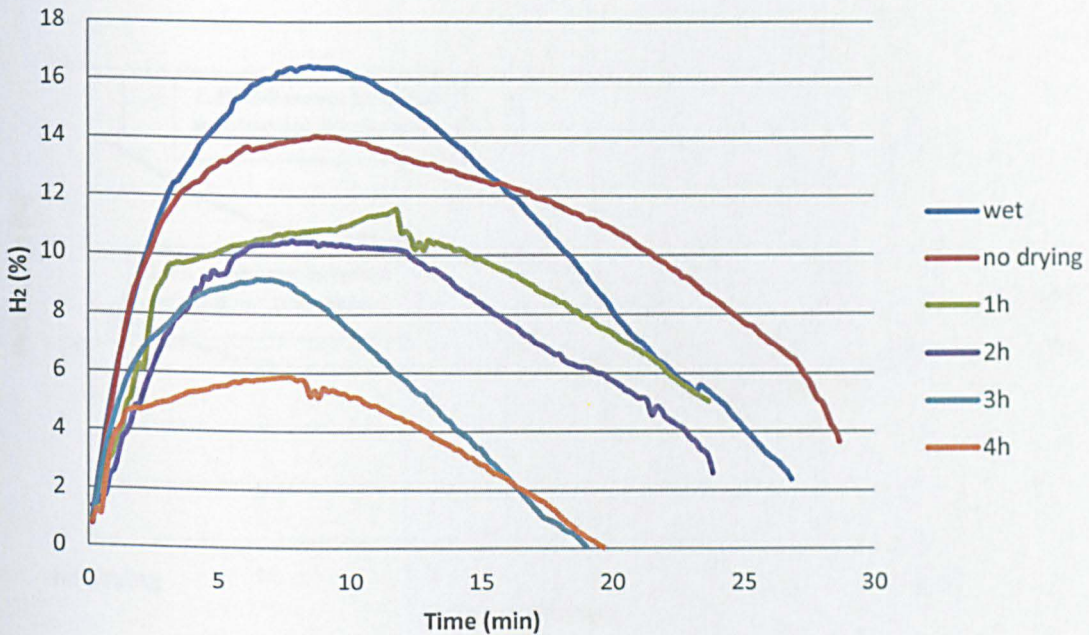


Figure 6.35: Moisture effects on H₂ production level.

Hydrogen production levels with different moisture cases are shown in figure 6.35. Similarly to CO; H₂ production level is lower when the samples are dried. However, and contrary to CO case, H₂ maximum level for the wet sample is higher than all of the other cases. This can be the result of soaking the sample in water (i.e. H₂O) thus more hydrogen molecules are available inside the sample.

The effects of the different moisture cases on syngas production is analysed in figure 6.36. It can be noticed from the figure that both CO and H₂ levels drop with low moisture content. However, the wet sample has given higher H₂ than the not dried sample but lower CO level.

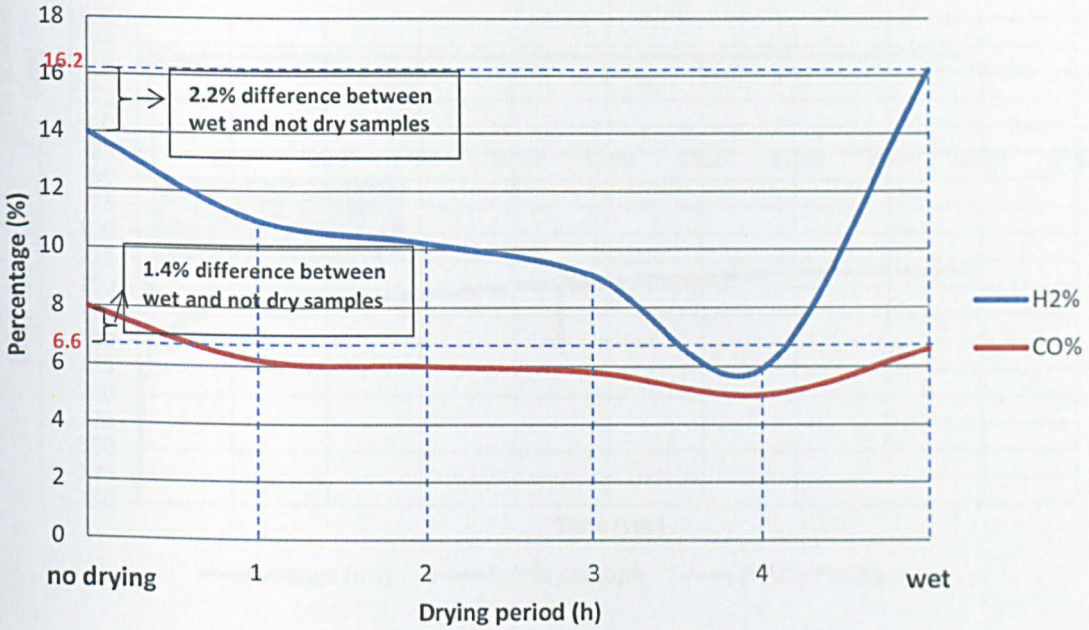


Figure 6.36: Syngas production change with different moisture levels.

6.4.6. Improvements of the Gasification Process

The improvements of the gasification system means the maximisation of syngas production. Through the previous experiments, optimal system parameters were specified to increase the syngas production. However, the system was manually controlled and the control algorithm was not applied. To study the effects of applying the control algorithm on syngas production, it is important to see the effects it has on the reflected power. Figures 6.37 and 6.38 show the relationship between the reflected voltage and the E-H tuner arms position. It can be noted that with the manually controlled arms state, the reflected voltage reaches to -140 mV. However, when applying the minimum reflected power algorithm, it drops down to -75 mV (figure 6.38) (i.e. nearly to half of the level of the reflected voltage without the algorithm).

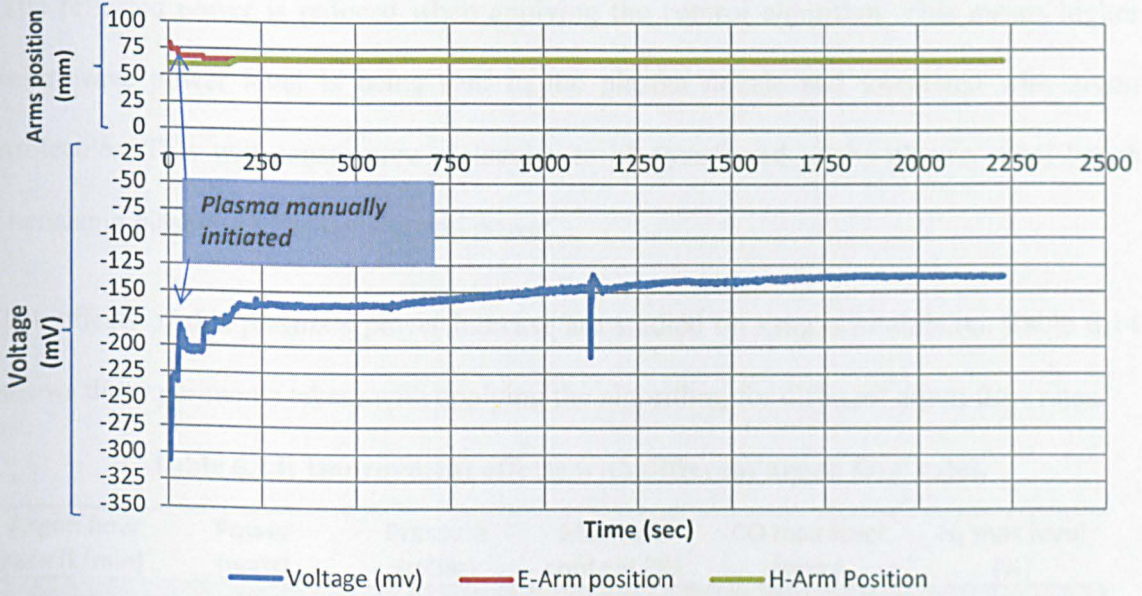


Figure 6.37: Manually controlled system behaviour.

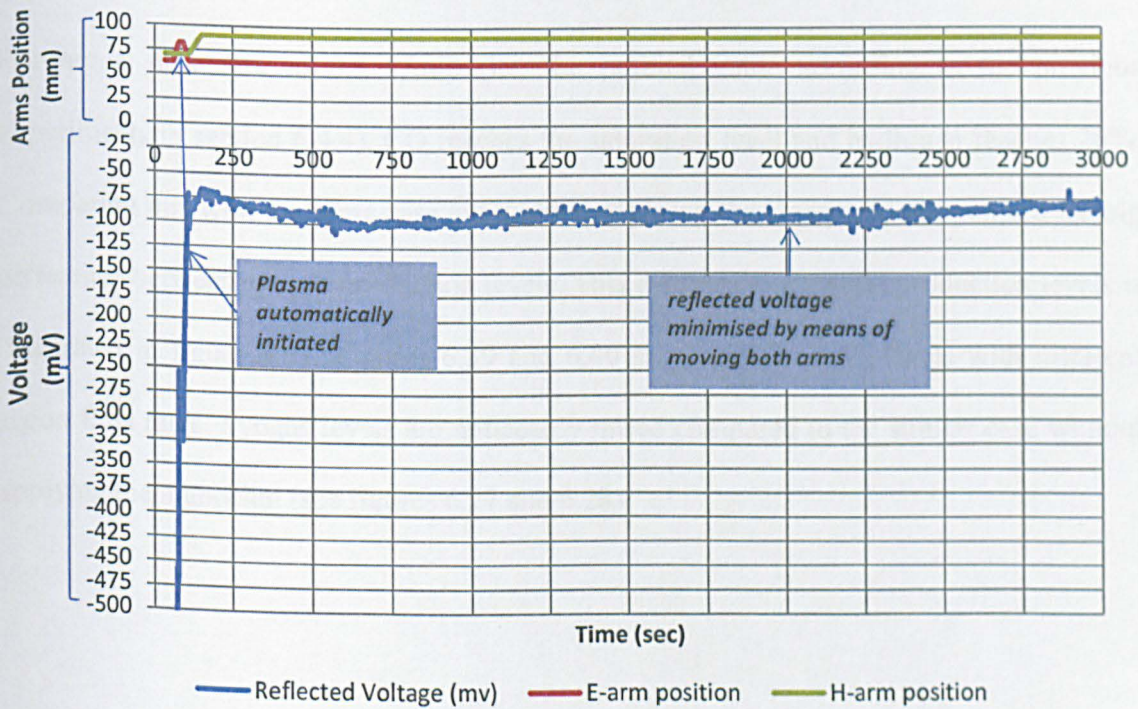


Figure 6.38: Tuned system behaviour.

The reflected power is reduced when applying the control algorithm. This means higher microwave power level is being sent to the plasma nozzle and interacted with argon molecules. This will cause more molecules to be transferred to the plasma state; hence increasing plasma's burst density and power.

The effects of this plasma's power increase are studied on syngas production. Table 6.14 shows the experiments taken, with applying the algorithm, for different argon flow rates.

Table 6.14: Improvement effects with different argon flow rates.

Argon flow rate (L/min)	Power (watt)	Pressure (mbar)	Moisture content (%)	CO max level (ppm)	H ₂ max level (%)
0.25	400	50	14	10000	11.5
0.5	400	50	14	Saturation	20
0.75	400	50	14	12000	19
1	400	50	14	81000	12

For argon flow rate of 0.5 L/min (i.e. the optimal value according to the previous experiments in section 6.4.4), CO reaches the saturation level and hydrogen reaches 20%. Comparing this with the same case but without applying the algorithm, one can see the big difference between syngas production levels. This difference in syngas production levels is illustrated in figure 6.41. Figures 6.39 and 6.40 shows CO and H₂ levels with different argon flow rates. Syngas levels are noticeably raised compared to the similar case without applying the algorithm (see figures 6.27 and 6.28).

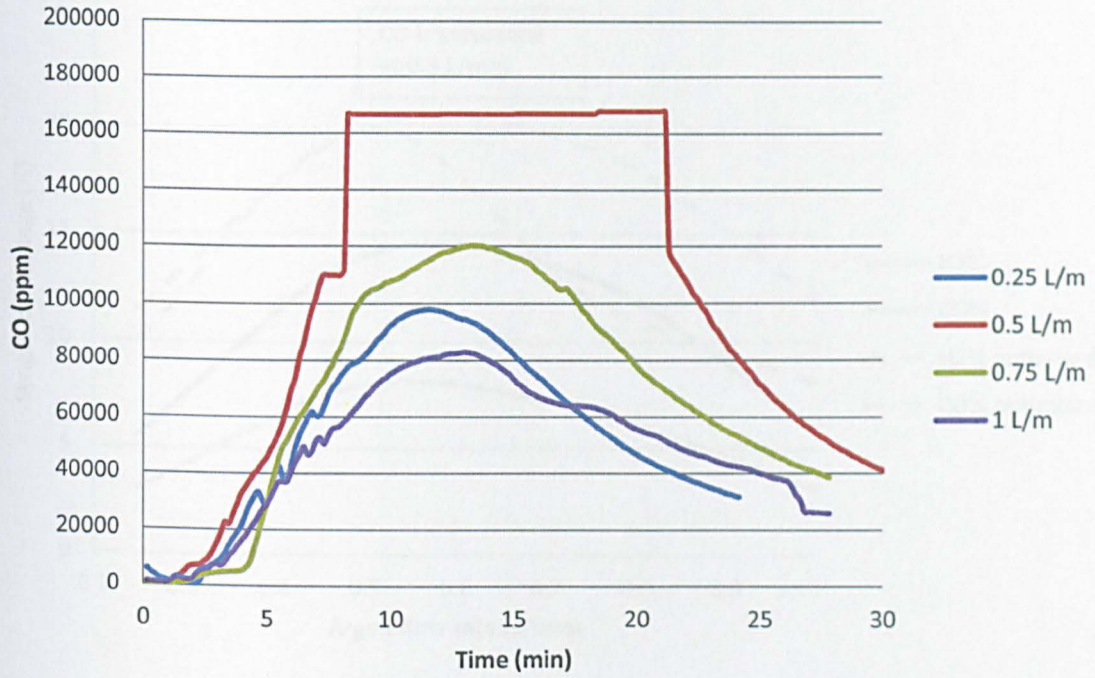


Figure 6.39: Algorithm effects on CO production.

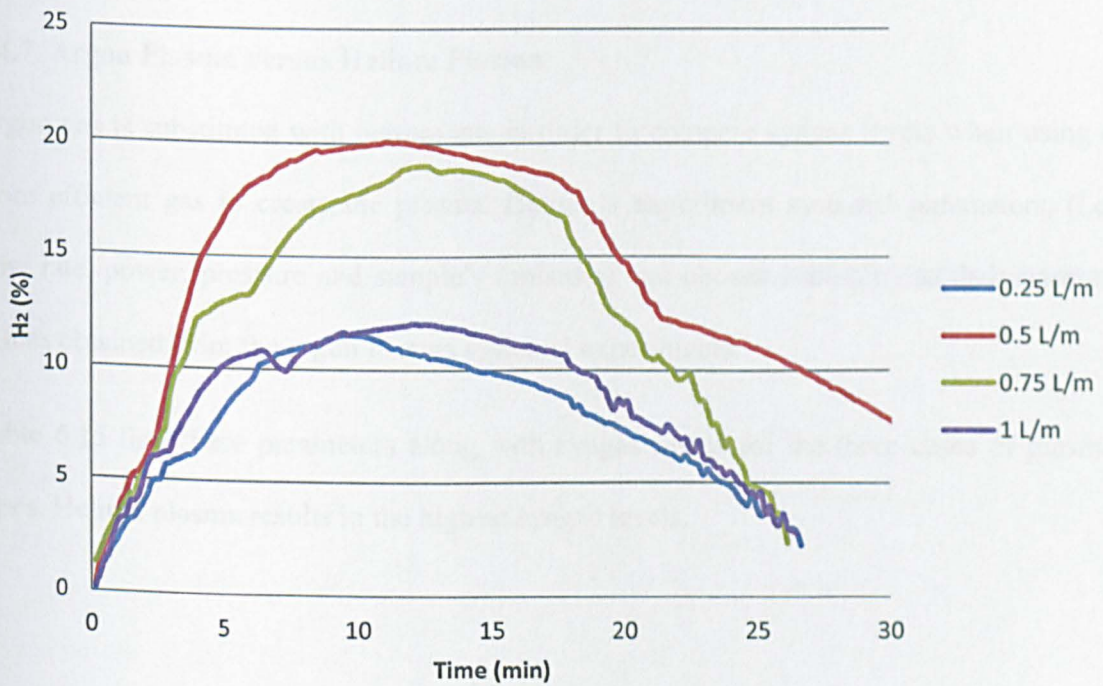


Figure 6.40: Algorithm effects on H₂ production.

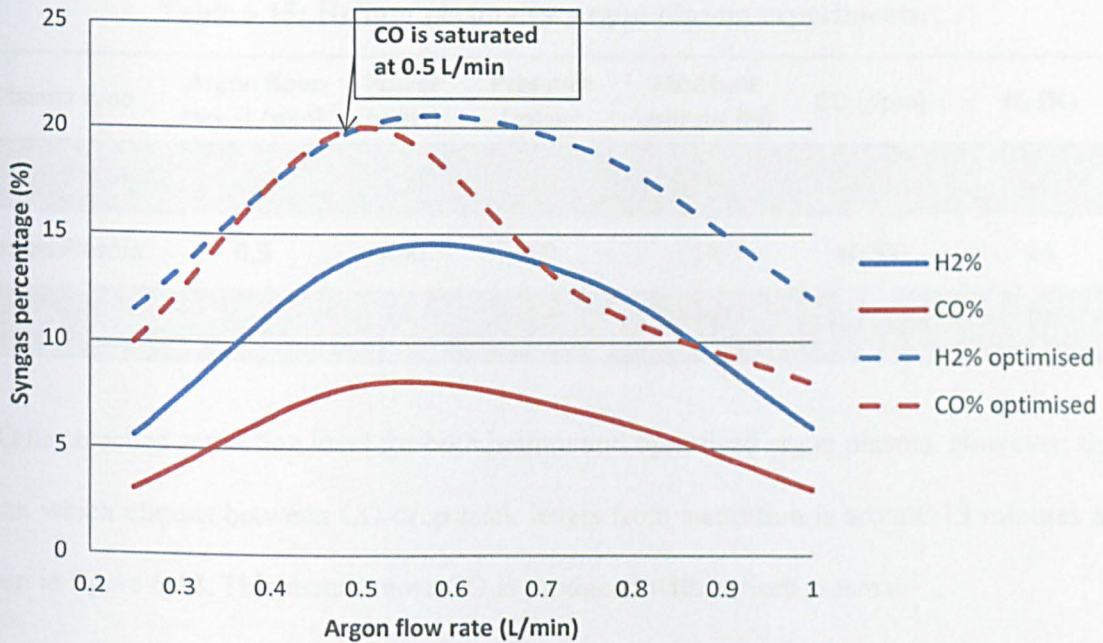


Figure 6.41: Comparison between syngas levels with and without applying the algorithm.

6.4.7. Argon Plasma versus Helium Plasma

Argon gas is substituted with helium gas in order to compare syngas levels when using a more efficient gas to create the plasma. Helium's experiment systems' parameters, (i.e. flow rate, power, pressure and sample's moisture), are chosen according to their optimal values obtained from the argon plasma systems' experiments.

Table 6.15 lists these parameters along with syngas levels for the three cases of plasma types. Helium plasma results in the highest syngas levels.

Table 6.15: Helium plasma vs. argon plasma experiments.

Plasma type	Argon flow rate (L/min)	Power (watt)	Pressure (mbar)	Moisture content (%)	CO (ppm)	H ₂ (%)
Helium Plasma	0.5	400	50	14	Saturation	26
Argon Plasma	0.5	400	50	14	80000	14
Optimised Argon Plasma	0.5	400	50	14	Saturation	20

CO has reached saturation level for both helium and optimised argon plasma. However, the time which elapses between CO drop back levels from saturation is around 13 minutes as seen in figure 6.42. This means more CO is produced with helium plasma.

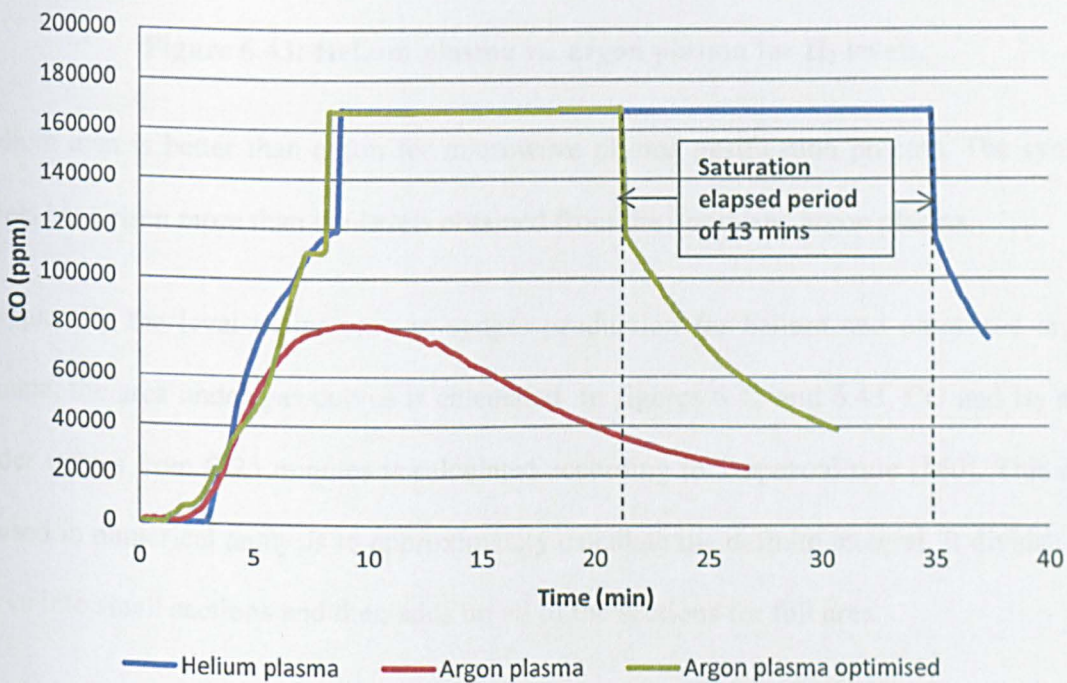


Figure 6.42: Helium plasma vs. argon plasma for CO levels.

H₂ production acts similarly to CO with the three types of plasma. The level difference of 6% between helium plasma and the optimised argon plasma can be observed from figure 6.43.

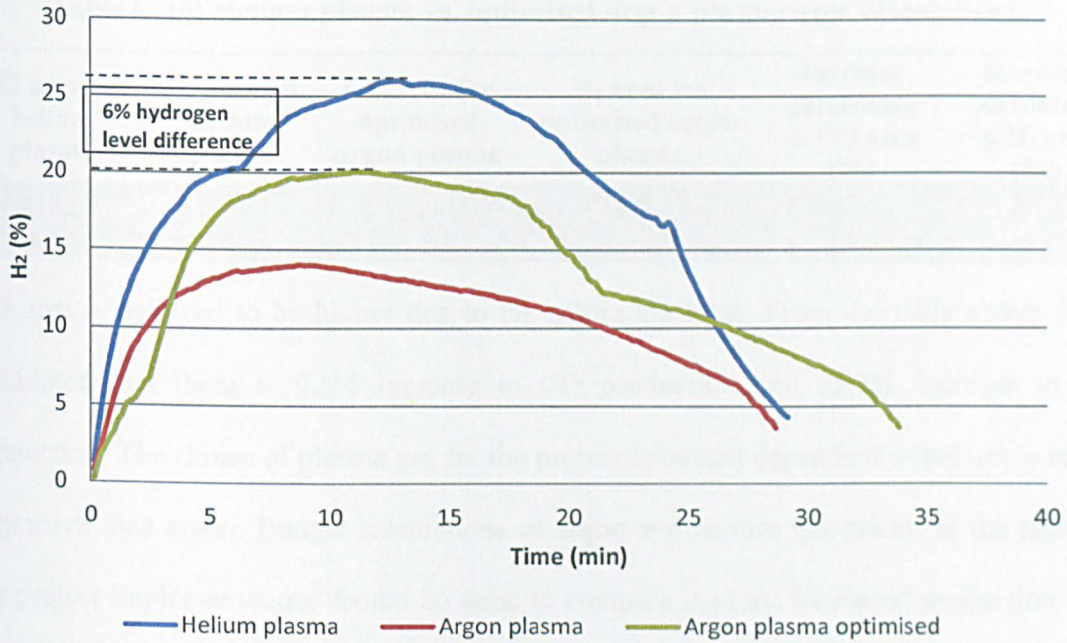


Figure 6.43: Helium plasma vs. argon plasma for H₂ levels.

Helium then is better than argon for microwave plasma gasification process. The syngas levels have risen more than the levels obtained from the optimised argon plasma.

To quantify the level of increase in syngas production for helium and optimised argon plasma, the area under gas curves is calculated. In figures 6.42 and 6.43, CO and H₂ area under curves from 0-25 minutes is calculated according to Trapezoid rule [160]. This rule is used in numerical analysis to approximately calculate the definite integral. It divides the curve into small sections and then adds up all of the sections for full area.

Table 6.16 shows the area calculations and the percentage increase between helium and optimised argon plasma.

Table 6. 16: Helium plasma vs. optimised argon plasma area calculations.

CO area for helium plasma	H ₂ area for helium plasma	CO area for optimised argon plasma	H ₂ area for optimised argon plasma	Increase percentage in CO area (%)	Increase percentage in H ₂ area (%)
319.4	519.9	289.2	386.5	9.5	25.7

CO area is believed to be higher due to the saturation limit. From the table above, it is calculated that there is 9.5% increase in CO production and 25.7% increase in H₂ production. The choice of plasma gas for the project is budget dependent as helium is more expensive than argon. Budget calculations of argon and helium gas prices, at the time of the project implementation, should be done to compare it to the increased production and choose the plasma gas.

6.4.8. Different Feedstock Study

Palm date seeds are tested in this experiment case as a substitute for timber feedstock. Figure 6.44 shows the seeds before and after the gasification process. The experiment is aimed to compare syngas levels between palm dates and timber blocks.

Table 6.17: Palm date seeds vs. timber for syngas levels.

Feedstock	Argon flow rate (L/min)	Power (watt)	Pressure (mbar)	Moisture content (%)	CO (ppm)	H ₂ (%)
Palm date seeds	0.5	400	50	11	Saturation	15
Timber	0.5	400	50	14	Saturation	20

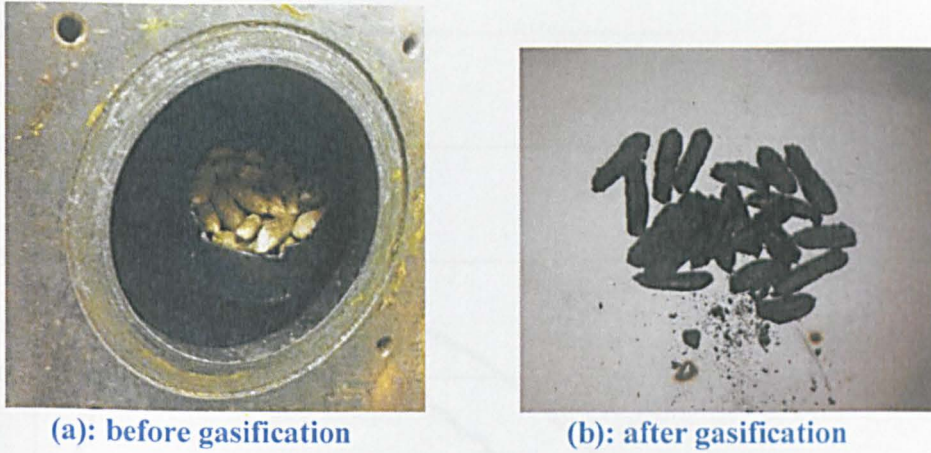


Figure 6.44: Palm date seeds samples.

Table 6.17 lists system’s parameters. These parameters are the ones specified from gasifying timber blocks (i.e. 0.5 L/min, 400 watt, 50 mbar for argon flow rate, power and pressure respectively). The similarity of syngas production between palm date seeds and timber can be observed from CO and H₂ levels, shown in figures 6.45 and 6.46.

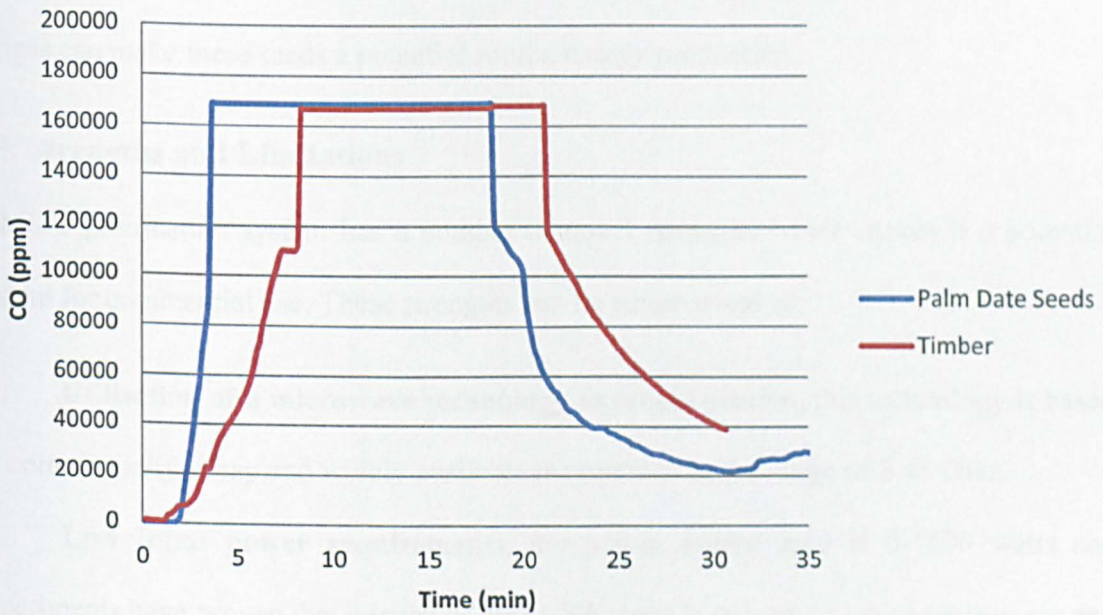


Figure 6.45: Palm date seeds vs. timber for CO levels.

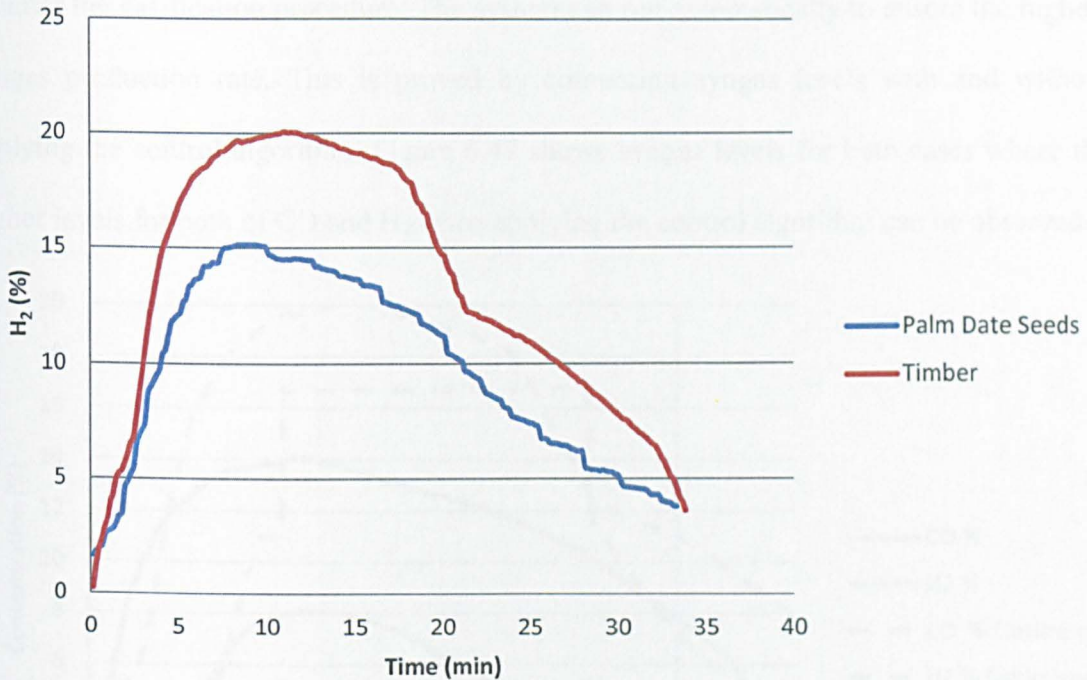


Figure 6.46: Palm date seeds vs. timber for H₂ levels.

However, the seeds are considered waste material, thus acquiring such high level of syngas can make these seeds a potential source energy production.

6.5. Strengths and Limitations

LJMU's gasification system has a number of novel strengths which makes it a potential system for commercial use. These strengths can be summarised as:

- 1- **Utilisation of a microwave technology to create plasma**, this technology is based on commercially cheap and widely available magnetrons in the range of 2.45 GHz.
- 2- **Low input power requirements**, the power source used is 0-1000 watts and experiments have proven that a range of 400-1000 watts is enough to ionise plasma gas and commence the gasification procedure.
- 3- **Automation control of the system**, this control enables the users to control and

monitor the gasification procedure. The system can run automatically to ensure the highest syngas production rate. This is proved by comparing syngas levels with and without applying the control algorithm. Figure 6.47 shows syngas levels for both cases where the higher levels for both of CO and H₂ when applying the control algorithm can be observed.

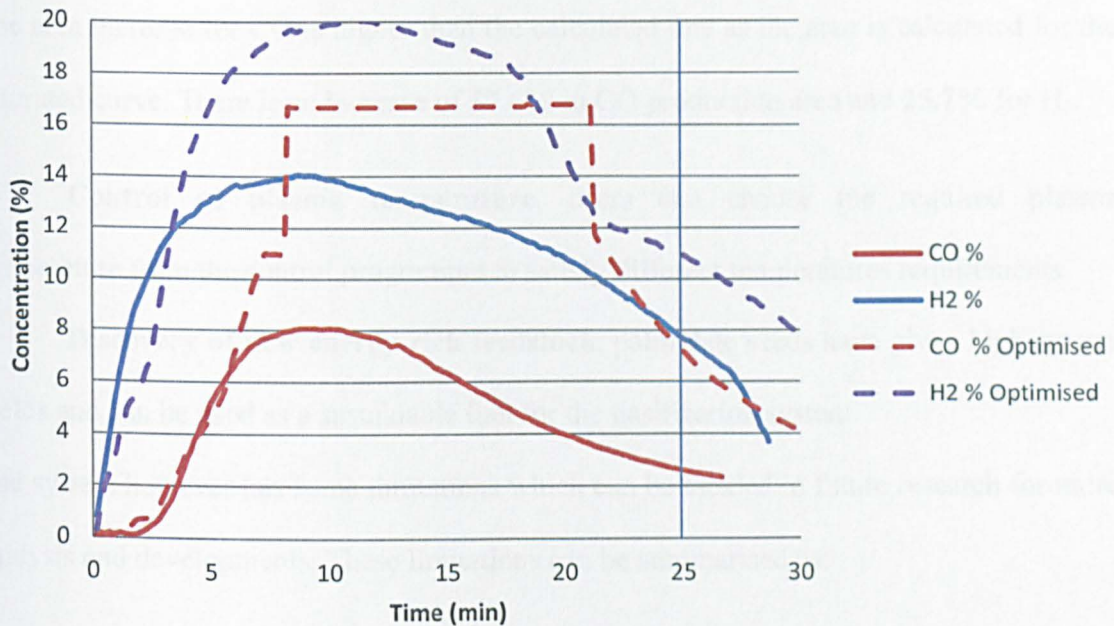


Figure 6.47: Syngas levels for the gasification process with and without the control algorithm applied.

To quantify the level of increase in syngas production for the improved and the manual control, the area under gas curves is calculated. In figure 6.47, CO and H₂ area under curves from 0-25 minutes is calculated according to Trapezoid rule.

The areas under curve are calculated by applying trapezoid rule in excel and table 6.18 lists the areas.

Table 6.18: Area calculations for syngas production.

CO area for manual control	H ₂ area for manual control	CO area for automatic control	H ₂ area for automatic control	Increase percentage in CO area (%)	Increase percentage in H ₂ area (%)
122.5	287.2	289.2	386.5	57.6	25.7

The area increase for CO is higher than the calculated one as the area is calculated for the saturated curve. There is an increase of **57.6%** in CO production area and **25.7%** for H₂.

4- **Control of plasma temperature**, users can choose the required plasma temperature from the control programme to satisfy different temperatures requirements

5- **Discovery of new energy rich feedstock**, palm date seeds have given high syngas yields and can be used as a sustainable fuel for the gasification system.

The system however has some limitations which can be tackled in future research for more analysis and developments. These limitations can be summarised as:

- 1- **Pressure limitation**, this limit is due to the design of the gasification chamber; it was designed to withstand pressures up to 300mbar. Thus higher pressure effects on syngas production could not be studied.
- 2- **Feedstock size limitation**, it is also due to the gasification chamber; it was designed to hold the feedstock in a crucible aligned with a hole in the chamber's wall from which plasma is initiated. This crucible could not hold larger volumes of feedstock.
- 3- **CO sensor limitation**, Quintox gas analyser has a limit on high CO levels measures of 17%. CO could not be accurately measured at high levels, thus Quintox limitation experiments were a must to see the effects of system parameters on syngas production.

6.6. Summary

In this chapter, the validation of the system's sensors calibration was examined first. Power control, argon flow, E-H tuner arms, and hydrogen sensor were tested for the full range of use of each of them. Error rates were calculated and listed for each sensor.

The second part of this chapter was about preparing the timber feedstock. Calculations of moisture content and ash content were made and were approximately equal to 14 % and 44% respectively. The calorific value of the timber was taken from a previous study and is equal to 19 MJ/Kg. For repeatability reasons, timber samples had to be homogenous. A microwave analysis was made for the samples used in order to check the similarity between the cut samples and only samples that had correlation factor of greater than 0.9 were chosen for the system experiments.

System experiments were done to specify the optimal systems parameters. These parameters are power, flow rate, pressure, and sample's moisture. However, Quintox CO limit of 17% was a problem as it is not possible to examine the effects of changing these parameters. Thus power and sample size needed to be chosen at values which do not generate high CO levels. Power of 400 watts with 10 g samples was chosen for this purpose. For repeatability reasons, some experiment cases in flow rate and pressure were repeated four times and error rates were calculated for syngas production. The work has proved to be repeatable.

The improvement of the syngas production by applying the control algorithm was examined, and syngas yielded at higher levels as a result of reducing the reflected power. CO production increased 57.6% and H₂ increased 25.7%.

Helium was tested as the plasma gas; it resulted in stronger and denser plasma which gave higher syngas levels. However, helium is an expensive gas and using it needs budget considerations for the system. This budget depends on the market value of the gas at the time of using the system. There is 9.5% increase in CO production and 25.7% in H₂ production. Argon was chosen as the plasma gas as it is cheaper.

Palm date seeds were used instead of timber feedstock as it is a waste material and gasifying it resulted in high syngas levels which can be compared to the levels produced when using timber. This puts palm date seeds as a potential fuel for energy from waste production.

Table 6.19 summarises the optimal parameters and the choices made for best syngas production.

Table 6.19: Optimal system's parameters.

Power (watt)	Argon Flow rate (L/m)	Pressure (mbar)	With or without control algorithm	Argon vs. helium plasma	Timber vs. palm date
400	0.5	50	With algorithm	Depends on cost	Palm date

Chapter Seven: Conclusion and Future Work

7.1. Conclusion

Green and sustainable energy is the path for a brighter and cleaner future. Research and development (R&D) is being conducted globally to reduce the dependency on fossil fuels as our main energy source. These developments are driven by both regulations and environmental concerns. Regulations such as the EU's renewables directive set a target to the energy producers to increase their electricity production from renewable sources to 20% by the year 2020. Environmental concerns on the other hand include the greenhouse gas (GHG) emissions, climate change and waste management. Governments are reducing GHG emissions and climate change effects by levying an added tax on the energy producers for any excess of their power plants' CO₂ emissions; this leads to further interest from these companies to invest in green energy R&D. However waste management remains as a challenge and landfills are reaching capacity.

Gasification is an answer for this brighter and cleaner future which the next generations depend on us to provide. Gasification does not only provide a sustainable energy production, but also contributes to solving the accumulated landfill problem. Gasification plants can be fuelled from municipal waste that often goes to landfills, making it the optimal solution for recycling and creating green energy simultaneously.

LJMU's gasification system is a state-of-the-art system. It uses microwave power in order to create plasma from argon gas. The microwave power is in the range of 0-1 KW and the frequency of 2.45 GHz. This microwave induced plasma is introduced to the gasification

chamber wherein the sample (feedstock) is placed. The plasma interacts with the sample to create syngas. In this thesis, the concept of gasification, plasma and microwave are explained as an introduction for the reader to understand the system. This thesis explains the simulation, the design and the implementation of the microwave plasma gasification system which has all been done in LJMU's BEST Research institute laboratory. After the system was implemented, it was fully controlled and computerised. Results have indicated that this control has led to improvements in syngas production. A 57.6% increase in CO and 25.7% increase in H₂ production were achieved by applying the control algorithm. The plasma parameters (through the power, argon flow rate and the tuning system), are controlled via a graphical user interface (LabVIEW). This control enabled us to study the effects of changing the parameters on syngas production. Results have shown that for an improved syngas production using a microwave argon plasma gasification system, argon flow rate should be 0.5 litre/minute, pressure at 50 mbar, and tuning system tracking the minimum reflected power for efficiency.

At 400 watt only and for 10g wood samples, LJMU's gasification system was able to produce more than 17 % CO (this number is believed to be much higher but due to CO sensor limitation, it was not able to record higher percentages) and 20% H₂. Palm date seeds were tested as well and have produced similar percentages of syngas (saturation level for CO and 15 % for H₂). This makes the proposed automated system a potential option for energy production from waste.

Helium was tested as the plasma gas instead of argon and the result has shown that it is more effective than argon at the same input power of 400 watt. However, helium is much more expensive than argon and a study should be made when deciding which gas to use.

This study should depend on the price of the KW/h of electricity and the difference between the argon and the helium price. However an increase of 9.5% in CO production and a 25.6% in H₂ production were achieved by using helium plasma comparing to argon plasma.

The aims and objectives of the project listed in chapter one have been all successfully met. The work packages, mentioned in chapter one, have all been explored and detailed. These work packages are;

Work package 1: Literature review of the necessity of an alternative energy sources and the available alternatives. Gasification microwave and plasma theory are looked at along with the available gasification technologies and research.

Work package 2: HFSS system analysis and development. HFSS model has been developed for further understanding of the system operation and for development of the system.

Work package 3: Instrumentation and LabVIEW interface with the different sensors needed for the automation and the control of the gasification process

Work package 4: Develop an automated monitoring and control system to tackle the complexity of manual control of the gasification process and to increase and maximise syngas production rates.

Work package 5: Interfacing with syngas sensors for the monitoring of the gasification procedure and as a proof of the benefits of the control system implemented.

Work package 6: Documentation of the study both in a thesis and in conference and journal papers as a contribution to the knowledge database and for future development and reference.

All of the parameters affecting the gasification procedure have been studied and controlled to deliver the complete, novel microwave plasma gasification system.

7.2. Future Work

This system deals with small samples (10-30g only). This is due to limitations in the gasification chamber and size. The project has already been granted a fund (technology strategy board, TSB project). This fund will be utilised in the further development of the system. This development will include the scale up to a small industrial scale. The scale up will make it possible to use samples in the range of hundred kilograms and the use of higher input power with more than one plasma torch. The increase in the number of the plasma torches from one will aid in rapidly and efficiently gasifying the feedstock. This scale up will be based on the study made in this thesis for best and performance.

Another future work might include a micro gasification system. This micro system would be for home use. Imagine your back garden transformed into a mini green power plant. This power plant would be able to “eat” your garbage and give electricity or heat to your house in return.

This concept however needs further development for a smaller system. Smaller waveguide system could be used with higher frequencies. Thus substituting the magnetron to higher frequency would potentially transform the system to a microsystem. However, there would still be the problem of how to utilise the syngas produced from the system, but future

development would eventually come up with a solution for this and make this green dream possible.

This was not applied in our gasification system as the aim of the study was to control and improve a microwave plasma gasification system that can be scaled up and commercially used to provide energy to a large number of consumers.

More future work can be done to develop the control algorithm to find the minimum reflected power. This algorithm is based on the reflected power as feedback. Other feedback parameters can be used to improve this algorithm, such as the strength and the temperature of the plasma. However, this needs alterations in the design of the gasification chamber to accommodate the temperature sensor for example inside the chamber.

Higher level CO sensor should be used as a future development to measure the maximum CO levels when using higher input power and bigger sample sizes.

References

- [1] Exxon Mobile, "2012 The Outlook for Energy: A View to 2040," Texas, 2012.
- [2] World Energy Council, "2010 Survey of Energy Resources," London, 2010.
- [3] David Archer, *The Long Thaw: How Humans are Changing the Next 100,000 Years of Earth's Climate*: Princeton University Press, 2009.
- [4] Nick Dallas, *Green Business Basics: 24 Lessons for Meeting the Challenges of Global Warming* McGraw-Hill, 2009.
- [5] Robert Henson and Duncan Clark, *The Rough Guide to Climate Change*, 2 ed. London: New York, 2008.
- [6] Janet Wood, *Nuclear Power*. London: IET, 2007.
- [7] Behram N. Kursunglu, Stephan L. Mintz, and Arnold Perlmutter, *The Challenges to Nuclear Power in the Twenty-first Century*. New York: Plenum, 2000.
- [8] James E. Doyle, *Nuclear Safeguards, Security, and Nonproliferation*. Oxford: Elsevier Inc., 2008.
- [9] REN21, "Renewables 2011, Global Status Report," 2011.
- [10] Legislation.gov.uk, *Utilities Act 2000*. London, 2000, Last accessed 28/05/2012.
- [11] Great Britain, *Electricity Act 1989*. London, 1989.
- [12] The European Parliament and The Council of The European Union, *The Promotion of Electricity Produced from Renewable Energy Sources in The Internal Electricity Market: Directive (2001/77/EC)*, 2001.
- [13] Department of Energy & Climate Change, "Energy Trends," London, 2010.
- [14] Renewable Energy Foundation, "Renewables Output in 2010," London, 2011.
- [15] The European Parliament and The Council of The European Union, *The Promotion of The Use of Energy from Renewable Sources and Amending and Subsequently Repealing Directives 2001/77/EC and 2003/30/EC: Directive 2009/28/EC*, 2009.
- [16] The National Academies, *Understanding and Responding to Climate Change*. Washington: National Academy of Science, National Academy of Engineering, Institute of Medicine, National Research Council, 2008.
- [17] S. Solomon, D. Qin, M. Manning, Z. Chen, M. Marquis, K.B. Averyt, M. Tignor, and H.L. Miller, "Climate Change 2007: The Physical Science Basis," *Contribution of Working Group 1 to the Fourth Assessment Report of the Intergovernmental Panel on Climate Change*, p. 996, 2007.
- [18] National Research Council, *Surface Temperature Reconstructions for the Last 2,000 Years* Washington, D.C., 2006.
- [19] U.S. Department of Transportation. *Transportation and Greenhouse Gas Emissions*. (2006)
- [20] U.S. Environmental Protection Agency. (2011, 20, June). *Greenhouse Gas Emissions*. Available: <http://www.epa.gov/climatechange/emissions/index.html#ggo>. Last accessed 2/4/2012.
- [21] National Oceanic and Atmospheric Administration (NOAA), "The NOAA Annual Greenhouse Gas Index (AGGI)," NOAA Earth System Research Laboratory, Broadway, 2011.

References

- [22] H.S. Eggleston, L. Buendia, K. Miwa, T Ngara, and K. Tanabe, "2006 IPCC Guidelines for National Greenhouse Gas Inventories," The National Greenhouse Gas Inventories Programme, The Intergovernmental Panel on Climate Change, 2006.
- [23] David JC MacKay, *Sustainable Energy — without the hot air*. Cambridge: UIT Cambridge Ltd., 2009.
- [24] Juniper for Renewables East, "Advanced Conversion Technology (Gasification) for Biomass Projects," Juniper, 2007.
- [25] John Twidell and Tony Weir, *Renewable Energy Resources*, 2nd ed. London: Taylor & Francis, 2006.
- [26] Susan Baker, *Sustainable Development*. New York: Routledge, 2006.
- [27] Peter P. Rogers, Kazi F. Jalal, and John A. Boyd, *An Introduction to Sustainable Development*: Earthscan, 2008.
- [28] Mohan Munasinghe, "Sustainable Development Triangle," Munasinghe Institute for Sustainable Development, 2007.
- [29] Actis. (2001, 27, June). *Renewable Energy Resources*. Available: <http://www.scienceonline.co.uk>. Last accessed 25/3/2012.
- [30] Michael Boxwell, *Solar Electricity Handbook*. Ryton on Dunsmore: Greenstream, 2010.
- [31] Antonio Luque and Steven Hegedus, *Handbook of Photovoltaic Science and Engineering*. Chichester: John Wiley & Sons Ltd., 2003.
- [32] Alyssa Kagel, Diana Bates, and Karl Gawell, "A guide to Geothermal Energy and The Environment," Geothermal Energy Association, Washington, 2007.
- [33] U.S Department of Energy. (2010, 4th, July). *How Wind Turbines Work*. Available: http://www1.eere.energy.gov/windandhydro/wind_how.html#a
- [34] Chianf Mei, "Capturing the Energy in Ocean Waves," MIT Energy Initiative, 2008.
- [35] Balazs Czech, Pavol Bauer, Henk Polinder, and Peter Korondi, "Modeling and Simulating an Archimedes Wave Swing Park in Steady State Conditions," presented at the Power Electronics and Applications, Barcelona, 2009.
- [36] Australian Institute of Energy, "Tidal Energy," 1999.
- [37] Tushar K. Ghosh and Mark A. Prelas, *Energy Resources and Systems: Renewable Resources*: Springer, 2011.
- [38] Tidal Stream. (07, July). *Harvesting Tidal Energy*. Available: <http://www.tidalstream.co.uk/html/background.html>
- [39] Department of Energy & Climate Change. (2011). *Hydroelectricity*. Available: http://www.decc.gov.uk/en/content/cms/meeting_energy/hydro/hydro.aspx
- [40] A.K. Raja, Amit Prakash Srivastava, and Manish Dwivedi, *Power Plant Engineering*: New Age International Ltd., 2006.
- [41] The McGraw Hill Companies, *Power Plant Engineering*, 3rd ed.: Tata McGraw-Hill, 2008.
- [42] Ralph P. Overend, "Biomass Conversion Technologies," Colorado 2002.
- [43] Erakhrumen andrew Agbontalor, "Overview of Various Biomass Energy Conversion Routes," *American-Euroasian Journal of Agricultural & Environmental Science*, vol. 2, pp. 662-671, 2007.

References

- [44] J. Woods and D.O. Hall, *Bioenergy for development - Technical and environmental dimensions*. Rome: FAO - Food and Agriculture Organization of the United Nations 1994
- [45] Ralph P. Overend, *Thermochemical Conversion of Biomass*. Colorado: EOLSS Publishers Co Ltd, 2009.
- [46] Ayhan Demirbas, *Biodiesel: A Realistic Fuel Alternative for Diesel Engines*. London: Springer, 2008.
- [47] Nicolaus Dahmen, Edmund Henrich, Andrea Kurse, and Klaus Raffelt, *Biomass Liquefaction and Gasification*: John Wiley & Sons Ltd., 2010.
- [48] Waste Balkan Network, "Biological Treatment," 2010.
- [49] Satoto Endar Nayono, *Anaerobic Digestion of Organic Solid Waste for Energy Production*: Karlsruhe Berichte zur Ingenieurbiologie, 2009.
- [50] Dawn A. Santoianni, Matthew F. Bingham, Dawn M. Woodard, and Jason C. Kinnell, "Power From Animal Waste: Economic, Technical, and Regulatory Landscape in the United States," *Journal of EUEC*, vol. 2, p. 37, 2008.
- [51] Mustafa Balat, "Biomass Energy and Biochemical Conversion Processing for Fuels and Chemicals," *Energy Sources*, vol. 28, pp. 517-525, 2006.
- [52] REN21, "Renewable Energy 2010: Key Facts and Figures for Decision Makers," 2010.
- [53] The Organisation for Economic Cooperation and Development (OECD). "OECD Environmental Data- Waste," 2008.
- [54] Timon Singh, "Meeting the Targets of the European Union Landfill Directive," *EU Infrastructure*, 2010.
- [55] The European Parliament and The Council of The European Union, "Directive 2008/98/EC on waste and repealing certain Directives," 2008.
- [56] Food and Rural Affairs (defra) Department for Environment, "Local Authority Collected Waste Management Statistics for England," London, 2012.
- [57] The Blue Ridge Environmental Defense League, "Waste Gasification, Impacts on the Environment and Public Health ", Technical Report, 2009.
- [58] Doug Orr and David Maxwell, "A Comparison of Gasification and Incineration of Hazardous Wastes," National Energy Technology Laboratory (NETL), West Virginia, 2000.
- [59] Malti Goel, Baleshwar Kumar, and S. Nirmal Charan, *Carbon Capture and Storage: R&D Technologies for a Sustainable Energy Future*: Alpha Science International Ltd, 2008.
- [60] Business Link. (2011, October). *Environmental tax obligations and breaks*. Available: <http://www.businesslink.gov.uk/bdotg/action/detail?itemId=1074404201&type=RESOURCES>
- [61] Robert B. Klepper. *Gasification*. Available: http://www.emnrd.state.nm.us/emnrd/biomass/docs/GF_presentations/combppt-Klepper.pdf
- [62] Irvin Glassman and Richard A. Yetter, *Combustion*, 4th ed.: Elsevier Inc., 2008.
- [63] Gasification Technologies Council. (October). *Gasification: Redefining Clean Energy*. Available: <http://www.gasification.org/>

References

- [64] R. Mark Bricka and Dave C. Swalm, "Energy Crop Gasification and Gasification Issues'," *School of Chemical Engineering Mississippi State University*.
- [65] A.V Bridgwater, "Thermal Conversion of Biomass and Waste: The Status," Bio-Energy Research Group, Aston University, Birmingham, 2008.
- [66] Christopher Higman and Maarten van der Burgt, *Gasification*, 2nd ed.: Gulf Professional Publishing, 2008.
- [67] Friends of the Earth, "Pyrolysis, Gasification and Plasma," Briefing of Friends of Earth Organisation, London, 2009.
- [68] Jared P. Ciferno and John J. Marano, "Benchmarking Biomass Gasification Technologies for Fuels, Chemicals and Hydrogen Production," U.S. Department of Energy, National Energy Technology Laboratory, 2002.
- [69] Jeffrey Phillips, "Different Types of Gasifiers and Their Integration with Gas Turbines," EPRI Advanced Coal Generation, 2008.
- [70] M. Morris, "Electricity Production from Solid Waste Fuels Using advanced Gasification Technologies," TPS Termiska Processer AB1998.
- [71] Stanislav Vassilev, David Baxter, Lars Andersen, and Christina Vassileva, "An Overview of The Chemical Composition of Biomass," IEA Bioenergy, Lyon2010.
- [72] Peter Quaak, Harrie Knoef, and Hubert Stassen, *Energy from Biomass: A Review of Combustion and Gasification Technologies* vol. 23-422. Washington: The International Bank for Reconstruction and Development, 1999.
- [73] John Moore, "Wood Properties and Uses of Sitka Spruce in Britain," Forestry Commission, Edinburgh, 2011.
- [74] Eija Alakangas, "Properties of Wood Fuels Used in Finland - Biosouth Project," VTT Processes, 2005.
- [75] Daniel Ciolkosz, *Renewable and Alternative Energy Fact Sheet*, 2010.
- [76] Michael R. Lindeburg, *Mechanical Engineering Reference Manual*, 12th ed.: Professional Publications, Inc., 2006.
- [77] U.S. Department of Energy. (2011, Feb 13). *How Coal Gasification Power Plants Work*. Available: <http://fossil.energy.gov/programs/powersystems/gasification/howgasificationworks.html>
- [78] Henry V. Krigmont, "Integrated Biomass Gasification Combined Cycle (IBGCC) Power Generation Concept: The Gateway to a Cleaner Future," Allied Environmental Technologies, Inc.1999.
- [79] Michael J.A. Tijmensen, Andre P.C. Faaij, Carlo N. Hamelinck, and Martijn R.M. van Hardeveld, "Exploration of the Possibilities for Production of Fischer Tropsch Liquids and Power via Biomass Gasification," *Biomass and Bioenergy, Elsevier*, vol. 23, pp. 129-152, 2002
- [80] Fred H. Hutchison. (2009). *Integrated Gasification Combined Cycle (IGCC)*. Available: <http://www.clean-energy.us/facts/igcc.htm>
- [81] H. Boerrigter and A. van der Drift, "Large-scale Production of Fischer-Tropsch Diesel from Biomass: Optimal Gasification and Gas Cleaning System," ECN Biomass2004.
- [82] Tom Miles, "What About Gasification for Village Energy?," T R Miles Technical Consultants2011.

References

- [83] Department of Energy & Climate Change. (2012, 10-Feb-2012). *Carbon Capture and Storage (CCS)*. Available: <http://www.decc.gov.uk/en/content/cms/emissions/ccs/ccs.aspx>
- [84] ENER-G. Available: <http://www.energ.co.uk/>
- [85] K. Umashankar, *Introduction to engineering electromagnetic fields*: World Scientific, 1989.
- [86] D.A. Fleisch, *A student's guide to Maxwell's equations*: Cambridge University Press, 2008.
- [87] The National Radio Astronomy Observatory. (2002). *How Radio Waves Are Produced*. Available: <http://www.nrao.edu/index.php/learn/radioastronomy/radiowaves>
- [88] Bhag S. Guru and Huseyin R. Hiziroglu, *Electromagnetic Field Theory Fundamentals*: Cambridge University Press, 2004.
- [89] John S. Seybold, *Introduction to RF Propagation*. New Jersey: John Wylie & Sons, Inc., 2005.
- [90] Hamish Meikle, *Modern Radar Systems*. London: Artech House, Inc., 2001.
- [91] Dynawave Inc., "Coaxial Cable RG 142 (Datasheet)."
- [92] Hongsen Cable, "Coaxial Cable RG 304 (Datasheet)."
- [93] Joseph F. White, *High Frequency Techniques, An Introduction to RF and Microwave Engineering*. New Jersey: John Wylie & Sons, Inc., 2004.
- [94] Cobham Defense Electronic Systems, "Waveguide Component Specifications and Design Handbook," Continental Microwave Division.
- [95] R. Gomez Martin, *Electromagnetic Field Theory for Physicists and Engineers: Fundamentals and Applications*. Granada: Electrodinamica, 2006.
- [96] R K Shevgaonkar, *Electromagnetic Waves*. New DELhi: McGraw-Hill 2006.
- [97] Annapurna Das and Sisir K. Das, *Microwave Engineering*: Tata McGraw-Hill, 2000.
- [98] Janusz A. Dobrowolski, *Microwave Network Design Using the Scattering Matrix*: Artech House, 2010.
- [99] Communications & Power Industries, "Magnetron Theory of Operation," Beverly Microwave Division, Massachusetts.
- [100] Joseph Helszajn, *The Stripline Circulator: Theory and Practice*: John Wiley & Sons, Inc., 2008.
- [101] G. J. Wheeler, *Introduction to Microwaves*: Prentic-Hall, 1963.
- [102] Annapurna Das and Sisir K Das, *Microwave Engineering*. New Delhi: Tata McGraw-Hill, 2009.
- [103] Rajeswari Chatterjee, *Antenna Theory And Practice*: New Age International, 2006.
- [104] Warren L. Stutzman and Gary A. Thiele, *Antenna Theory and Design*: John Wiley & Sons, 2012.
- [105] ANSYS, "Ansoft HFSS - User Guide," ANSYS, Inc.2009.
- [106] Vector Fields Concerto, "Manual guide," 2001.
- [107] J.A. Bittencourt, *Fundamentals of Plasma Physics*, 3rd ed. New York: Springer, 2004.
- [108] John Howard, *Introduction to Plasma Physics*: Plasma Research Laboratory, Research School of Physical Sciences and Engineering, 2002.

References

- [109] Maher I. Boulos, Pierre Fauchais, and Emil Pfender, *Thermal Plasmas: Fundamental and Applications*. New York: Plenum Press, 1994.
- [110] Grill. A, *Cold Plasma Materials Fabrication: From Fundamentals to Applications*, 1st ed.: Wiley-IEEE 1994.
- [111] Eric Seymour, "Performance Considerations of High-Power AC Plasma Deposition Power Supplies," Advanced Energy Industries, Colorado, 2004.
- [112] A I Al-Shamma'a, S R Wylie, J Lucas, and C F Pau, "Design and Construction of a 2.45 GHz Waveguide-based Microwave Plasma Jet At Atmospheric pressure for Material Processing," *Journal of Physics: Applied Physics*, vol. 34, pp. 2734-2741, 2001.
- [113] A. L. Hughes and J. H. McMillen, "Inelastic and Elastic Electron Scattering in Argon," *Physical Review*, vol. 39, pp. 585-600, 1932.
- [114] Hiroshi Uchida, "Effects of Central Argon Flow Rate on Characteristics of Inductively Coupled Plasma," *Spectroscopy Letters: An International Journal for Rapid Communication* vol. 14, pp. 665-674, 1981.
- [115] Jeroen Jonkers, Marco van de Sande, Antonio Sola, Antonio Gamero, and Joost van der Mullen, "On the Differences Between Ionizing Helium and Argon Plasmas At Atmospheric Pressure," *Plasma Sources Science and Technology (IoP)*, vol. 12, pp. 30-38, 2003.
- [116] Brenda S. Sheppard, Wei-Lung Shen, Timothy M. Davidson, and Joseph A. Carusot, "Helium - Argon Inductively Coupled Plasma for Plasma Source Mass Spectrometry," *Journal of Analytical Atomic Spectrometry*, vol. 5, pp. 697-700, 1990.
- [117] Krzysztof Jankowski and Adrianna Jackowska, "Spectroscopic Diagnostics for Evaluation of the Analytical Potential of Argon + Helium Microwave-Induced Plasma with Solution Nebulization," *Journal of Analytical Atomic Spectrometry*, vol. 22, pp. 1076-1082, 2007.
- [118] E. Gomez, D. Amutha Rani, C.R. Cheeseman, D. Deegan, M. Wise, and A.R. Boccaccini, "Thermal plasma technology for the treatment of wastes: A critical review," *Journal of Hazardous Materilas*, vol. 161, pp. 614-626, 2009.
- [119] Shlomo Wald, Alex Pokryvailo, Gabriel Appelbaum, Moshe Katz, and Eyal I. Weiss, "Hazardous Waste Treatment and Recovery of Valuable Products with a Thermal Pulsed-Plasma Technology," *IEEE Transactions on Plasma Science*, vol. 28, pp. 1576-1580, 2000.
- [120] T.W. Cheng, J.P. Chu, C.C. Tzeng, and Y.S. Chen, "Treatment and Recycling of Incinerated Ash Using Thermal Plasma Technology," *Waste Management*, vol. 22, pp. 485-490, 2002.
- [121] Gasification Technologies Council, "Gasification: An Investment in Our Energy Future," Allngton, 2011.
- [122] Advanced Plasma Power. (2011). *Swindon Gasplasma Plant*. Available: <http://www.advancedplasmapower.com>
- [123] David Beckman, "Energy Innocations: Demonstrating new cellulosic ethanol process technology," HATCH, Ontario, 2010.
- [124] Waste Technology Reports, "The Alter NRG/Westinghouse Plasma Gasification Process," Juniper Consultancy Services Limited, Bisley, 2008.

References

- [125] Djamal Djebabra, Odile Dessaux, and Pierre Goudmand, "Coal Gasification by Microwave Plasma in Water Vapour," *Fuel*, vol. 7, pp. 1479-1475, 1991.
- [126] P.M Kaniloa, V.I Kazantsev, N.I Rasyukc, K Schünemannd, and D.M Vavriv, "Microwave Plasma Combustion of Coal " *Fuel*, vol. 82, pp. 187-193, 2003.
- [127] L. Tang and H. Huang, "Plasma Pyrolysis of Biomass for Production of Syngas and Carbon Adsorbent," *Energy and Fuels*, vol. 19, pp. 1174-1178, 2005.
- [128] Osamu Kamei, Kaoru Onoe, Wataru Marushima, and Tatsuaki Yamaguchi, "Brown Coal Conversion by Microwave Plasma Reactions Under Successive Supply of Methane," *Fuel*, vol. 77, pp. 1503-1506, 1998.
- [129] Antonio León Sánchez, "Technological Status "ABA Process for Microwave Induced Plasma Gasification", " Centro de Calidad Ambiental ITESM Campus Monterrey, Monterrey, 2011.
- [130] Hidetoshi Sekiguchi and Yoshihiro Mori, "Steam plasma reforming using microwave discharge," *Thin Solid Films*, vol. 435, pp. 44-48, 2003.
- [131] Gary C. Young, *Municipal Solid Waste to Energy Conversion Processes: Economic, Technical and renewable comparisons*: John Wiley & Sons, Inc., 2010.
- [132] National Instruments, "Industrial Isolator: Product Information," Richardson Electronics, Ltd.
- [133] M. Moisan, Z. Zakrzewski, R. Pantel, and P. Leprince, "A Waveguide-Based Launcher to Sustain Long Plasma Columns Through the Propagation of an Electromagnetic Surface Wave," *IEEE Transactions on Plasma Science*, vol. 3, 1984.
- [134] M. Moisan and Z. Zakrzewski, "New Surface Wave Launcher for Sustaining Plasma Columns at Submicrowave Frequencies (1-300 MHz)," *American Institute of Physics*, vol. 10, 1987.
- [135] M. Moisan, Z. Zakrewski, R. Etemadi, and J. C. Rostaing, "Multiple Surface-wave Discharge for Increased Gas Throughput at Atmospheric Pressure," *Journal of Applied Physics*, vol. 83, 1998.
- [136] T. Fleisch, Y. Kabouzi, M. Moisan, J. Pollak, E. Castanos-Martinez, H. Nowakowska, and Z. Zakrzewski, "Designing an Efficient Microwave-plasma Source, Independent of Operating Conditions, at Atmospheric Pressure," *IoP, Plasma Sources Science and Technology*, vol. 16, pp. 173-182, 2007.
- [137] M. Moisan, Z. Zakrzewski, and J. C. Rostaing, "Waveguide-based Single and Multiple Nozzle Plasma Torches: The TIAGO Concept," *IoP, Plasma Sources Science and Technology*, vol. 10, pp. 387-394, 2001.
- [138] Gary W. Johnson and Richard Jennings, *LabVIEW Graphical Programming*: McGraw-Hill, 2006.
- [139] National Instruments, "16-Channel Analog Output Module NI 9264," 2010.
- [140] National Instruments, "NI 9219: 24-Bit Universal Analog Input," 2012.
- [141] National Instruments, "NI 9401: 8 Ch, 5V/TTL High-Speed Bidirectional C Series Digital I/O Module," 2012.
- [142] National Instruments, "NI 9211: 4-Channel, 14 S/s, 24-Bit, +80 mV C Series Thermocouple Input Module," 2012.
- [143] Alter Power Systems, "Switching Power Supply fo Magnetron, Technical Note SM745G," 2010.
- [144] Songle Relay, "Relay ISO9002, SM1-12VDC-SD-2C, Technical Sheet."

References

- [145] Brooks Mass Flow Meter/Controller Model 5850TR, "Installation and Operating Manual," 1992.
- [146] Astrosyn, "Stepper Motor, Technical Data."
- [147] Panasonic, "Mono Faders for Audio Mixers, Slide Potentiometer/ EVANF Data Sheet," 2005.
- [148] Omron, "Ultra Subminiature Basic Switch, Microswitch Data Sheet."
- [149] McLennan, "Unipolar Stepper Motor Translators User Handbook."
- [150] TC Direct, "Temperature Measurement and Control , N-type Thermocouple Data Sheet," 2012.
- [151] Hitech Instruments, "K1550 Gas Analyser Instruction Manual."
- [152] Keison Products, "KM9106 Operators Manual."
- [153] (2009, 05). Available: http://www.keison.co.uk/kane_fireworks.shtml
- [154] Jerry Luecke, *Analog and Digital Circuits for Electronic Control System Applications*: Elsevier, 2004.
- [155] A.K. Sharma, *Text Book Of Correlations And Regression*: Discovery Publishing House, 2005.
- [156] Simon Nelms, *Inductively Coupled Plasma Mass Spectrometry Handbook*: Blackwell Publishing, 2005.
- [157] Krzysztof J. Jankowski and Edward Reszke, *Microwave Induced Plasma Analytical Spectrometry*: The Royal Society of Chemistry, 2011.
- [158] Farnell UK, "ST-125 Moisture Meter," Farnell datasheet 2012.
- [159] Valter Francescato, Eliseo Antonini, and Luca Zuccoli Beromi, "Wood Fuels Handbook," Italian Agriforestry Energy Association, Italy, 2008.
- [160] James F. Epperson, *An Introduction to Numerical Methods and Analysis*: John Wiley & Sons, 2007.

Appendix A – Publications List

1. B. Kabalan, S. Wylie, A. Mason, R. Al-khaddar and A. Al-Shamma'a, C. Lupa, B Herbert and E Maddocks, "*Real-time Optimisation of a Microwave Plasma Gasification System*", Journal of Physics: Conference Series 307, 2011.
2. N. Al-Rubaye, D. Al-Khafagiy, B. Kabalan, and A. Al-Shamma'a, "*Syngas Production from Date Palm Seeds by Using Advanced Microwave Technology*", British Journal of Science, Vol. 3 (2), February 2012.
3. N. Al-Rubaye, D. Al-Khafagiy, and B. Kabalan, "*Biogas Production from Date Palm Seeds: CFD Simulation and Quality Assessment in Thermal Plasma Reactor*", Journal Conference on Environmental Science and Development (JCESD 1st), 2012.
4. B. Kabalan, A. Mason A. Shaw and A. Al-Shamma'a, "*The Effects of Parameters Changing on Syngas Production Using Microwave Plasma Gasification System*", Built Environment & Natural Environment 7th Conference, Liverpool, 2012
5. B. Kabalan, S. Wylie, A.Mason, and A. Al-Shamma'a, "*Microwave plasma gasification: control, automation and analysis*", Built Environment & Natural Environment 6th Conference, Liverpool, 2011

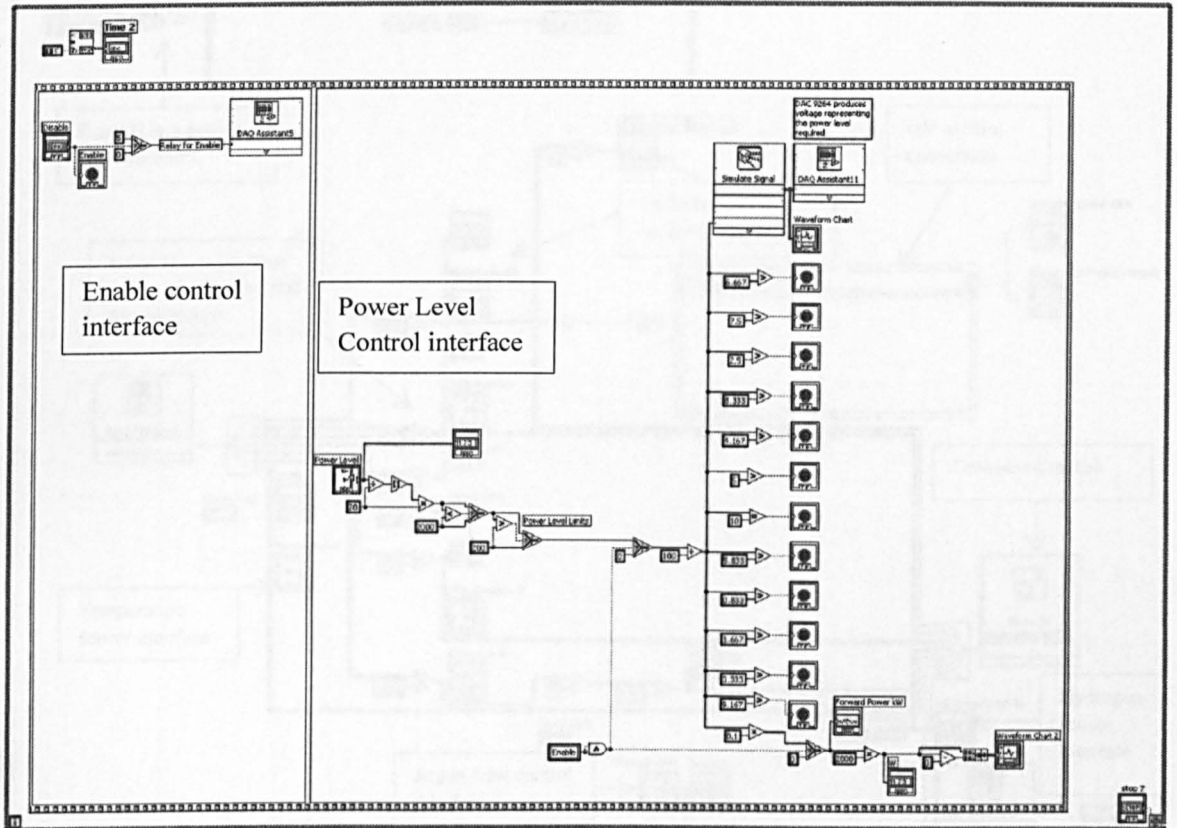
Appendix B – Gasification Plants Worldwide

Technology Provider	Plant Locations	Technology Description	Details	Wastes Treated
Mitsui Babcock	Yame Seibu, Japan Toyoashi City, Japan	R21: Pyroly. + Combust. R21: Pyroly. + Combust.	70,000 tpa. 2000 120,000 tpa. 2002	MSW, ASR MSW
Okadora	Kanagawa Prefecture, Japan	Carbonizing-Melting-Gasification	1,750 tpa. May 2004. Experimental plant for one year test-run to establish a full-scale facility of 350,000 tpa.	Biomass (including MSW,)
PKA	Freiberg, Germany	Pyrolysis	Research Plant	Industrial and municipal solid industrial waste with a high content of aluminium MSW
	Freiberg, Germany	Pyrolysis (Alu-Rec Pyrolysis)	2001.	
	Aalen, Germany	Pyrolysis (element of MSW combustion plant)	Full-scale Plant. 2001	
Serpac/Basse Sambre	Iceland	Pyrolysis (PIT Pyroflam)	12,000 tpa. Dec. 2003	Waste min. 6,800 kJ/kg
Thermoselect	Karlsruhe, Germany	Pyrolysis + gasification	225,000 tpa. 1998 - 2002	MSW and commercial waste Industrial waste MSW
	Chiba, Japan	Pyrolysis + gasification	100,000 tpa. 1999	
	Mutsu, Japan	Pyrolysis + gasification	50,000 tpa. 2003	
Thide Environment	Dreux, Paris	Pyrolysis/thermolysis	Small scale pilot, 6,400 tpa. 1992	Shredded MSW MSW, Industrial waste and sludge
	Arras, France		50,000 tpa. 2004	
	Izumo, Japan		70,000 tpa. 2003	
	Itogawa, Japan		25,000 tpa. 2002	
TPS	Nakaminato, Japan	Gasification	8,000 tpa. 1999	Pelletised RDF
	Greve-in-Chianti, Italy		67,000 tpa. 1992	
Von Roll		Pyrolysis + Melting	Technology not ready for market yet	MSW, ASR
WasteGen/Techtrade	Burgau, Germany	Pyrolysis	2 x 24,000 tpa. 1983	MSW and sewage sludge
	Hamm, Germany	Pyrolysis	100,000 tpa. 2002	MSW and sewage sludge

Technology Provider	Plant Locations	Technology Description	Details	Wastes Treated
Brightstar Environment	Wollongong, Australia	Pyrolysis + gasification	Demonstration Ceased	MSW
Compact Power	Avonmouth, UK	Pyrolysis, gasification and high temperature oxidation	8,000 tpa. (MSW smallest plant: 30,000 tpa)	Special wastes, Mainly clinical waste
Ebara	Japan	TwinRec Process: Fluidized Bed Gasification and Ash Melting	From 2 x 34,300 to 5 x 49,000 tpa. From 2002 to 2004	MSW
Energos	Ranheim, Norway Averoy, Norway Hurum, Norway Sarpsborg, Norway Forus, Norway Minden, Germany	Gasificat. + combustion Gasificat. + combustion Gasificat. + combustion Gasificat. + combustion Gasificat. + combustion Gasificat. + combustion	10,000 tpa. 1998 30,000 tpa, 2000 35,000 tpa, 2001 70,000 tpa, 2002 37,000 tpa, 2002 37,000 tpa, 2002	Commercial and industrial waste MSW MSW and industrial waste MSW and industrial waste MSW MSW and commercial waste
Energem / Novera (has the exclusive rights for UK and Ireland)	Castellon, Spain Quebec, Canada	Fluidized bed gasification Fluidized bed gasification	25,000 tpa, 2002 1,600 tpa. Pilot plant	Plastics Plastics, sludges, wood, MSW pellets
Ferco	Vermont, USA	FERCO SilvaGas™: Fluidized bed gasification	165,000 tpa. Demonstration plant. 1997	RDF
Foster Wheeler Energy Oy	Lathi, Finland Varkaus, Finland	Circulating Fluidized-Bed Boiler with gasification Bubbling Fluidized-Bed Boiler with gasification	116,100 tpa. 1998 No 2000/76/EC 2100 metric tpa. 2000	Biomass fuels (up to 40% RDF) Aluminium
Future Energy GmbH (formerly Noell)	Sekundärrohstoff-Verwertungszentrum, Germany Freiberg, Germany	Gasification Pyrolysis and entrained flow gasification	3 x 80,000 tpa 12,000 tpa sewage sludge + 5,760 tpa MSW. Demonstration plant. 1996/1997	Waste oil and slurries Sewage sludge + MSW
IET Energy	Hong Kong, Taiwan, Australia, Indonesia, Malaysia, Korea Poland	Entech Renewable Energy System™: pyrolytic gasification Entech Renewable Energy System™: pyrolytic gasification	From 1,750 to 20,300 tpa. From 1990 to 2003 1,750 tpa. 2004	MSW MSW
Lurgi + British Gas	Schwarze Pumpe, Germany	Gasification	500,000 tpa. 1993 rotating grate gasifier. 2000 slagging gasifier.	Plastics, RDF, wood, sewage, sludge, lubricants, coal
Lurgi	Rudersdorf, Germany		100 MW th, 1996	RDF

Appendix C – LabVIEW Block Diagram

A_ Power Control Block Diagram



B_ E-H Tuner, Reflected Power, Argon Flow, Temperature, and Hydrogen Sensor Block Diagram

